Université Ferhat ABBAS Sétif 1

Ferhat ABBAS University Setif -1-
Faculty of Technology
Department of Process Engineering
Option: Chemical Engineering

PhD Thesis

Synthesis and Development of Deep Eutectic Solvents: Characterization Using Quantitative Structure-Property Relationship, and Application as New Solvents in Diesel Purification

Presented by

LEMAOUI Tarek

Presented publicly on: 14 / 05 / 2022 to the jury committee of:

BENTOUHAMI Embarek	Professor	U.F.A. Setif 1	President
BENGUERBA Yacine	Professor	U.F.A. Setif 1	Supervisor
BENAICHA Mohamed	Professor	U.F.A. Setif 1	Co-Supervisor
MEROUANI Slimane	Professor	U. Constantine 3	External Examiner
SOBHI Widad	Professor	U.F.A. Setif 1	Internal Examiner
CHAFAI Nadjib	Assoc. Prof.	U.F.A. Setif 1	Internal Examiner

Academic Year: 2021/2022

Dedication

I **dedicate** this **work** to

My Dear **Parents**,

I will never be able to find the words that could give justice to all my deep love,

appreciation, and gratitude for all the sacrifices

that you have made for me.

I pray to God, that will give you a long life full of happiness and joy, and to

forgive me any pain and hardships I caused you during my Ph.D. period.

My dear **Wife**

My Dear Brothers: **Salah Eddine** and **Amine**

My Lovely Sister: **Soumaya**

All the Family Members of **Lemaoui** and **Layadi**

Especially, to My Dear Uncle: **Ferhat**

My Precious Colleagues: **Ahmad** and **Ayoub**

My Dear Friends:

Aimen, **Walid**, **Khalil**, **Abdessalam** and **Sofiane**.

Finally,

To all those who helped me to do this humble work, from near and far.

To all those who sacrificed their efforts for me.

I tell you with great love:

Thank You So Much

Acknowledgement

I would first like to thank **Allah** for the **Almighty** who gave me the power and patience to carry out this modest work.

I feel that I have learned a lot from this Ph.D. thesis. This is a great treasure that I will keep not only in my future academic career but in my entire life. I would like to take this opportunity to express my immense gratitude to all of the people who have given me their invaluable support.

First and foremost, I am very grateful to **Prof. Inas ALNASHEF** for his guidance, motivation, assistance, and valuable advice. I learned a lot from your advice and experiences in research. I highly appreciate all your time, effort, and contributions throughout my Ph.D years. Also, for giving me the opportunity to work with you on your projects. I would like to express my gratitude to you from the bottom of my heart for your kindness and good dealings with me throughout my stay with you. I hope that our cooperation will continue together in the future.

I would like to thank my utmost gratitude to my advisor, **Prof. Yacine BENGUERBA**, for his continuous support during my Ph.D. years, patience, kindness, benevolence, motivation, enthusiasm, diligence, wisdom, immense knowledge, intelligence, unlimited advice, infinite passion for learning. He gave me a lifetime's worth of unforgettable memories. I was extremely lucky to have the chance to be one of your students. Your kind and supportive personality made you a wonderful professor. I will evermore be indebted to you for all your time and effort in teaching me. I will forever treasure all our fruitful discussions and will be grateful for what I learned from you and your guidance throughout these years. You also gave me the trust and the freedom to pursue research of my interest. If I had to describe you in two words, I

Acknowledgement

would have to choose the words "Great Teacher". Thank you again for everything!

I would like to express my gratitude to my Co-adviser, **Prof. Mohamed BENAICHA**, who gave me valuable guidance. I would like to thank him for his kindness, interest in this modest work, and for encouraging my research, also for allowing me to grow as a research scientist. Your advice to me on both my research and academic career has been invaluable.

I would like to thank the PhD thesis Committee , **Prof. Embarek BENTOUHAMI, Prof. Slimane MEROUANI, Dr. Widad SOBHI**, and **Dr. Nadjib CHAFAI**, for their presence as members of my committee. I also want to thank you for letting my PhD defense be an enjoyable moment, and for your brilliant comments and suggestions, It will be a great honor to have them throughout hours of my PhD discussion, as I will undoubtedly learn from all their expertise and knowledge.

I am also very thankful to Ferhat Abbas Setif University 1 (**Algeria**), and Khalifa University (**United Arab Emirates**) for all their support throughout these Ph.D. years. I would also like to state my gratitude towards the Multiphase Polymer Materials Laboratory (**LMPMP**), and Center for Membrane and Advanced Water Technology (**CMAT**), for all the support that they have given me.

I would like to thank the wonderful, excellent, serious, great, legendary **Team** for all the hard work, support, and cooperation that we have done together, all words are not enough to express the best team. I'm so proud to be part of this team. We weren't just a team; we were a family. I hope that we will continue our partnership and cooperation in the future.

Acknowledgement

My deep and sincere gratitude to **My Family** for their continuous and unparalleled love, help and support. I am forever indebted to **My Parents** for giving me the opportunities and experiences that have made me who I am. They selflessly encouraged me to explore new directions in life and seek my own destiny. This journey would not have been possible if not for them, and I devote this milestone to them.

Last but certainly not least, I must express my deep gratitude to **My Wife** for giving me her infinite support, encouragement, and kindness throughout the PhD Years. She has inspired me to work even harder every day. Nothing would have been possible without her love and compassion.

T. Lemaoui

List of Figures

Abbreviation

AA	Acetic acid
AD	Applicability domain
Ala	Alanine
ANN	Artificial neural networks
ANOVA	Analysis of variance
ARD	Average relative deviation
ATPPB	Allyltriphenylphosphonium bromide
B3LYP	Becke, 3-parameter, Lee-Yang-Parr
Bet	Betaine
BMimBF4	Butyl-3-methylimidazolium tetrafluoroborate
Bor	Borneol
BP86	Becke-Perdew 86
BTPPC	Benzyltriphenylphosphonium chloride
But	Butanediol
CA	Citric acid
Cam	Camphor
ChCl	Choline chloride
COSMO-RS	Conductor like screening model for real solvents
CV	Cross-validation
DA	Decanoic acid
DEA	Diethanolamine
Dec	1-Decanol
DEEAC	N,N-Diethylethanolammonium chloride
def-TZVP	Triple-ζ Valence Polarized
DEG	Diethylene glycol
DESs	Deep eutectic solvents
DFT	Density functional theory
DL-Men	DL-Menthol
DMSO	Dimethyl sulfoxide
DoA	Dodecanoic Acid
DSC	Differential scanning calorimetry
EAC	Ethylammonium chloride
EG	Ethylene glycol
Ethp	Ethylparaben
Fru	D-Fructose
FT-IR	Fourier Transform Infrared Spectroscopy
GC	Gas Chromatography
GGA	Generalized gradient approximation
Glu	D-Glucose
Gly	Glycerol
GlyA	Glycolic acid
Glyi	Glycine
HBA	Hydrogen bond acceptor
HBD	Hydrogen bond donor
HBenA	3-Hydroxy Benzoic Acid
HDESs	Hydrophobic deep eutectic solvents
HexdA	Hexadecanoic acid
Ibp	Ibuprofen
Ils	Ionic Liquids
LacA	Lactic Acid
LevA	Levulinic Acid
Lid	Lidocaine
LLE	Liquid-liquid equilibrium

L-Men	L-Menthol
MA	Malic acid
MalA	Malonic acid
MDEA	Methyl diethanolamine
MEA	Monoethanolamine
MLR	Multiple linear regression
MM	Molecular mechanics
MOAB	Methyltrioctylammonium bromide
MOAC	Methyltrioctylammonium chloride
MP-ol	2-Methyl-2,4-pentanediol
MTPPB	Methyltriphenylphosphonium bromide
MTPPC	Methyltriphenylphosphonium chloride
NADES	Natural deep eutectic solvent
NFM	N-Formylmorpholine
NMP	N-Methyl-2-Pyrrolidone
NoA	Nonanoic Acid
NRTL	Non-random two-liquid model
OA	Oxalic acid
OcA	Octanoic acid
OcdA	Octadecanoic acid
OleA	Oleic acid
Ph	Phenol
Pro	Proline
PyA	Pyruvic acid
QSPR	Quantitative structure-property relationship
RMSD	Root mean square deviation
RMSE	Root mean square error
RTILs	Room temperature ionic liquids
SDR	Standardized residual
Ses	Sesamol
Sob	trans-Sobrerol
SoD	Sodium dodecanoate
Suc	Sucrose
TBAB	Tetrabutylammonium bromide
TBAC	Tetrabuthylammonium chloride
TEA	Triethanolamine
TEAC	Tetraethylammonium chloride
TedA	Tetradecanoic acid
TEG	Triethylene glycol
TetDec	1-Tetradecanol
TFA	2,2,2-Trifluoroacetamide
THAC	Tetraheptylammonium chloride
THF	Tetrahydrofuran
Thy	Thymol
TMAB	Tetramethylammonium bromide
TOAB	Tetraoctylammonium bromide
TOAC	Tetraoctylammonium chloride
TOPO	Trioctyl-phosphine oxide
TPAB	Tetrapropylammonium bromide
Ur	Urea
VFT	Vogel-Fulcher-Tammann
[2-HEAF]	2-Hydroxyethylammonium formate
[4empy][Tf2N]	1-Ethyl-4-methylpyridinium
[Bmim][NO3]	1-Butyl-3-methylimidazolium nitrate
[Bmim][SCN]	1-Butyl-3-methylimidazolium thiocyanate

[Bmim][SCN]	1-Butyl-3-methylimidazolium thiocyanate
[Emim][DCA]	1-Ethyl-3-methylimidazolium dicyanamide
[Emim][MeSO4]	1-Ethyl-3-methylimidazolium methyl sulfate
[Hmim][SCN]	1-Hexyl-3-methylimidazolium thiocyanate
[Omim][NO3]	1-Octyl-3-methylimidazolium nitrate
[Omim][SCN]	1-Octyl-3-methylimidazolium thiocyanate

Nomenclature

β_i	Distribution ratio of component i
γ_i	Activity coefficient of component i
η	Viscosity, mPa·s
ρ	Density, g·cm^{-3}
τ_{ij}	NRTL binary interaction parameter of component i with j
τ_{ji}	NRTL binary interaction parameter of component j with i
σ	Surface charge density, e/Å
$S_{\sigma\text{-}profile}$	Area under the surface charge density distribution, e/Å^2
$P(\sigma)$	σ-profile
$\delta-$	Partial negative charge
$\delta+$	Partial positive charge
α	NRTL non-randomness parameter of the mixture
α_0	Multiple linear regression intercept
α_i	Descriptor i coefficient
α_{i-j}	Interaction coefficient of descriptor i with j
AARD	Absolute-average-relative-deviation
AcO$^-$	Acetate
$AD_{coverage}$	Applicability domain coverage
AIC	Akaike information criterion
AIC_i	Corrected Akaike information criterion
BF$_4$	Tetrafluoroborate
b_k	Intercept bias of hidden neuron k
d^*	Total number of model descriptors
CF$_3$CONH$_2$	Trifluoroacetamide
CoCl$_2$	Cobalt chloride
Cu	Copper
D_i	Descriptor i
$\overline{D_i}$	Mean value of the descriptor i
E_i	Extraction efficiency of component i, %
E_{stage}	Constant single-stage extraction efficiency, %
$E_{targeted}$	Targeted extraction efficiency after n stages, %
F$^-$	Fluoride
F-Ratio	Fisher's statistic
H$_2$S	Hydrogen sulfide
h_i	Leverage value
$\widehat{h}$	Diagonal matrix containing the h_i values of each data point
h^*	Warning leverage value
H_k	Activation function of hidden neuron k
k	Electrical conductivity, mS·cm^{-1}
L	Maximum value of the likelihood function
NC	Total number of components in the HES mixture
NO$_3$	Nitrate
p	Total number of data points in training set
p_{inside}	Total number of points within the AD boundaries

p_{total}	Total number of data points in training and testing
P_{value}	t-test probability value
Q^2_{LMO}	Leave-many-out cross validation coefficient
Q^2_{LOO}	Leave-one-out cross validation coefficient
R^2	Coefficient of determination
$R^2_{adjusted}$	Adjusted coefficient of determination
$R^2_{external}$	External coefficient of determination
$R^2_{scramble}$	y-scrambling coefficient of determination
SO_2	Sulfur dioxide
S_i	Descriptor i
$\bar{S}_\iota$	Mean value of the descriptor i
S_{ij}	Selectivity of component i over component j
T	Temperature, K
T (superscript)	Matrix transpose operator
T_f	Freezing temperature, K
T_m	Melting temperature, K
$t\text{-}_{Ratio}$	t-test ratio
w_i	Weight fraction of component i, $wt\%$
$w_{i,E}$	Weight fraction of component i in the extract phase, $wt\%$
$w_{i,R}$	Weight fraction of component i in the raffinate phase, $wt\%$
$w_{i,intial}$	Initial weight fraction of component i in the feed, $wt\%$
w_{H2O}	Weight fraction of water in the DES, $wt\%$
$w_{k,input}$	Weight coefficient of each input with hidden neuron k
x_i	Mole fraction of component i, $mol\%$
x_j	Mole fraction of component j, mol%
x_{H2O}	Mole fraction of water in the DES, $mol\%$
y	Macroscopic property of the DES
Y_k	Linear combination of the inputs linked to hidden neuron k
Z	$p \times d^*$ matrix containing the data points and the model descriptors
Z^T	Transpose of matrix Z
z_i	Row-vector matrix containing the descriptors of the HES
$z_i{}^T$	Transpose of matrix z_i

Table of Contents

Table of Contents

Chapter III: Physio-chemical Properties of Deep Eutectic Solvents

Chapter IV: Deep Eutectic Solvents as Extraction Solvents

Table of Contents

Appendixes

General Introduction

The use of solvents in many industrial applications is of paramount importance. Large-scale applications include industrial separations in different fields such as pharmaceutical, food, metal refining, biochemical, and wastewater treatment. While the extraction methods have now become a routine procedure in separation technologies, the correct identification of the optimal solvent with adequate properties for a specific application still represents one of the challenges in this research field. The choice of an appropriate solvent is essential for both technical and economic reasons since it represents about 80% of the total volume of chemicals used in a generic process (Anastas & Kirchhoff, 2002). Solvents present many environmental, health, and safety concerns, including human and ecotoxicological problems, process safety hazards, and waste management issues (Gani et al., 2005). Most organic solvents do not fulfill the requirements for their use in green technologies because they have intrinsic toxicity and high volatility (Anastas & Kirchhoff, 2002).

In recent decades, efforts have been made to replace organic solvents with alternative classes of chemical compounds. These approaches include the use of easily recyclable systems, such as fluorinated solvents, the elimination of solvents from the productive cycle (whenever possible), and the use of non-volatile compounds, such as ionic liquids (ILs) and deep eutectic solvents (DESs).

Ionic Liquids (ILs) are most commonly defined in the literature as "salts which are liquid at temperatures below 373.2 K" (freezing point below 373.2 K) (Endres & Zein El Abedin, 2006). Thus, ILs are liquids that consist of exclusively cations and anions. This definition is very brief and the temperature selected does not have any chemical or physical significance, however, this temperature was selected as the temperature that distinguishes ILs from molten salts. It is worth noting that these ILs usually consist of organic cations while molten salts consist of inorganic cations.

The asymmetry of organic cations lowers the lattice energy, disrupting the ion-ion packing, and thus causing a decrease in the freezing point. This is the reason why ILs can have low freezing points as supposed to other ionic compounds such as Na^+Cl^-. ILs that have freezing points below 298.2 K are also called room-temperature ionic liquids (RTILs). ILs are most commonly known for their very low volatility which is a result of the ionic bonds between the charged cations and the anions in the liquid. They are also characterized by their high chemical/thermal stability, and low flammability (Ali et al., 2009). ILs have also been described as "designer solvents" as their properties can be tuned by the combination choice of cation and anion. However, their main disadvantages include the difficulty of their processing, mainly due to their general high viscosity.

Besides, the cost of ILs is high compared to commercially available solvents. This is due to their relatively complicated synthesis and purification (Petkovic et al., 2011). To overcome these disadvantages, Deep eutectic solvents (DESs) have been proposed as a new class of analogs of the ILs. Although they share many characteristics and properties with ILs, they represent different types of solvents and have different chemical nature (Smith et al., 2014).

DESs have emerged as a new generation of sustainable "green" alternatives to classical organic solvents (Francisco et al., 2013; Smith et al., 2014; Zhang et al., 2012). DESs were first reported in the literature in 2003 by Abbott et al.(Abbott et al., 2003), where the mixture of choline chloride and urea at a 1:2 molar ratio was presented. Accordingly, the subject of DESs is considered to be still in its infancy when compared to ILs, which were discovered in 1914.At the time of writing, there are several definitions of DESs available in the literature. The most common definition describes DESs as a mixture of a hydrogen bond acceptor (HBA) and a hydrogen bond donor (HBD) that when mixed interact with each other via hydrogen bonding leading to the formation of a eutectic mixture with a freezing point far below that of its constituents (Abbott et al., 2003; Quijano et al., 2011; Romero et al., 2008).

The research trend of DESs can be seen in Figure 1. Since their discovery, DESs have been used in several applications including separation, electrochemistry, catalysis, biochemistry, and nanotechnology (Paiva et al., 2014; Smith et al., 2014). DESs have similar properties to that of ILs in terms of their low vapor pressure and wide liquid range. However, they can be easily prepared by simply applying heat (no chemical synthesis required), and they are generally cheaper than ILs.
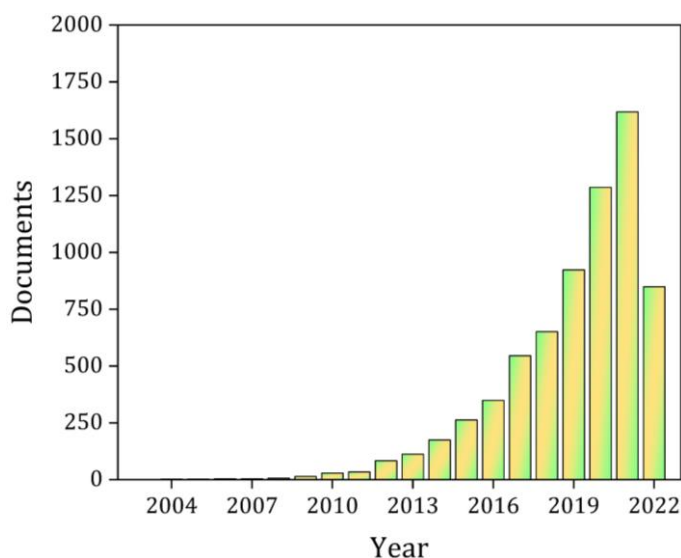
Figure 1. The number of research papers with "DES" in the title was adopted from Scopus.

DESs have also been described as "designer solvents" (Francisco et al., 2013) as their physical properties and solvation properties can easily be altered by changing the HBA, the HBD, or their mixing ratio. Therefore, based on the HBA and HBD selection, it is possible to prepare a low-cost, naturally occurring, and biodegradable solvent with high solvation properties.

There are many potential applications of DESs, for example, they can be used in the electrochemical treatment of metals, as reaction media for various industrial processes, biochemical processes, drug delivery, etc. Since DESs serve as an environmentally friendly alternative to organic solvents, their field of applications can be potentially further enlarged in the next years.

The properties of a DES regarding its biodegradability and biocompatibility are solely dependent on the substances used. Therefore, Naturally-based DESs can be prepared using primary metabolites, namely amino acids, organic acids, sugars, or choline derivatives (Paiva et al., 2014). These DESs perfectly fulfill the principles of green chemistry and engineering. Although there is a large group of DESs with known properties and many of them have been already used in different applications, the mechanism of their formation is not well understood and the prediction of their phase diagrams is difficult since various interactions can simultaneously occur. On the other hand, since the possible combinations of constituents is potentially infinite (in terms of both substances and their relative concentrations), the ability to predict the properties of a given DES would be an invaluable tool for the rapid and inexpensive identification of suitable high performances materials. The best option would be the availability of a calculation tool for testing many possible mixtures and determining their properties before preparing them, based on the knowledge of single constituents' properties. Also, important information about construction principles and intermolecular interactions could be retrieved, which could help in the prediction of their behavior when used in industrial processes.

In the past decade, the application of mathematical models to predict the properties of DESs has been studied in several papers. The first study for predicting the properties of DESs was done by Shahbaz *et al* (Shahbaz et al., 2011). In their research, they applied the group contribution method and the modified Rackett equation to predict the densities of DESs. Lloret *et al* (Lloret et al., 2017) and Zubeir *et al* (Zubeir et al., 2016). Both used molecular-based equations of state to compare two different methods to model DESs: once as a *pseudo*-pure component and another as two individual components. The studies concluded that both methods give very comparable and accurate results (Lloret et al., 2017; Zubeir et al., 2016). However, they also discussed that

modeling of the DES as two individual components is more universally applicable as only one set of interaction parameters "for each species" is required (Lloret et al., 2017; Zubeir et al., 2016).

One of the most widely adopted methods to augment experimental analytical techniques is the use of Computer-assisted quantitative structure-property relations (QSPR) (Coutinho et al., 2012), which have proven to be an accurate, reliable, and cost-effective method for predicting DESs properties (Zhao et al., 2015). The general idea is to derive the physicochemical properties of DESs from a set of molecular descriptors, which can be represented by Physico-chemical properties or theoretical molecular properties of the used chemicals.

The use of QSPR models can also significantly help in the comprehension of the relationships between the microscopic properties of molecular components and the properties of the macroscopic material. Many experimental data of DESs properties formed by a specific HBA and HBD are currently available in the literature. Simultaneously, it is well known that the type of the HBD and HBA and their molar ratio in a DES can drastically affect the properties of the DES. However, since very few methods are currently available for the prediction of DESs properties without the need for an experimental activity, the set-up of a predictive modeling tool is of great interest in the current literature scenario. To achieve a reliable model for DESs properties prediction, the availability of an extensive set of experimental data is necessary, for both model set-up and tuning.

Eckert *et al.* (Eckert & Klamt, 2002) developed a solvent screening method so-called "COnductor like Screening MOdel for Real Solvents" (COSMO-RS) based on quantum chemistry to determine the physiochemical and thermodynamical properties of mixed and pure solvents utilizing molecular surface polarity distributions (σ-profiles) only. The distribution area of these σ-profiles (S_σ-profile), was adopted in the literature as a quantitative description of a molecule's surface (Benguerba et al., 2019; Zhao et al., 2015) using S_σ-profiles as molecular descriptors.

Since their discovery, DESs have been used in many applications such as electrochemistry (Brett, 2018), catalysis (Williamson et al., 2017), material preparation (Tomé et al., 2018), nanotechnology (Abo-Hamad et al., 2015), and analytical chemistry (Makoś et al., 2018). Moreover, the use of DESs as an extraction solvent has been extensively studied for fuel purification processes; desulfurization (Ahmed Rahma et al., 2017), denitrification (Hizaddin et al., 2016), or dearomatization (Naik et al., 2016). DESs have been extensively applied in the separation of aromatics, sulfur-containing, and nitrogen-containing aromatics from *n*-alkanes(Gonzalez et al., 2013; Warrag, Peters, et al., 2017; Warrag, Rodriguez, et al., 2017).

However, most studies investigated the removal of only one impurity (either an aromatic, a sulfur-containing aromatic, or a nitrogen-containing aromatic) from *n*-alkanes. To the best of our knowledge, the application of DESs in simultaneous dearomatization, desulfurization, and denitrogenation of fuels have only been reported in a few research works by Kučan *et al*.(Kučan et al., 2018; Rogošić & Kučan, 2018).

Our research investigates the creation of novel mathematical models for predicting the physicochemical properties of deep eutectic solvents (density, viscosity, electrical conductivity, pH), as well as the extraction of fuel impurities utilizing deep eutectic solvents. This study is split into four chapters detailed as follows:

Chapter I: Provides general information on deep eutectic solvents.

Chapter II: Consists of bibliographical reminder on quantitative structure-property relationships (QSPRs), molecular modeling, conductor-like screening model for real solvent (COSMO-RS), and calculation rules for the liquid-liquid extraction method.

Chapter III: New mathematical models have been developed to predict the physicochemical properties of deep eutectic solvents using the QSPR methodology.

Chapter IV: Insights were provided about the performance of deep eutectic solvents in a process that mimics the multicomponent dearomatization, desulfurization, and denitrogenation used industrially. Furthermore, DESs were applied in simultaneous extraction of toluene, thiophene, pyridine, and pyrrole from n-decane.

References

Abbott, A. P., Capper, G., Davies, D. L., Rasheed, R. K., & Tambyrajah, V. (2003). Novel solvent properties of choline chloride/urea mixtures. *Chemical Communications*, *1*, 70–71. https://doi.org/10.1039/b210714g

Abo-Hamad, A., Hayyan, M., AlSaadi, M. A. H., & Hashim, M. A. (2015). Potential applications of deep eutectic solvents in nanotechnology. *Chemical Engineering Journal*, *273*, 551–567. https://doi.org/10.1016/j.cej.2015.03.091

Ahmed Rahma, W. S., Mjalli, F. S., Al-Wahaibi, T., & Al-Hashmi, A. A. (2017). Polymeric-based deep eutectic solvents for effective extractive desulfurization of liquid fuel at ambient conditions. *Chemical Engineering Research and Design*, *120*, 271–283. https://doi.org/10.1016/j.cherd.2017.02.025

Ali, S. H., Hamad, D. M., Albusairi, B. H., & Fahim, M. A. (2009). Removal of dibenzothiophenes from fuels by oxy-desulfurization. *Energy and Fuels*, *23*(12), 5986–5994. https://doi.org/10.1021/ef900683d

Anastas, P. T., & Kirchhoff, M. M. (2002). Origins, current status, and future challenges of green chemistry. *Accounts of Chemical Research*, *35*(9), 686–694. https://doi.org/10.1021/ar010065m

Benguerba, Y., Alnashef, I. M., Erto, A., Balsamo, M., & Ernst, B. (2019). A quantitative prediction of the viscosity of amine based DESs using Sσ-profile molecular descriptors. *Journal of Molecular Structure*, *1184*(February), 357–363. https://doi.org/10.1016/j.molstruc.2019.02.052

Brett, C. M. A. (2018). Deep eutectic solvents and applications in electrochemical sensing. *Current Opinion in Electrochemistry*, *10*, 143–148. https://doi.org/10.1016/j.coelec.2018.05.016

Coutinho, J. A. P., Carvalho, P. J., & Oliveira, N. M. C. (2012). Predictive methods for the estimation of thermophysical properties of ionic liquids. *RSC Advances*, *2*(19), 7322–7346. https://doi.org/10.1039/c2ra20141k

Eckert, F., & Klamt, A. (2002). Fast Solvent Screening via Quantum Chemistry: COSMO-RS Approach. *AIChE Journal*, *48*(2), 369–385. https://doi.org/10.1002/aic.690480220

Endres, F., & Zein El Abedin, S. (2006). Air and water stable ionic liquids in physical chemistry. *Physical Chemistry Chemical Physics*, *8*(18), 2101–2116. https://doi.org/10.1039/b600519p

Francisco, M., Van Den Bruinhorst, A., & Kroon, M. C. (2013). Low-transition-temperature mixtures (LTTMs): A new generation of designer solvents. *Angewandte Chemie - International Edition*, *52*(11), 3074–3085. https://doi.org/10.1002/anie.201207548

Gani, R., Jiménez-González, C., & Constable, D. J. C. (2005). Method for selection of solvents for promotion of organic reactions. *Computers and Chemical Engineering*, *29*(7), 1661–1676. https://doi.org/10.1016/j.compchemeng.2005.02.021

Gonzalez, A. S. B., Francisco, M., Jimeno, G., De Dios, S. L. G., & Kroon, M. C. (2013). Liquid-liquid equilibrium data for the systems {LTTM+benzene+hexane} and {LTTM+ethyl acetate+hexane} at different temperatures and atmospheric pressure. *Fluid Phase Equilibria*, *360*, 54–62. https://doi.org/10.1016/j.fluid.2013.09.010

Hizaddin, H. F., Hadj-Kali, M. K., Ramalingam, A., & Ali Hashim, M. (2016). Extractive denitrogenation of diesel fuel using ammonium- and phosphonium-based deep eutectic solvents. *Journal of Chemical Thermodynamics*, *95*, 164–173.

https://doi.org/10.1016/j.jct.2015.12.009Kučan, K. Z., Perković, M., Cmrk, K., Načinović, D., & Rogošić, M. (2018). Betaine + (Glycerol or Ethylene Glycol or Propylene Glycol) Deep Eutectic Solvents for Extractive Purification of Gasoline. *ChemistrySelect*, *3*(44), 12582–12590. https://doi.org/10.1002/slct.201803251

Lloret, J. O., Vega, L. F., & Llovell, F. (2017). Accurate description of thermophysical properties of Tetraalkylammonium Chloride Deep Eutectic Solvents with the soft-SAFT equation of state. *Fluid Phase Equilibria*, *448*, 81–93. https://doi.org/10.1016/j.fluid.2017.04.013

Makoś, P., Przyjazny, A., & Boczkaj, G. (2018). Hydrophobic deep eutectic solvents as "green" extraction media for polycyclic aromatic hydrocarbons in aqueous samples. *Journal of Chromatography A*, *1570*, 28–37. https://doi.org/10.1016/j.chroma.2018.07.070

Naik, P. K., Dehury, P., Paul, S., & Banerjee, T. (2016). Evaluation of Deep Eutectic Solvent for the selective extraction of toluene and quinoline at T = 308.15 K and p = 1 bar. *Fluid Phase Equilibria*, *423*, 146–155. https://doi.org/10.1016/j.fluid.2016.04.018

Paiva, A., Craveiro, R., Aroso, I., Martins, M., Reis, R. L., & Duarte, A. R. C. (2014). Natural deep eutectic solvents - Solvents for the 21st century. *ACS Sustainable Chemistry and Engineering*, *2*(5), 1063–1071. https://doi.org/10.1021/sc500096j

Petkovic, M., Seddon, K. R., Rebelo, L. P. N., & Pereira, C. S. (2011). Ionic liquids: A pathway to environmental acceptability. *Chemical Society Reviews*, *40*(3), 1383–1403. https://doi.org/10.1039/c004968a

Quijano, G., Couvert, A., Amrane, A., Darracq, G., Couriol, C., Le Cloirec, P., Paquin, L., & Carrié, D. (2011). Toxicity and biodegradability of ionic liquids: New perspectives towards whole-cell biotechnological applications. *Chemical Engineering Journal*, *174*(1), 27–32. https://doi.org/10.1016/j.cej.2011.07.055

Rogošić, M., & Kučan, K. Z. (2018). Deep eutectic solvents based on choline chloride and ethylene glycol as media for extractive denitrification/desulfurization/dearomatization of motor fuels. *Journal of Industrial and Engineering Chemistry*, *72*, 87–99.

Romero, A., Santos, A., Tojo, J., & Rodríguez, A. (2008). Toxicity and biodegradability of imidazolium ionic liquids. *Journal of Hazardous Materials*, *151*(1), 268–273. https://doi.org/10.1016/j.jhazmat.2007.10.079

Shahbaz, K., Mjalli, F. S., Hashim, M. A., & Alnashef, I. M. (2011). Prediction of deep eutectic solvents densities at different temperatures. *Thermochimica Acta*, *515*(1–2), 67–72. https://doi.org/10.1016/j.tca.2010.12.022

Smith, E. L., Abbott, A. P., & Ryder, K. S. (2014). Deep Eutectic Solvents (DESs) and Their Applications. *Chemical Reviews*, *114*(21), 11060–11082. https://doi.org/10.1021/cr300162p

Tomé, L. I. N., Baião, V., da Silva, W., & Brett, C. M. A. (2018). Deep eutectic solvents for the production and application of new materials. *Applied Materials Today*, *10*, 30–50. https://doi.org/10.1016/j.apmt.2017.11.005

Warrag, S. E. E., Peters, C. J., & Kroon, M. C. (2017). Deep eutectic solvents for highly efficient separations in oil and gas industries. *Current Opinion in Green and Sustainable Chemistry*, *5*, 55–60. https://doi.org/10.1016/j.cogsc.2017.03.013

Warrag, S. E. E., Rodriguez, N. R., Nashef, I. M., Van Sint Annaland, M., Siepmann, J. I., Kroon, M. C., & Peters, C. J. (2017). Separation of Thiophene from Aliphatic Hydrocarbons

UsingTetrahexylammonium-Based Deep Eutectic Solvents as Extracting Agents. *Journal of Chemical and Engineering Data*, *62*(9), 2911–2919. https://doi.org/10.1021/acs.jced.7b00168

Williamson, S. T., Shahbaz, K., Mjalli, F. S., AlNashef, I. M., & Farid, M. M. (2017). Application of deep eutectic solvents as catalysts for the esterification of oleic acid with glycerol. *Renewable Energy*, *114*, 480–488. https://doi.org/10.1016/j.renene.2017.07.046

Zhang, Q., De Oliveira Vigier, K., Royer, S., & Jérôme, F. (2012). Deep eutectic solvents: Syntheses, properties and applications. *Chemical Society Reviews*, *41*(21), 7108–7146. https://doi.org/10.1039/c2cs35178a

Zhao, Y., Huang, Y., Zhang, X., & Zhang, S. (2015). A quantitative prediction of the viscosity of ionic liquids using Sσ-profile molecular descriptors. *Physical Chemistry Chemical Physics*, *17*(5), 3761–3767. https://doi.org/10.1039/c4cp04712e

Zubeir, L. F., Held, C., Sadowski, G., & Kroon, M. C. (2016). PC-SAFT Modeling of CO2 Solubilities in Deep Eutectic Solvents. *Journal of Physical Chemistry B*, *120*(9), 2300–2310. https://doi.org/10.1021/acs.jpcb.5b07888

Chapter I

Deep Eutectic Solvents

I.1. Introduction

In the broad sense, a solvent is a substance that dissolves a solute, resulting in a solution. A solvent is usually a liquid but can also be a solid, a gas, or a supercritical fluid. Solvents are therefore of considerable importance in most industries. They can be used as cleaning agents, diluents in paint, packaging supports in the cosmetic sector, or even reaction media in chemical synthesis, where their role can be essential. Solvents are currently classified based on the type of chemical bonds that they interact with. Molecular solvents are the most commonly used solvents (example: organic solvents). They are essentially composed of a single neutral type with only covalent bonds. More recently, new solvents dominated by ionic interactions have been developed. These solvents are known as ionic liquids (ILs), and they result from the combination of two charged molecules (cation/anion) organic and/or inorganic, and they correspond to liquid salts that differ from all salts by having a freezing point below 100 °C.

Finally, in the early 2000s, Prof. A.P. Abbott's group at the University of Leicester in England was interested in synthesizing, characterizing, and developing a new type of solvent called deep eutectic solvents (DESs). These liquids are made by combining a neutral molecule (a positively charged organic salt, and a negatively charged counter ion) with a hydrogen bond donor.

I.2. Fundamentals of Deep Eutectic Solvents

I.2.1. Definition

DESs are made by mixing two or more compounds in an exact proportion that equals the eutectic point (Smith et al., 2014). The majority of these solvents are liquid at room temperature, making them easier to use. A mixture of choline chloride (ChCl) and urea (Ur) in the molar ratio of 1: 2 has been observed as one of the most important eutectic phenomena. At room temperature, this mixture has a eutectic freezing point of 12 °C (much lower than the freezing point of ChCl and Ur of 302 °C and 133 °C, respectively) (Abbott et al., 2003).

The most common definition describes DESs as a mixture of a hydrogen bond acceptor (HBA) and a hydrogen bond donor (HBD) that when mixed interact with each other via hydrogen bonding leading to the formation of a eutectic mixture with a freezing point far below that of its constituents. As with any new field, the definition of DESs should still be improved as it is still not very clear which mixtures can be considered a DES or not.
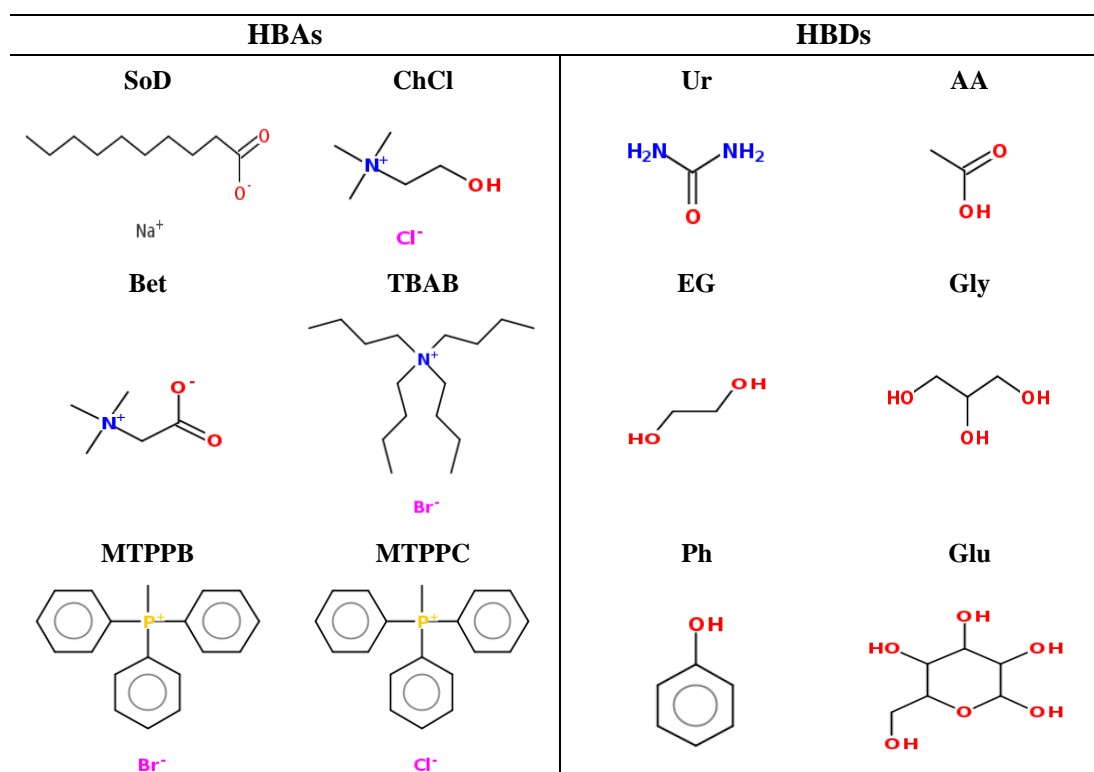
Figure I.1. Typical structure of some HBAs and HBDs.

I.2.2. Types of Deep Eutectic Solvents

The first generation of DESs was based on mixtures of quaternary ammonium salts with hydrogen bond donors such as amines and carboxylic acids. In general, three types of DESs are defined (Abbott et al., 2007).

- Type I: Metal salt + organic salt (e.g. $ZnCl_2$ + choline chloride).
- Type II: Metal salt hydrate + organic salt (e.g. $CoCl_2 \cdot 6H_2O$ + choline chloride).
- Type III: Hydrogen bond donor + organic salt (e.g. urea + choline chloride).

I.2.3. Naturel Deep Eutectic Solvents

Natural deep eutectic solvents (NADESs), this term was very recently introduced by Choi et al (Choi et al., 2011) to describe all of the eutectic mixtures obtained by combining molecules abundantly present in the active world. According to these authors, these mixtures are composed of two or more compounds that are generally plant-based primary metabolites, i.e. organic acids, sugars, alcohols, amines, and amino acids. Examples of different NADES have been shown in the table below (Table I.1).

Table I.1. Composition and molar ratio of some NADES.

Composition of NADES	Molar ratio
Choline Chloride: Aconitic Acid	1:1
Malic Acid: Glucose	1:1
Malic Acid: Fructose	1:1
Malic Acid: Sucrose	1:1
Citric Acid: Sucrose	1:1

I.2.4. Synthesis of Deep Eutectic Solvents

The synthesis of DESs is easy and clean compared to that of ionic liquids which need several stages of chemical synthesis and purification. It is simply a well-proportioned mixture of the products that make up the DES, heated until a homogeneous and transparent liquid is obtained. These components are a mixture of HBA and HBD. The composition of the DES can be identified by differential scanning calorimetry (DSC), this method measures the variations in heat exchange between a sample to be analyzed and a reference, which makes it possible to determine phase transitions, or by simply observing the freezing point of mixtures with different molar compositions (Andrew P. Abbott, Capper, Davies, et al., 2006). This technique makes it possible to create a phase diagram linking the freezing point of the medium to its composition (Figure I.2).

As aforementioned, the first DES to be reported was the mixture of choline chloride and urea. The solid-liquid phase diagram of the mixture is shown in Figure I.2. As it can be observed, the freezing point of pure choline chloride (at 0 mol% urea) is 302°C and the freezing point of pure urea (at 100 mol% urea) is 133°C. The mixture between choline chloride and urea at a 1:2 molar ratio (at 66.7 mol% urea) has a eutectic freezing point of only 12°C. This finding implies that two solids at room temperature can be mixed to form a new solvent with unique properties.
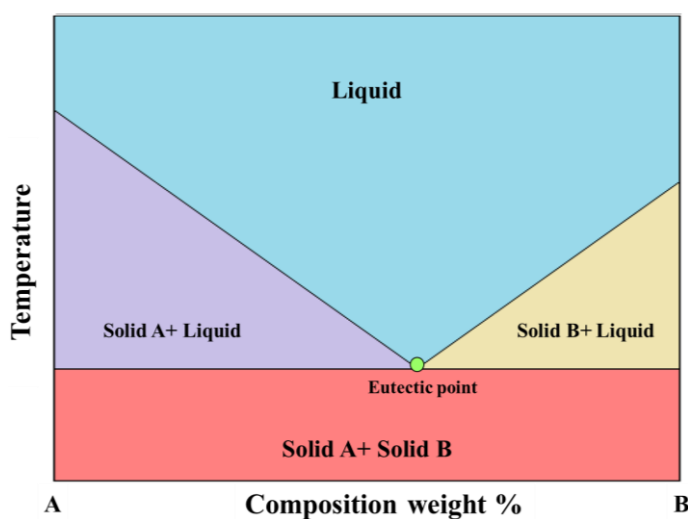
Figure I.2. Solid-Liquid phase diagram of a DES.

I.2.5. Hydrophilic and hydrophobic Deep Eutectic Solvents

DESs may be divided into two categories (hydrophilic and hydrophobic DESs) based on their water solubility. Most hydrophilic DESs are used in many fields, including, separation (extraction) (Wang et al., 2016), electrochemical devices (Andrew P. Abbott et al., 2012), pharmaceuticals (Morrison et al., 2009). Compared to hydrophilic DESs, there are fewer hydrophobic DESs and they are less widely used. Figure I.3 shows some applications of hydrophilic and hydrophobic DESs.
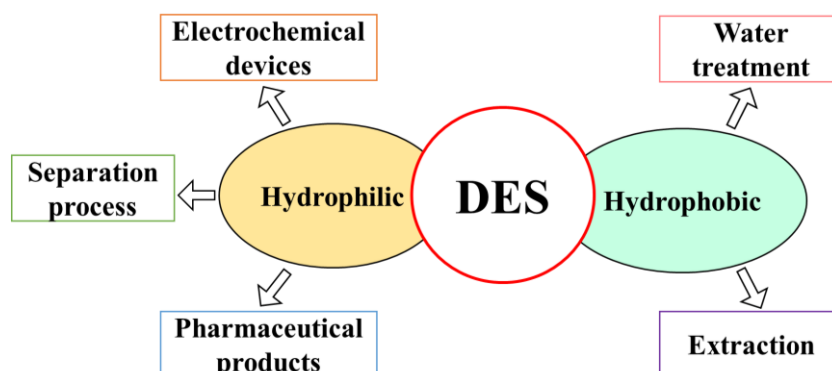
Figure I.3. Applications of hydrophilic and hydrophobic DESs.

I.3. Properties of Deep Eutectic Solvents

I.3.1. Freezing Point

DESs are characterized by relatively low freezing points. As mentioned previously, this new liquid phase is obtained by mixing two compounds, the freezing point is much lower than those of the compounds taken separately. For example, the mixture between choline chloride ($T_m = 302$ °C) and urea ($T_m = 133$ °C) at a 1:2 molar ratio (at 66.7 mol% urea) has a eutectic freezing point of only 12ºC.

At the time of the finding, Abbott et al (Zhang et al., 2012) proposed that the considerable drop in freezing point was caused by the interaction between the HBD molecule and the anionic species given by the salt. According to these authors, HBD works as a complexing agent for anionic species, allowing them to grow in size while reducing interactions with the cation. As a result, the freezing point decreases. The strength of the hydrogen bonds can be correlated with the phase transition temperature and the stability of the mixture. In general, the greater the ability to donor / or accept hydrogen bonds of the constituents, the freezing point will be decreased. In addition, the symmetry and radius of the cation, also the electronegativity of the anion will influence this phase transition. As already mentioned, the eutectic corresponds to the single and lowest freezing point of the phase diagram of the mixture.

Therefore, a variation in the molar ratio of HBA or HBD will have a significant impact on the freezing point of the DES. Thus, in the above example, when ChCl is mixed with urea at a molar ratio of 1: 1 or 1: 2 (eutectic), the temperature of the mixture decreases considerably from more than 50 °C to 12 °C (Andrew P. Abbott et al., 2003). Even if there is no clear relationship between the nature of the constituents utilized and the freezing point of a mixture, the phase transition will be mostly a function of:

➢ The structure of the hydrogen bond donor (volume, nature, and number of potential hydrogen bonds) (Table I.2). For example, the DES formed from (ChCl) and different HBD, even if the molar ratios to the mixture remain the same, the freezing point can vary from -66 °C to 149 °C (Andrew P. Abbott, Cullis, et al., 2007; Maugeri & Domínguez De María, 2012).

Table I.2. Freezing point based on choline chloride and various HBDs.

Cationic salt	Anion	Hydrogen bond donor	Molar ratio	Freezing point (°C)
Choline (Ch)	Cl^-	Ethylene glycol	1:2	-66
Choline (Ch)	Cl^-	Glycerol	1:2	-40
Choline (Ch)	Cl^-	Urea	1:2	12
Choline (Ch)	Cl^-	Levulinic Acid	1:2	RT
Choline (Ch)	Cl^-	Vanillin	1:2	17
Choline (Ch)	Cl^-	Acetamide	1:2	51
Choline (Ch)	Cl^-	1,1-Dimethylurea	1:2	149

➢ The structure of the cationic salt (Table I.3), the mixture of urea with different cationic salts (molar ratio of 1:2) containing the same chloride anion, resulted in DESs with drastically varying freezing points (- 38 °C to 26 °C) (Andrew P. Abbott et al., 2003).

Table I.3. Freezing point based on urea and different cationic salts (Maugeri & Domínguez De María, 2012).

Cationic salt	Anion	Hydrogen bond donor	Molar ratio	Freezing point (°C)
Monoethylcholine	Cl^-	Urea	1:2	-38
Acetylcholine	Cl^-	Urea	1:2	-14
Trimethyl ammonium	Cl^-	Urea	1:2	15
Benzyltrimethyl ammonium	Cl^-	Urea	1:2	26

➢ The nature (electronegativity and polarizability) of the anion (Table I.4), For example, varying the nature of the anion, the choline salt mixed with urea (molar ratio salt: urea of 1: 2) the freezing point of the DES decreases according to the order $F^- > NO_3^- > Cl^- > AcO^- > BF_4^-$, This implies a relationship between hydrogen bond strength and freezing point (Andrew P. Abbott et al., 2003).

Table I.4. Freezing point based on choline and urea with different anions.

Cationic salt	Anion	Hydrogen bond donor	Molar ratio	Freezing point (°C)
Choline (Ch)	F^-	Urea	1:2	1
Choline (Ch)	NO_3^-	Urea	1:2	4
Choline (Ch)	Cl^-	Urea	1:2	12
Choline (Ch)	AcO^-	Urea	1:2	18
Choline (Ch)	BF_4^-	Urea	1:2	67

I.3.2. Viscosity, Surface tension, Conductivity and Density

The fluidity of the mixture can easily be adjusted according to the nature of the cationic salt, HBD, structure of the components, molar ratio, water content, or even the temperature. However, the viscosity (Table I.5) and the surface tension of DESs are considerably higher than most conventional solvents, nevertheless comparable to those of ionic liquids (Andrew P. Abbott et al., 2011; Kareem et al., 2010).

Table I.5. Composition and viscosity of different DESs.

Cationic salt	Anion	Hydrogen bond donor	Molar ratio	Viscosity (cP)
Choline (Ch)	Cl^-	Urea	1:2	750(25˚C)
Choline (Ch)	Cl^-	Ethylene glycol	1:2	36(20˚C)
Choline (Ch)	Cl^-	Glycerol	1:2	376(20˚C)
Choline (Ch)	Br^-	Imidazole	3:7	810(20˚C)
Choline (Ch)	AcO^-	Glycerol	1:1.5	93(50˚C)

The fluidity of the mixture is ruled by the large network of hydrogen bonds established between each constituent, also by Van der Waals or electrostatic interactions. However, the nature of the HBD is undoubtedly the most influential parameter on the viscosity. DESs derived from dicarboxylic acids or sugars have significantly higher viscosities than all other DESs, which could partly be explained by a much more robust three-dimensional network of intermolecular hydrogen bonds.

Importantly, adding an HBA (ChCl) to an HBD (EG or But) increases the viscosity of the mixture. On the other hand, in DESs derived from glycerol, the opposite phenomenon occurs with a decrease in viscosity by adding ChCl (Choi et al., 2011). This observation confirms the influence of hydrogen bonding.

Conductivity can be increased by lowering the surface tension using small volume particles. Consequently, the use of small quaternary ammonium cations or fluorine-type hydrogen bond donors will make it possible to obtain DESs with low viscosities (Andrew P. Abbott, Capper, & Gray, 2006). In addition, the viscosity of DESs decreases significantly when the temperature increases and is inversely proportional to the conductivity (Andrew P. Abbott et al., 2004). There

is a strong correlation between conductivity and viscosity. DESs show poor conductivity (lower than 2 mS cm-1 at room temperature) due to their high viscosity.

DESs generally have a higher density than water. They are similar to those of ILs ranging from 1.1 g.cm^{-3} to 2.4 g.cm^{-3} (Wasserscheid & Welton, 2003). The mixture of organic salt and HBDs affects the density. A DES with a lower density than pure HBD be explained by an increase in free volume, as shown in the eutectic mixture ChCl: Gly. Conversely, a DES with a density greater than pure HBD will be attributable to a decrease in unoccupied areas. Table I.6 below gives the values of the conductivity and the density of certain DESs.

Table I.6. Conductivity and density of several DESs.

Cationic Salt	Anion	Hydrogen Bond Donor	Molar Ratio	Conductivity (mS.cm^{-1})	Density (g.cm^{-3})
Choline (Ch)	Cl$^-$	Urea	1:2	0.199(40˚C)	1.24(40˚C)
Choline (Ch)	Cl$^-$	Ethylene glycol	1:2	1.13(25˚C)	1.13(25˚C)
Choline (Ch)	Cl$^-$	Glycerol	1:2	1.19(25˚C)	1.19 (25˚C)
Ethyl ammonium	Cl$^-$	2,2,2-Trifluoroacetamide	1:1,5	1.273(40˚C)	1.273(40˚C)
Ethyl ammonium	Cl$^-$	Acetamide	1:1.5	1.041(40˚C)	1.041(40˚C)
Ethyl ammonium	Cl$^-$	Urea	1:1.5	1.14(40˚C)	1.14(40˚C)
Diethylenethanol ammonium	Cl$^-$	Glycerol	1:4	1.22(40˚C)	1.22(40˚C)
Diethylenethanol ammonium	Cl$^-$	Ethylene glycol	1:3	1.12(25˚C)	1.12(25˚C)
Diethylenethanol ammonium	Cl$^-$	2,2,2-Trifluoroacetamide	1:2	1.346(25˚C)	1.346(25˚C)
Methyltriphenyl phosphonium	Br$^-$	Glycerol	1:3	1.30(25˚C)	1.30(25˚C)
Methyltriphenyl phosphonium	Br$^-$	Ethylene glycol	1:4	1.25(25˚C)	1.25(25˚C)
Methyltriphenyl phosphonium	Br$^-$	Triethylene glycol	1:5.25	1.19(25˚C)	1.19(25˚C)

I.3.3. Acidity and Alkalinity

Regarding the pH value, the measurement in such systems is very complex due to the very low chemical activity of hydrogen ions. Indeed, in non-aqueous or very weakly hydrated DESs (<5% by mass) it becomes very difficult to measure the state of the mixture by a traditional method using a pH meter.

Nevertheless, various methods developed by Hammett in 1932, based on a spectrophotometric of the ionization state of an indicator, make it possible to provide reliable indications on the acidity or the basicity of a non-aqueous system. Thus, the measurement of pH in DES discovered that the nature of the hydrogen bond donor conditioned the state of acidity or basicity of the corresponding medium, with a very small influence on the temperature.

Some DESs have basic pH, as in the case of ChCl: Ur with a value of 10.86 (W. Li et al., 2008), or neutral as observed in MTPPB: Gly and in most DESs of the ChCl: sugars (Maugeri & Domínguez De María, 2012), or even acidic (pH MTPPB: $CF_3CONH_2 \approx 3$) (Kareem et al., 2010). In addition, a very small amount of water (1-3%) in a DES type (ChCl: Ur) has very little impact on pH values (10.77-10.65). On the other hand, in this same solvent, the dissolution of a small amount of CO_2 can reduce the pH from 10.86 to 6.25.

I.3.4. Thermal stability and Polarity

Thermogravimetric analyzes of DES have revealed very high thermal stability of these solvents with high decomposition temperatures, especially above 200 °C (Zhao et al., 2011).

The polarity of these solvents could be measured by the free transfer energies calculation determined empirically by Reichardt. This method is based on the development of a reference dye's absorption maximum, which represents the influence of the solvent on the energy difference between ground and excited state molecules. The polarity values for the DESs in (Table I.7) were calculated using Reichardt's Dye 30. The very strong polarity of DESs compared with other solvents can be explained by the large network of hydrogen bonds responsible for the formation of these mixtures (Gorke et al., 2008).

Table I.7. Polarity of several DESs obtained using Reichardt's Dye 30 concept.

Salt	Hydrogen Bond Donor	Molar ratio	Polarity
Choline chloride	Acetamide	1:2	0.77
Choline chloride	Ethylene glycol	1:2	0.80
Choline chloride	Glycerol	1:2	0.84
Choline chloride	Urea	1:2	0.84
Ethylammonium chloride	Acetamide	1:1.5	0.85
Ethylammonium chloride	Ethylene glycol	1:1.5	0.88
Ethylammonium chloride	Glycerol	1:4	0.93
Solvent			
Water	-	-	1.00
Trimethylsilane	-	-	0.00
Methanol	-	-	0.76

I.3.5. Toxicity, Biodegradability

The toxicity and biodegradability of this type of solvent will depend almost exclusively on the elements that compose it (cationic salt, anion and, HBD). Thus, choline chloride (ChCl) whose biodegradability (more than 93% degradation in 14 days) and non-toxicity (food additive) are verified, when mixed with HBD of very low toxicity (glycerol, urea, etc.) will give a durable and

biocompatible DES. This has been confirmed by toxicity studies on bacteria (gram + and -) which have revealed no toxic effect from these mixtures (Hayyan et al., 2013).

I.4. Solvation Properties of Deep Eutectic solvents

I.4.1. Miscibility of Deep Eutectic Solvents with Organic Solvents

DESs exhibit unusual solvation properties which are strongly influenced by intermolecular hydrogen bonds, resulting in a very high affinity for all compounds capable of donating electrons or protons.

As a result, solvents capable of forming hydrogen bonds, such as methanol or ethanol, will tend to be miscible with DESs.Consequently, these compounds can be utilized as analytical solvents to homogenize the reaction medium at the end of the procedure. In contrast, non-polar solvents such as hexane or toluene are entirely immiscible with DESs because they are unable to form this type of bond.

The same is for conventional polar solvents such as acetone, acetonitrile, or THF, which, although being hydrophilic and HBAs will have very low miscibility with these media. These solvents can then be used to perform biphasic systems or for the extraction of molecules.

I.4.2. Miscibility of Deep Eutectic Solvents with Water

These solvation properties and this very particular affinity for portal polar substances make almost all DESs very hygroscopic. This is why precautions must be taken to minimize the absorption of water by these solvents. For example, a DES formed from choline chloride and levulinic acid is capable of absorbing more than 8% mass of water from ambient humidity in one hour (Maugeri & Domínguez De María, 2012). However, this characteristic can make these solvents an inexpensive and biodegradable material as a moisture absorber.

The affinity of this type of solvent with water has been highlighted in numerous experiments based on the physical and thermodynamic properties (Leron & Li, 2012; Wu et al., 2012). These studies revealed an increase in interactions within the binary mixture (DES-water) compared to those obtained in the pure eutectic mixture, which confirms the increase in the number of hydrogen bonds. Furthermore, according to the results of Gutierrez et al. (Gutiérrez et al., 2009), a large amount of water must be added to a DES to lose the supramolecular complex between the anion of the salt and the HBD in this mixture, and to obtain an equivalent system to a simple dilution of the components in water. From these experiments, the maximum "authorized" mass water content in a eutectic mixture ChCl: Ur is near to 50% so as not to cause the rupture between the urea and the halide. It should be noted that DES derived from fluorinated hydrogen bond donors will have

very different water solvation properties (Andrew P. Abbott, Capper, & Gray, 2006). Indeed, a eutectic mixture obtained by combining of choline chloride with trifluoroacetamide (ChCl: CF_3CONH_2) in a molar ratio of 1 to 2, will be completely immiscible with water.

I.5. Applications of Deep Eutectic Solvents

I.5.1. In Separation Processes

The DESs can be used for many applications, including dissolving, solubilizing, and extracting molecules.

I.5.1.1. Dissolution of Gas (CO_2 and SO_2)

Dissolving gases in DESs could allow these solvents to be used in many processes as well as separation, purification, catalysis, and gas fixation. Preliminary studies on the solubilization of gases such as CO_2 or SO_2 in this type of solvent have been carried out, with particularly promising results. Thus, Li et al. (X. Li et al., 2008) have determined the solubility of CO_2 in a ChCl: U mixture at different temperatures, pressures, and molar ratios. The results showed that the solubility of CO_2 in this solvent increased with pressure but reduced with increasing temperature. In addition, the molar ratio had considerable importance on the solubilization of the gas, thus, a 1: 2 ratio (corresponding to the eutectic) allowed a greater efficiency of solubilization than those at 1: 1.5 or 1: 2.5. More recently, Su et al. (Su et al., 2009) studied the solubility of CO_2 in this same solvent in a binary mixture with water at different temperatures and constant pressure. The results revealed a decrease in the solubility of the gas in ChCl: Ur (ratio 1: 2) when the water content in the solvent increased. Even more interesting in this same study, the calculation of the enthalpy of CO_2 adsorption discovered that the adsorption phenomenon was endothermic when the DES/water ratio was greater than 0.231 and exothermic when it was lower.

In 2013, Liu et al. (Liu et al., 2013) measured the absorption of SO2 in five DES derived from caprolactam and various HBD (acetamide, imidazole, furoic acid, benzoic acid, and toluic acid). The results showed that increasing the temperature had a negative influence on the solubility of the gas in DESs. Furthermore, DESs produced from amino-type hydrogen bond donors demonstrated higher SO_2 absorption efficiency than DESs derived from organic acids. The DES caprolactam: acetamide showed the best SO_2 solubility values, with higher absorption capacities than in the ionic liquid $BMimBF_4$, but weaker than in DMSO.

I.5.1.2. *Solubilization of Active Ingredient, Metal Oxide and Other Molecules*

Numerous studies aimed at determining the solubilization of various molecules in DESs have been undertaken. Thus, Abbott et al found that it was possible to dissolve in ChCl: U a wide range of compounds such as inorganic salts (e.g. LiCl or AgCl) (Andrew P. Abbott et al., 2003), aromatic compounds (benzoic acid), or acids amines (D-alanine). In 2003, Abbott was the first to test the potential of a DES (ChCl: U) for the dissolution of copper oxide. Shortly after, this same author studied the solubility of three metal oxides (ZnO, CuO, and Fe_3O_4) in various DESs synthesized by ChCl with different carboxylic acids. The results revealed significant changes in the solubility of these metals depending on the nature of the HBD, highlighting the significant differences in solubility between solvents based on the nature of one of their components. Other investigations have succeeded in quantifying metal oxide dissolution in DESs, and quantum chemistry simulations have even been performed to calculate the binding energy involved in the connection of metallic elements with DES constituents (Rimsza & Corrales, 2012). Furthermore, the solubility of organic molecules in DESs has been tested, even though such research has been extremely rare too far. Morisson et al. (Morrison et al., 2009) investigated the solubilization of several active components (griseofulvin, danazol) in two DESs (ChCl: Ur and ChCl: MalA), either alone or in a binary mixture with water. These active compounds were found to be 5 to 22000 times more soluble in DESs than in pure water. For example, the solubility of danazol in water is <0. 0005mg.ml^{-1} while it is respectively 0.048 mg.ml^{-1} and 0.160 mg.ml^{-1} in ChCl:Ur and ChCl:MalA.

I.5.1.3. *Molecule Extraction*

To date, the extent of research dealing with the effectiveness of eutectic mixtures as solvents in procedures for extracting or separating molecules remains relatively small. In particular, it would be very interesting to use the adaptability of these solvents, their heat resistance, and their low saturation vapor pressure for the liquid-solid or liquid-liquid extraction of molecules of interest. For example, were tested for their ability to extract polyphenols from the leaf of Chamaecyparis obtusa (Co) (Bi et al., 2013). They tested different molar ratios of DES synthesized from ChCl and seven HBDs with an alcohol function. The parameters (temperature, content of water, solid/liquid ratio) were optimized by the response surface method (RSM) and the results were compared with different extraction methods (ultrasound, mechanical agitation). The best extraction conditions were obtained at 70 °C in the presence of 30% water in ChCl:1,4-Butanediol with a 1:5 ratio. These results have been compared (quantity of polyphenols extracted and cost of the process) with other extraction methods using organic solvents. In addition to the essential

results on improving the extraction of these polyphenols, this process allows a significant reduction in the cost of the processes.

In the same vein, we might mention the separation of phenol from vegetable oil using ammonium salts (TMAB, TEAC, TBAC) (Guo et al., 2013). In contrast to traditional methods of extracting phenolic compounds from oils, this method involves the formation of eutectic mixtures with ammonium salts and avoids the use of bases and acids. The results showed that quaternary ammonium salts, composed of symmetrical cations with suitable chain lengths and a highly electronegative anion, were the most efficient. Thus, the maximum extraction (99.9%) was reached with TEAC, for a TEAC: Ph in the mole ratio of 0.8: 1.

I.5.2. In Electrochemical Processes

Electrochemistry includes a wide range of applications that investigate the link between chemical transformations and the passage of electric current. Electroplating is one of them. It is a process that allows the production of solid materials by electrochemical reactions in a liquid phase (electrolyte). To put it simply, the cation form contained in an electrolyte is reduced to the cathode and deposited as metal. The electrolyte must be chemically inert and resistant to electrochemical reductions and oxidations. In other words, the electrolyte must be able to benefit from the largest possible electrochemical gap, i.e., have a range of potentials on which it is neither oxidized nor reduced on the surface of the electrode. Although the possible spaces for DESs are significantly smaller than those of certain ILs, they are wide enough to allow the deposition of metals with reasonable yields. In addition, the very high thermal and chemical resistance of DESs, their low cost of use, their biodegradability, and their water content are all supplementary advantages for this type of application. Their usage as an electrolyte was one among the very earliest uses, with the most publications to date.

Thus, a certain number of works have been able to demonstrate the applicability of this class of solvents as electroplating media for a range of transition metals and alloys, Cu and Ni (A. P. Abbott et al., 2008), In addition, the eutectic mixture ChCl: EG (1:2 ratio) has been used successfully for electropolishing (chemical surface treatment technique by electrolytic action) of stainless steel.

I.5.3. Other Applications

DES has grown in popularity in recent years, their scope has also increased. The solvation of biomass, such as lignocellulose and cellulose, is a fascinating issue that has gotten a lot of consideration (Francisco et al., 2012). Furthermore, DES is utilized to create well-defined

nanomaterials involving structure-controlled nanoparticles, organometallic structures, colloidal assemblies, and architectures, as well as a durable medium for nanomaterials and functional materials (Wagle et al., 2014). DESs are also employed as organic templates for the synthesis of materials and zeolite analogs (Parnham et al., 2006). Their potential as drug solubilization vehicles has also been explored (Morriso et al., 2006).

I.6. Conclusion

Deep eutectic solvents (DESs) are now widely acknowledged as a new class of ionic liquid (IL) analogs because they share many characteristics and properties with ILs. The physical-chemical properties of DESs can be nearly infinitely tuned by changing the nature of the HBA and the HBD, making possible the preparation of task-specific DESs. Regarding physicochemical properties, we conclude the following points:

❖ The drastic decrease in the freezing point of the DES, possibly due to the type of interactions between the HBAs and HBDs.

❖ The viscosity and surface tension of DESs are notably higher when compared to the majority of traditional solvents, but they are close to ionic liquids.

❖ DES has relatively low densities and can be liquid over a wide range of temperatures.

❖ The toxicity and biodegradability of DESs are linked to those of their components (HBA and HBD).

Deep eutectic solvents have many applications as well as, solubilization of active principle, metal oxide, dissolution of gas CO_2 and SO_2, and extraction of molecules.

References

Abbott, A. P., El Ttaib, K., Ryder, K. S., & Smith, E. L. (2008). Electrodeposition of nickel using eutectic based ionic liquids. *Transactions of the Institute of Metal Finishing*, *86*(4), 234–240. https://doi.org/10.1179/174591908X327581

Abbott, A. P., Barron, J. C., Ryder, K. S., & Wilson, D. (2007). Eutectic-based ionic liquids with metal-containing anions and cations. *Chemistry-A European Journal*, *13*(22), 6495–6501. https://doi.org/10.1002/chem.200601738

Abbott, A.P., Boothby, D., Capper, G., Davies, D. L., & Rasheed, R. K. (2004). Deep Eutectic Solvents formed between choline chloride and carboxylic acids: Versatile alternatives to ionic liquids. *Journal of the American Chemical Society*, *126*(29), 9142–9147. https://doi.org/10.1021/ja048266j

Abbott, A. P., Capper, G., Davies, D. L., McKenzie, K. J., & Obi, S. U. (2006). Solubility of metal oxides in deep eutectic solvents based on choline chloride. *Journal of Chemical and Engineering Data*, *51*(4), 1280–1282. https://doi.org/10.1021/je060038c

Abbott, A.P., Capper, G., Davies, D. L., Rasheed, R. K., & Tambyrajah, V. (2003). Novel solvent properties of choline chloride/urea mixtures. *Chemical Communications*, *1*, 70–71. https://doi.org/10.1039/b210714g

Abbott, A. P., Capper, G., & Gray, S. (2006). Design of improved deep eutectic solvents using hole theory. *ChemPhysChem*, *7*(4), 803–806. https://doi.org/10.1002/cphc.200500489

Abbott, A. P., Cullis, P. M., Gibson, M. J., Harris, R. C., & Raven, E. (2007). Extraction of glycerol from biodiesel into a eutectic based ionic liquid. *Green Chemistry*, *9*(8), 868–887. https://doi.org/10.1039/b702833d

Abbott, A. P., Harris, R. C., Ryder, K. S., D'Agostino, C., Gladden, L. F., & Mantle, M. D. (2011). Glycerol eutectics as sustainable solvent systems. *Green Chemistry*, *13*(1), 82–90. https://doi.org/10.1039/c0gc00395f

Abbott, A. P., Ttaib, K. El, Frisch, G., Ryder, K. S., & Weston, D. (2012). The electrodeposition of silver composites using deep eutectic solvents. *Physical Chemistry Chemical Physics*, *14*(7), 2443–2449. https://doi.org/10.1039/c2cp23712a

Bi, W., Tian, M., & Row, K. H. (2013). Evaluation of alcohol-based deep eutectic solvent in extraction and determination of flavonoids with response surface methodology optimization. *Journal of Chromatography A*, *1285*, 22–30. https://doi.org/10.1016/j.chroma.2013.02.041

Choi, Y. H., Van Spronsen, J., Dai, Y., Verberne, M., Hollmann, F., Arends, I. W. C. E., Witkamp, G. J., & Verpoorte, R. (2011). Are natural deep eutectic solvents the missing link in understanding cellular metabolism and physiology? *Plant Physiology*, *156*(4), 1701–1705. https://doi.org/10.1104/pp.111.178426

D'Agostino, C., Harris, R. C., Abbott, A. P., Gladden, L. F., & Mantle, M. D. (2011). Molecular motion and ion diffusion in choline chloride based deep eutectic solvents studied by 1H pulsed field gradient NMR spectroscopy. *Physical Chemistry Chemical Physics*, *13*(48), 21383–21391. https://doi.org/10.1039/c1cp22554e

Francisco, M., Van Den Bruinhorst, A., & Kroon, M. C. (2012). New natural and renewable low transition temperature mixtures (LTTMs): Screening as solvents for lignocellulosic biomass processing. *Green Chemistry*, *14*(8), 2153–2157. https://doi.org/10.1039/c2gc35660k

Francisco, M., Van Den Bruinhorst, A., & Kroon, M. C. (2013). Low-transition-temperature mixtures (LTTMs): A new generation of designer solvents. *Angewandte Chemie - International Edition*, *52*(11), 3074–3085. https://doi.org/10.1002/anie.201207548

García, G., Aparicio, S., Ullah, R., & Atilhan, M. (2015). Deep eutectic solvents: Physicochemical properties and gas separation applications. *Energy and Fuels*, *29*(4), 2616–2644. https://doi.org/10.1021/ef5028873

Gorke, J. T., Srienc, F., & Kazlauskas, R. J. (2008). Hydrolase-catalyzed biotransformations in deep eutectic solvents. *Chemical Communications*, *10*, 1235–1237. https://doi.org/10.1039/b716317g

Guo, W., Hou, Y., Wu, W., Ren, S., Tian, S., & Marsh, K. N. (2013). Separation of phenol from model oils with quaternary ammonium salts via forming deep eutectic solvents. *Green Chemistry*, *15*(1), 226–229. https://doi.org/10.1039/c2gc36602a

Gutiérrez, M. C., Ferrer, M. L., Mateo, C. R., & Monte, F. Del. (2009). Freeze-drying of aqueous solutions of deep eutectic solvents: A suitable approach to deep eutectic suspensions of self-assembled structures. *Langmuir*, *25*(10), 5509–5515. https://doi.org/10.1021/la900552b

Hayyan, M., Hashim, M. A., Hayyan, A., Al-Saadi, M. A., AlNashef, I. M., Mirghani, M. E. S., & Saheed, O. K. (2013). Are deep eutectic solvents benign or toxic? *Chemosphere*, *90*(7), 2193–2195. https://doi.org/10.1016/j.chemosphere.2012.11.004

Kareem, M. A., Mjalli, F. S., Hashim, M. A., & Alnashef, I. M. (2010). Phosphonium-based ionic liquids analogues and their physical properties. *Journal of Chemical and Engineering Data*, *55*(11), 4632–4637. https://doi.org/10.1021/je100104v

Leron, R. B., & Li, M. H. (2012). Molar heat capacities of choline chloride-based deep eutectic solvents and their binary mixtures with water. *Thermochimica Acta*, *530*, 52–57. https://doi.org/10.1016/j.tca.2011.11.036

Li, W., Zhang, Z., Han, B., Hu, S., Song, J., Xie, Y., & Zhou, X. (2008). Switching the basicity of ionic liquids by CO2. *Green Chemistry*, *10*(11), 1142–1145. https://doi.org/10.1039/b811624e

Li, X., Hou, M., Han, B., Wang, X., & Zou, L. (2008). Solubility of CO2 in a choline chloride + urea eutectic mixture. *Journal of Chemical and Engineering Data*, *53*(2), 548–550. https://doi.org/10.1021/je700638u

Liu, B., Zhao, J., & Wei, F. (2013). Characterization of caprolactam based eutectic ionic liquids and their application in SO2 absorption. *Journal of Molecular Liquids*, *180*(3), 19–25. https://doi.org/10.1016/j.molliq.2012.12.024

Maugeri, Z., & Domínguez De María, P. (2012). Novel choline-chloride-based deep-eutectic-solvents with renewable hydrogen bond donors: Levulinic acid and sugar-based polyols. *RSC Advances*, *2*(2), 421–425. https://doi.org/10.1039/c1ra00630d

Morrison, H. G., Sun, C. C., & Neervannan, S. (2009). Characterization of thermal behavior of deep eutectic solvents and their potential as drug solubilization vehicles. *International Journal of Pharmaceutics*, *378*(1–2), 136–139. https://doi.org/10.1016/j.ijpharm.2009.05.039

Parnham, E. R., Drylie, E. A., Wheatley, P. S., Slawin, A. M. Z., & Morris, R. E. (2006). Ionothermal materials synthesis using unstable deep-eutectic solvents as template-delivery agents. *Angewandte Chemie - International Edition*, *45*(30), 4962–4966. https://doi.org/10.1002/anie.200600290

Rimsza, J. M., & Corrales, L. R. (2012). Adsorption complexes of copper and copper oxide in the deep

eutectic solvent 2:1 urea-choline chloride. *Computational and Theoretical Chemistry*, *987*, 57–61. https://doi.org/10.1016/j.comptc.2011.11.003

Smith, E. L., Abbott, A. P., & Ryder, K. S. (2014). Deep Eutectic Solvents (DESs) and Their Applications. *Chemical Reviews*, *114*(21), 11060–11082. https://doi.org/10.1021/cr300162p

Su, W. C., Wong, D. S. H., & Li, M. H. (2009). Effect of water on solubility of carbon dioxide in (aminomethanamide + 2-hydroxy-N,N,N-trimethylethanaminium chloride). *Journal of Chemical and Engineering Data*, *54*(6), 1951–1955. https://doi.org/10.1021/je900078k

Wagle, D. V., Zhao, H., & Baker, G. A. (2014). ChemInform Abstract: Deep Eutectic Solvents: Sustainable Media for Nanoscale and Functional Materials. *ChemInform*, *45*(41), no-no. https://doi.org/10.1002/chin.201441292

Wang, Y., Hou, Y., Wu, W., Liu, D., Ji, Y., & Ren, S. (2016). Roles of a hydrogen bond donor and a hydrogen bond acceptor in the extraction of toluene from: N -heptane using deep eutectic solvents. *Green Chemistry*, *18*(10), 3089–3097. https://doi.org/10.1039/c5gc02909k

Wasserscheid, P., & Welton, T. (2003). Ionic Liquids in Synthesis. In *Synthesis* (Vol. 2003, Issue 11). https://doi.org/10.1055/s-2003-40869

Wu, S. H., Caparanga, A. R., Leron, R. B., & Li, M. H. (2012). Vapor pressure of aqueous choline chloride-based deep eutectic solvents (ethaline, glyceline, maline and reline) at 30-70 °c. *Thermochimica Acta*, *544*, 1–5. https://doi.org/10.1016/j.tca.2012.05.031

Zhang, Q., De Oliveira Vigier, K., Royer, S., & Jérôme, F. (2012). Deep eutectic solvents: Syntheses, properties and applications. *Chemical Society Reviews*, *41*(21), 7108–7146. https://doi.org/10.1039/c2cs35178a

Zhao, H., Baker, G. A., & Holmes, S. (2011). New eutectic ionic liquids for lipase activation and enzymatic preparation of biodiesel. *Organic and Biomolecular Chemistry*, *9*(6), 1908–1916. https://doi.org/10.1039/c0ob01011a

Chapter II

Theories and Methods

II.1. Introduction

With the advent of progressively sophisticated theoretical methods of computing and more accessible calculating resources, computational chemistry is gradually becoming a useful tool for both industry and academia. Among these tools :(i) quantitative structure-property relationship (QSPR) and (ii) molecular modeling.

Computer-assisted QSPR has proven to be an accurate, reliable, and cost-effective method in predicting the physicochemical properties of solvents, via a set of molecular descriptors. Molecular modeling has undergone a very important development in many applications involving the electronic structure of atoms, molecules, and metal-organic complexes. This set of techniques study and deal with chemical issues on a computer without the need to go to the treatment room for experiments. Besides, in this chapter, we aim to provide comprehensive knowledge on theoretical equations in the calculation of the liquid-liquid extraction process.

II.2. Quantitative Structures-Property Relationship

II.2.1. Definition of QSPR

A QSPR analysis is a promising approach to correlate molecular-level structure with physicochemical properties (Hartman, 1962; Yousefinejad & Hemmateenejad, 2015). This modeling approach showed its reliability in predicting the physical, chemical, and biological properties of many solvents (Blay et al., 2016; Calvo-Serrano et al., 2019; Liu et al., 2020).

In an attempt to develop a QSPR model, the following should be obtained: (1) an extensive dataset that covers different chemicals for sufficient statistical analysis, (2) selection of molecular descriptors, (3) calculation and generating the molecular descriptors of these compounds, (4) selecting a proper algorithm to relate the molecular descriptors with the dependent variable, and (5) performing a statistical analysis to ensure the robustness and the applicability of the predictive model.

II.2.2. Principe

Molecular descriptor-based QSPR is an accurate, reliable, and cost-effective method for predicting the properties of solvents (deep eutectic solvents and ionic liquids) (Papa & Gramatica, 2010; Torrecilla et al., 2010). The principle of QSPR methods is to create a model that links the descriptors and physicochemical properties of a series of similar chemical compounds using data analysis methods (Figure II.1). The general form of such a model is as follows:

$$\text{Propriety} = f\,(\text{Descriptors}) \tag{II.1}$$

The objective of such a method is to predict and screen the properties of a certain solvent (Papa & Gramatica, 2010; Torrecilla et al., 2010). They are also capable of obtaining insights and uncovering relationships between the molecular-level structure and the macroscopic-level properties of solvents (Papa & Gramatica, 2010; Torrecilla et al., 2010). To do this, different types of tools can be used: multiple linear regression (MLR) (Myles et al., 2004), partial least squares regression (PLS regression), artificial neural network (ANN) (Gasteiger & Zupan, 1993).

Descriptors
- Electronics
- Topological

Properties
- Viscosity, Density
- Conductivity

QSPR model
- Multiple Linear Regression
- Artificial Neural Networks
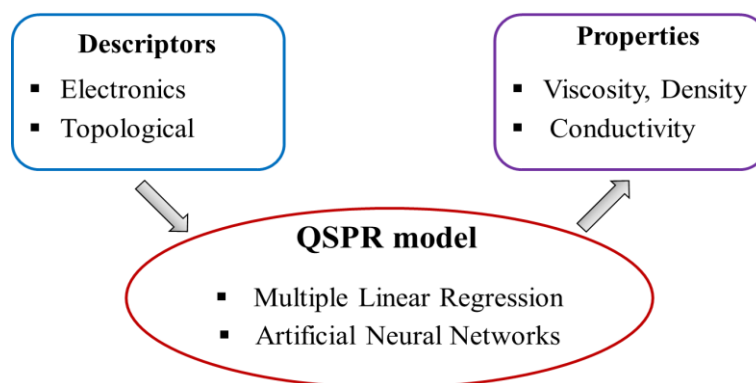
Figure II.1. Principle of the QSPR method.

II.2.3. Importance of Database

The QSPR study conducts statistical analyzes, one of the crucial steps is the selection of the database. Indeed, a QSPR model is dependent on an experimental database.

The choice of an adequate database is decisive in developing a model. In most cases, the experimental data are available in the literature. An effective database must be composed of highly reliable experimental data obtained by following a single protocol since any error would impact the final model. Several issues must be checked in the protocol progress to set a database. First, we must ensure that the structures are correct from a chemical point of view; wrong structures generate bad descriptors and therefore bad models.

II.2.4. Molecular Descriptors

Molecular structures are transformed into a series of quantities that determine physical, chemical, and structural properties. These quantities are called descriptors. For years, enormous work has been carried out to develop thousands of descriptors capable of describing the molecular structures as comprehensively as possible (Balaban, 2012). Since they are essential to be measured, the calculated descriptors are chosen. Detailed information on descriptors is available in Karelson's book (Karelson et al., 1996). Molecular descriptors are generally classified into three categories; physicochemical, topological, and electronic descriptors. These descriptors differ from the bi- and three-dimensional structures of the molecule. The most descriptors used in the QSPR study (Chtita

et al., 2015) are the total energy (E_T), the energy of the highest occupied molecular orbital (E_{HOMO}), the energy of the lowest unoccupied molecular orbital (E_{LUMO}) and the dipole moment (DM), as electronic descriptors. There are also physio-chemical and topological descriptors such as molar refractivity (MR), molar volume (MV), molecular weight (MW), and density (D).

II.2.5. Data Analysis Methods

A data analysis method is required to develop a QSPR model, this method quantifies the relationship between property and structure (descriptors). There are several methods to build and analyze the statistical data of the model, some are linear such as multiple linear regression (MLR), partial least squares regression (PLS), others are nonlinear like non-linear multiple linear regression (MNLR), artificial neural networks (ANN). Among the methods used in our study are multiple linear regression (MLR) and artificial neuron network (ANN).

II.2.5.1. Multiple Linear Regression

Multiple Linear Regression (MLR) is a machine learning technique reported extensively in the literature for its reliability and interpretability in expressing a simple linear relation between the dependent variable (*i.e.,* physicochemical properties) and the independent variables (*i.e.,* molecular descriptors) (Gu et al., 2019). The linear equation can be expressed as follows:

$$y = a_0 + \sum_{i=1}^{n} a_i S_i + \sum_{i=1}^{n} \sum_{j=i+1}^{n} a_{i-j}(S_i - \overline{S_i})(S_j - \overline{S_j}) \tag{II.2}$$

where a_0 represents the intercept of the linear equation, S_i represents a descriptor i, a_i is coefficient of descriptor i, n is the total number of descriptors, and $a_{i-j}(S_i - \overline{S_i})(S_j - \overline{S_j})$ represents the binary interactions between a pair of descriptors.

The MLR model was developed through the multilinear fitting toolbox of the JMP statistical software. The discretized $S_{\sigma\text{-profile}}$ descriptors and the temperature were selected as the inputs, while the property of the deep eutectic solvents (DESs) was selected as the output. The binary interactions between a pair of descriptors were added by selecting the 2nd-degree factorial option. The fitting method was set as 'forward stepwise' with the parameter cost function (stopping rule) selected as a minimum AIC_c "Corrected Akaike Information Criterion", which can be defined as follows:

$$AIC = 2K - 2\ln(L) \tag{II.3}$$

$$AIC_c = AIC + \frac{2K^2 + 2K}{p - K - 1} \tag{II.4}$$

where K represents the number of estimated parameters in the model, L represents the maximum value of the likelihood function in the model, and p represents the number of training experimental data points. Note that as $p \rightarrow \infty$, the extra corrected penalty term in AIC_c converges to 0, and thus AICc converges to AIC. Using the stepwise AIC_c algorithm, only the significant descriptors that enhanced the model's information criterion were added to the model, while the ones that had an insignificant effect were eliminated (Gramatica, 2007).

II.2.5.2. Artificial Neural Networks

Artificial neural networks (ANN) were originally an attempt at mathematical modeling of nervous systems, initiated in 1943 by McCulloch and Pitts (Mcculloch & Pitts, 1990). A neuron is a non-linear function for real variables with parameters and finite values. Most often, the neurons perform a linear combination of the usual inputs, then apply to this value an "activation function" f, generally non-linear. The value obtained is the output of the neuron. A neuron is seen in Figure II.2.
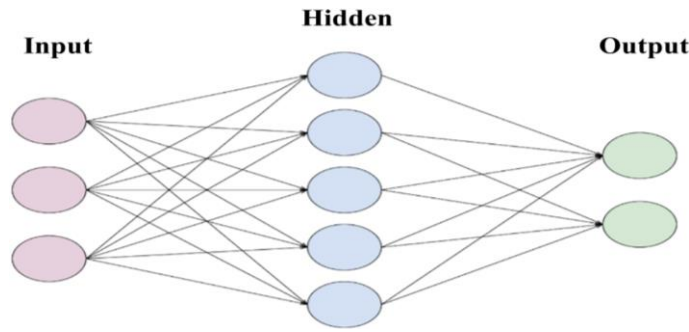
Figure II.2. Representation of a neuron.

The (ANN) has also been utilized to develop a robust non-linear correlation between the descriptors and the properties of DESs. The network consists of several processing elements denoted as "neuron nodes". The neurons are associated with each other by direct communication activation functions that contain the information required to generate the output (Adeyemi et al., 2018; Shahbaz et al., 2012). The hyperbolic tangent sigmoid activation function of each hidden neuron (H_k) can be computed as follows (Adeyemi et al., 2018):

$$H_k = tanh\left(\frac{1}{2}Y_k\right) \tag{II.5}$$

The $tanh$ activation function transforms the Y_k values to be between -1 and 1. Y_k is a linear combination of the inputs linked to hidden neuron k, which can be calculated as follows:

$$Y_k = \sum_{k=1}^{M}(W_{k,input})(S_i) + b_k \tag{II.6}$$

where $W_{k,input}$ represents the weight coefficient of the link between each input and hidden neuron k, and b_k represents the intercept bias of hidden neuron k.

The neural network was developed through the neural network toolbox of the JMP statistical software. The discretized $S_{\sigma\text{-profile}}$ descriptors and the temperature were selected as the network's inputs, while the property of the DESs was selected as the output. The network's learning rate was fixed at 0.1 with a squared penalty method and an internal cross-validation holdback proportion of 25%.

II.2.6. Validation

In general, a *QSPR* model is evaluated by analyzing many statistical indicators of the regression, such as the coefficient of determination R^2, the adjusted coefficient of determination R^2_{Adjust} and the root mean squared error (RMSE). According to these parameters, the robustness and reliability of the *QSPR* model can be estimated (Afantitis et al., 2009; Patel et al., 2014).

II.2.6.1. Internal Validation

The most common technique used to determine the stability of the predictive model is to test the influence of each sample on the last model, to do this, we utilized a cross-validation technique (CV). This method consists of taking out a certain number *n* from an initial number *k* of molecules, then building a new model with the residual *n-k* molecules using the chosen descriptors. This new model is then used for the prediction of the *n* molecules removed. This method is continued until all of the molecules' values in the training set have been predicted and removed. Depending on whether one or more molecules are eliminated, we shall use the terms Leave-One-Out (LOO) or Leave-Many-Out (LMO) (Zhang et al., 2008). The coefficient that describes this validation is given by the equation below:

$$Q^2_{cv} = 1 - \frac{\Sigma(y_i - \hat{y}_i)^2}{\Sigma(y_i - \bar{y})^2} \qquad \text{(II.7)}$$

where y_i is the measured value of the training set compounds, $\hat{y}_i$ is the predicted value of the training set compounds and $\bar{y}$ is the average property of all molecules of the training set (Adeniji et al., 2018; Tropsha et al., 2003).

II.2.6.2. External Validation

Additional experimental data called test set are needed to fix the ability of the prediction model. The model generated by the training set is used to predict the properties of the testing set

(Adeniji et al., 2018; Tropsha et al., 2003) R_{pred}^2 is the coefficient that describes this validation, and it is obtained from the following equation:

$$R_{test}^2 = 1 - \frac{\sum(y_i - \hat{y}_i)^2}{\sum(y_i - \bar{y})^2} \tag{II.8}$$

where y_i is the measured value of the test set compounds, $\hat{y}_i$ is the predicted value of the test set compounds and $\bar{y}$ is the average property of all molecules of the test set.

II.2.7. Applicability Domain Analysis

The development of QSPR models is based on a defined domain of molecules with known structures and properties (Ojha & Roy, 2011). Accordingly, it should be mentioned that no matter how validated a model may be, a reliable QSPR prediction for the entire universe of molecules cannot be guaranteed (Tropsha et al., 2003). Therefore, it is essential to quantitatively define the scope and extent of extrapolation in a QSPR model before it is used in designing and screening solvents (Gramatica et al., 2007; Tropsha et al., 2003). The Applicability Domain (AD) analysis is a standard method that has been utilized extensively in QSPR models as a means to (i) identify the presence of structural outliers, and (ii) define the domain of molecules for which a QSPR prediction may be considered reliable (*i.e.,* the extent of extrapolation and the uncertainty in prediction) (He et al., 2017; Ojha & Roy, 2011). The AD of a model is defined as the theoretical physicochemical or structural space where the QSPR model is developed (Gramatica et al.,, 2007; Tropsha et al., 2003). Therefore, to enable more reliable predictions of new molecules, a QSPR model must include a high diversity of data points to ensure that the AD of the model is defined as widely as possible (Hammoudi et al., 2020).

Following the leverage method (Tropsha et al., 2003), the AD in a QSPR model can be defined using the leverage values (h_i), and the standardized residuals (SDR). The leverage value is a measure of the similarity of a certain molecule *i* from the majority of the molecules in training set (Gramatica et al., 2007). Therefore, by using the difference in leverage values, structural outliers that are considered to be "chemically different" from most of the molecules used in the training set of a model can be identified. The leverage values of each DES were calculated as follows (Gramatica et al., 2007; Tropsha et al., 2003):

$$\hat{h} = z_i (Z^T Z)^{-1} * z_i^{\ T} \tag{II.9}$$

where z_i is a row-vector matrix containing the descriptors of DES i, Z is a $p \times d^*$ the matrix in which p is the data points used in the training set and d^* is the number of significant model descriptors, and $\hat{h}$ is a diagonal matrix containing the h_i values of each data point. The superscript

"T" refers to the transpose of the matrices. The SDR of each data point can be defined as follows (Hammoudi et al., 2020):

$$SDR = \frac{y_{pred} - y_{exp}}{\sqrt{\dfrac{\sum_{m=1}^{p}(y_{pred} - y_{exp})^2}{p}}} \tag{II.10}$$

where y_{pred} and y_{exp} represent the predicted and the experimental property, respectively. Using both the calculated leverage values and the calculated standardized residuals, the domain of applicability can be defined between the (i) horizontal boundaries $-3 < SDR < +3$, and (ii) vertical boundaries $0 < h_i < h^*$, in which h^* is the warning leverage threshold calculated as follows (Hammoudi et al., 2020):

$$h^* = \frac{3(d^* + 1)}{p} \tag{II.11}$$

The predictions of new DESs that are within the AD of the model are considered to be more reliable due to their high interpolation degree (*i.e.,* structurally similar to the DESs used in the training set) (Gramatica et al., 2007; Tropsha et al., 2003). On the other hand, the predictions of new DESs with leverage values higher than h^* could also be considered correct but less reliable due to their extrapolation degree (He et al., 2017; Ojha & Roy, 2011). The most common visual method to detect AD outliers is through the use of William plots (Mitra et al., 2010; Tropsha et al., 2003), which are constructed by plotting the SDR against the h_i of each data point. The coverage of the domain of applicability in a William plot can be defined as follows (Gramatica et al., 2016):

$$AD_{coverage} = \frac{p_{inside}}{p_{total}}(100) \tag{II.12}$$

where p_{inside} denotes the total number of points within the AD boundaries, while p_{total} denotes the total number of data points (including both the training and testing set).

II.2.8. Interpretation of Models

The interpretation of models in terms of elementary mechanisms is also an important point recommended in the process of validation of the models (Stanton, 2003). Besides the aspect of clean interpretation of models, this provides for a better knowledge of the underlying chemical phenomenon. The use of interpretation parameters in prediction models can help to reduce the risks of a random selection of parameters. It is not always easy to interpret molecular descriptors.

For instance, a large number of descriptors makes an equation difficult to interpret due to the size of information. Likewise, some non-linear models make it completely impossible to

interpret descriptors. The interpretation of models might be considered as early as the data selection step. Indeed, it may be required to choose between two descriptors that are statistically quite similar during the procedure. For example, at the molecular level, an automatic technique can make us choose the least signifying descriptor, providing a very slightly higher correlation with the experimental property.

II.3. Molecular Modeling

The term "molecular modeling"refers to approaches for simulating the behavior of a particle system. The studied system size can range from a simple diatomic molecule to biological macromolecules of several tens of thousands of atoms. Molecular modeling involves the use of theoretical calculation methods to determine the graphic representation of the geometry or configuration of molecule atoms and evaluate the physicochemical properties of the studied molecule. Molecular modeling aims to predict the structure and reactivity or the systems of molecules. Molecular modeling methods can be classified into three categories (Mostefaoui, 2011): Quantum mechanics, Molecular mechanics, and Molecular dynamics.

II.3.1. Quantum Mechanics

Quantum mechanics (QM) is an extension of the quantum theory, resulting from the work of Planck, their interpretation by Einstein, and their application to atomic theory by Bohr and Sommerfeld. QM explains the quantification of certain quantities (energy, kinetic moment) and brings out the Pauli exclusion principle. The new particle design that results from the wave-particle duality revealed in Broglie's (1923) work leads to wave mechanics.

The methods of QM, which use the distribution of electrons in orbitals around the molecule, imply often computing for long times, which limits their use to small molecules, or requires the use of numerous approximations. They are particularly suitable for calculating charges and electrostatic potentials. The main objective of QM is to determine the energy and electronic distribution (Mostefaoui, 2011). QM defines the molecular structure as being a nucleus around electrons and is described by their probability of presence at a point and represented by orbitals (Boyd, 1983).

II.3.1.1. Semi-Empirical Methods

A semi-empirical method is a method in which a part of the calculations necessary for Hartree-Fock calculations is replaced by parameters adjusted to experimental values (the Hamiltonian is always parameterized by comparison with reference compounds). In general, this method is very precise for the families of given products close to those used for parameterization.

Semi-empirical methods consider electrons from the valence layer; the electrons of the internal layers are included in the nuclear core.

o   Neglect of Diatomic Differential Overlap (NDDO) method: proposed by Pople in 1965. All bicentric bioelectronic integrals are retained.

o   Modified Neglect of Diatomic Differential Overlap (MNDO) method: proposed by Dewar in 1977.

o   Austin Model1(AM1) method: proposed by Dewar in 1985. It corrects the term heart-heart repulsion.

o   Parametric Method 3 (PM3) method: proposed by Stewart in 1989. It uses an automatic parameterization procedure during calculations.

II.3.1.2. Density Functional Theory

The electronic density functional theory (DFT) was developed in two periods, in 1964 and 1965, by Hohenberg, Kohn, and Sham [Hohenberg-1964, Kohn-1965]. DFT is now commonly employed to study the electronic structure of semiconductors. Traditionally, functionals such as the local density approximation (LDA) or the generalized gradient approximation (GGA) have been used, producing accurate results for many structural and energetic properties not only of bulk materials but also of surfaces and interfaces (Lyons et al., 2009).

II.3.2. Molecular Mechanics

Molecular Mechanics (MM) is a calculation method that makes it possible to obtain results of molecular geometries and energies based on classical mechanics. The MM appeared in 1930 (Andrews, 1930), but developed only during the sixties when computers became more accessible and more efficient. The MM is based on the Born-Oppenheimer approximation that supposes that electrons are much faster than nuclei. MM is a non-quantum method but has an interest in large systems; as in the case of biological systems which cannot be approached with quantum methods. In these methods, we associate a potential energy empirical function with each degree of freedom of the molecule: elongation of the bonds, variation of the valence angles, and the dihedrons (rotation around a bond). MM aims to calculate the potential energy of a molecule (or system of molecules) according to the coordinates of the atoms.

II.3.2.1. Force Field

In molecular mechanics, the force field is the mathematical model that represents the potential energy of a molecule. The force field is a realistic expression of the mean electronic

interactions between atoms (N. L. Allinger, 1976). It provides access to the energetic hypersurface of a molecule by creating a link between the structural deformations of the system and its potential energy. It designates both the mathematical equation (potential energy function) and the parameters that compose it (N .L. Allinger, 1977).The potential energy function defines empirical energy and the total energy is decomposed into a sum of additive terms representing each of the interatomic interactions. It is expressed as a sum of contributions from several types of interaction. It can be broken down into intramolecular and intermolecular interactions terms. Intramolecular interactions depend only on the internal coordinates of the molecules, i.e. bonds, valence angles, and torsions. The intramolecular potential can be written in general:
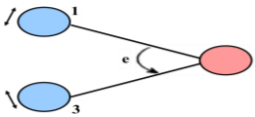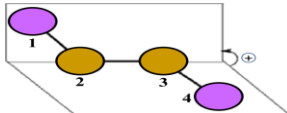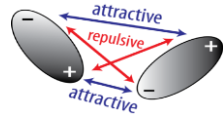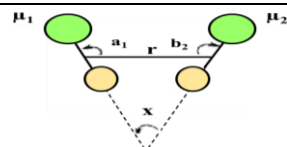
$$V_{intramolecular} = \sum_{liaison} V_{elongation} + \sum_{angle} V_{curvature} + \sum_{\substack{dihedral \\ angle}} V_{elongation} + \sum V_{cross}$$

Intermolecular interactions take into account interactions that do not include a bond, an angular curvature, or an angle of twist. The non-binding potential is expressed in two terms: Van der Walls and electrostatic energy terms so we have:

$$V_{intermolecular} = \sum V_{Van\ der\ Waals} + \sum V_{electrostatic}$$

The expression "force field" covers all of the functions as well as the parameters related to the different types of atoms they contain. Table II.1 shows the most important potential energies of the force field are :

Table II.1. The potential energies of a particle in a force field.

Energy	Type	Figures
Elongation	Elongation between two atoms	
Binding	Deformation of valence angles.	
Torsion	Dihedral angle formed by atoms 1-2-3-4	
Van der Waals	Interaction between two dipoles	
Electrostatic	Electrostatic interactions between two atoms	

II.3.2.2. *Different Force Fields in Molecular Mechanics*

Different force fields are proposed in the literature, varying from one another in terms of the development of the expression of molecular energy. Each one has a specific application field so that the choice of force field depends on the properties and application of the system such as:

- ➢ Type of compound: carbohydrate, metal complex.
- ➢ Environment: gas, solution.
- ➢ Type of interaction: hydrogen bond.

These force fields were first seen in the early 1970s and are still being studied today. Among the various force fields are:

a. MM2/MM3/MM4

Molecular mechanics 2 (MM2) is the first force field developed by Allinger et al.(N. L. Allinger et al., 1989). It was originally designed for simple molecules (alkanes, alkenes, alkynes, amines, etc.), then its improved versions MM3 (1989) and MM4 (1996) allow it to process progressively complex organic molecules.

b. OPLS

The Optimized Potentials for Liquid Simulations (OPLS) program, as its name suggests, is designed to optimize the potential for describing solvation properties. It is by W.L Jorgensen Jorgensen and J. Tirado Rives (Jorgensen et al., 1996).

c. UFF

Universal Force Field (UFF). Rappé and his collaborators have strained to design a universal force field (Rappé et al., 1992) capable of simulating molecules containing any combination of atoms in the periodic table.

d. AMBER

Assisted Model Building Energy Refinement(AMBER) was written by Kollman (Cornell et al., 1995). The field is configured for proteins and nucleic acids (UCSF, 1994). It has been used for polymers and other small molecules. In the context of this work, we will use this force field, since we will treat proteins.

II.4. COSMO-RS

COSMO-RS (short for COnductor like Screening MOdel for Real Solvents) (Andreas Klamt, 1995) is a quantum chemistry-based equilibrium thermodynamics method to predict

chemical potentials μ in liquids. It processes the screening charge density σ on the surface of molecules to calculate the chemical potential μ of each species in solution. Perhaps in dilute solution, a constant potential must be considered. As an initial step, a quantum chemical COSMO (A. Klamt & Schüürmann, 1993) calculation for all molecules is performed and the results (e.g. the screening charge density) are stored in a database. In a separate step, COSMO-RS uses the stored COSMO results to calculate the chemical potential of the molecules in a liquid solvent or mixture.

II.4.1. Generating the Molecular Descriptors

In order to generate the COSMO-RS based molecular descriptors, first, the SMILES of each hydrogen bond acceptor (HBA) and hydrogen bond donor (HBD) molecule were imported to the Turbomole software (TmoleX version 4.5.1). Then, the 3D structures were geometrically optimized at the DFT level by combining the def-TZVP "triple-ζ valence polarized" functions with the BP86 "Becke-Perdew 86" generalized gradient approximation. The SCF margin for the calculations was set to 1×10^{-6} Hartree (Alareeqi et al., 2020). The files generated for each molecule were then exported as "COSMO" files and then imported into the COSMO-RS software "COSMOThermX".

Using the COSMOThermX software, the 51 points of the *σ-profile* within the range of $\pm$ 0.025 e/Å were then extracted as "prf" data. The *σ-profile* data were then converted into molecular descriptors denoted as $S_{\sigma\text{-profiles}}$ by entering their data into MATLAB to calculate the integral of the area under the *σ-profile* curves. After calculating the $S_{\sigma\text{-profile}}$ descriptor of each HBA and HBD, the $S_{\sigma\text{-profile}}$ of the DESs were calculated as follow (Benguerba et al., 2019):

$$S_i^{ES} = (x_{HBA})\left(S_i^{HBA}\right) + (x_{HBD})\left(S_i^{HBD}\right) + (x_{H2O})\left(S_i^{H2O}\right) \qquad (\text{II.13})$$

where S_i is the descriptor in region i (e/Å^2), while x_{HBA}, x_{HBD}, and x_{H2O} are the mole fractions of the HBA, the HBD, and water, respectively.

This method of modeling is superior to the conventional method of defining the DES as a *pseudo*-pure component. Here, the DES is considered to be a mixture of three components; the HBA, the HBD, and water. The benefit of considering the DES as a mixture is that the resulting model would be much more flexible with regards to modeling new combinations of DES as it enables changing the HBA, the HBD, or their molar ratio with ease (Lloret et al., 2017; Zubeir et al., 2016).

II.5. Liquid-Liquid Extraction

II.5.1. Extraction Efficiency

The extraction efficiency (E_i) of each fuel impurity is defined by Eq. II.14 as follows:

$$E_i\,(\%) = \frac{w_{i,Initial} - w_{i,Raffinate}}{w_{i,initial}} \tag{II.14}$$

where the subscript i denotes a particular species; $w_{i,Initial}$ represents the initial weight fraction in the feed and $w_{i,Raffinate}$ represents the final weight fraction in the raffinate after extraction.

II.5.2. Distribution Ratio and Selectivity

The distribution ratio (β_i) can be defined by Eq. II.15 as follows:

$$\beta_i = \frac{w_{i,E}}{w_{i,R}} \tag{II.15}$$

where the E and R subscripts refer to the extract phase "DES-rich phase" and raffinate phase "n-alkane-rich phase", respectively; w_i refers to the weight fraction of species i.

The solute distribution ratio is used to compare the amount of the solute "contaminant" in the DES-rich phase compared to that in the n-alkane-rich phase, and thus, the higher the distribution ratio, the less amount of solvent would be required for high extraction. On the other hand, the selectivity (S) "also known as the separation factor" is defined by Eq. II.16 as follows:

$$S = \frac{\beta_2}{\beta_1} \tag{II.16}$$

where β_2 is the distribution ratio of each fuel contaminant while β_1 is the distribution ratio of n-alkane.

The selectivity measures the solvent's ability to selectively extract the fuel contaminants over n-alkane. High selectivity values indicate that smaller size equipment "less number of extraction stages" would be needed for extraction, which leads to lower initial capital costs (Warrag et al., 2020).

II.5.3. Consistency Tests

The Othmer−Tobias (OTHMER et al., 1945) and Hand (Li et al., 2013) empirical correlations, shown by Eq. II.17 and Eq. II.18, respectively, were used to check the consistency of the pseudo-ternary equilibrium data.

$$\ln\left(\frac{1\text{-}x_{1,\,R}}{x_{1,\,R}}\right) = a + b\,\ln\left(\frac{1\text{-}x_{3,E}}{x_{3,E}}\right) \tag{II.17}$$

$$\ln\left(\frac{1\text{-}x_{2,\,R}}{x_{1,\,R}}\right) = c + d \ln\left(\frac{1\text{-}x_{2,\,E}}{x_{3,E}}\right) \tag{II.18}$$

where x_1, x_2, and x_3 represent the mole fraction of *n*-alkane, the fuel contaminants, and the DES, respectively; a, b, c, and d are the fitting parameters of the consistency empirical correlations.

II.5.4. NRTL Regression

The non-random two-liquid (NRTL) model has been used for several ternary systems in literature and was found to be successful in correlating partially-miscible systems of two phases (Rodriguez et al., 2015). Therefore, the NRTL model was used to estimate the binary interaction parameters that can fit the experimental data successfully. The activity coefficient using NRTL is defined using Eq. II.19 as follows (Rodriguez et al., 2015):

$$\ln\gamma_i = \frac{\sum_j x_j \tau_{ji} G_{ji}}{\sum_k x_k G_{ki}} + \sum_j \frac{x_j G_{ij}}{\sum_k x_k G_{kj}}\left(\tau_{ij} - \frac{\sum_k x_k \tau_{kj} G_{kj}}{\sum_k x_k G_{kj}}\right) \tag{II.19}$$

in which: $G_{ij} = e^{(-\alpha_{ij}\tau_{ij})}$, $\tau_{ij} = a_{ij} + \frac{b_{ij}}{T}$, and $\tau_{ii} = 0$.

where *x* represents the mole fraction, γ represents the activity coefficient, τ_{ij} and τ_{ji} are the NRTL binary interaction parameters, and α_{ij} is the non-randomness parameter of the mixture, which was arbitrarily chosen as $\alpha_{ij} = \alpha_{ji} = \alpha = 0.25$. The selected value is within the recommended range of 0.1−0.3 used for nonpolar substances with polar non-associated liquids (Rodriguez et al., 2015). The binary interaction parameters were estimated using Aspen Plus; however, the mole fractions in Eq. II.29 were replaced with weight fractions as this is a common strategy in correlating *pseudo*-ternary systems containing DESs (Warrag et al., 2019). The NRTL regression was then applied by minimizing Eq. II.20, which is the objective function based on the Maximum-Likelihood method.

$$OF = \sum_{k=1}^{N}\sum_{j=1}^{P}\sum_{i=1}^{M}\left(w_{ijk}^{exp} - w_{ijk}^{cal}\right)^2 \tag{II.20}$$

where *N* represents the number of equilibrium tie lines, *P* represents the number of phases (either raffinate or extract), and *M* represents the number of fuel components in equilibrium; w_{ijk} refers to the weight fraction of species *i* in phase *j* of the equilibrium tie line *k*; the superscripts *exp* and *cal* denote the experimentally measured and NRTL calculated values, respectively. Finally, to evaluate the accuracy of the regression parameters, the root-mean-square deviations (RMSD) between the calculated and the experimental values were determined using Eq. II.21.

$$RMSD\ (\%) = \sqrt{\frac{\sum_{k=1}^{N}\sum_{j=1}^{P}\sum_{i=1}^{M}\left(w_{i,j,k}^{exp} - w_{i,j,k}^{cal}\right)^2}{NPM}} \tag{II.21}$$

II.6. Conclusion

From this chapter we can conclude the following points:

➢ QSPR models are an effective, reliable, and accurate method for predicting and screening the properties of a certain solvent. They are also capable of obtaining insights and uncovering relationships between the molecular-level structure and the macroscopic-level properties of solvents.

➢ Molecular modeling covers a wide variety of theoretical and computational methods used to represent the structure of molecules, ions, and/or particles.

➢ COSMO-RS "Conductor-like Screening Model for Real Solvents" is a molecular modeling technique that utilizes both quantum chemistry and statistical mechanics to predict various physicochemical properties and thermodynamic behavior of solvents.

➢ Liquid-liquid extraction technologies appeared to be one of the most promising alternatives to conventional hydrotreatment.

References

Adeniji, S. E., Uba, S., & Uzairu, A. (2018). QSAR Modeling and Molecular Docking Analysis of Some Active Compounds against Mycobacterium tuberculosis Receptor (Mtb CYP121) . *Journal of Pathogens*, *2018*, 1–24. https://doi.org/10.1155/2018/1018694

Adeyemi, I., Abu-Zahra, M. R. M., & AlNashef, I. M. (2018). Physicochemical properties of alkanolamine-choline chloride deep eutectic solvents: Measurements, group contribution and artificial intelligence prediction techniques. *Journal of Molecular Liquids*, *256*, 581–590. https://doi.org/10.1016/j.molliq.2018.02.085

Afantitis, A., Melagraki, G., Sarimveis, H., Igglessi-markopoulou, O., & Kollias, G. (2009). *Original article A novel QSAR model for predicting the inhibition of CXCR3 receptor by 4- N -aryl- [1 , 4] diazepane ureas*. *44*. https://doi.org/10.1016/j.ejmech.2008.05.028

Alareeqi, S., Bahamon, D., Nogueira, R. P., & Vega, L. F. (2020). Understanding the relationship between the structural properties of three corrosion inhibitors and their surface protectiveness ability in different environments. *Applied Surface Science*. https://doi.org/10.1016/j.apsusc.2020.148600

Allinger, N. L. (1976). Calculation of Molecular Structure and Energy by Force-Field Methods. *Advances in Physical Organic Chemistry*, *13*(C), 1–82. https://doi.org/10.1016/S0065-3160(08)60212-9

Allinger, N. L. (1977). Conformational Analysis. 130. MM2. A Hydrocarbon Force Field Utilizing V1and V2Torsional Terms1,2. *Journal of the American Chemical Society*, *99*(25), 8127–8134. https://doi.org/10.1021/ja00467a001

Allinger, Norman L., Quinn, M. I., Chen, K., Frierson, M. R., Sciences, C., & A, G. A. U. S. (1989). Molecular Mechanics Calculations Organometallanes OF Germanium , (MM2) on Tin , and Lead * Molecular mechanics has become a standard tool for the study of molecular structure in recent years [1 , 21 . The MM2 force field has been widely used , and is a. *Science*, *194*, 1–18.

Andrews, D. H. (1930). The Relation Between the raman Spectra and the Structure of Organic Molecules. *Physical review*, *36*.

Balaban, A. T. (2012). Review of "Statistical Modelling of Molecular Descriptors in QSAR/QSPR" by Matthias Dehmer, Kurt Varmuza, and Danail Bonchev. *Journal of Cheminformatics*, *4*(1), 1–2. https://doi.org/10.1186/1758-2946-4-36

Benguerba, Y., Alnashef, I. M., Erto, A., Balsamo, M., & Ernst, B. (2019). A quantitative prediction of the viscosity of amine based DESs using Sσ-profile molecular descriptors. *Journal of Molecular Structure*, *1184*(February), 357–363. https://doi.org/10.1016/j.molstruc.2019.02.052

Blay, V., Gullón-Soleto, J., Gálvez-Llompart, M., Gálvez, J., & García-Domenech, R. (2016). Biodegradability Prediction of Fragrant Molecules by Molecular Topology. *ACS Sustainable Chemistry and Engineering*, *4*(8), 4224–4231. https://doi.org/10.1021/acssuschemeng.6b00717

Boyd, D. B. (1983). Quantum mechanics in drug design: Methods and applications. *Therapeutic Innovation & Regulatory Science*, *17*(3), 121–131. https://doi.org/10.1177/009286158301700301

Calvo-Serrano, R., González-Miquel, M., & Guillén-Gosálbez, G. (2019). Integrating COSMO-Based σ-Profiles with Molecular and Thermodynamic Attributes to Predict the Life Cycle Environmental Impact of Chemicals. *ACS Sustainable Chemistry and Engineering*, *7*(3), 3575–3583. https://doi.org/10.1021/acssuschemeng.8b06032

Chtita, S., Larif, M., Ghamali, M., Bouachrine, M., & Lakhlifi, T. (2015). QSAR Studies of Toxicity Towards Monocytes with (1,3-benzothiazol-2-yl) amino-9-(10H)-acridinone Derivatives Using

Electronic Descriptors. *Orbital - The Electronic Journal of Chemistry*, *7*(2). https://doi.org/10.17807/orbital.v7i2.677

Cornell, W. D., Cieplak, P., Bayly, C. I., Gould, I. R., Merz, K. M., Ferguson, D. M., Spellmeyer, D. C., Fox, T., Caldwell, J. W., & Kollman, P. A. (1995). A Second Generation Force Field for the Simulation of Proteins, Nucleic Acids, and Organic Molecules. *J. Am. Chem. SOC*, *117*, 5179–5197. https://doi.org/10.1080/07391102.2005.10507028

Gasteiger, J., & Zupan, J. (1993). Neural networks in chemistry. *C'hem. Intr. Ed. EngI*, *32*(4), 503–527. https://doi.org/10.1063/1.47749

Gramatica, P. (2007). Principles of QSAR models validation: Internal and external. *QSAR and Combinatorial Science*, *26*(5), 694–701. https://doi.org/10.1002/qsar.200610151

Gramatica, P., Cassani, S., & Sangion, A. (2016). Aquatic ecotoxicity of personal care products: QSAR models and ranking for prioritization and safer alternatives' design. *Green Chemistry*, *18*(16), 4393–4406. https://doi.org/10.1039/c5gc02818c

Gu, G. H., Noh, J., Kim, I., & Jung, Y. (2019). Machine learning for renewable energy materials. *Journal of Materials Chemistry A*, *7*(29), 17096–17117. https://doi.org/10.1039/c9ta02356a

Hammoudi, N. E. H., Benguerba, Y., Attoui, A., Hognon, C., Lemaoui, T., Sobhi, W., Benaicha, M., Badawi, M., & Monari, A. (2020). In silico drug discovery of IKK-β inhibitors from 2-amino-3-cyano-4-alkyl-6-(2-hydroxyphenyl) pyridine derivatives based on QSAR, docking, molecular dynamics and drug-likeness evaluation studies. *Journal of Biomolecular Structure and Dynamics*, *0*(0), 1–17. https://doi.org/10.1080/07391102.2020.1819878

Hartman, G. H. (1962). A Short History Of. *Chicago Review*, *15*(4), 122. https://doi.org/10.2307/25293701

He, W., Yan, F., Jia, Q., Xia, S., & Wang, Q. (2017). Description of the Thermal Conductivity $\lambda(T, P)$ of Ionic Liquids Using the Structure-Property Relationship Method. *Journal of Chemical and Engineering Data*, *62*(8), 2466–2472. https://doi.org/10.1021/acs.jced.7b00422

Jorgensen, W. L., Maxwell, D. S., & Tirado-Rives, J. (1996). Development and testing of the OPLS all-atom force field on conformational energetics and properties of organic liquids. *Journal of the American Chemical Society*, *118*(45), 11225–11236. https://doi.org/10.1021/ja9621760

Karelson, M., Lobanov, V. S., & Katritzky, A. R. (1996). Quantum-chemical descriptors in QSAR/QSPR studies. *Chemical Reviews*, *96*(3), 1027–1043. https://doi.org/10.1021/cr950202r

Klamt, A., & Schüürmann, G. (1993). COSMO: A new approach to dielectric screening in solvents with explicit expressions for the screening energy and its gradient. *Journal of the Chemical Society, Perkin Transactions 2*, *5*, 799–805. https://doi.org/10.1039/P29930000799

Klamt, A. (1995). Conductor-like screening model for real solvents: A new approach to the quantitative calculation of solvation phenomena. *Journal of Physical Chemistry*, *99*(7), 2224–2235. https://doi.org/10.1021/j100007a062

Li, C., Li, D., Zou, S., Li, Z., Yin, J., Wang, A., Cui, Y., Z. Yaoa, & Zhaoa, Q. (2013). Extraction desulfurization process of fuels with ammonium based deep eutectic solvents. *Green Chemistry*, 1–7. https://doi.org/10.1039/b000000x

Lipkowitz, K. B. (1995). Abuses of Molecular Mechanics. *Journal of Chemical Education*, *72*, 1070–1075. https://doi.org/10.1007/978-981-10-8363-1_8

Liu, X., Wang, C., Lan, T., He, M., & Zhang, Y. (2020). Prediction of Thermal Conductivity for Guiding Molecular Design of Liquids. *ACS Sustainable Chemistry and Engineering*, *8*(15), 6022–6032. https://doi.org/10.1021/acssuschemeng.0c00801

Lloret, J. O., Vega, L. F., & Llovell, F. (2017). Accurate description of thermophysical properties of Tetraalkylammonium Chloride Deep Eutectic Solvents with the soft-SAFT equation of state. *Fluid Phase Equilibria*, *448*, 81–93. https://doi.org/10.1016/j.fluid.2017.04.013

Lyons, J. L., Janotti, A., & Van De Walle, C. G. (2009). Why nitrogen cannot lead to p -type conductivity in ZnO. *Applied Physics Letters*, *95*(25), 1–4. https://doi.org/10.1063/1.3274043

Mcculloch, W. S., & Pitts, W. (1990). A logical calculus nervous activity. *Bulletin of Mathematical Biology*, *52*(l), 99–115. https://doi.org/10.1007/BF02478259

Mitra, I., Saha, A., & Roy, K. (2010). Exploring quantitative structure-activity relationship studies of antioxidant phenolic compounds obtained from traditional Chinese medicinal plants. *Molecular Simulation*, *36*(13), 1067–1079. https://doi.org/10.1080/08927022.2010.503326

Moondra, S., Maheshwari, R., Taneja, N., Tekade, M., & Tekadle, R. K. (2018). Bulk Level Properties and its Role in Formulation Development and Processing. In *Dosage Form Design Parameters* (Vol. 2). Elsevier Inc. https://doi.org/10.1016/B978-0-12-814421-3.00006-3

Mostefaoui, L. (2011). *Contribution à la description et à la compréhension de la solvatation des biomolécules*. l'Universite Abou Bekr Belkaid Tlemcen UABT.

Myles, A. J., Feudale, R. N., Liu, Y., Woody, N. A., & Brown, S. D. (2004). An introduction to decision tree modeling. *Journal of Chemometrics*, *18*(6), 275–285. https://doi.org/10.1002/cem.873

Ojha, P. K., & Roy, K. (2011). Comparative QSARs for antimalarial endochins: Importance of descriptor-thinning and noise reduction prior to feature selection. *Chemometrics and Intelligent Laboratory Systems*, *109*(2), 146–161. https://doi.org/10.1016/j.chemolab.2011.08.007

Othmer, D. F., Bergen, W. S., Shlechter, N., & Bruins, P. F. (1945). LIQUID-LIQUID EXTRACTION DATA Systems Used in Butadiene Uauufaclure from Butylene Glycol. *Industrial & Engineering Chemistry Research*, *37*, 890–894.

Papa, E., & Gramatica, P. (2010). QSPR as a support for the EU REACH regulation and rational design of environmentally safer chemicals: PBT identification from molecular structure. *Green Chemistry*, *12*(5), 836–884. https://doi.org/10.1039/b923843c

Patel, K., Tyagi, C., Goyal, S., & Grover, A. (2014). *CHEMISTRY Curcumin-based IKK b inhibiting anticancer lead design using novel fragment-based group QSAR modelling*. https://doi.org/10.1007/s00044-014-1274-8

Rappé, A. K., Casewit, C. J., Colwell, K. S., Goddard III, W. A., & Skiff, W. . (1992). UFF, a Full Periodic Table Force Field for Molecular Mechanics and Molecular Dynamics Simulations. *American Chemical Society*, *114*, 10024–10035. https://doi.org/10.1007/978-3-642-04431-1_17

Rodriguez, N. R., Requejo, P. F., & Kroon, M. C. (2015). Aliphatic-Aromatic Separation Using Deep Eutectic Solvents as Extracting Agents. *Industrial and Engineering Chemistry Research*, *54*(45), 11404–11412. https://doi.org/10.1021/acs.iecr.5b02611

Shahbaz, K., Baroutian, S., Mjalli, F. S., Hashim, M. A., & Alnashef, I. M. (2012). Densities of ammonium and phosphonium based deep eutectic solvents: Prediction using artificial intelligence and group contribution techniques. *Thermochimica Acta*, *527*, 59–66. https://doi.org/10.1016/j.tca.2011.10.010

Stanton, D. T. (2003). On the Physical Interpretation of QSAR Models. *Journal of Chemical Information and Computer Sciences*, *43*(5), 1423–1433. https://doi.org/10.1021/ci0340658

Torrecilla, J. S., Palomar, J., Lemus, J., & Rodríguez, F. (2010). A quantum-chemical-based guide to analyze/quantify the cytotoxicity of ionic liquids. *Green Chemistry*, *12*(1), 123–13. https://doi.org/10.1039/b919806g

Tropsha, A., Gramatica, P., & Gombar, V. K. (2003). The importance of being earnest: Validation is the absolute essential for successful application and interpretation of QSPR models. *QSAR and Combinatorial Science*, *22*(1), 69–77. https://doi.org/10.1002/qsar.200390007

Warrag, S. E. E., Alli, R. D., & Kroon, M. C. (2019). Liquid–Liquid Equilibrium Measurements for the Extraction of Pyridine and Benzothiazole from n -Alkanes Using Deep Eutectic Solvents. *Journal of Chemical & Engineering Data*. https://doi.org/10.1021/acs.jced.9b00413

Warrag, S. E. E., Darwish, A. S., Abuhatab, F. O. S., Adeyemi, I. A., Kroon, M. C., & Alnashef, I. M. (2020). Combined Extractive Dearomatization, Desulfurization, and Denitrogenation of Oil Fuels Using Deep Eutectic Solvents: A Parametric Study. *Industrial and Engineering Chemistry Research*, *59*(25), 11723–11733. https://doi.org/10.1021/acs.iecr.0c01360

Watkins, J. A., Cusanovich, M. A., Meyer, T. E., & Tollin, G. (1994). A "parallel plate" electrostatic model for bimolecular rate constants applied to electron transfer proteins. *Protein Science*, *3*(11), 2104–2114. https://doi.org/10.1002/pro.5560031124

Yousefinejad, S., & Hemmateenejad, B. (2015). Chemometrics tools in QSAR/QSPR studies: A historical perspective. *Chemometrics and Intelligent Laboratory Systems*, *149*, 177–204. https://doi.org/10.1016/j.chemolab.2015.06.016

Zhang, L., Zhu, H., Oprea, T. I., Golbraikh, A., & Tropsha, A. (2008). QSAR modeling of the blood-brain barrier permeability for diverse organic compounds. *Pharmaceutical Research*, *25*(8), 1902–1914. https://doi.org/10.1007/s11095-008-9609-0

Zubeir, L. F., Held, C., Sadowski, G., & Kroon, M. C. (2016). PC-SAFT Modeling of CO2 Solubilities in Deep Eutectic Solvents. *Journal of Physical Chemistry B*, *120*(9), 2300–2310. https://doi.org/10.1021/acs.jpcb.5b07888

Chapter III

Physicochemical Properties of Deep Eutectic Solvents

Chapter III   Physicochemical Properties of Deep Eutectic Solvents

III.1. Introduction

The interest in green and sustainable solvents has been dramatically increasing in recent years because of the growing awareness of the impact of classical organic solvents on environmental pollution and human health. As a solution to these issues, several greener and more sustainable solvents have been proposed in recent years such as the deep eutectic solvents (DESs).

DESs have many advantageous characteristics and could be considered as a potential replacement for both ionic liquids (ILs) and classical solvents. However, choosing the right DES with the required physiochemical properties for a certain application is an extremely difficult task, especially since large-scale experimental measurements are expensive and time-consuming. Thus, the development of predictive models capable of estimating the properties of these solvents could be considered a powerful tool in screening new green and sustainable DESs.

III.2. Density and Viscosity of Hydrophilic Deep Eutectic Solvents

III.2.1. DESs Experimental Data

As aforementioned previously in chapter II, quantitative structure-property relationship (QSPR) constitutes a powerful analytical method for understanding how the chemical structure of a DES can be correlated with its physicochemical properties. The starting point for deriving QSPR models is the availability of reliable experimental data. A total of 49 DESs reported in the literature (Table III.1) were considered. Each DES was individuated by hydrogen bond acceptor (HBA), hydrogen bond donor (HBD), and molar ratio.

The DESs reported in Table III.1 contain a total number of five HBAs: benzyltriphenyl phosphonium chloride (BTPPC), choline chloride (ChCl), methyltriphenylphosphonium bromide (MTPPB), N,N-diethylethanolammonium chloride (DEEAC), and tetrabutylammonium bromide (TBAB)) and nine HBDs (D-fructose (Fru), diethanolamine (DEA), ethylene glycol (EG), malonic acid (MalA), glycerol (Gly), methyl diethanolamine (MDEA), monoethanolamine (MEA), oxalic acid (OA), triethanolamine (TEA).

Chapter III   Physicochemical Properties of Deep Eutectic Solvents

Table III.1. Deep eutectic solvents were used in the model with their compositions.

HBA	HBD	Mole ratio	Abbrev	Ref
BTPPC	EG	1: 3	DES 1	(Kareem et al., 2010)
	Gly	1: 5	DES 2	
ChCl	Fru	1: 1	DES 3	
	Fru	1.5: 1	DES 4	(Hayyan et al., 2012)
	Fru	2: 1	DES 5	
	Fru	2.5: 1	DES 6	
	DEA	1: 6	DES 7	
	DEA	1: 8	DES 8	(Adeyemi et al., 2018)
	DEA	1: 10	DES 9	
	EG	1: 1.8	DES 10	
	EG	1: 2	DES 11	
	EG	1: 2.5	DES 12	(Shahbaz et al., 2011)
	Gly	1: 1	DES 13	
	Gly	1: 2	DES 14	
	Gly	1: 3	DES 15	
	MalA	1: 1	DES 16	(Bahadori et al., 2013)
	MDEA	1: 6	DES 17	
	MDEA	1: 8	DES 18	
	MDEA	1: 10	DES 19	
	MEA	1: 4	DES 20	
	MEA	1: 5	DES 21	
	MEA	1: 6	DES 22	(Adeyemi et al., 2018)
	MEA	1: 7	DES 23	
	MEA	1: 8	DES 24	
	MEA	1:10	DES 25	
	TEA	1: 2	DES 26	
	OA	1: 1	DES 27	(Bahadori et al., 2013)
MTPPB	EG	1: 3	DES 28	(Shahbaz et al., 2011)
	EG	1: 4	DES 29	(Kareem et al., 2010)
	EG	1: 5	DES 29	
	Gly	1: 2	DES 30	
	Gly	1: 3	DES 31	(Shahbaz et al., 2011)
	Gly	1: 4	DES 32	
	Gly	1: 1.8	DES 33	(Kareem et al., 2010)
	MEA	1: 6	DES 34	
	MEA	1: 7	DES 35	(Adeyemi et al., 2018)
	MEA	1: 8	DES 36	
	MEA	1: 9	DES 37	
DEEAC	MalA	1: 1	DES 38	(Bahadori et al., 2013)
	EG	1: 2	DES 39	
	EG	1: 3	DES 41	
	EG	1: 4	DES 42	(Shahbaz et al., 2011)
	Gly	1: 2	DES 43	
	Gly	1: 3	DES 44	
	Gly	1: 4	DES 45	
TBAB	MEA	1: 4	DES 46	
	MEA	1: 5	DES 47	(Adeyemi et al., 2018)
	MEA	1: 6	DES 48	
	MEA	1: 7	DES 49	

III.2.2. Development of the *σ-Profiles*

Figure III.1 shows the chemical structures of the HBAs and HBDs used to form the 49 DESs. The green-colored area represents the nonpolar part of the DES, the blue-colored area is the HBD part and the red one is the HBA part of the DES.

Hydrogen bond Acceptors

1) Benzyltriphenyl phosphonium chloride	2) Choline chloride	3) N,N- Diethylethanol ammonium chloride	4) Methyltriphenyl phosphonium-bromide	5) Tetrabutyl ammonium bromide

Hydrogen bond donors

1) D-Fructose	2) Diethanolamine	3) Ethylene glycol	4) Glycerol	5) Malonic Acid	6) Methyl diethanolamine

7) Monoethanolamine	8) Oxalic acid	9) Triethanolamine

Key:

Atoms:
- Carbon
- Hydrogen
- Oxygen
- Nitrogen
- Phosphorus
- Bromide
- Chloride
- Fluorine

Colors:
Highly negative	(+0.02 e/Å)
Slightly negative	(+0.01 e/Å)
Neutral	(≈0.00 e/Å)
Slightly positive	(–0.01 e/Å)
Highly positive	(–0.02 e/Å)

Figure III.1. COSMO surfaces and chemical structures of HBAs and HBDs.

III.2.3. Results and Discussion

III.2.3.1. Interpretation of the σ-profile

Figure III.2 and Figure III.3 show the probability distribution (P(σ)) of a molecular surface segment having a specific charge density for the investigated HBAs and HBDs, respectively.
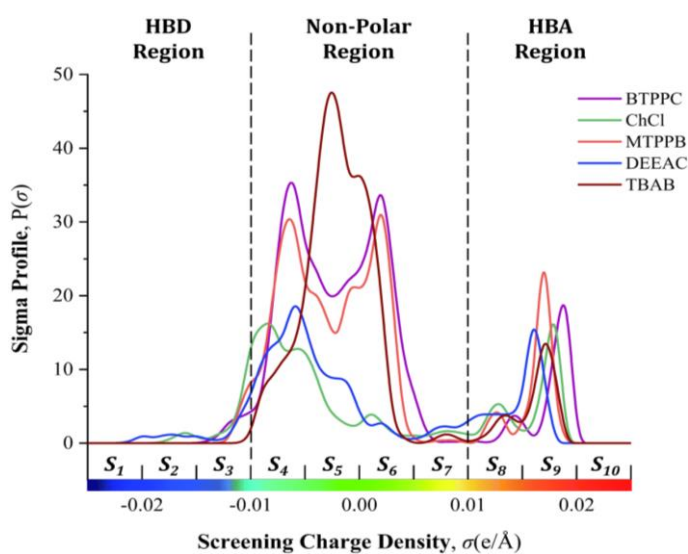
Figure III.2. σ-profiles of the HBAs.
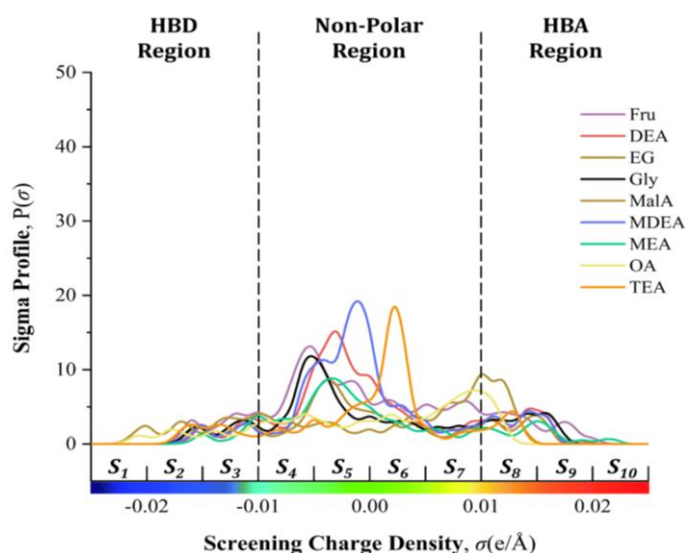
Figure III.3. σ-profiles of the HBDs.

Based on the σ values, the σ-profile curve can be divided into three regions corresponding to HBD, nonpolar, and HBA. In the region of HBD, [-0.025, -0.008], the characteristic peaks of the hydrogen atoms (e.g. in N-H or O-H bonds) are present. The nonpolar region [-0.008, 0.008] is characteristic of the CH_3 and CH_2 alkyl groups. Finally, the region [0.008, 0.025] is characteristic of hydrogen acceptor atoms (e.g. N, O).

III.2.3.2. Density Model

The DES properties were analyzed and the corresponding model equations were derived using the experimental data listed in Table III.1. For the determination of the model expression for density, 310 experimental data points for 17 DESs were used (Table III.2).

Table III.2. DESs used for the density model.

Number of experiments	DESs
310	10-15, 28, 30-33, 40-45

The stepwise regression algorithm was used for the analysis of the experimental density data expressed by the MLR model descriptors of the σ-profile's surfaces, temperature, and the interaction between them. The summary of MLR performance for the entire data set is given in Table III.3. From the obtained value of the coefficient of determination (R^2) and the root mean squared error (*RMSE*), 0.9924, 0.0097, respectively, it can be concluded that the MLR model fits well the experimental data set. The relationship between the density and the descriptors is satisfactorily multi-linear.

Table III.3. Statistical parameters of the MLR model for density.

R^2	0.9924
$R^2_{adjusted}$	0.9919
RMSE	0.0097

Chapter III   Physicochemical Properties of Deep Eutectic Solvents

The parameters of the ANOVA analysis carried out for the individuation of the descriptors that have a significant influence, while the corresponding coefficients of the significant descriptors are listed in Table III.4:

Table III.4. Estimation of the model coefficients for the density model.

Term	Coefficient	Estimate	Standard Error	$|t\text{-}Ratio|$	P_{value}
Intercept	a_0	-4.37	1.93	2.27	0.0240
S_2	a_2	6152.85	2269.48	2.71	0.0071
S_3	a_3	380.74	69.029	5.52	<.0001
S_4	a_4	-591.00	229.37	2.58	0.0105
S_5	a_5	169.87	64.90	2.62	0.0093
S_6	a_6	1196.74	433.66	2.76	0.0062
S_7	a_7	-3881.25	1416.35	2.74	0.0065
S_8	a_8	204.35	75.16	2.72	0.0069
S_9	a_9	-289.62	62.216	4.66	<.0001
T	a_{11}	-7.01×10^{-4}	2.53×10^{-5}	28.73	<.0001
$(S_2\text{-}\bar{S_2})\,(T\text{-}\bar{T})$	a_{211}	-0.62	0.04	15.41	<.0001
$(S_3\text{-}\bar{S_3})\,(T\text{-}\bar{T})$	a_{311}	-0.55	0.07	8.30	<.0001
$(S_4\text{-}\bar{S_4})\,(T\text{-}\bar{T})$	a_{411}	-0.06	0.01	5.48	<.0001
$(S_6\text{-}\bar{S_6})\,(T\text{-}\bar{T})$	a_{611}	-0.09	0.01	10.09	<.0001
$(S_7\text{-}\bar{S_7})\,(T\text{-}\bar{T})$	a_{711}	0.14	0.02	8.41	<.0001
$(S_9\text{-}\bar{S_9})\,(T\text{-}\bar{T})$	a_{911}	0.24	0.036	6.60	<.0001
$(S_2\text{-}\bar{S_2})\,(S_4\text{-}\bar{S_4})$	a_{24}	3023.52	1048.02	2.88	0.0042
$(S_2\text{-}\bar{S_2})\,(S_8\text{-}\bar{S_8})$	a_{28}	-264.91	73.73	3.59	0.0004
$(S_3\text{-}\bar{S_3})\,(S_5\text{-}\bar{S_5})$	a_{35}	3297.00	264.86	12.45	<.0001
$(S_3\text{-}\bar{S_3})\,(S_6\text{-}\bar{S_6})$	a_{36}	-6274.55	1043.71	6.01	<.0001
$(S_5\text{-}\bar{S_5})\,(S_9\text{-}\bar{S_9})$	a_{59}	-1823.41	168.17	10.84	<.0001

$\bar{T}$: Average temperature values; $\bar{S_i}$: mean values of the descriptors S_i; $\bar{S_2} = 1.70 \times 10^{-3}$; $\bar{S_3} = 6.00 \times 10^{-3}$; $\bar{S_4} = 1.77 \times 10^{-2}$; $\bar{S_5} = 7.60 \times 10^{-2}$; $\bar{S_6} = 3.03 \times 10^{-2}$; $\bar{S_7} = 1.38 \times 10^{-2}$; $\bar{S_9} = 8.80 \times 10^{-3}$; $\bar{T} = 333.15$

In particular, it was found that S_1 and S_{10} have no significant effect on the dependent variable with a p-value greater than 5%. Therefore, a_1 and a_{10} were set equal to zero. However, all the other descriptors were significant with a p-value lower than 5% and accordingly were retained in the model (Table III.4). It was found that there was a combined effect on the density of S_2 with S_4 (+), S_8 (-) and T(-); of S_3 with S_5 (+), S_6 (-) and T(-); of S_5 with S_9 (-); of S_6 with T(-); and finally S_7 and S_9 with T(+). Where the sign, given between parenthesis, indicates positive (+) or negative (-) effects. It should be noted that temperature has a double effect on density: a simple negative effect (a_{11}<0) and a combined effect with sigma surface segments, which could be positive or negative, e.g., S_7 and S_9 (a_{711} and a_{911}>0). The temperature has an effect on polarity which in turn influences density. The positive sign of a_{711} and a_{911} is due to the fact that the negative effect of S_7 and S_9 (a_7<0, a_9<0) combined with the negative effect of temperature (a_{11}<0) gives a positive effect on density which means a relaxation of the DES system at the molecular level, i.e. reduction of the HBA-HBD interactions strength when the increasing temperature. The experimental and calculated values are shown as a parity diagram in Figure III.4. In conclusion, the best expression of the MLR model for density is as follows:

$\rho = -4.37 + 6152.85\ (S_2) + 380.74\ (S_3) - 591.00\ (S_4) + 169.87\ (S_5) + 1196.74\ (S_6) - 3881.25\ (S_7) + 204.35\ (S_8) - 289.62\ (S_9) - 7.00\times10^{-4}\ (T) + 3023.52\ (S_2 - \overline{S_2})(S_4 - \overline{S_4}) - 264.91\ (S_2 - \overline{S_2})(S_8 - \overline{S_8}) - 0.62\ (S_2 - \overline{S_2})(T - \overline{T}) + 3297.00\ (S_3 - \overline{S_3})(S_5 - \overline{S_5}) - 6274.55\ (S_3 - \overline{S_3})(S_6 - \overline{S_6}) - 0.55\ (S_3 - \overline{S_3})(T - \overline{T}) - 0.06\ (S_4 - \overline{S_4})(T - \overline{T}) - 1832.41\ (S_5 - \overline{S_5})(S_9 - \overline{S_9}) - 0.09\ (S_6 - \overline{S_6})(T - \overline{T}) + 0.14\ (S_7 - \overline{S_7})(T - \overline{T}) + 0.24\ (S_9 - \overline{S_9})(T - \overline{T})$

$$(III.1)$$
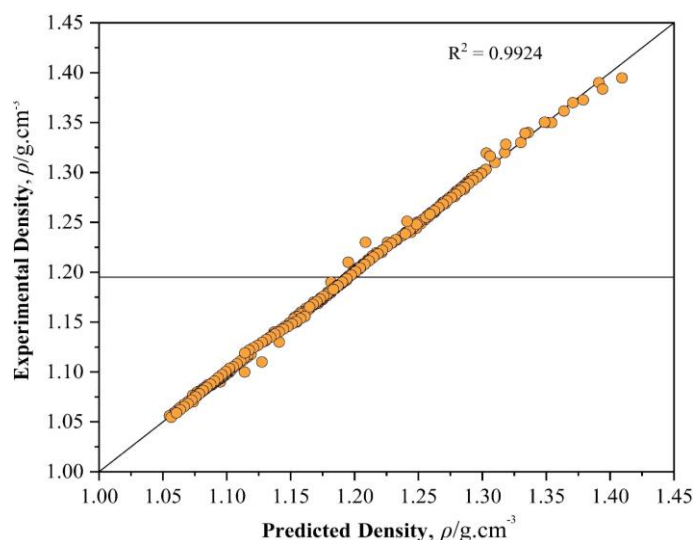
Figure III.4. Experimental values of density versus predicted values using MLR model.

Remarkably, all density points lie on the diagonal line, with a very narrow dispersion. There was only one point that have a fairly acceptable difference between observed and predicted values. The good prediction of the data is confirmed by the residue analysis (Figure III.5), which in all cases was less than 0.02 (absolute value).
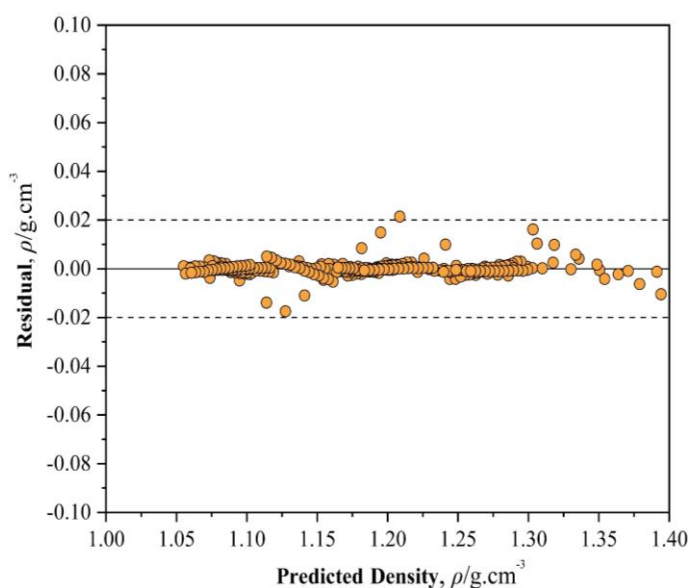
Figure III.5. Residuals vs. predicted values of density.

III.2.3.3. Viscosity Model

The viscosity of DES is of paramount importance for industrial applications of these solvents. To develop an appropriate model for the prediction of DES viscosity, 193 experimental points retrieved from the literature, corresponding to 24 of the DES listed in Table III.5, were used.

The stepwise regression algorithm was used for the regression analysis of the experimental viscosity data expressed by the MLR descriptors: *σ-profile* surfaces and temperature. A summary of MLR performances for the entire data set is given in Table III.6.

In general, the values of R^2 =0.9874, and *RMSE*=0.1047 indicate that the MLR model for viscosity shows very good performance as it provides a precise fit of the experimental data set. The relationship between the viscosity and the descriptors $S_{\sigma\text{-profiles}}$ and temperature is satisfactorily multilinear.

Table III.5. DESs used in the development of the viscosity model.

Number of experiments	DESs
193	1-5, 8-9, 16-18, 21-25, 29, 34-37, 46-49

Table III.6. Statistical Parameters of the MLR for viscosity determination.

R^2	0.9874
$R^2_{adjusted}$	0.9845
RMSE	0.1047

A detailed statistical analysis to identify the descriptors that have a significant influence on the description of the experimental viscosity values. The purpose behind this analysis is to find a reduced expression of the MLR model equation similar to the generic (Eq. II.2). To this end, ANOVA analysis was used to determine the model expression coefficients, as indicated in Table III.7 and Table III.8.

Table III.7. Analysis of variance of the MLR for viscosity.

Source	Degrees of freedom	Sum of squares	Mean squares	F-ratio
Model	9	134.8731	14.9859	341.3182
Residuals	183	1.7123	0.0094	Prob. > F
Total	192	136.5854	-	<0.0001

The ANOVA analysis showed that the sigma surface S_1, …, S_{10} descriptors have no significant effect on the viscosity with a p-value of acceptance stated at 0.05. Therefore, the constants $a_1, .., a_{10}$ were set to 0 in the model expression. On the other hand, the description of the viscosity is significantly affected by the temperature and the interaction between temperature and sigma surfaces (except S_3 and S_8) at a level of confidence greater than 95% (Table III.8).

Table III.8. Estimation of the model coefficients for the viscosity model.

Term	Coefficient	Estimate	Standard Error	$\|t\text{-}Ratio\|$	P_{value}
T	a_{11}	-0.02	3.00×10^{-4}	51.95	<.0001
$(S_1\text{-}\bar{S_1})\,(T\text{-}\bar{T})$	a_{111}	-34.55	11.91	2.90	0.0043
$(S_2\text{-}\bar{S_2})\,(T\text{-}\bar{T})$	a_{211}	3.86	0.78	4.96	<.0001
$(S_4\text{-}\bar{S_4})\,(T\text{-}\bar{T})$	a_{411}	-2.51	0.68	3.72	0.0003
$(S_5\text{-}\bar{S_5})\,(T\text{-}\bar{T})$	a_{511}	-0.62	0.20	3.03	0.0028
$(S_6\text{-}\bar{S_6})\,(T\text{-}\bar{T})$	a_{611}	0.60	0.09	6.95	<.0001
$(S_7\text{-}\bar{S_7})\,(T\text{-}\bar{T})$	a_{711}	2.69	1.27	2.11	0.0361
$(S_9\text{-}\bar{S_9})\,(T\text{-}\bar{T})$	a_{911}	3.09	1.19	2.61	0.0100
$(S_{10}\text{-}\bar{S_{10}})\,(T\text{-}\bar{T})$	a_{1011}	18.64	2.14	8.73	<.0001

$\bar{T}$: Average temperature values; $\bar{S_i}$: mean values of the descriptors S_i ; $\bar{S_1}$=1.42 $\times10^{-5}$; $\bar{S_2}$=1.10 $\times10^{-3}$; $\bar{S_4}$=4.50 $\times10^{-2}$; $\bar{S_5}$=9.87 $\times10^{-2}$; $\bar{S_6}$=8.31 $\times10^{-2}$; $\bar{S_7}$=1.93 $\times10^{-2}$; $\bar{S_9}$=1.94 $\times10^{-2}$; $\bar{S_{10}}$=7.00 $\times10^{-4}$; $\bar{T}$=326.98

As expected, the temperature was found to have a negative effect on viscosity. The interaction's terms with a p-value lower than 5%, describe the combined effect of sigma surfaces (polarity) with temperature on viscosity.

It was found that the negative effect of temperature when combined with the positive effect of S_2, S_6, S_7, S_9 and S_{10} (the direct effect of these descriptors is found statistically insignificant), gives a negative effect on the viscosity. This means that S_2 (HBD region: medium polarity), {S_6, S_7}(nonpolar region: negative charges), and S_9, S_{10} (HBA region), are the important regions when searching for reducing viscosity with increasing temperature. On the contrary, if we want to increase viscosity with temperature, we have to increase the surface S_1 (HBD region: high polarity), and S_4, S_5 (nonpolar region: positive charges). The MLR model for viscosity is given as follows:

$Log(\eta) = -\ 0.02\ (T) - 34.55\ (S_1-\bar{S_1})(\,T-\bar{T})\ +\ 3.86\ (S_2-\bar{S_2})(\,T-\bar{T}) - 2.51\ (S_4-\bar{S_4})(\,T-\bar{T})\ -\ 0.55\ (S_5-\bar{S_5})(\,T-\bar{T})\ +\ 2.51\ (S_6-\bar{S_6})(\,T-\bar{T})\ +\ 2.69\ (S_7-\bar{S_7})(\,T-\bar{T})+\ 3.09\ (S_9-\bar{S_9})(\,T-\bar{T})\ +\ 18.64\ (S_{10}-\bar{S_{10}})(\,T-\bar{T})$

(III.2)

The parameters that are preceded by a negative sign cause a decrease in the viscosity of the DES, while a positive sign gives a positive effect (increases the viscosity-value). (Eq. III.2) was determined by the regression analysis performed on 193 total experimental data points. In Figure III.6, the model results were represented as a parity diagram.
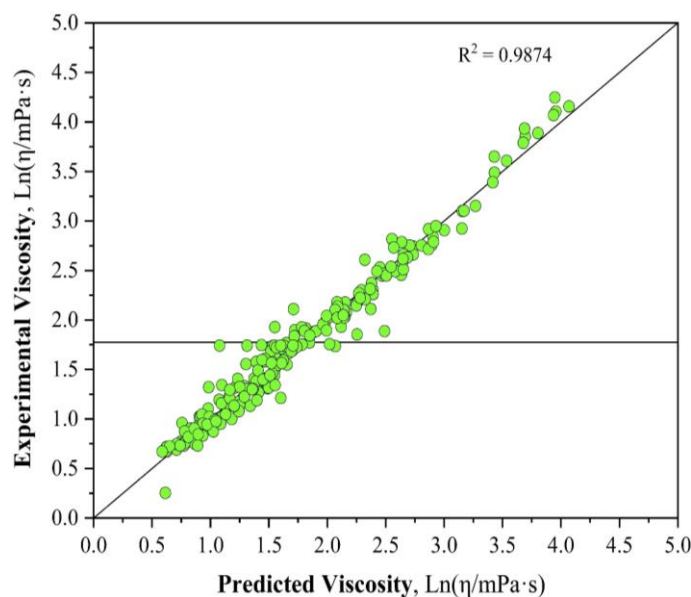
Figure III.6. Observed values of viscosity as a function of the predicted values.

As can be observed, most of the viscosity values were correctly predicted by the model as the points are very close to the diagonal line with no significant dispersion. The same result can be retrieved by the analysis of the residue (Figure III.7), which is in most cases less than 0.3 (absolute value), and confirm the optimal prediction of the data.
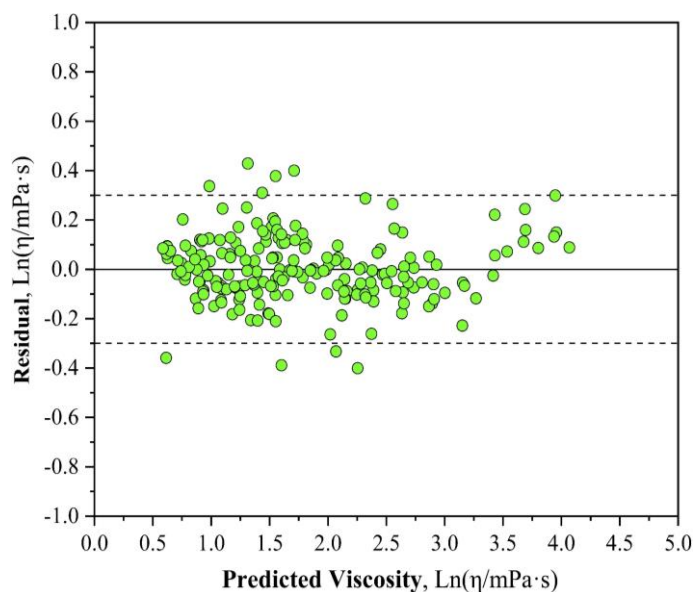
Figure III.7. Residues vs predicted values of viscosity.

III.2.3.4. Applicability Domain

The Applicability Domain (AD) of a model is one of the most critical parameters, especially in QSPR studies, as it defines the theoretical "chemical scope" where a QSPR model is considered reliable (Gramatica, 2007; Tropsha et al., 2003). Therefore, to help evaluate the proposed QSPR models, the William plots of both models are presented in Figure III.8. The AD boundaries are

defined between (i) the leverage threshold $0 < h_i < h^*$ (vertical dashed line), and (ii) the standardized residuals $-3 < SDR < +3$ (horizontal dashed line).

a) Density Model
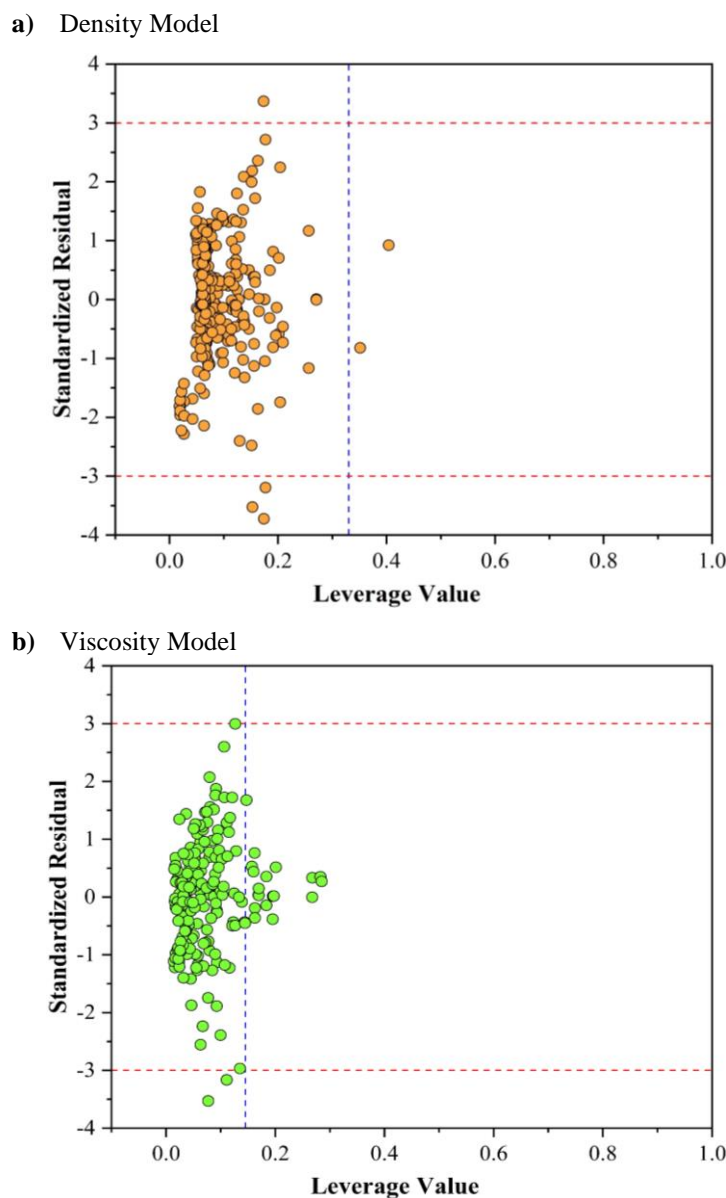
b) Viscosity Model

Figure III.8. William plot for (a) density and (b) viscosity models.

When comparing the domains of applicability of the density and viscosity models in Figure III.8, it can be observed that the density model AD is slightly wider than that of the viscosity model $(h_\rho^* = 0.2129 > h_\eta^* = 0.1554)$. Also, it can be seen that remarkably the AD structural range of both the density and viscosity models are very large ($AD_{coverage} > 95\%$). However, that being said, predictions of some DESs at several exception temperatures could be regarded as "borderline AD". The borderline DESs have been split into two main categories, (i) structural borderline outlier "DESs with an h_i value close to h^*", and (ii) response borderline outlier "DESs with SDR values close to ± 3".

Chapter III   Physicochemical Properties of Deep Eutectic Solvents

III.3. Density and Viscosity of Hydrophobic Deep Eutectic Solvents

III.3.1. Experimental Dataset

Two datasets, one for density and one for viscosity, obtained from the literature were utilized in the development of the QSPR models. The density dataset (ρ/g·cm^{-3}) consisted of 606 experimental points and the viscosity dataset (η/mPa·s) consisted of 530 experimental points. To the best of our knowledge, the dataset utilized includes all the temperature-dependent density and viscosity measurements reported in the literature for HDESs. The complete datasets are available in Table 1 in (Appendix A). The collected dataset includes 54 HDESs that are prepared from 34 HBAs and HBDs. Table III.9 lists the HDESs used with their corresponding compositions and references. The HDESs cover a wide range of molecules with different cations, anions, and functional groups. Also, both datasets cover a varied range of density (1.0716 – 0.8200 g·cm^{-3}) and viscosity (1,706.2 – 1.3 mPa·s) measurements that also include a wide range of temperatures (373.2 – 278.2 K) and molar ratios (19:1 – 0.73:1) measured at atmospheric pressure (1.01 bar). This wide range of data and molecular structural coverage is expected to enhance the robustness and scope of the models by accounting for the HDES constituents, the molar ratio, and the temperature. It is worth noting that the effect of pressure on the properties of the HDESs was not accounted for in the models due to the lack of pressure-dependent experimental data in the literature.

Table III.9. Hydrophobic Deep Eutectic Solvents with their compositions, densities, viscosities.

HDES#	Const 1	Const 2	Molar Ratio	ρ (g·cm^{-3})	η (mPa·s)	T (K)	Ref.
HDES1	DA	TBAC	2:1	0.917	265.3	298.2	
HDES2		THAC	2:1	0.891	172.9	298.2	
HDES3		MOAB	2:1	0.942	576.5	298.2	
HDES4		MOAB	2:1	0.896	783.4	298.2	(Van Osch et al., 2015)
HDES5		TOAB	2:1	0.930	636.4	298.2	
HDES6		TOAC	2:1	0.889	472.6	298.2	
HDES7		TOAC	1.5:1	0.888	-	298.2	(Zubeir et al., 2018)
HDES8		Lid	2:1	0.958	237.5	298.2	
HDES9		Lid	3:1	0.950	208.5	298.2	(Dietz et al., 2019; Van Osch et al., 2016)
HDES10		Lid	4:1	0.942	142.0	298.2	
HDES11		SoD	4:1	0.924	60.5	298.2	(Florindo et al., 2018)
HDES12	DoA	OcA	1:3	0.901	7.1	298.2	
HDES13		NoA	1:3	0.897	8.6	298.2	(Florindo, Celia-Silva, et al., 2018)
HDES14		DeA	1:2	0.894	10.8	298.2	
HDES15	Ethp	MOAC	2:1	0.995	957.5	298.2	(Li et al., 2019)
HDES16	Ibp	TOAC	3:7	0.892	1029.0	298.2	(Tereshatov et al., 2016)
HDES17	DL-Men	AA	1:1	0.931	8.7	298.2	(Ribeiro et al., 2015)

HDES18		LacA	1:2	1.033	218.9	298.2	
HDES19		PyA	1:2	0.995	30.0	298.2	
HDES20		DoA	2:1	0.894	24.4	298.2	Verma & Banerjee, 2018)
HDES21		HexdA	12:1	0.890	-	298.2	(Verma & Banerjee, 2019)
HDES22		HBenA	7:1	0.920	≈1420	298.2	(Mat Hussin et al., 2020)
HDES23		Mpen	2:1	0.901	68.4	298.2	
HDES24		Dec	2:1	0.871	28.0	298.2	(Almustafa et al., 2020)
HDES25		Ses	1:1	1.072	≈360	298.2	
HDES26		Thy	1:1	0.929	≈180	298.2	(Mat Hussin et al., 2020)
HDES27	L-Men	OcA	1.5:1	0.900	15.3	298.2	
HDES28		DeA	1.5:1	0.897	18.9	298.2	(Martins et al., 2018)
HDES29		DeA	1:1	0.896	22.0	298.2	(Dietz et al., 2019)
HDES30		DoA	3:1	0.893	28.1	298.2	
HDES31		TedA	4:1	0.892	34.0	298.2	
HDES32		HexdA	5.67:1	0.881	15.3	313.2	(Martins et al., 2018)
HDES33		OcdA	9:1	0.881	16.6	313.2	
HDES34		TedA	2:1	0.869	31.7	298.2	(Van Osch et al., 2020)
HDES35		Bor	7:3	0.915	110.4	298.2	
HDES36		Cam	1:1	0.924	16.4	298.2	
HDES37		Sob	19:1	0.876	6.7	333.2	(Martins et al., 2019)
HDES38		Thy	1:1	0.933	38.1	298.2	
HDES39	OleA	THAC	2:1	0.867	244.7	298.2	(Tereshatov et al., 2016)
HDES40	Thy	MP-ol	2:1	0.959	32.7	298.2	
HDES41		Dec	2:1	0.915	14.4	298.2	(Almustafa et al., 2020)
HDES42		OcA	0.73:1	0.930	8.0	298.2	
HDES43		DeA	1:1	0.930	12.2	298.2	
HDES44		DodA	1.22:1	0.922	12.4	303.2	
HDES45		TedA	3:1	0.928	8.7	313.2	(Martins et al., 2018)
HDES46		HexdA	4:1	0.929	9.2	313.2	
HDES47		OcdA	9:1	0.936	6.9	318.2	
HDES48		Bor	1:1	0.963	43.1	308.2	
HDES49		Cam	1:1	0.967	20.8	298.2	(Martins et al., 2019)
HDES50		Lid	2:1	0.989	99.0	298.2	(Dietz et al., 2019)
HDES51	TOPO	DA	1:1	0.881	39.0	298.2	
HDES52		DodA	1:1	0.880	46.5	298.2	(Riveiro et al., 2020)
HDES53		Ph	1:2	0.933	12.4	298.2	
HDES54		Ph	1:1	0.907	43.0	298.2	(Gilmore et al., 2018)

III.3.2. Development of the σ-Profiles

The 3D molecular structures of each HBA and HBD were first built *via* the Turbomole software (TmoleX version 4.2) by inputting the SMILES "Simplified Molecular Input Line Entry Specification" of each molecule into the software. Figure III.9 shows the 3D structures of the 34 modeled HBAs and HBDs plotted *via* COSMOThermX.

1) Tetraoctyl-ammonium Bromide

2) Tetraoctyl-ammonium Chloride

3) Tetraheptyl-ammonium Chloride

4) Methyltrioctyl-ammonium Bromide

5) Methyltrioctyl-ammonium Chloride

6) Trioctyl-phosphine oxide

7) Tetrabutyl-ammonium Chloride

8) Sodium Dodecanoate

9) Camphor

10) DL-Menthol

11) L-Menthol

12) Thymol

13) trans-Sobrerol

14) Sesamol

15) Phenol

16) Ethylparaben

17) Lidocaine

18) Acetic Acid

19) Lactic Acid

20) Pyruvic Acid

21) Octanoic Acid

22) Nonanoic Acid

23) Decanoic Acid

24) Dodecanoic Acid

25) Tetradecanoic Acid

26) Hexadecanoic Acid

27) Octadecanoic Acid

28) Oleic Acid

| 29) 3-Hydroxybenzoic Acid | 30) 1-Decanol | 31) 1-Tetradecanol | 32) Borneol |

| 33) 2-Methyl-2,4-pentanediol | 34) Ibuprofen | Key: |

Atoms:
- ● Carbon
- ○ Hydrogen
- ● Oxygen
- ● Nitrogen
- ● Phosphorus
- ● Bromide
- ● Chloride
- ● Sodium

Colors:
- ■ Highly negative   (+0.02 e/Å)
- ■ Slightly negative (+0.01 e/Å)
- ■ Neutral   (≈0.00 e/Å)
- ■ Slightly positive (–0.01 e/Å)
- ■ Highly positive   (–0.02 e/Å)

Figure III.9. 3D structures of the 34 modeled HBAs and HBDs.

III.3.3. Model Evaluation

To evaluate the predictive capability of the models, the datasets were divided into a training and a testing set before model development. The training set consisted of nearly ≈70% of the experimental data, while the remaining 30% was utilized as a testing set. The HDESs in the testing set were never utilized in the development of the models and were only used to test the final models. The dataset was split through the structural similarity technique (Gramatica, 2007; Gramatica et al., 2016). In this technique, first, the molecular descriptors of each HDES in the ten regions were combined and averaged into one descriptor denoted as $S_{1-10,avg}^{HDES}$. Second, the HDESs were sorted according to their $S_{1-10,avg}^{DES}$, and then, one out of every three or four HDESs (≈30%) were put into the external testing set. By utilizing this method, the selection of a structurally meaningful training and external testing set was realized.

The division of the datasets for both the density and viscosity models are shown in Table III.10. The external predictive power of the model was then evaluated *via* the external coefficient of determination ($R^2_{external}$).

Table III.10. Division of the density and viscosity experimental data into a training and a testing set.

	Density Model	Viscosity Model
Total number of HDESs	52	45
HDESs in training set	37	32
HDESs in testing set	15	13
Total number of data points	606	530
Data points in training set	419	377
Data points in testing set	187	153
HDESs considered in training set	HDESs 1-3, 5, 7-8, 10-11, 13-17, 19-20, 23-27, 30-31, 33-38, 40-41, 43-45, 47-48, 51-53	HDESs 1-4, 6, 8, 10-11, 15-16, 18-20, 28, 30-34, 36-38, 42-44, 46, 48-52, 54
HDESs considered in testing set	HDESs 4, 6, 9, 12, 18, 21, 22, 28, 32, 36, 39, 42, 46, 49, 54	HDESs 5, 9, 12-14,17, 27, 29, 35, 39, 45, 47, 53

III.3.4. Dataset Interpretation

we aim to identify trends from the density and viscosity experimental data of the HDESs previously reported in the literature Table III.9.

III.3.4.1. Density Model

The density of a mixture is associated with (i) the molecular packing of the individual constituents, and (ii) the molecular interactions between the constituents (Van Osch et al., 2020). As it can be observed from Table III.9, the density of HDESs covers a relatively wide range of densities (0.867 – 1.072 g·cm^{-3}) at 298.2 K. This is valuable from a solvent design perspective as it enables more opportunities for an objective-oriented solvent selection process. Also, all the HDESs in Table III.9 were reported to exhibit a linear decrease of density with temperature, which was expected as this is a universal tendency in the density of solvents (Van Osch et al., 2020). The effect of saturating the HDESs with water on the density was reported by Ribeiro *et al.*(Ribeiro et al., 2015). Their results showed that the addition of water tends to increase the density of the HDESs. The amount of the increase was highly dependent on the hydrophobicity of the HDES constituents.

With regards to ionic-based HDESs, it can be seen that an increase in the chain length of the cation leads to a decrease in the density of an HDES (Van Osch et al., 2015) (*e.g.,* tetrabutyl-ammonium > tetraheptyl-ammonium). Conversely, for the same cation and HBD, the bromide anion was observed to exhibit higher densities than that of chloride anion (*e.g.*, tetraoctyl-ammonium bromide > tetraoctyl-ammonium chloride) (Van Osch et al., 2015). These trends are in agreement with the trends observed for the density of Ils (Rocha et al., 2013). It can also be seen that when comparing different HBDs, the HDESs containing acids had slightly higher densities than the HDESs containing alcohols (*e.g.,* decanoic acid > 1-decanol). The HBD chain length was

also observed to affect the density of the HDESs, where HDESs containing longer chains exhibited lower densities (*e.g.,* octanoic acid > dodecanoic acid, and 1-decanol > 1-tetradecanol). In terms of the effect of the molar ratio, a proportional relationship of the density of HDESs with the components molar ratio is observed. For instance, the density of trioctyl-phosphine oxide and phenol was higher at a 1:2 ratio > 1:1 ratio, which is consistent with the individual component's density (phenol > trioctyl-phosphine oxide). Another example can be observed by fixing a component such as thymol at a 2:1 ratio with other components, thymol: lidocaine > thymol:2-methyl-2,4-pentanediol > thymol:1-decanol, which is consistent with the trend of the individual component density of component 2 (lidocaine > 2-methyl-2,4-pentanediol > 1-decanol).

III.3.4.2. Viscosity Model

From an industrial and application standpoint, the viscosity of solvents is one of the most critical solvent selection parameters. The viscosity of mixtures is usually governed by the strength of intermolecular interactions between the mixture's constituents. Generally, solvents that are more polar tend to be more viscous than similar non-polar solvents (van Osch et al., 2020) (*e.g.,* nonanoic acid > nonane). Since DESs are formed based on hydrogen bonding molecular interactions, it is expected that high viscosities of these solvents would be observed as the hydrogen bonds formed between the molecules limit their mobility within the mixture. For instance, glucose-based DESs such as choline chloride: glucose were reported to have high viscosities in the range of 8,000 – 10,000 mPa·s at 298.2 K (Hayyan et al., 2013). However, since HDESs are considered to be much less polar than their hydrophilic counterparts, viscosities as low as 6.7 and 7.1 mPa·s have been reported for L-menthol: sobrerol (19:1)(Martins et al., 2019) and dodecanoic acid: octanoic acid (1:3) (Florindo, Romero, et al., 2018), respectively. As it can be observed from Table III.9, the viscosity of HDESs covers a relatively wide range of viscosities (1420 – 7 mPa·s) at 298.2 K. As aforementioned, this is of great significance as it enables an objective-oriented solvent design process. Furthermore, all the viscosities of the HDESs listed in Table III.9 were reported to be very sensitive to temperature following an exponential Arrhenius behavior. A significant decrease in the viscosity of the HDESs is observed when increasing the temperature. The effect of the addition of water on the viscosity of HDESs was also reported by Ribeiro *et al.* (Ribeiro et al., 2015), where they found that the saturation of water decreases the viscosity of the HDESs, relative to the hydrophobicity of the HDES constituents.

When comparing ionic based and non-ionic based HDESs, it can be observed that the viscosities of non-ionic based HDESs are generally lower than that of the ionic based HDESs (*e.g.,* tetraalkylammonium anion: decanoic acid > menthol/thymol: decanoic acid). This trend could be

attributed to the fact that molecular-based HDESs have less molecular interactions when compared to ionic-based HDESs. Also, regarding ionic-based HDESs, the viscosity was generally observed to increase as the chain length of the cation increases (*e.g.,* tetraoctyl-ammonium > tetrabutyl-ammonium). While, for the same cation and HBD, the bromide anion was generally observed to have higher viscosities than that of the chloride anion (*e.g.,* tetraoctyl-ammonium bromide > tetraoctyl-ammonium chloride). These trends are also in agreement with the trends observed for the viscosities of Ils (Rocha et al., 2013). In terms of comparing different HBDs, it can be observed that HDESs with longer chain lengths were observed to have slightly higher viscosities (*e.g.,* menthol: decanoic acid > menthol octanoic acid). Finally, when investigating the effect of the molar ratio it should be noted that, unlike density, when fixing a particular HBA with an HBD no clear trend was observed on the viscosity of the HDESs. This is presumably because the effect of the molar ratio on viscosity is highly dependent on the intermolecular interactions between the HDES constituents, and hence, should be studied on a case-by-case basis.

III.3.5. Results and Discussion

III.3.5.1. Physical Meaning of $S_{\sigma-profile}$ Molecular Descriptors

Figure III.10 shows the relative probability distributions, *σ-profiles*, of the 34 investigated hydrophobic HBAs and HBDs. The *σ-profiles*, $P(\sigma)$, describes the amount of surface segments with a certain screening charge density of σ on its molecular surface (Kahlen et al., 2010). Positive charge densities ($\sigma > 0$) correspond to the negative polarity surfaces within a molecule, while the negative charge densities ($\sigma < 0$) represent the positive polarity surfaces. The neutral charge densities ($\sigma \approx 0$) correspond to the non-polar (hydrophobic) surfaces within a molecule (Kahlen et al., 2010; Moity et al., 2012). Thus, on the basis of the σ values, the curve can qualitatively be categorized into 3 regions: the HBD region ($- 0.025 < \sigma < - 0.010$), the non-polar region ($- 0.010 < \sigma < + 0.010$), and the HBA region ($+ 0.010 < \sigma < + 0.025$). The separation of the regions (by vertical dashed lines) and their respective $S_{\sigma-profile}$ molecular descriptors ($S_1 - S_{10}$) are shown in Figure III.10.
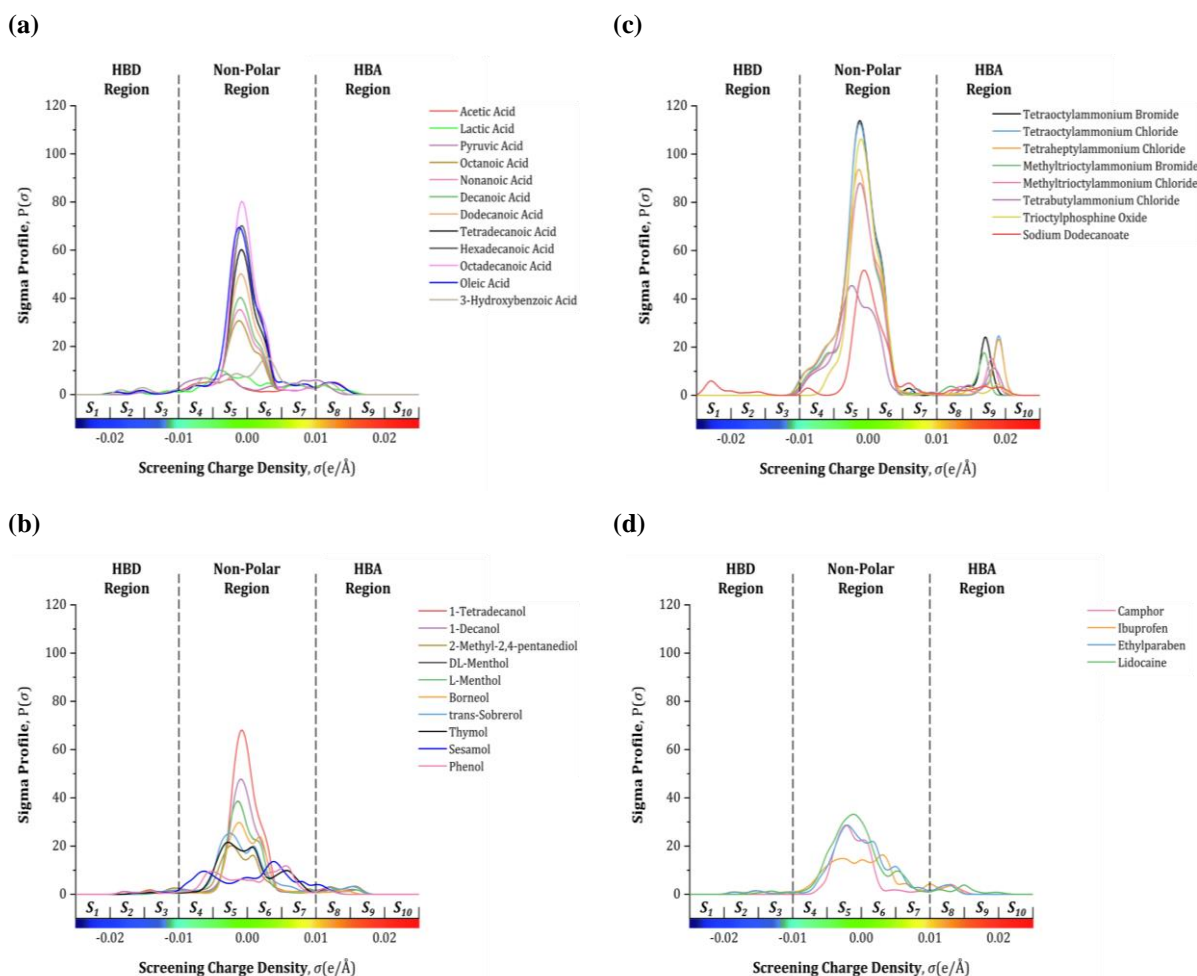
Figure III.10. The calculated σ-profiles of the 34 constituents.

It should be noted that in Figure III.10, the molecules have not been clearly categorized as "HBA" or "HBD". This is due to the dual nature of many hydrophobic HBAs and HBDs, where most of the molecules could be categorized both as an HBA in some HES mixtures and as an HBD in other types of HDES mixtures (Florindo et al., 2018; Martins et al., 2019) (*e.g.,* acids, terpenes, *etc.*). For instance, when analyzing the *σ-profile* of oleic acid, peaks in both the HBA and HBD regions of the *σ*-range can be found. Nevertheless, Figure III.10 has been divided into four parts as follows: (a) acids, (b) alcohols, (c) salts, and the remaining cyclic molecules are grouped in (d).

The concentration and nature of each constituent atom in the *σ-profile* curve can be identified by its location, height, and width in the *σ*-range. For example, the peaks in the non-polar region around zero charge densities correspond to the non-polar alkyl groups of the molecules (–CH$_3$, –CH$_2$, and –CH). Figure III.10 shows that the longer the chain lengths of the molecules, the higher height of the peaks in the S_5 and S_6 range (*e.g.,* decanoic acid peak > octanoic acid peak). The peaks in the HBD region mainly represent the H$^+$ parts of the molecules (in S_2 and S_3) and the Na$^+$ cation (in S_1). The positively charged ammonium (N$^+$) and phosphonium (P$^+$) parts of the

molecules are represented in the peaks of the S_4 range. The electron-withdrawing parts of the molecules are represented in the HBA region. For example, the peaks contained within the S_9 and S_{10} range correspond to the Cl$^-$ and Br$^-$ anions, while the negatively polarized O$^{\delta-}$ and N$^{\delta-}$ atoms belonging to the O–H and N–H functional groups are represented by the S_8 range. The slightly electron withdrawing C=C atoms in the aromatics (*e.g.,* Thymol, Lidocaine, *etc.*) are represented by the S_7 range.

III.3.5.2. Interpretation of Density Model

Based on the 419 data points in the density training set, an MLR relationship using the ten $S_{\sigma-profile}$ molecular descriptors, the temperature descriptor, and the 55 interaction descriptors were established by utilizing a stepwise regression algorithm. Thereafter, an analysis of variance study was conducted to screen the molecular descriptors that have a high statistical influence in predicting the density. The goal of this study is to (i) find a reduced model with fewer terms that can adequately predict the density of HDESs, and (ii) estimate the coefficients of the significant terms in the model. The results of this analysis are listed in Table III.11.

Table III.11. The coefficients of the 53 significant terms of the density model. [a,b]

Term	Estimate	Standard Error	$\lvert t\text{-}_{Ratio}\rvert$	P_{value}
Intercept	−436.67	90.01	4.85	<0.0001
S_1	1964059.50	1284969.00	1.53	0.1272
S_2	4185.64	1609.10	2.60	0.0097
S_3	−73.95	57.53	1.29	0.1995
S_4	18334.62	1380.77	13.28	<0.0001
S_5	3340.69	237.79	14.05	<0.0001
S_6	−1808.78	192.38	9.40	<0.0001
S_7	5325.28	898.46	5.93	<0.0001
S_8	−13370.76	750.14	17.82	<0.0001
S_9	−17041.24	2078.86	8.20	<0.0001
S_{10}	1045402.80	62170.60	16.82	<0.0001
T	-7.49×10^{-4}	1.43×10^{-6}	522.90	<0.0001
$(S_1\text{-}\bar{S}_1)(T\text{-}\bar{T})$	8.90×10^{-3}	3.65×10^{-3}	2.44	0.0152
$(S_4\text{-}\bar{S}_4)(T\text{-}\bar{T})$	-1.19×10^{-3}	4.00×10^{-4}	2.99	0.0030
$(S_6\text{-}\bar{S}_6)(T\text{-}\bar{T})$	1.63×10^{-3}	1.02×10^{-4}	16.09	<0.0001
$(S_9\text{-}\bar{S}_9)(T\text{-}\bar{T})$	6.19×10^{-3}	7.64×10^{-4}	8.10	<0.0001
$(S_{10}\text{-}\bar{S}_{10})(T\text{-}\bar{T})$	-3.43×10^{-2}	9.93×10^{-3}	3.45	0.0006
$(S_1\text{-}\bar{S}_1)(S_2\text{-}\bar{S}_2)$	31824292.00	21565041.00	1.48	0.1409
$(S_1\text{-}\bar{S}_1)(S_4\text{-}\bar{S}_4)$	29444360.00	10743143.00	2.74	0.0064
$(S_1\text{-}\bar{S}_1)(S_7\text{-}\bar{S}_7)$	102308630.00	12234614.00	8.36	<0.0001
$(S_2\text{-}\bar{S}_2)(S_4\text{-}\bar{S}_4)$	266768.64	17241.93	15.47	<0.0001
$(S_2\text{-}\bar{S}_2)(S_5\text{-}\bar{S}_5)$	54175.49	3856.90	14.05	<0.0001
$(S_2\text{-}\bar{S}_2)(S_6\text{-}\bar{S}_6)$	−29025.23	3127.61	9.28	<0.0001
$(S_2\text{-}\bar{S}_2)(S_7\text{-}\bar{S}_7)$	−37257.12	5414.97	6.88	<0.0001
$(S_2\text{-}\bar{S}_2)(S_8\text{-}\bar{S}_8)$	−215925.90	12038.93	17.94	<0.0001
$(S_2\text{-}\bar{S}_2)(S_9\text{-}\bar{S}_9)$	−285103.80	33596.51	8.49	<0.0001
$(S_2\text{-}\bar{S}_2)(S_{10}\text{-}\bar{S}_{10})$	17044937.00	1013086	16.82	<0.0001
$(S_3\text{-}\bar{S}_3)(S_4\text{-}\bar{S}_4)$	98403.99	22309.27	4.41	<0.0001
$(S_3\text{-}\bar{S}_3)(S_5\text{-}\bar{S}_5)$	4907.89	1704.24	2.88	0.0042
$(S_3\text{-}\bar{S}_3)(S_6\text{-}\bar{S}_6)$	−43958.20	2411.79	18.23	<0.0001

$(S_3-\bar{S}_3)(S_7-\bar{S}_7)$	–45901.26	3109.96	14.76	<0.0001
$(S_3-\bar{S}_3)(S_8-\bar{S}_8)$	16830.22	7371.19	2.28	0.0230
$(S_3-\bar{S}_3)(S_9-\bar{S}_9)$	–320639.90	21766.59	14.73	<0.0001
$(S_3-\bar{S}_3)(S_{10}-\bar{S}_{10})$	10288598	631153.90	16.30	<0.0001
$(S_4-\bar{S}_4)(S_5-\bar{S}_5)$	–5057.58	1482.68	3.41	0.0007
$(S_4-\bar{S}_4)(S_6-\bar{S}_6)$	–9100.96	1561.46	5.83	<0.0001
$(S_4-\bar{S}_4)(S_7-\bar{S}_7)$	–12453.08	1021.79	12.19	<0.0001
$(S_4-\bar{S}_4)(S_8-\bar{S}_8)$	–3663.32	1342.09	2.73	0.0066
$(S_4-\bar{S}_4)(S_9-\bar{S}_9)$	12120.55	883.04	13.73	<0.0001
$(S_5-\bar{S}_5)(S_6-\bar{S}_6)$	–37.76	9.45	4.00	<0.0001
$(S_5-\bar{S}_5)(S_7-\bar{S}_7)$	207.11	302.25	0.69	0.4936
$(S_5-\bar{S}_5)(S_8-\bar{S}_8)$	–8662.26	912.53	9.49	<0.0001
$(S_5-\bar{S}_5)(S_9-\bar{S}_9)$	–10448.68	1891.15	5.53	<0.0001
$(S_5-\bar{S}_5)(S_{10}-\bar{S}_{10})$	672267.87	37902.85	17.74	<0.0001
$(S_6-\bar{S}_6)(S_7-\bar{S}_7)$	3387.22	345.21	9.81	<0.0001
$(S_6-\bar{S}_6)(S_8-\bar{S}_8)$	14384.78	1181.99	12.17	<0.0001
$(S_6-\bar{S}_6)(S_9-\bar{S}_9)$	20700.78	2227.69	9.29	<0.0001
$(S_6-\bar{S}_6)(S_{10}-\bar{S}_{10})$	–621133.10	37079.77	16.75	<0.0001
$(S_7-\bar{S}_7)(S_8-\bar{S}_8)$	–1391.28	571.74	2.43	0.0154
$(S_7-\bar{S}_7)(S_9-\bar{S}_9)$	–41.40	107.06	0.51	0.6992
$(S_7-\bar{S}_7)(S_{10}-\bar{S}_{10})$	–206979.30	11379.79	18.19	<0.0001
$(S_8-\bar{S}_8)(S_9-\bar{S}_9)$	–31524.15	3712.65	8.49	<0.0001
$(S_8-\bar{S}_8)(S_{10}-\bar{S}_{10})$	–2283677.00	141873.00	16.10	<0.0001
$(S_9-\bar{S}_9)(S_{10}-\bar{S}_{10})$	426372.69	48649.90	8.76	<0.0001

[a] Mean values: $\bar{S}_1$ =7.40×10^{-5}; $\bar{S}_2$ =6.33×10^{-2}; $\bar{S}_3$ =2.30×10^{-3}; $\bar{S}_4$ =9.70×10^{-3}; $\bar{S}_5$ =8.93×10^{-2}; $\bar{S}_6$ =7.24×10^{-2}; $\bar{S}_7$ =9.40×10^{-3}; $\bar{S}_8$ =9.60×10^{-3}; $\bar{S}_9$ =3.50×10^{-3}; $\bar{S}_{10}$ =7.52×10^{-5}; $\bar{T}$ =323.95

[b] Excluded descriptors: $\{S_2, T\}$, $\{S_3, T\}$, $\{S_5, T\}$, $\{S_7, T\}$, $\{S_8, T\}$, $\{S_1, S_3\}$, $\{S_1, S_5\}$, $\{S_1, S_6\}$, $\{S_1, S_8\}$, $\{S_1, S_9\}$, $\{S_1, S_{10}\}$, $\{S_2, S_3\}$, and $\{S_4, S_{10}\}$

As it can be seen from Table III.11, 53 descriptors were found to have a significant influence on the density of HDESs, while the remaining 13 insignificant descriptors were excluded from the model by setting their coefficient values equal to 0. It is worth noting that the majority of the descriptors (48 out of 53) had P_{value} less than 0.05. However, the remaining 5 descriptors, particularly S_1, S_3, $\{S_1, S_2\}$, $\{S_5, S_7\}$ and $\{S_7, S_9\}$, were still included in the model as they had a relatively significant influence on $R^2_{adjusted}$, which only increases if the new term improves the model more than it would be expected by chance. This can also be further backed up by the high Fisher statistic test in Table III.12 indicating that there exists a much larger variation due to observed differences in the descriptors rather than variations due to chance (F_{-Ratio} = 47654.40; $P_{value, Fisher}$ <0.0001). It should also be mentioned that even though the descriptors S_1 and S_3 exhibited a P_{value} of 0.1272 and 0.1995, respectively, their interactions with other descriptors, namely $\{S_1, T\}$, $\{S_1, S_4\}$, $\{S_1, S_7\}$, $\{S_3, S_4\}$, $\{S_3, S_5\}$, $\{S_3, S_6\}$, $\{S_3, S_7\}$, $\{S_3, S_8\}$, $\{S_3, S_9\}$, and $\{S_3, S_{10}\}$, all exhibit a P_{value} less than 0.05, and thus, the S_1 and S_3 molecular descriptors should be included in the model to conserve coherence of the regression.

Table III.12. Statistical parameters of the density model.

HDESs in training set	37
Data points in training set	419
R^2	0.9998
$F\text{-}_{Ratio}$	47654.40
$P_{value,\ Fisher}$	<0.0001
$R^2_{adjusted}$	0.9997
Q^2_{LOO}	0.9998
Q^2_{LMO}	0.9983
$R^2_{scramble}$	0.0043
HDESs in testing set	15
Data points in training set	187
$R^2_{external}$	0.9956
RMSE	0.0005
SD_{avg}	$\pm 0.0001\ \text{g·cm}^{-3}$
AARD	$\pm 0.1\%$

Regarding the binary interactions between the 10 molecular descriptors with the temperature descriptor $\{S_i, T\}$, it can be observed that the interactions between S_2, S_3, S_5, S_7, and S_8 with the temperature descriptor, T, were found to not influence the density of the HDESs. Regarding the binary interactions between a pair of molecular descriptors $\{S_i, S_j\}$, it was found that the pairs $\{S_1, S_3\}, \{S_1, S_5\}, \{S_1, S_6\}, \{S_1, S_8\}, \{S_1, S_9\}, \{S_1, S_{10}\}, \{S_2, S_3\}$, and $\{S_4, S_{10}\}$ did not influence the density of HDESs. Conversely, all 10 molecular descriptors, the temperature descriptor, and the remaining 42 interaction descriptors were found to be significant in predicting the density of HDESs. In conclusion, the resulting density model can be expressed as follows:

$$
\begin{aligned}
\rho = &-436.67 + 1964059.50\,(S_1) - 4185.64\,(S_2) - 73.95\,(S_3) + 18334.62\,(S_4) + 3340.69\,(S_5) - 1808.78 \\
&(S_6) + 5325.28\,(S_7) - 13370.76\,(S_8) - 17041.24\,(S_9) + 104502.80\,(S_{10}) - 7.49\times10^{-4}\,(T) + 31824292.00 \\
&(S_1-\overline{S_1})(S_2-\overline{S_2}) + 29444360.00\,(S_1-\overline{S_1})(S_4-\overline{S_4}) + 102308630.00\,(S_1-\overline{S_1})(S_7-\overline{S_7}) + 8.90\times10^{-3} \\
&(S_1-\overline{S_1})(T-\overline{T}) + 266768.64\,(S_2-\overline{S_2})(S_4-\overline{S_4}) + 54175.49\,(S_2-\overline{S_2})(S_5-\overline{S_5}) - 29025.23 \\
&(S_2-\overline{S_2})(S_6-\overline{S_6}) - 37257.12\,(S_2-\overline{S_2})(S_7-\overline{S_7}) - 215925.90\,(S_2-\overline{S_2})(S_8-\overline{S_8}) - 285103.80 \\
&(S_2-\overline{S_2})(S_9-\overline{S_9}) + 17044937.00\,(S_2-\overline{S_2})(S_{10}-\overline{S_{10}}) + 98403.99\,(S_3-\overline{S_3})(S_4-\overline{S_4}) + 4907.89 \\
&(S_3-\overline{S_3})(S_5-\overline{S_5}) - 43958.20\,(S_3-\overline{S_3})(S_6-\overline{S_6}) - 45901.26\,(S_3-\overline{S_3})(S_7-\overline{S_7}) + 16830.22 \\
&(S_3-\overline{S_3})(S_8-\overline{S_8}) - 320639.90\,(S_3-\overline{S_3})(S_9-\overline{S_9}) + 10288598.00\,(S_3-\overline{S_3})(S_{10}-\overline{S_{10}}) - 5057.58 \\
&(S_4-\overline{S_4})(S_5-\overline{S_5}) - 9100.96\,(S_4-\overline{S_4})(S_6-\overline{S_6}) - 12453.08\,(S_4-\overline{S_4})(S_7-\overline{S_7}) - 3663.32\,(S_4-\overline{S_4})(S_8-\overline{S_8}) \\
&+ 12120.55\,(S_4-\overline{S_4})(S_9-\overline{S_9}) - 1.19\times10^{-3}\,(S_4-\overline{S_4})(T-\overline{T}) - 37.76\,(S_5-\overline{S_5})(S_6-\overline{S_6}) + 207.11 \\
&(S_5-\overline{S_5})(S_7-\overline{S_7}) - 8662.26\,(S_5-\overline{S_5})(S_8-\overline{S_8}) + 10448.68\,(S_5-\overline{S_5})(S_9-\overline{S_9}) + 672267.87 \\
&(S_5-\overline{S_5})(S_{10}-\overline{S_{10}}) + 3387.22\,(S_6-\overline{S_6})(S_7-\overline{S_7}) + 14384.79\,(S_6-\overline{S_6})(S_8-\overline{S_8}) + 20700.78 \\
&(S_6-\overline{S_6})(S_9-\overline{S_9}) - 621133.10\,(S_6-\overline{S_6})(S_{10}-\overline{S_{10}}) + 1.63\times10^{-3}\,(S_6-\overline{S_6})(T-\overline{T}) - 1391.28 \\
&(S_7-\overline{S_7})(S_8-\overline{S_8}) - 41.40\,(S_7-\overline{S_7})(S_9-\overline{S_9}) - 206979.30\,(S_7-\overline{S_7})(S_{10}-\overline{S_{10}}) - 31524.15 \\
&(S_8-\overline{S_8})(S_9-\overline{S_9}) - 2283677.00\,(S_8-\overline{S_8})(S_{10}-\overline{S_{10}}) + 426372.69\,(S_9-\overline{S_9})(S_{10}-\overline{S_{10}}) + 6.19\times10^{-3} \\
&(S_9-\overline{S_9})(T-\overline{T}) - 3.43\times10^{-2}\,(S_{10}-\overline{S_{10}})(T-\overline{T})
\end{aligned}
\tag{III.3}
$$

where S_i is the HDES molecular descriptor of region i (e/Å^2), $\overline{S_i}$ is the mean value of the molecular descriptor in region i (e/Å^2), T is the temperature (K), $\overline{\text{T}}$ is the mean value of the temperature (K), and ρ is the density (g·cm^{-3}).

A statistical summary of the performance of the model is given in Table III.12. The high coefficient of determination ($R^2 = 0.9998$) and the high Fisher's statistic ($F\text{-}_{Ratio} = 47654.40$) suggest that the model provides an excellent fit to the experimental dataset. Also, the high cross-validation coefficients ($Q^2_{LOO} = 0.9998$; $Q^2_{LMO} = 0.9983$) suggest that the model is internally stable and robust. Chance correlation tests were also conducted to verify the regression of the model. The high adjusted coefficient of determination ($R^2_{adjusted} = 0.9997$) and the low y-scrambling coefficient of determination ($R^2_{scramble} = 0.0043$) indicate that the regression of the model is not correlated by chance.

It should be noted that even though the model exhibits a high number of descriptors, 53 degrees of freedom, all the degrees of freedom are based on only ten simple molecular descriptors ($S_1 - S_{10}$) and temperature (T). The rest of the descriptors are just simple multiplications of two descriptors expressing their interactions. For instance, the interaction between $\{S_1 \& S_2\}$ is mathematically described as $(S_1 - \overline{S_1})(S_2 - \overline{S_2})$. Consequently, the developed model can be used for screening *a priori* a large number of HDESs (that are yet to be prepared) using only ten molecular descriptors, which can be obtained using basic COSMO-RS modeling of each HDES constituent, allowing for significant time and cost savings. Furthermore, it has been reported previously that in QSPR studies the number of total data points to significant descriptors should be at least in the ratio of 5 to 1 (Dearden et al., 2009; Topliss & Costello, 1972), which is in agreement with the developed model at 11.4 to 1. It should also be mentioned that if the binary interactions between the descriptors were to be removed the developed model would be a lot simpler, however, the accuracy of the model will also decrease substantially. Therefore, there exists somewhat of a compromise between the accuracy of the model and its complexity.

All molecular descriptors in the MLR model have physical meaning that stems from their description of the molecule's structural features (Torrecilla et al., 2010; Zhao et al., 2015), and these descriptors can account for the factors affecting the density of HDESs. A positive coefficient sign indicates a positive correlation between the descriptor and the density (*i.e.,* increasing the density), while a negative coefficient sign indicates a negative correlation. First, it can be observed that the temperature descriptor is negatively correlated with the density of the HDESs, which was expected as this is a universal tendency in the density of solvents (Van Osch et al., 2020). Also,

according to the t-test ratio, the temperature descriptor is the most statistically significant descriptor in the model as it has the highest t-$_{Ratio}$ value.

Second, it can also be seen that the majority of the hydrophobic region molecular descriptors S_4, S_5, and S_7 are positively correlated, while the S_6 molecular descriptor is negatively correlated. When comparing the HBA and HBD regions of the HDESs, the HBA region was observed to have higher statistical significance on the density as their t-$_{Ratio}$ values were considerably higher than that of those in the HBD region. The HBA region descriptors S_8 and S_9 were observed to be negatively correlated with the density, while the S_{10} region was positively correlated. Instead, the HBD region descriptors S_1 and S_2 were observed to have positive effects on the density of the HDESs, while the S_3 descriptor was observed to have negative effects.

Regarding the interactions between the molecular descriptors and the temperature descriptor, it can be seen that the most statistically important interactions were $\{S_6, T\}$ and $\{S_9, T\}$ as they had the highest t-$_{Ratio}$ values. It can also be observed that the interactions $\{S_1, T\}$, $\{S_6, T\}$, and $\{S_9, T\}$ were positively correlated with the density, while $\{S_4, T\}$ and $\{S_{10}, T\}$ were negatively correlated. In terms of the interactions between a pair of molecular descriptors, it can be observed from Table III.11 that 20 interaction pairs exhibit a negative correlation, while the remaining 17 exhibit a positive correlation. The most statistically significant interactions with high t-$_{Ratio}$ (>15) values were as follows: $\{S_2, S_4\}$, $\{S_2, S_8\}$, $\{S_2, S_{10}\}$, $\{S_3, S_6\}$, $\{S_3, S_{10}\}$, $\{S_5, S_{10}\}$, $\{S_6, S_{10}\}$, $\{S_7, S_{10}\}$, $\{S_8, S_{10}\}$.

Figure III.11 (a) shows the experimental densities plotted against the predicted densities calculated by the model for 37 HDESs (419 data points) in training. As it can be seen, all the points are almost perfectly on the diagonal line with nearly no dispersion ($R^2 = 0.9998$). The model was then evaluated for its performance in predicting 15 external HDESs (187 data points) that were not included in the training of the model.

The results shown in Figure III.11 (b) demonstrate the excellent predictive power of the developed model as there is a very narrow dispersion between the experimental and predicted densities ($R^2_{external} = 0.9956$). The excellent prediction was further verified using the relative deviations between the experimental and predicted values in both training and testing datasets. Figure III.12 shows that the density relative deviations are always within a maximum of ±1% with an AARD of ±0.1%. The standard deviations between the experimental and predicted values were also calculated to be within an average of ±0.0001 g·cm^{-3}. Based on the obtained results, it can be concluded that QSPR models based on $S_{\sigma-profiles}$ and their interactions are excellent at predicting the density of HDESs.

(a) Training
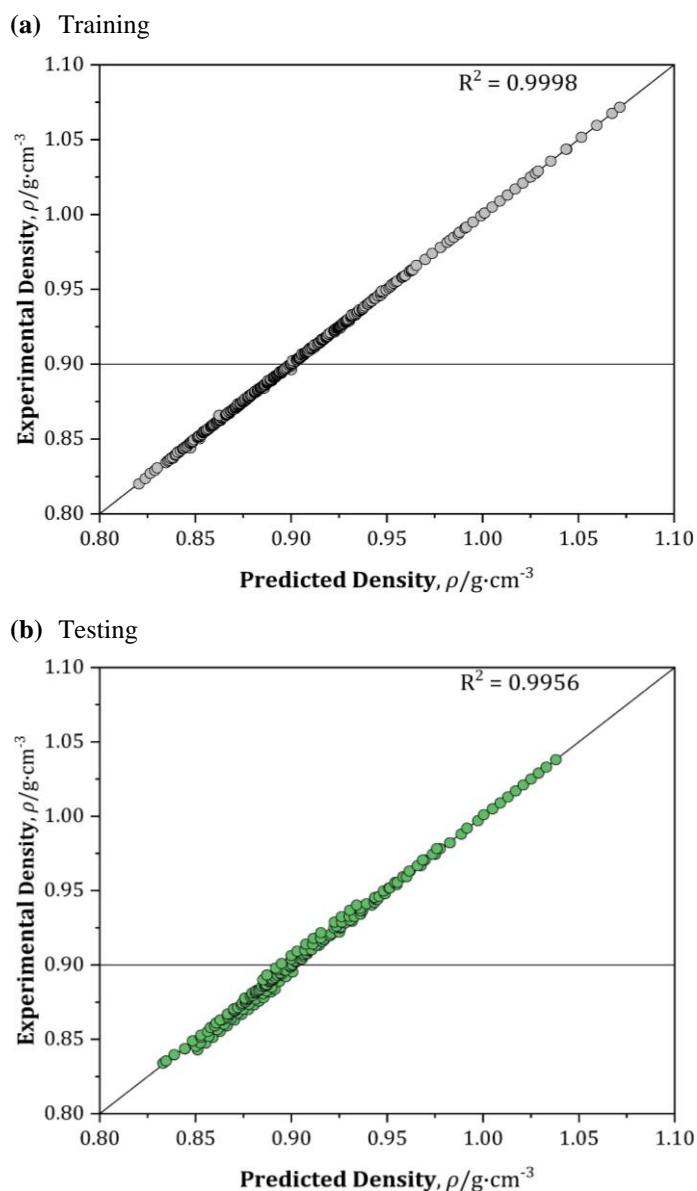
(b) Testing

Figure III.11. The experimental densities *versus* the predicted densities of the model in (a) training and (b) external testing.
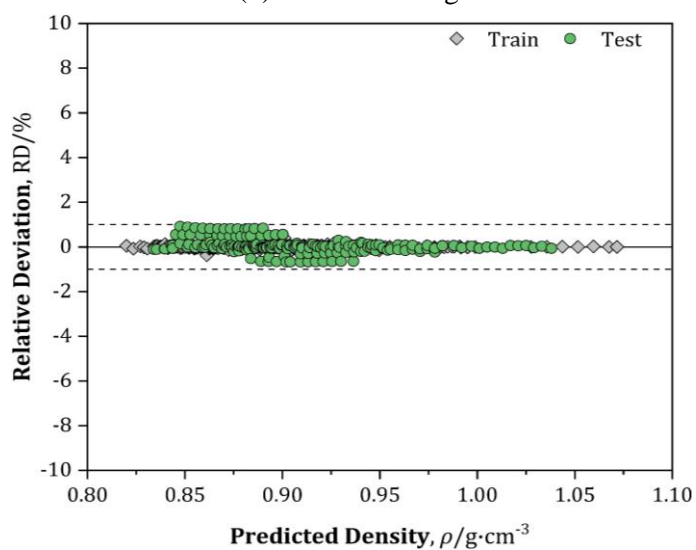
Figure III.12. Relative deviation between the experimental and predicted densities.

III.3.5.3. Interpretation of Viscosity Model

The same procedure utilized in the development of the density model was used in the viscosity model. The results of the analysis of variance on the 377 collected data points in training are listed in Table III.13. As it can be observed from Table III.13, only 38 descriptors in the viscosity model were found to have a high statistical influence on the viscosity of the HDESs (simpler model compared to density model with 53 significant descriptors). The remaining 28 insignificant descriptors were excluded from the model. It should be noted that similar to the density model the majority of the significant descriptors (36 out of 38) had P_{value} less than 0.05. As explained in the previous section, the remaining 2 descriptors, $\{S_5, T\}$ and $\{S_2, S_4\}$, were still included in the model as they had a relatively significant influence on $R^2_{adjusted}$, which was then again further validated by the use of the Fisher statistic test ($F\text{-}_{Ratio} = 1319.58$; $P_{value, Fisher} < 0.0001$).

Table III.13. The coefficients of the 38 significant terms of the viscosity model.[a,b]

Term	Estimate	Standard Error	$\lvert t\text{-}_{Ratio}\rvert$	P_{value}
Intercept	−1138.10	406.57	2.80	0.0054
S_1	13569128.00	4438149.00	3.06	0.0024
S_2	45498.77	15193.05	2.99	0.0029
S_3	3131.48	391.36	8.00	<0.0001
S_4	−16463.29	2977.75	5.53	<0.0001
S_5	−264.70	79.87	3.31	0.0010
S_6	242.96	62.63	3.88	0.0001
S_7	−424.56	67.49	6.29	<0.0001
S_8	−734.34	254.53	2.89	0.0041
S_9	1348.82	388.46	3.47	0.0006
S_{10}	7195.197	2600.05	2.77	0.0059
T	-3.75×10^{-2}	4.16×10^{-4}	90.24	<0.0001
$(S_2\text{-}\bar{S_2})(T\text{-}\bar{T})$	-1.30×10^{-2}	0.005125	2.53	0.0119
$(S_3\text{-}\bar{S_3})(T\text{-}\bar{T})$	−14.91	2.74	5.45	<0.0001
$(S_4\text{-}\bar{S_4})(T\text{-}\bar{T})$	3.90×10^{-1}	1.28×10^{-1}	3.05	0.0024
$(S_5\text{-}\bar{S_5})(T\text{-}\bar{T})$	4.90×10^{-2}	3.66×10^{-2}	1.34	0.1810
$(S_7\text{-}\bar{S_7})(T\text{-}\bar{T})$	0.39	0.11	3.66	0.0003
$(S_9\text{-}\bar{S_9})(T\text{-}\bar{T})$	−4.23	0.32	13.19	<0.0001
$(S_1\text{-}\bar{S_1})(S_2\text{-}\bar{S_2})$	535855509.00	$1.75\times10^{+8}$	3.05	0.0024
$(S_1\text{-}\bar{S_1})(S_4\text{-}\bar{S_4})$	$-1.91\times10^{+8}$	41887784.00	4.56	<0.0001
$(S_2\text{-}\bar{S_2})(S_4\text{-}\bar{S_4})$	−10432.05	26212.73	0.51	0.6909
$(S_2\text{-}\bar{S_2})(S_8\text{-}\bar{S_8})$	−44042.87	8287.30	5.31	<0.0001
$(S_3\text{-}\bar{S_3})(S_6\text{-}\bar{S_6})$	98871.30	23699.00	4.17	<0.0001
$(S_3\text{-}\bar{S_3})(S_7\text{-}\bar{S_7})$	368987.71	40513.89	9.11	<0.0001
$(S_3\text{-}\bar{S_3})(S_8\text{-}\bar{S_8})$	1128384.60	184605.90	6.11	<0.0001
$(S_3\text{-}\bar{S_3})(S_9\text{-}\bar{S_9})$	2370362.60	558408.80	4.24	<0.0001
$(S_3\text{-}\bar{S_3})(S_{10}\text{-}\overline{S_{10}})$	−25604624.00	3875056.00	6.61	<0.0001
$(S_4\text{-}\bar{S_4})(S_5\text{-}\bar{S_5})$	5393.90	1021.79	5.28	<0.0001
$(S_4\text{-}\bar{S_4})(S_7\text{-}\bar{S_7})$	35629.87	12190.22	2.92	0.0037
$(S_4\text{-}\bar{S_4})(S_8\text{-}\bar{S_8})$	−84371.96	24810.63	3.40	0.0007
$(S_4\text{-}\bar{S_4})(S_9\text{-}\bar{S_9})$	−97815.38	22942.15	4.26	<0.0001
$(S_5\text{-}\bar{S_5})(S_7\text{-}\bar{S_7})$	17537.30	7777.87	2.25	0.0247
$(S_5\text{-}\bar{S_5})(S_9\text{-}\bar{S_9})$	8027.65	3827.48	2.10	0.0366
$(S_5\text{-}\bar{S_5})(S_{10}\text{-}\overline{S_{10}})$	−581696.70	87477.05	6.65	<0.0001
$(S_6\text{-}\bar{S_6})(S_7\text{-}\bar{S_7})$	−13705.01	5683.85	2.41	0.0164

$(S_6-\bar{S}_6)(S_{10}-\bar{S}_{10})$	723935.40	128115.40	5.65	<0.0001
$(S_7-\bar{S}_7)(S_8-\bar{S}_8)$	–34118.32	8659.07	3.94	<0.0001
$(S_7-\bar{S}_7)(S_9-\bar{S}_9)$	–531913.30	113305.50	4.69	<0.0001
$(S_7-\bar{S}_7)(S_{10}-\bar{S}_{10})$	4087362.60	798165.70	5.12	<0.0001

[a]Mean values: $\bar{S}_1 = 8.55\times10^{-5}$; $\bar{S}_2 = 2.89\times10^{-2}$; $\bar{S}_3 = 2.26\times10^{-2}$; $\bar{S}_4 = 1.02\times10^{-2}$; $\bar{S}_5 = 9.06\times10^{-2}$; $\bar{S}_6 = 7.42\times10^{-2}$; $\bar{S}_7 = 1.01\times10^{-2}$; $\bar{S}_8 = 1.04\times10^{-2}$; $\bar{S}_9 = 3.00\times10^{-3}$; $\bar{S}_{10} = 1.00\times10^{-4}$; $\bar{T} = 324.80$

[b]Excluded descriptors: $\{S_1,T\}$, $\{S_6,T\}$, $\{S_8,T\}$, $\{S_{10},T\}$, $\{S_1,S_3\}$, $\{S_1,S_5\}$, $\{S_1,S_6\}$, $\{S_1,S_7\}$, $\{S_1,S_8\}$, $\{S_1,S_9\}$, $\{S_1,S_{10}\}$, $\{S_2,S_3\}$, $\{S_2,S_5\}$, $\{S_2,S_6\}$, $\{S_2,S_7\}$, $\{S_2,S_9\}$, $\{S_2,S_{10}\}$, $\{S_3,S_4\}$, $\{S_3,S_5\}$, $\{S_4,S_6\}$, $\{S_4,S_{10}\}$, $\{S_5,S_6\}$, $\{S_5,S_8\}$, $\{S_6,S_8\}$, $\{S_6,S_9\}$, $\{S_8,S_9\}$, $\{S_8,S_{10}\}$, and $\{S_9,S_{10}\}$.

A list of the 28 excluded descriptors can be found in the notes under Table III.13. It was observed that the interactions between $S_1, S_6, S_8,$ and S_{10} with the temperature descriptor, T, had no statistical significance on the viscosity of the HDESs. As for the binary interactions between a pair of molecular descriptors, it was found that 24 binary interactions had no influence on the viscosity of the HDESs. Conversely, all 10 molecular descriptors, the temperature descriptor, and the remaining 27 interaction descriptors were found to be statistically significant in predicting the viscosity of the HDESs. Therefore, the resulting viscosity model can be expressed as follows:

$$ln(\eta) = -1138.10 + 13569128.00\,(S_1) + 45498.77\,(S_2) + 3131.48\,(S_3) - 16463.29\,(S_4) - 264.70\,(S_5) + 242.96\,(S_6) - 424.56\,(S_7) - 734.34\,(S_8) + 1348.82\,(S_9) + 7195.20\,(S_{10}) - 3.75\times10^{-2}(T) + 535855509.00\,(S_1-\bar{S}_1)(S_2-\bar{S}_2) - 1.91\times10^{+8}\,(S_1-\bar{S}_1)(S_4-\bar{S}_4) - 10432.05\,(S_2-\bar{S}_2)(S_4-\bar{S}_4) - 44042.87\,(S_2-\bar{S}_2)(S_8-\bar{S}_8) - 1.30\times10^{-2}\,(S_2-\bar{S}_2)(T-\bar{T}) + 98871.30\,(S_3-\bar{S}_3)(S_6-\bar{S}_6) + 368987.71\,(S_3-\bar{S}_3)(S_7-\bar{S}_7) + 1128384.60\,(S_3-\bar{S}_3)(S_8-\bar{S}_8) + 2370362.60\,(S_3-\bar{S}_3)(S_9-\bar{S}_9) - 25604624.00\,(S_3-\bar{S}_3)(S_{10}-\bar{S}_{10}) - 14.91\,(S_3-\bar{S}_3)(T-\bar{T}) + 5393.90\,(S_4-\bar{S}_4)(S_5-\bar{S}_5) - 35629.87\,(S_4-\bar{S}_4)(S_7-\bar{S}_7) - 84371.96\,(S_4-\bar{S}_4)(S_8-\bar{S}_8) - 97815.38\,(S_4-\bar{S}_4)(S_9-\bar{S}_9) + 0.39\,(S_4-\bar{S}_4)(T-\bar{T}) + 17537.30\,(S_5-\bar{S}_5)(S_7-\bar{S}_7) + 8027.65\,(S_5-\bar{S}_5)(S_9-\bar{S}_9) - 581696.70\,(S_5-\bar{S}_5)(S_{10}-\bar{S}_{10}) + 4.90\times10^{-2}\,(S_5-\bar{S}_5)(T-\bar{T}) - 13705.01\,(S_6-\bar{S}_6)(S_7-\bar{S}_7) + 723935.40\,(S_6-\bar{S}_6)(S_{10}-\bar{S}_{10}) - 34118.32\,(S_7-\bar{S}_7)(S_8-\bar{S}_8) - 531913.30\,(S_7-\bar{S}_7)(S_9-\bar{S}_9) + 4087362.60\,(S_7-\bar{S}_7)(S_{10}-\bar{S}_{10}) + 0.39\,(S_7-\bar{S}_7)(T-\bar{T}) - 4.23\,(S_9-\bar{S}_9)(T-\bar{T})$$

(III.4)

Where S_i is the HDES molecular descriptor of region i (e/Å^2), $\bar{S}_i$ is the mean value of the molecular descriptor in region i (e/Å^2), T is the temperature (K), $\bar{T}$ is the mean value of the temperature (K), and ln (η) is the natural logarithm of the viscosity (mPa·s).

A statistical summary of the performance of the viscosity model is given in Table III.14. It can be observed that the viscosity model also demonstrated high statistical performances: good fit of the experimental dataset (high $R^2 = 0.9921$; $F_{-Ratio} = 1319.58$), robust and internally validated (high $Q^2_{LOO} = 0.9921$; $Q^2_{LMO} = 0.9906$), and is not correlated by chance (high $R^2_{adjusted} = 0.9912$; low $R^2_{scramble} = 0.0081$).

Table III.14. Statistical parameters of the viscosity model.

HDESs in training set	32
Data points in training set	377
R^2	0.9921
$F_{\text{-}Ratio}$	1319.58
$P_{value,\ Fisher}$	<0.0001
$R^2_{adjusted}$	0.9912
Q^2_{LOO}	0.9921
Q^2_{LMO}	0.9906
$R^2_{scramble}$	0.0081
HDESs in testing set	13
Data points in training set	153
$R^2_{external}$	0.9871
$RMSE$	0.2188
SD_{avg}	±0.6 mPa·s
$AARD$	±4.7%
$AD_{coverage}$	100.0%

By analyzing the results presented in Table III.13, it can be observed that the temperature descriptor is the most statistically significant descriptor in the model as it has the highest $t_{\text{-}Ratio}$ value, which is similar to the result obtained in the density model. The temperature was also found to be negatively correlated with the viscosity, which is consistent with the experimental data obtained from the literature (Van Osch et al., 2020). However, opposite to the density model, the majority of the non-polar region molecular descriptors, S_4, S_5, and S_7, were found to be negatively correlated with the viscosity, while the S_6 molecular descriptor is positively correlated. This result is presumably due to the trends discussed in section III.3.4, where it was generally found that the structural features in the non-polar region that increase the density were also the same structural features that decrease the viscosity of the HDESs (*i.e.,* effect of cation chain length, effect of HBD chain length).

Additionally, it can be observed that the $t_{\text{-}Ratio}$ values for both the HBA and HBD regions are almost similar suggesting that both regions are statistically significant, unlike the density model, which had higher significance in the HBA region. It can also be observed that all molecular descriptors in the HBA region (S_1, S_2, S_3) and the majority of the molecular descriptors in the HBD region (S_9, S_{10}) had a positive correlation with the viscosity of the HDESs, with the only exception being the S_8 molecular descriptor which was negatively correlated. Regarding the interactions of the molecular descriptors with the temperature descriptor, it can be seen that the interactions $\{S_2, T\}, \{S_3, T\}$, and $\{S_9, T\}$ were all negatively correlated with the viscosity, while the interactions $\{S_4, T\}, \{S_5, T\}$, and $\{S_7, T\}$ were observed to be positively correlated. Finally, with regards to the interactions between a pair of molecular descriptors, it can be seen from Table III.13 that 11 interaction pairs were positively correlated, while the remaining 10 were negatively correlated.

The most statistically significant interactions with high t-$_{Ratio}$ (>5) values were as follows: $\{S_2, S_8\}$, $\{S_3, S_7\}$, $\{S_3, S_8\}$, $\{S_3, S_{10}\}$, $\{S_4, S_5\}$, $\{S_5, S_{10}\}$, $\{S_6, S_{10}\}$, $\{S_7, S_{10}\}$.

Figure III.13 shows the experimental viscosities plotted against the predicted viscosities calculated by the model in (a) training set (32 HDESs; 377 points) and in (b) external testing set (13 HDESs; 153 points). It can be seen that the majority of the points on both plots are on the diagonal lines with a narrow dispersion (R^2 = 0.9921; $R^2_{external}$ = 0.9871). The relative deviations between the experimental and predicted viscosities in both training and testing datasets are shown in Figure III.14 (a). The relative deviations of the viscosity are always within a maximum of ±25% with an AARD of ±4.7%. The distribution of the relative deviations in different deviation ranges is also shown in Figure III.14 (b). It can be seen that (i) around 2/3 of the data points had less than 5% relative deviation, (ii) 88.7% of the data points had a relative deviation between 0 – 10%, and (iii) only 11.3% of the data points had a relative deviation between 10 – 25%. Finally, the standard deviations between the experimental and predicted viscosities were calculated and were found to be within an average of ±0.6 mPa·s.

Overall, it can be observed that the external validation of the model is fairly reliable except for the predictions of a few HDES with low viscosities ($\ln(\eta_{exp}) \leq 2.5$). The model tends to underestimate the viscosities of (HDES12) dodecanoic acid: octanoic acid, (HDES13) dodecanoic acid: nonanoic acid, and (HDES14) dodecanoic acid: decanoic acid. However, despite these deviations, the model still captures the correct qualitative trend where the viscosity of HDES14 > HDES13 > HDES12, which is consistent with the trend in the experimental data. These lower performances in predicting viscosity compared to density can be attributed to the high dependence of intermolecular interactions between the two HDES constituents and how they change the viscosity on a case-by-case basis as explained in section III.3.4.2. Hence, the limited dataset available in the literature could be affecting the viscosity predictions, and thus, the usage of a more diverse dataset would be required to improve the performance of the model. Also, the viscosities of the HDESs cover a wide range from as low as 1.3 mPa·s to as high as 1,706.2 mPa·s, which also could be affecting the predictions. For example, comparing HDES1 with HDES41 in terms of numerical values only, it can be observed that the densities are almost similar 0.942 and 0.915 g·cm^{-3}, respectively, while the viscosities highly deviate from each other with values of 576.5 and 14.4 mPa·s, respectively. Furthermore, it is worth noting that when comparing the experimental uncertainties that were reported in the literature for the density and viscosity data points, such errors in the viscosity model can be considered acceptable.

Taking all the results into account, it can be said that even though these statistical performances of the viscosity model are lower than that of the density model, the viscosity model still demonstrates a highly reliable fit of the experimental data and good external predictive power. Therefore, it can be concluded that QSPR models based on $S_{\sigma-profiles}$ and their interactions proven to be accurate for density predictions, are also great at predicting the viscosity of HDESs.

(a) Training
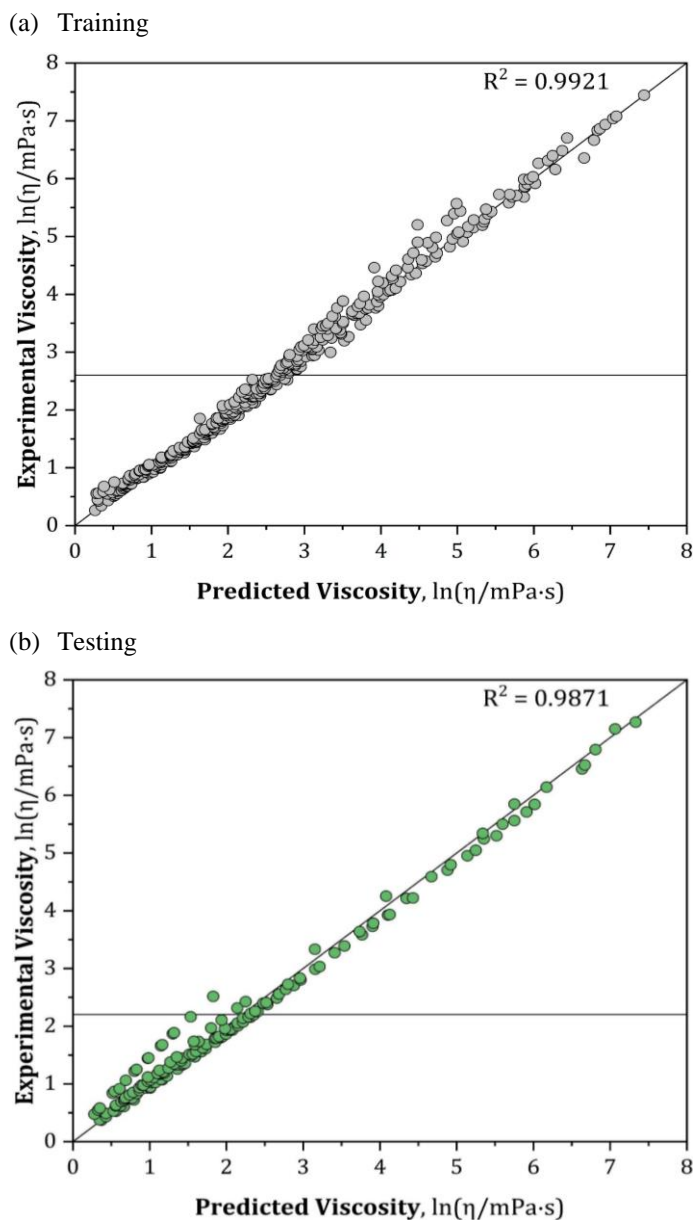
(b) Testing

Figure III.13. The experimental viscosities *versus* the predicted viscosities of the model in (a) training and (b) external testing.

(a)

(b)
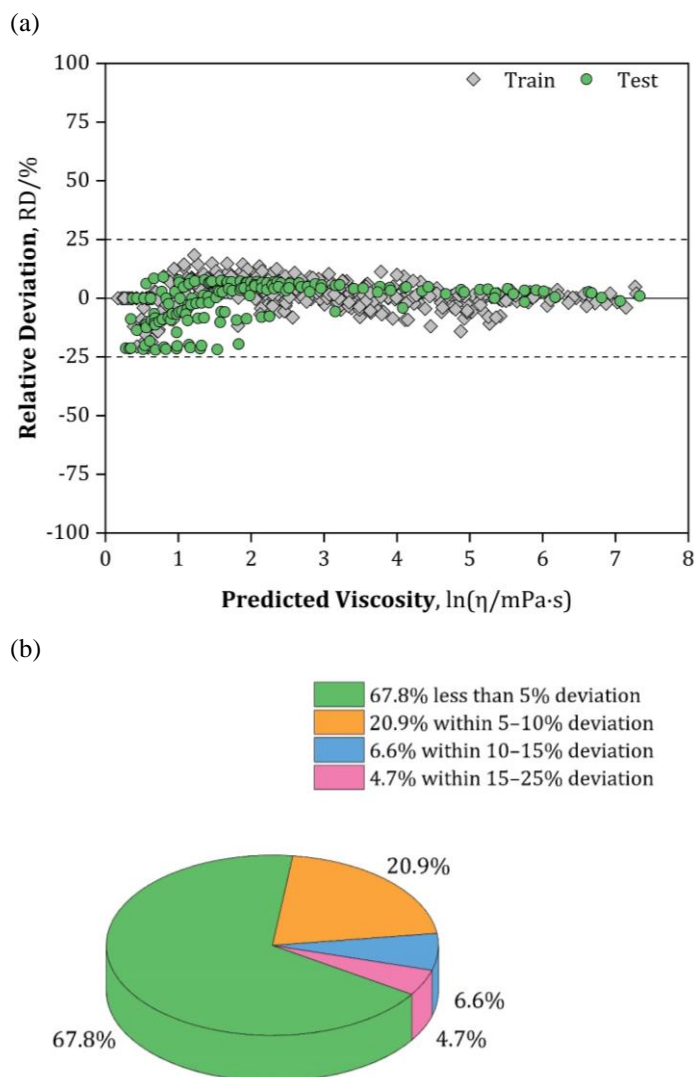
Figure III.14. (a) Relative deviation between the experimental and predicted viscosities, and (b) the distribution of the relative deviation in different deviation ranges.

III.3.5.4. Applicability Domain

The William plots of both models are presented in Figure III.15. The AD boundaries are defined between (i) the leverage threshold $0 < h_i < h^*$ (vertical dashed line), and (ii) the standardized residuals $-3 < SDR < +3$ (horizontal dashed line).
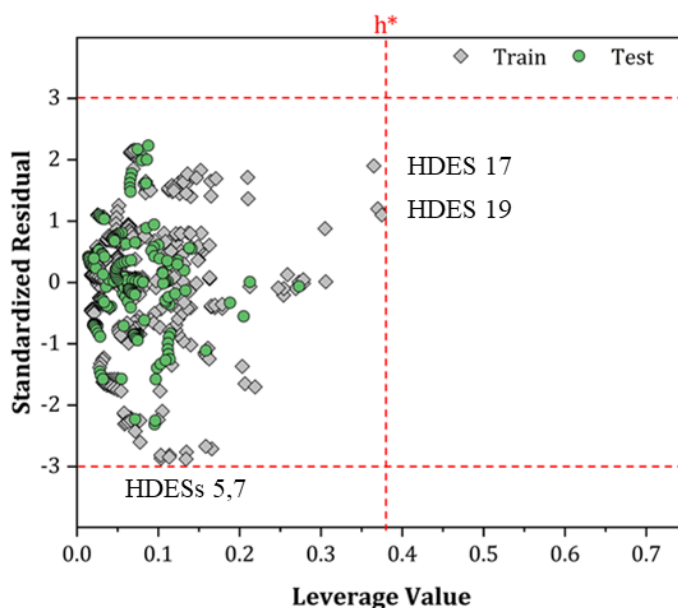
a)   Density Model
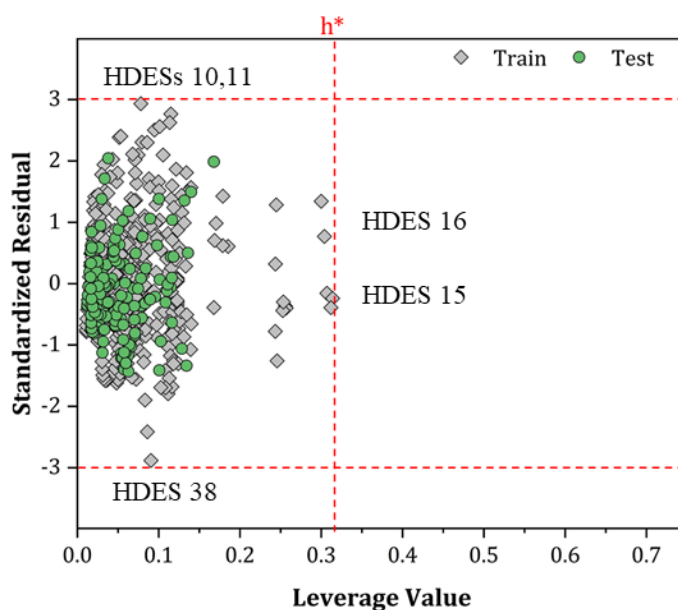
b)   Viscosity Model

Figure III.15. William plot for (a) density and (b) viscosity models.

When comparing the domains of applicability of the density and viscosity models in Figure III.15, it can be observed that the density model AD is slightly wider than that of the viscosity model ($h_\rho^* = 0.3795 > h_\eta^* = 0.3129$). Also, it can be seen that remarkably the AD structural range of both the density and viscosity models are very large ($AD_{coverage} = 100\%$) as none of the HDESs were considered as an outlier. However, that being said, predictions of some HDESs at several exception temperatures could be regarded as "borderline AD". The borderline HDESs have been split into two main categories, (i) structural borderline outlier "HDESs with an h_i value close to h^*", and (ii) response borderline outlier "HDESs with SDR values close to ±3". Table III.15 lists a summary of all the HDESs that were considered borderline AD. If the borderline points are

considered as outliers, then the $AD_{coverage}$ of the models reduces to 98.0% and 97.7% for the density and viscosity models, respectively.

Table III.15. List of HDESs that are considered borderline AD.

Structural Borderline Outlier	Response Borderline Outlier
Density Model	
DL-menthol: acetic acid (1:1)	decanoic acid: tetraoctyl-ammonium bromide (2:1)
DL-menthol: pyruvic acid (1:2)	decanoic acid: tetraoctyl-ammonium chloride (2:1)
Viscosity Model	
ethylparaben: methyltrioctyl-ammonium chloride (2:1)	decanoic acid: lidocaine (4:1)
ibuprofen: tetraheptyl-ammonium chloride (3:7)	decanoic acid: sodium dodecanoate (4:1)
DL-menthol: thymol (1:1)	

In conclusion, the results of the AD analysis indicate that the proposed QSPR models show high reliability and generalizability due to their wide domain of applicability and structural coverage. The results also suggest that the prediction of new HDESs that fall within the same domain of applicability could be considered reliable for initial solvent screening studies in the absence of experimental data. However, the prediction of external HDESs that fall outside the domain of applicability of the QSPR models may also be considered correct but less reliable due to their extrapolation degree, and thus, should be treated with greater care.

III.4. Electrical Conductivity of Deep Eutectic Solvents

III.4.1. Electrical Conductivity Dataset

An electrical conductivity (k / mS·cm^{-1}) dataset of 236 experimental points was used as a basis for the development of the QSPR models. The data points were taken from previous works (Bagh et al., 2013; Kareem et al., 2010) and are summarized in Table 2 in (Appendix A). The collected experimental data include a total of 21 DESs (9 phosphonium-based and 11 ammonium-based DESs). The data covered a wide range of temperatures (298.15 − 368.15 K) and molar ratios (1:1-1:8) at atmospheric pressure. The DESs were comprised of combinations of 4 HBAs and 3 HBDs mixed at various molar ratios.
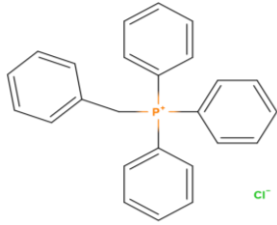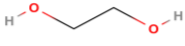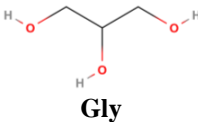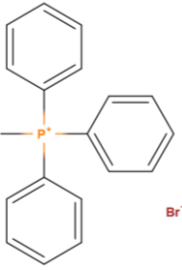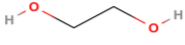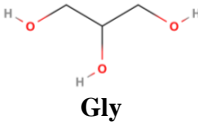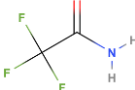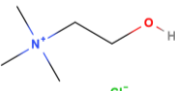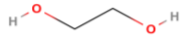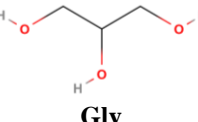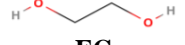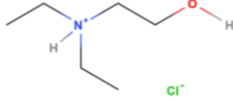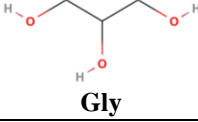
Table III.16 lists the DESs used with their chemical structures and compositions. The HBAs considered are as follows : (i) benzyltriphenylphosphonium chloride (BTPPC), (ii) methyltriphenylphosphonium bromide (MTPPB), (iii) choline chloride (ChCl), and (iv) N,N-diethylethanolammonium chloride (DEEAC). As for HBDs, the following were considered : (i) ethylene glycol (EG), (ii) glycerol (Gly), and (iii) 2,2,2-Trifluoroacetamide (TFA). The choice of DESs was done with the intent of covering a range of HBA and HBD molecules with different

cations, anions, functional groups, and molar ratios. This is expected to improve the robustness of the developed model and allow for better predictions of the electrical conductivity of DESs. Additionally, since the temperature is one of the main parameters affecting electrical conductivity, the choice of the data was made based on having a wide range of temperatures to extend the field of investigation to include both the DES structure and the temperature dependence on electrical conductivity. The measurements reported from the literature were done in triplicates and the uncertainties in measurement were reported as ± 0.003 mS·cm^{-1} and ± 0.1 K for electrical conductivity and temperature, respectively. It is worth noting that based on the data selected, the developed model will not be able to predict the electrical conductivity of hydrophobic DESs as they are considered to be "chemically different" than the DESs selected in Table III.16.

Table III.16. Compositions of the deep eutectic solvents.

Hydrogen Bond Acceptor (HBA)	Hydrogen Bond Donor (HBD)	Molar Ratio	DES
(i) Phosphonium-based DESs			
BTPPC	EG	(1:3)	DES 1
	Gly	(1:5)	DES 2
MTPPB	EG	(1:5.25)	DES 3
		(1:4)	DES 4
		(1:3)	DES 5
	Gly	(1:4)	DES 6
		(1:3)	DES 7
		(1:1.75)	DES 8
	TFA	(1:8)	DES 9
(ii) Ammonium-based DESs			
ChCl	EG	(1:2.5)	DES 10
		(1:2)	DES 11
		(1:2)	DES 12
	Gly	(1:3)	DES 13
		(1:2)	DES 14
		(1:1)	DES 15
DEEAC	EG	(1:4)	DES 16
		(1:3)	DES 17
		(1:2.5)	DES 18
	Gly	(1:4)	DES 19
		(1:3)	DES 20
		(1:2)	DES 21

III.4.2. Molecular Descriptors using COSMO-RS

Utilizing the generated COSMO files of the HBA and HBD molecules, COSMO calculations were performed to calculate: (i) the molecular surface polarity distributions (σ-profile), and (ii) the molecular descriptors (S_σ-profile), which is the integral of the σ-profile. Figure III.16 shows the 3D molecular structures and surface charge densities of the HBAs and HBDs. The σ-profile of a molecule provides the probability distribution of obtaining a segment of the molecular surface with a particular screening charge density (σ). Also, the possible molecular interactions of the mixture of HBA and the HBD (*i.e.* electrostatic, polar, and hydrogen bonding interactions) can be predicted through σ-profiles (Eckert & Klamt, 2002; Diedenhofen & Klamt, 2010; Aissaoui et al., 2016). Additionally, it is worth noting that the position, width, and height of the σ-profile peaks differ based on the concentration of contributing atoms and the nature of the molecule. Therefore, to prepare the DESs the $S\sigma$-profiles of the HBA and HBD were adjusted to account for changes in the molar ratio of the DES.

Figure III.17 shows the 3D molecular structures and surface charge densities of the DES descriptor sets used at a 1:1 molar ratio plotted using COSMOThermX.
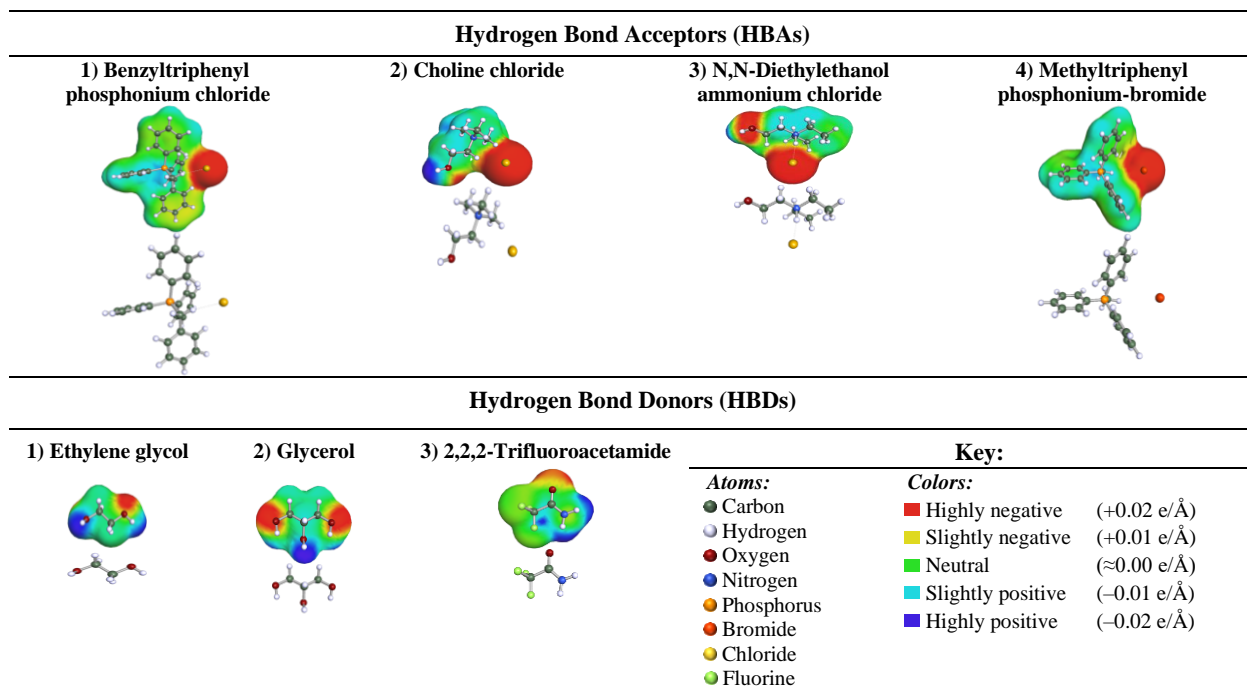
Figure III.16. 3D structures and charge densities of the HBAs and HBDs.

		Deep Eutectic Solvents (DESs)		
BTPPB:EG	MTPPB:Gly	ChCl:Gly	BTPPB:Gly	MTPPB:TFA
DEEAC:EG	MTPPB:EG	ChCl:EG		DEEAC:Gly
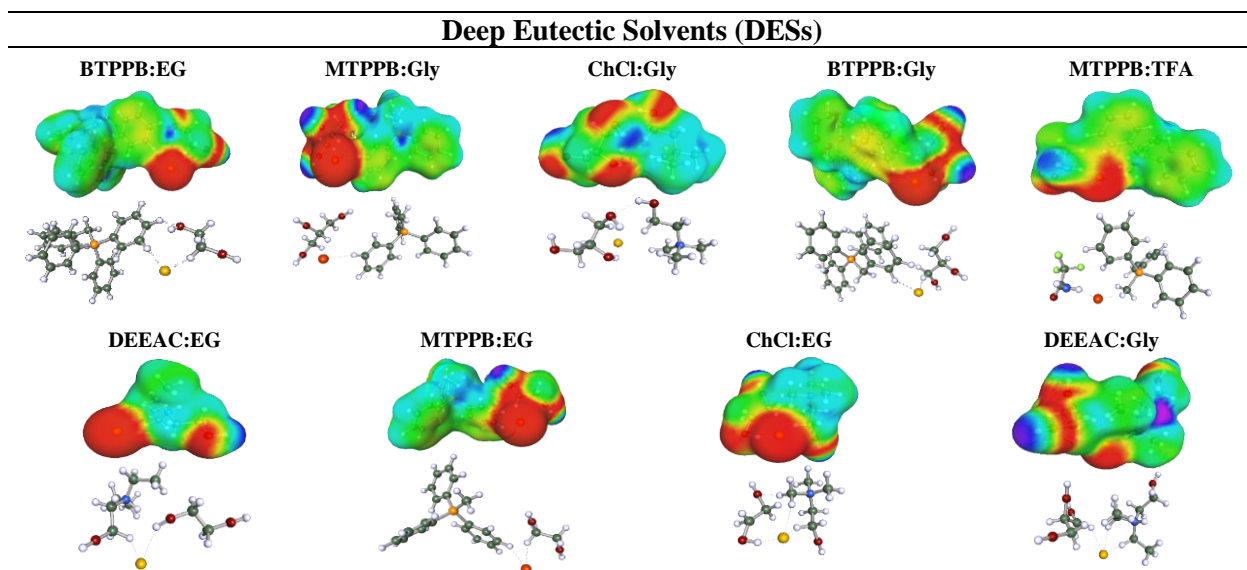
Figure III.17. 3D structures and charge densities of the deep eutectic solvents at a 1:1 molar ratio.

III.4.3. Development of the Quantitative Structure-Property Relationship Models

As aforementioned, the σ-profiles obtained from applying the COSMO-RS method contain the necessary chemical information for predicating the possible interactions between the HBA and the HBD. Thus, it is possible to develop a relationship between the structure and certain property of the DES, such as electrical conductivity.

Thus, the first step of developing the QSPR model was to divide the σ-profiles for each HBA and HBD molecule into 10 regions from –0.025 e/Å up until +0.025 e/Å with each region being 0.005 e/Å wide. Afterward, the integral of each region was calculated and their numerical area value was utilized as a molecular descriptor. The 10 molecular descriptors and their representations are listed in Table III.17.

Table III.17. The 10 molecular descriptors and their representations.

Molecular Descriptor	Screening Charge Density Range (e/Å)	Representation
S_{DES}^{1}	$-0.025 < \sigma < -0.020$	HBD region
S_{DES}^{2}	$-0.020 < \sigma < -0.015$	
S_{DES}^{3}	$-0.015 < \sigma < -0.010$	
S_{DES}^{4}	$-0.010 < \sigma < -0.005$	Non-polar region with negative charges density
S_{DES}^{5}	$-0.005 < \sigma <\ \ 0.000$	
S_{DES}^{6}	$0.000 < \sigma < +0.005$	Non-polar region with positive charges density
S_{DES}^{7}	$+0.005 < \sigma < +0.010$	
S_{DES}^{8}	$+0.010 < \sigma < +0.015$	HBA region
S_{DES}^{9}	$+0.015 < \sigma < +0.020$	
S_{DES}^{10}	$+0.020 < \sigma < +0.025$	

III.4.4. Results and Discussion

III.4.4.1. σ-Profile of the HBA and HBD Molecules

The σ-profiles of the HBAs and the HBDs were calculated and are shown in Figure III.18 and Figure III.19, respectively. The σ-profile can be divided into 3 main regions: (i) the HBD region "negative charge densities", (ii) the non-polar region "almost neutral charge densities", and (iii) the HBA region "positive charge densities".
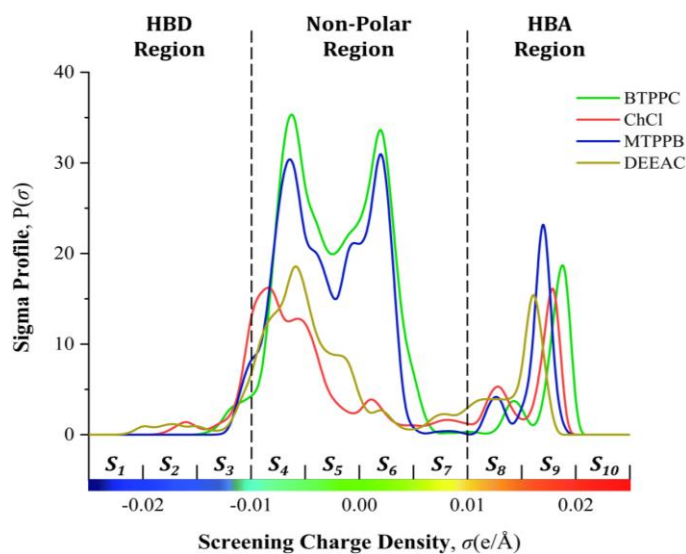
Figure III.18. σ-profiles of the hydrogen bond acceptors.
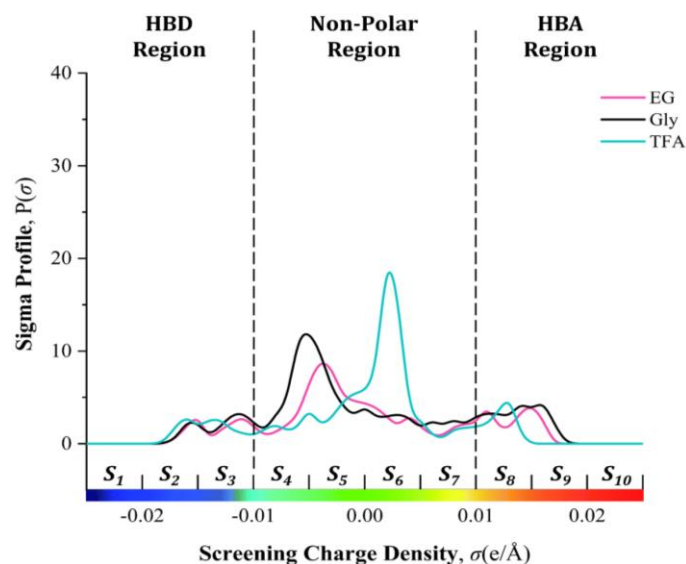
Figure III.19. σ-profiles of the hydrogen bond donors.

III.4.4.2. Model 1: Linear QSPR Model Excluding Descriptor Interactions

The first MLR-based QSPR model was developed by taking into account the 10 molecular descriptors (S_{DES}^1 - S_{DES}^{10}) and the temperature descriptor (T) without considering the interactions between these 11 descriptors. A statistical summary for evaluating the linear model in predicting

the dataset is listed in Table III.18.

Table III.18. Statistical parameters of the model excluding descriptor interactions.

R^2	0.8023
$R^2_{adjusted}$	0.8011
RMSE	3.2770

From the obtained coefficient of determination (R^2) of 0.8023, it can be concluded that the accuracy of the fit without considering the interactions between the descriptors is quite low. Nevertheless, an Analysis of Variance (ANOVA) was conducted to identify which descriptor terms have an important influence on the model. The ANOVA results and the calculated model coefficients are listed in Table III.19 and Table III.20, respectively.

Table III.19. Analysis of the first linear QSPR model excluding descriptor interactions.

Source	Degrees of Freedom	Sum of Squares	Mean Squares	F-Ratio
Model	6	10246.98	1707.83	158.9410
Error	229	2460.61	10.75	Prob. > F
Total	235	12707.59	-	<0.0001

Table III.20. Estimation of the model coefficients for the first linear QSPR model.

Term	Coefficient	Estimate	Standard Error	$|t_{\text{-Ratio}}|$	P_{value}
S_4	a_4	1382.61	555.54	2.49	0.0135
S_6	a_6	–465.36	126.65	3.67	0.0003
S_7	a_7	–4145.11	704.97	5.88	<.0001
S_9	a_9	–2379.13	1076.47	2.21	0.0281
S_{10}	a_{10}	–1477.70	329395.40	4.49	<.0001
T	a_{11}	0.19	0.01	15.48	<.0001

The ANOVA results indicated that the descriptors S_1, S_2, S_3, S_5, S_8 and the intercept has no significant influence on the electrical conductivity model (P-value > 5%). Therefore, their corresponding coefficients were set to $a_0 = a_1 = a_2 = a_3 = a_5 = a_8 = 0$. On the other hand, the descriptors $S_4, S_6, S_7, S_9, S_{10}$ and T were found to have a significant influence on the electrical conductivity (P-value < 5%). Their corresponding estimated coefficient values are listed in Table III.20. The resulting electrical conductivity (k) linear model can be expressed as follows :

$$k = 1382.61\ (S_4) - 465.36\ (S_6) + 2379.13\ (S_7) - 2379.13\ (S_9) - 1477.70\ (S_{10}) + 0.19\ (T) \qquad \text{(III.5)}$$

where k is in units of mS·cm^{-1}, S_i is in units of e/Å^2, and T is in units of K.

The signs of the model coefficients listed in Table III.20, or Eq. (III.5), indicate whether a descriptor has a positive effect on the electrical conductivity or a negative effect. A positive sign indicates a positive effect and vice versa. It can be observed that the temperature has a positive effect (*i.e.* increases the electrical conductivity of the DES), which is consistent with the results obtained from the literature (Bagh et al., 2013). In terms of molecular descriptors, the only

descriptor with a positive effect was the S_4 descriptor (HBD region), while the others (non-polar and HBA region) were observed to have negative effects on the electrical conductivity.

Figure III.20 shows a parity diagram where the experimental values were plotted versus the predicted values. The experimental electrical conductivity points were deviating from the diagonal line with visible dispersion. Similar results were displayed by the residual analysis depicted in Figure III.21, where residuals were highly deviating from the horizontal zero line (between +7.5 and –5). Thus, it can be concluded that this model is considered to be "qualitative at best" and is not sufficient enough as a quantitative predictive model for electrical conductivity. Therefore, in the next section, another approach is considered.
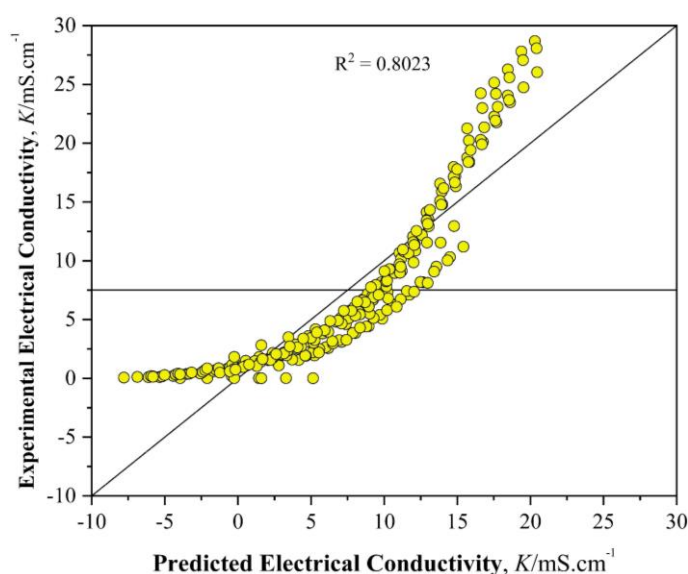
Figure III.20. Experimental versus predicted values of electrical conductivity calculated via Eq. (III.5).
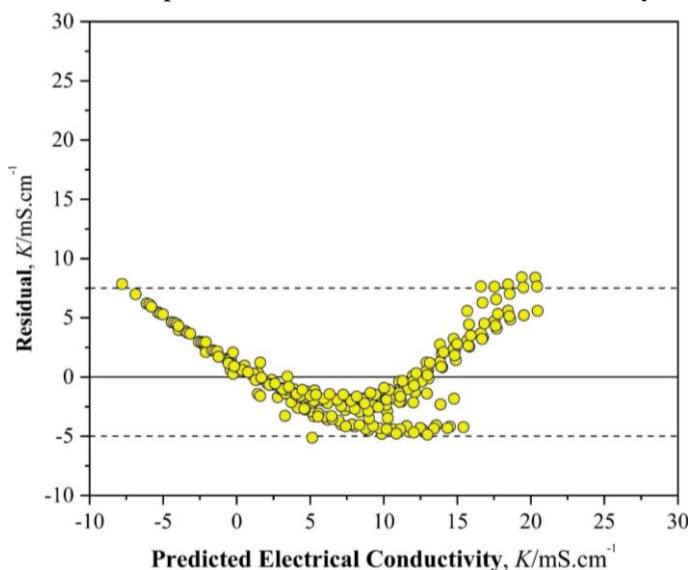
Figure III.21. Residual versus predicted values of electrical conductivity calculated via Eq. (III.5).

III.4.4.3. Model 2: Linear QSPR Model Including Descriptor Interactions

The second MLR-based QSPR model was developed by taking into account the 10 molecular descriptors (S_{DES}^1 - S_{DES}^{10}) and the temperature descriptor (T). However, unlike the previous model, the binary interactions between the 11 descriptors were also taken into account. A statistical summary for evaluating the linear model in predicting the dataset is listed in Table III.21 The obtained coefficient of determination (R^2) of 0.9901 suggests that the accuracy of the fit after considering the interactions improved drastically (from 0.8023). Therefore, it can be concluded that the electrical conductivity and the descriptors (including their interactions) can be expressed satisfactorily via the use of a linear equation.

Table III.21. Statistical parameters of the model including descriptor interactions.

R^2	0.9901
$R^2_{adjusted}$	0.9897
$RMSE$	0.8960

However, since the number of terms using this approach is quite high (11 descriptors and 110 interactions descriptors), an ANOVA analysis was conducted to identify which terms have an important influence on the model. The main objective of this analysis is to find a reduced expression (*i.e.* having less terms) that can satisfactorily predict the electrical conductivity of the DESs. The ANOVA results and the calculated model coefficients are listed in Table III.22 and Table III.23, respectively.

Table III.22. Analysis of the second linear QSPR model including descriptor interactions.

Source	Degrees of Freedom	Sum of Squares	Mean Squares	F-Ratio
Model	16	12531.86	783.24	976.1019
Error	219	175.73	0.80	Prob. > F
Total	235	12707.59	-	<0.0001

Table III.23. Estimation of the model coefficients for the second linear QSPR model.

Term	Coefficient	Estimate	Standard Error	$|t\text{-}Ratio|$	P_{value}
Intercept	a_0	−45.58	5.59	−8.16	<.0001
S_4	a_4	−2531.74	579.22	−4.37	<.0001
S_5	a_5	−809.74	92.23	−8.78	<.0001
S_6	a_6	371.83	139.70	2.66	0.0084
S_7	a_7	1824.68	848.23	2.15	0.0326
S_9	a_9	4738.82	1072.56	4.42	<.0001
T	a_{11}	0.19	3.40×10^{-3}	56.36	<.0001
$(S_4\text{-}\bar{S}_4)(S_9\text{-}\bar{S}_9)$	a_{49}	−31037.51	3870.61	−8.02	<.0001
$(S_5\text{-}\bar{S}_5)(S_6\text{-}\bar{S}_6)$	a_{56}	13402.87	3994.97	3.35	0.0009
$(S_5\text{-}\bar{S}_5)(S_7\text{-}\bar{S}_7)$	a_{57}	107281.33	14428.93	7.44	<.0001
$(S_6\text{-}\bar{S}_6)(S_7\text{-}\bar{S}_7)$	a_{67}	90000.56	8921.17	10.09	<.0001
$(S_4\text{-}\bar{S}_4)(T\text{-}\bar{T})$	a_{411}	2.61	0.66	3.97	<.0001
$(S_6\text{-}\bar{S}_6)(T\text{-}\bar{T})$	a_{611}	−5.07	0.30	−16.82	<.0001
$(S_7\text{-}\bar{S}_7)(T\text{-}\bar{T})$	a_{711}	−45.86	2.57	−17.87	<.0001
$(S_{10}\text{-}\bar{S}_{10})(T\text{-}\bar{T})$	a_{1011}	−22835.82	5437.27	−4.20	<.0001

[a]$\bar{S}_4$ = 2.34×10^{-2} ; $\bar{S}_5$ = 3.47×10^{-2} ; $\bar{S}_6$ = 1.90×10^{-2}; $\bar{S}_7$ = 7.70×10^{-3} ; $\bar{S}_{10}$ = 1.69×10^{-7} ; $\bar{T}$ = 326.50

Table III.23 lists the terms that have a significant influence on the electrical conductivity (P-value < 5%), while all the other terms that are insignificant (P-value > 5%) have been set to 0. It can be seen from the results that the number of required terms reduced drastically after applying the ANOVA analysis. The resulting electrical conductivity (k) linear model can be expressed using Eq. (III.6) as follows :

$$k = -45.58 - 2531.74\ (S_4) - 809.74\ (S_5) + 371.83\ (S_6) + 1824.68\ (S_7) + 4738.82\ (S_9) + 0.19\ (T) - 31037.51\ (S_4-\overline{S_4})(S_9-\overline{S_9}) + 2.61\ (S_4-\overline{S_4})(T-\overline{T}) + 13402.87\ (S_5-\overline{S_5})(S_6-\overline{S_6}) + 107281.33\ (S_5-\overline{S_5})(S_7-\overline{S_7}) + 90000.56\ (S_6-\overline{S_6})(S_7-\overline{S_7}) - 5.07\ (S_6-\overline{S_6})(T-\overline{T}) - 45.86\ (S_7-\overline{S_7})(T-\overline{T}) - 22835.82\ (S_{10}-\overline{S_{10}})(T-\overline{T})$$

(III.6)

where k is in units of mS·cm^{-1}, S_i and $\overline{S_i}$ are in units of e/Å^2, and T is in units of K.

In terms of positive and negative effects, it can be seen that the temperature has a positive effect on the electrical conductivity of the DESs, which is consistent with the earlier results from Model 1. As for the molecular descriptors, it can be observed that the descriptors from the non-polar region with negative charge densities (S_4 and S_5) have negative effects on the electrical conductivity of the DES. On the other hand, the descriptors from the non-polar region with positive charge densities (S_6 and S_7) and the HBA region (S_9) have positive effects on the electrical conductivity of DESs. Regarding the interactions between molecular descriptors, the interactions between $\{S_5, S_6\}$, $\{S_5, S_7\}$, and $\{S_6, S_7\}$ are observed to have positive effects, while interactions between $\{S_4, S_9\}$ resulted in negative effects on electrical conductivity. Finally, in terms of the interactions between molecular descriptors and the temperature descriptor, the interactions between $\{S_4, T\}$ resulted in positive effects, while the interactions between $\{S_6, T\}$, $\{S_7, T\}$, and $\{S_{10}, T\}$ are observed to have negative effects on the electrical conductivity of the DES.
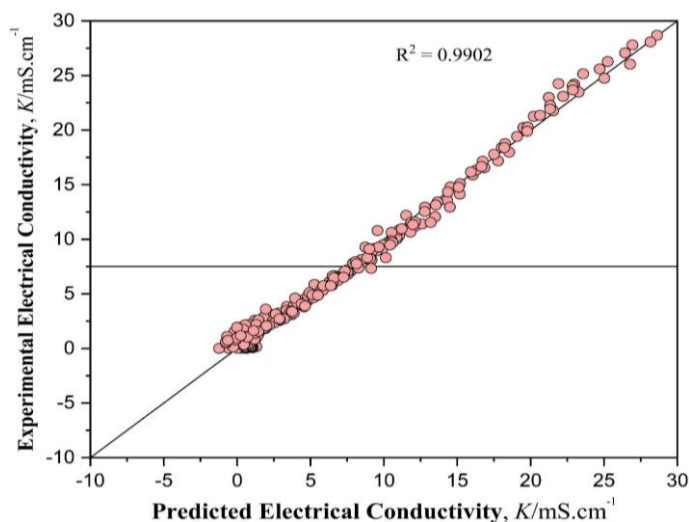
Figure III.22. Experimental versus predicted values of electrical conductivity calculated via Eq. (III.6).

Figure III.22 shows a parity diagram where the experimental values were plotted versus the predicted values. The experimental electrical conductivity points were on the diagonal line with very narrow dispersion. The reliable predictions were also confirmed by the residual analysis depicted in Figure III.23, where residuals were deviating between +2.5 and –2.5.
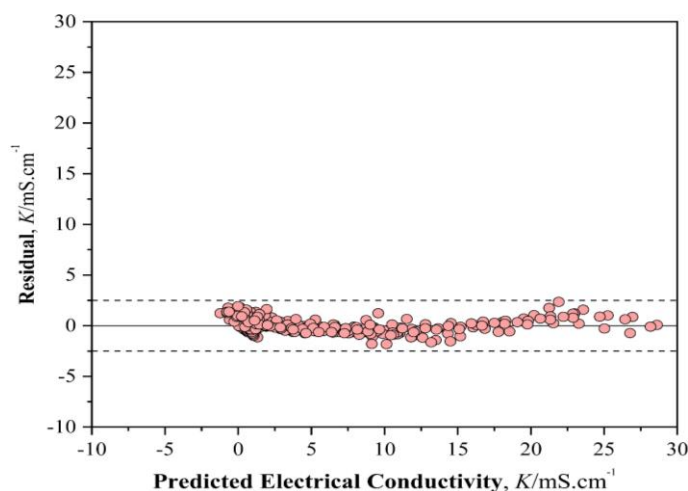
Figure III.23. Residual versus predicted values of electrical conductivity calculated via Eq. (III.6).

III.4.4.4. Applicability Domain of the Developed QSPR Models

As it can be seen from Figure III.24, the AD plot of the first model, Eq. (III.5), showed that most of the investigated DESs were within the AD boundaries of the proposed model $(0.000 < h_i < 0.088)$; $(-3 < SDR < +3)$. However, it was observed that DES 1 at the temperatures of $\{338.15–368.15 \text{ K}\}$ and DES 8 at 353.15 K presented h_i values higher than threshold h^* value (0.088). Therefore, it can be concluded that these two DESs are outside the domain of applicability of the proposed model. It should be noted that all values were within the suggested standardized residual boundary of $-3 < SDR < +3$.
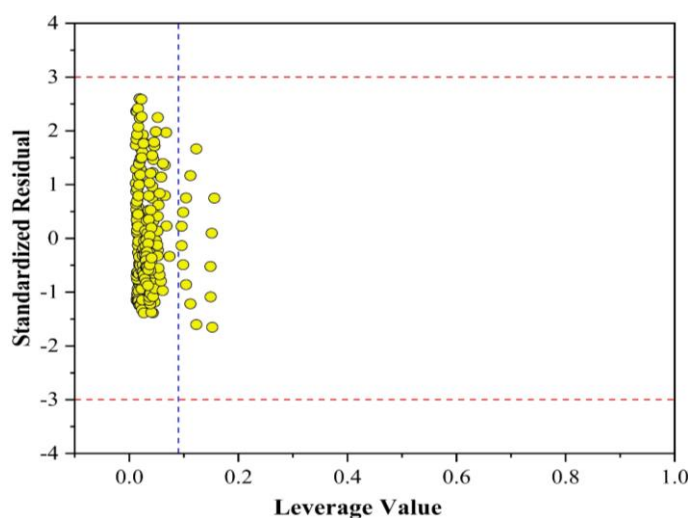
Figure III.24. William plot showing the Applicability Domain (AD) boundaries of the first model excluding descriptor interactions.

As illustrated in Figure III.25, the AD plot of the second model, Eq. (III.6), showed that most of the investigated DESs were within the AD boundaries of the proposed model $(0.000<h_i<0.2161)$; $(-3<SDR<+3)$. It can be also observed that no data points had an h_i value higher than threshold h^* value (0.2161). However, it was observed that DES 1 at the temperatures of {338.15–368.15 K} fell outside the suggested standardized residual boundary of $-3<SDR<+3$. Therefore, based on the results obtained, it was concluded that this DES is outside the domain of applicability of the proposed model.
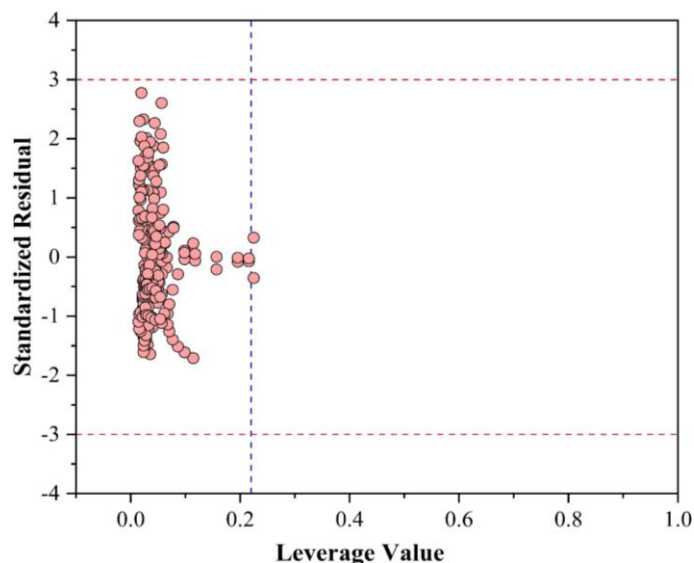
Figure III.25. William plot showing the Applicability Domain (AD) boundaries of the second model including descriptor interactions.

III.5. pH of Deep Eutectic Solvents

III.5.1. Experimental Data

To the best of our knowledge, the dataset reported in the literature covered 84 DESs prepared from 9 HBAs and 21 HBDs resulting in a total of 648 experimental points covering a variety of cations, anions, and functional groups. The DESs utilized in the dataset are considered to be a representative batch of a sufficiently extensive range of molecules that allow for a robust approach to predict the pH property of hydrophilic DESs. The utilized pH measurements also include a broad range of temperatures (358.15 – 293.15 K) and molar ratios (9:1 – 1:16) all measured at 1.01 bar, which is also anticipated to improve the robustness of the model. Table III.24 summarizes the DESs used with their corresponding molar ratios and experimental pH measurements. The complete experimental dataset is available in Table 3 in (Appendix A).

It should be noted that each DES listed in Table III.24 has been treated as a distinct DES, and not as a mixture of two compounds. This is because it has been reported by several papers that the physiochemical, thermal, and solvation properties of DESs depend on the choice of the HBA,

Chapter III   Physicochemical Properties of Deep Eutectic Solvents

the HBD, their synergetic mixing effects, and the molar ratio (Hayyan et al., 2012; Jibril et al., 2014; Mjalli et al., 2014; Saputra et al., 2020). Also, since the presence of water is an important parameter that affects the pH of DESs, the water contents of all the DESs have been accounted and their respective water molar ratio is shown in Table III.24.

Table III.24. The constituents of the deep eutectic solvents with their corresponding molar ratios, water contents, and experimental pH measurements.

DES#	Abbreviation	Mole ratio	pH	Temperature	Ref
DES1	ATPPB:DEG:H_2O	1:4:0.17	1.49 – 0.50	293.15 – 343.15	
DES1.1	ATPPB:DEG:H_2O	1:10:0.31	4.05 – 3.23	293.15 – 343.15	
DES1.2	ATPPB:DEG:H_2O	1:16:0.39	4.21 –3.34	293.15 – 343.15	(Ghaedi et al., 2018)
DES2	ATPPB:TEG:H_2O	1:4:0.18	1.40 – 0.15	293.15 – 343.15	
DES2.1	ATPPB:TEG:H_2O	1:10:0.35	3.15 –1.90	293.15 – 343.15	
DES2.2	ATPPB:TEG:H_2O	1:16:0.56	3.42 – 2.47	293.15 – 343.15	
DES3	BTPC:EG	1:3	5.71 – 5.59	298.15 – 353.15	(Kareem et al., 2010)
DES4	BTPC:Gly	1:5	6.90 – 7.02	298.15 – 353.15	
DES5	ChCl:CA:H_2O	1:1:1.33	1.72 – 0.92	298.15 – 333.15	
DES5.1	ChCl:CA:H_2O	2:1:1.44	1.33 – 0.98	298.15 – 333.15	
DES6	ChCl:DEA	1:6	11.47 – 9.98	295.15 – 353.15	
DES7	ChCl:EG:H_2O	1:2:0.33	4.38 – 4.00	298.15 – 333.15	
DES8	ChCl:Fru	1:1	6.10 – 4.43	298.15 – 358.15	
DES8.1	ChCl:Fru	1.5:1	6.91 – 6.32	298.15 – 358.15	
DES8.2	ChCl:Fru	2:1	6.65 – 4.85	298.15 – 358.15	
DES8.3	ChCl:Fru	2.5:1	7.10 – 6.41	298.15 – 358.15	
DES9	ChCl:Glu	1:1	6.83 – 6.25	298.15 – 353.15	
DES9.1	ChCl:Glu	1.5:1	7.10 – 5.99	298.15 – 353.15	
DES9.2	ChCl:Glu	2:1	7.00 – 6.45	298.15 – 353.15	
DES9.3	ChCl:Glu	2.5:1	7.11 – 6.47	298.15 – 353.15	(Skulcova et al., 2018)
DES10	ChCl:Gly:H_2O	1:2:0.33	4.47 – 4.12	298.15 – 333.15	
DES11	ChCl:GlyA:H_2O	1:3:0.44	1.24 – 0.99	298.15 – 333.15	
DES12	ChCl:LacA:H_2O	1:5:0.67	1.73 – 0.99	298.15 – 333.15	
DES12.1	ChCl:LacA:H_2O	1:10:1.22	1.77 – 1.04	298.15 – 333.15	
DES13	ChCl:MA:H_2O	1:1:0.22	1.61 – 0.94	298.15 – 333.15	
DES13.1	ChCl:MA:H_2O	2:1:0.33	1.93 – 1.19	298.15 – 333.15	
DES14	ChCl:MalA:H_2O	1:1:0.22	1.28 – 0.41	298.15 – 333.15	
DES15	ChCl:MDEA	1:6	11.04 – 9.89	295.15 – 353.15	
DES16	ChCl:MEA	1:6	12.81 – 11.12	295.15 – 353.15	
DES17	ChCl:OA:H_2O	1:1:2.44	1.21 – 0.06	298.15 – 333.15	
DES18	ChCl:TFA	1:2	3.97 – 3.86	298.15 – 353.15	
DES19	DEEAC:MalA	1:1	2.41 – 2.29	298.15 – 353.15	(Bahadori et al., 2013)
DES20	EAC:Gly:H_2O	1:3:0.64	2.04 – 1.97	303.15 – 353.15	
DES20.1	EAC:Gly:H_2O	1:4:0.95	2.42 – 2.33	303.15 – 353.15	(Saputra et al., 2020)
DES20.2	EAC:Gly:H_2O	1:5:1.02	2.57 – 2.44	303.15 – 353.15	
DES21	LacA:Ala:H_2O	9:1:1.11	2.15 – 1.42	298.15 – 333.15	
DES22	LacA:Bet:H_2O	2:1:0.33	2.45 – 1.85	298.15 – 333.15	
DES23	LacA:Glyi:H_2O	2:1:0.33	2.74 –2.18	298.15 – 333.15	(Skulcova et al., 2018)
DES23.1	LacA:Glyi:H_2O	9:1:1.11	2.27 – 1.54	298.15 – 333.15	
DES24	MA:Suc:H_2O	1:1:0.22	2.05 – 1.35	298.15 – 333.15	
DES25	MTPPB:EG	1:4	6.35 – 5.86	298.15 – 353.15	
DES26	MTPPB:Gly	1:1.75	6.97 – 6.70	298.15 – 353.15	(Kareem et al., 2010)
DES27	MTPPB: TFA	1:8	2.71 – 3.34	298.15 – 353.15	
DES28	TBAC:EG	1:2	9.10 – 7.51	293.15 – 353.15	
DES28.1	TBAC:EG	1:3	9.20 – 7.76	293.15 – 353.15	
DES28.2	TBAC:EG	1:4	9.35 – 8.19	293.15 – 353.15	(Mjalli et al., 2014)
DES29	TBAC:Gly	1:3	6.51 – 6.11	293.15 – 353.15	
DES29.1	TBAC:Gly	1:4	8.95 – 7.50	293.15 – 353.15	
DES29.2	TBAC:Gly	1:5	6.81 – 6.42	293.15 – 353.15	

DES30	TBAC:TEG	1:1	6.40 – 5.92	293.15 – 353.15	
DES30.1	TBAC:TEG	2:1	6.97 – 6.21	293.15 – 353.15	
DES30.2	TBAC:TEG	3:1	7.70 – 6.73	293.15 – 353.15	
DES30.3	TBAC:TEG	4:1	8.06 – 7.03	293.15 – 353.15	
DES31	TPAB:EG	1:3	6.41 – 5.97	293.15 – 353.15	
DES31.1	TPAB:EG	1:4	6.53 – 6.14	298.15 – 353.15	
DES31.2	TPAB:EG	1:5	7.23 – 6.57	298.15 – 353.15	
DES32	TPAB:Gly	1:2	6.40 – 6.03	298.15 – 353.15	
DES32.1	TPAB:Gly	1:3	5.96 – 5.85	298.15 – 353.15	(Jibril et al., 2014)
DES32.2	TPAB:Gly	1:4	5.85 – 5.64	298.15 – 353.15	
DES33	TPAB:TEG	1:2.5	5.09 – 4.80	298.15 – 353.15	
ES33.1	TPAB:TEG	1:3	5.22 – 4.94	298.15 – 353.15	
DES33.2	TPAB:TEG	1:4	5.15 – 4.87	298.15 – 353.15	
DES34	ChCl:LacA:H_2O	1:9:1.11	1.61 – 0.80	298.15 – 333.15	(Skulcova et al., 2018)
DES35	Bet:MA:H_2O	1:1:1.5	3.39 – 2.62	288.15 – 328.15	
DES35.1	Bet:MA:H_2O	1:1:6	3.40 – 2.90	288.15 – 328.15	
DES35.2	Bet:MA:H_2O	1:1:13.9	2.95 – 2.50	288.15 – 328.15	
DES36	ChCl:CA:H_2O	2:1:3	0.63 – 0.67	288.15 – 328.15	
DES36.1	ChCl:CA:H_2O	2:1:11.5	0.88 – 0.98	288.15 – 328.15	
DES36.2	ChCl:CA:H_2O	2:1:26.7	1.11 – 1.18	288.15 – 328.15	
DES37	ChCl:MA:H_2O	1:1:1.7	0.22 – 0.34	288.15 – 328.15	
DES37.1	ChCl:MA:H_2O	1:1:6.5	0.55 – 0.78	288.15 – 328.15	
DES37.2	ChCl:MA:H_2O	1:1:15.2	1.10 – 1.11	288.15 – 328.16	
DES38	Bet:CA:H_2O	1:1:1.9	2.81 – 2.15	288.15 – 328.15	
DES38.1	Bet:CA:H_2O	1:1:7.4	2.77 – 2.15	288.15 – 328.15	(Mitar et al., 2019)
DES38.2	Bet:CA:H_2O	1:1:17.2	2.75 – 2.12	288.15 – 328.15	
DES39	ChCl:Pro:MA:H_2O	1:1:1:2.4	3.63 – 3.58	288.15 – 328.15	
DES39.1	ChCl:Pro:MA:H_2O	1:1:1:9.3	3.35 – 2.80	288.15 – 328.15	
DES39.2	ChCl:Pro:MA: :H_2O	1:1:1:21.6	2.95 – 3.03	288.15 – 328.15	
DES40	Pro:MA:H_2O	1:1:1.5	2.17 – 2.19	288.15 – 328.15	
DES40.1	Pro:MA:H_2O	1:1:5.9	2.87 – 2.29	288.15 – 328.15	
DES40.2	Pro:MA:H_2O	1:1:13.8	2.86 – 2.28	288.15 – 328.15	
DES41	MA:Glu:H_2O	1:1:1.9	0.37 – 0.46	288.15 – 328.15	
DES41.1	MA:Glu:H_2O	1:1:7.5	0.45 – 0.67	288.15 – 328.15	
DES41.2	MA:Glu:H_2O	1:1:17.4	0.76 – 0.81	288.15 – 328.15	

III.5.2. Concept of pH in Deep Eutectic Solvents

The knowledge of a solvent's pH is vital in designing many industrial processes and optimizing their operating conditions (Carvalheda et al., 2013; Farias et al., 2018; Paris et al., 2019; Uslu & Bamufleh, 2016). In this section, the dataset collected from the literature (Table III.24) were analyzed to study and identify the structural factors influencing the pH value of the DESs. It has been previously reported by Abbott *et al.*(Abbott et al., 2018) that the concept of pH in ILs and DESs is poorly understood. According to their discussion, the pH of ILs and DESs is based on the ability of the DES's cation, anion, and HBD to act as proton acceptors and proton donors in the same way that any other molecular liquid can.

III.5.3. Interpretation of the Experimental Trends

In terms of the temperature effect, as expected, all the DESs in Table III.24 showed a linear acidity behavior; a decrease in the pH value when increasing the temperature, except for some DESs *e.g.*, MTPPB:TFA (1:8) and BTPPC:Gly (1:5) where the increase in the temperature

increases the pH values (Kareem et al., 2010). As for the effect of water content, it can be observed from Table III.24 that the increase in the water content had a dual effect; either increasing the acidity of the DESs (*e.g.* ChCh:Pro:MA:H_2O or Bet:CA:H_2O DESs) or decreasing it (*e.g.* ChCl:CA:H_2O or Pro:MA:H_2O). Regarding the effect of DES's structure on pH values, the following was found: by keeping the HBD constant *i.e.,* tri-ethylene glycol (TEG), the acidity of ATPPB:TEG:H_2O (1:4:0.18) was much higher than TPAB:TEG (1:4). This could be attributed to the aromaticity of the ATPPB and the addition of water (Ghaedi et al., 2018). Also, when comparing EAC:Gly (1:4) (Saputra et al., 2020) and TBAC:Gly (1:4) (Mjalli et al., 2014), the pH values of TBAC:Gly (1:4) were higher than EAC:Gly (1:4). It can be seen that the increase in the number of alkyl chains increases the value of pH.

Considering the effect of HBD by keeping choline chloride (ChCl) constant, it can be seen that DESs with organic acid (Skulcova et al., 2018) HBDs (*i.e.,* citric acid, glycolic acid, lactic acid, malic acid, malonic acid, and oxalic acid) had the highest acidity, followed by polyols (Skulcova et al., 2018) HBDs (*e.g.* ethylene glycol, glycerol)> sugars (Hayyan et al., 2012, 2013) (*e.g.* fructose and glucose)> and finally amines (Adeyemi et al., 2018) (*e.g.* ethanolamine and diethanolamine). Moreover, for the same HBD family, *i.e.,* polyols (Ghaedi et al., 2018), it can be seen that the TEG, which contains three hydroxyl groups showed higher acidity compared to DEG with two hydroxyl groups when comparing ATPPB:TEG:H_2O (1:10:0.35) to ATPPB:DEG:H_2O (1:10:0.31). Likewise, for constant HBA *i.e.,* TBAC, ethylene glycol (EG) was more basic compared to glycerol (Gly) when comparing TBAC:EG (1:3) to TBAC: Gly (1:3), which could be explained again based on the number of hydroxyl functional groups attached to each molecule (Mjalli et al., 2014). Additionally, for amine HBDs, the primary amines (EA) showed higher basicity (high pH) compared to secondary (DEA) and tertiary (MDEA) amines (Adeyemi et al., 2018). From the dataset available, it can be said that the nature of the HBD was significantly influencing the acidity of the DES relative to the effect of HBAs (Bahadori et al., 2013; Kareem et al., 2010).

Another important feature is the molar ratio, which plays a significant role in altering the properties of DESs. It can be observed that the increase in the molar ratio had inconsistent trends. For example, the increase in the molar ratio of TPAB:Gly from (1:2) to (1:4) increases the acidity of the DES (Jibril et al., 2014). Conversely, increasing the molar ratio of ATPPB:DEG:H_2O (Ghaedi et al., 2018) from (1:4:0.17) to (1:10:0.31) reduces the acidity of the DES. It should be noted that the further increase in the molar ratio of ATPPB:DEG:H_2O to (1:16:0.39) had an insignificant effect on the pH. This behavior could be attributed to the pH value of the DES

converging towards the pH of the pure HBD (pH ≈7) in addition to the increase in the water content (Ghaedi et al., 2018). The same behavior was observed for ATPPB:TEG:H_2O, EAC:Gly:H_2O, and ChCl:Fru (Hayyan et al., 2012). Other DESs showed an insignificant change in the pH when the molar ratio is increased as in the case of increasing the molar ratio of ChCl:LaA:H_2O from (1:5:0.67) to (1:10:1.22) (Skulcova et al., 2018) and the increase in the molar ratio of TBAC:EG from (1:2) to (1:4) (Mjalli et al., 2014). Other DESs showed exceptional changes in their pH value when changing the HBA molar ratio. For instance, increasing the molar ratio of ChCl:Glu from (1:1) to (1.5:1) increased the basicity of the DES, however, the basicity is decreased with further increase in the molar ratio to (2:1), yet increased again at a molar ratio of (2.5:1) (Hayyan et al., 2013). The same behavior was observed with TBAC:Gly (Mjalli et al., 2014). Thus, it can be concluded that no clear trend can be deduced by changing the molar ratio. The observed behavior could be attributed to the fact that the pH property significantly depends on the molecular-level interactions between the HBA and the HBD, and therefore, each case should be studied independently.

III.5.4. Result and Discussions

III.5.4.1. Physical Meaning of COSMO-RS σ-Profiles

Figure III.26 and Figure III.27 show the 2D chemical structures and the 3D geometrically optimized COSMO-RS molecular structures of the HBAs and the HBDs.

1) allyltriphenyl phosphonium bromide

2) benzyltriphenyl phosphonium chloride

3) betaine

4) choline chloride

5) ethyl ammonium chloride

6) methyltriphenyl phosphonium bromide

7) N,N-diethylethanol ammonium chloride

8) tetrabutyl ammonium chloride

9) tetrapropyl ammonium bromide

Key:

Atoms:
- Carbon
- Hydrogen
- Oxygen
- Nitrogen
- Phosphorus
- Bromide
- Chloride
- Fluorine

Colors:
- Highly negative   (+0.02 e/Å)
- Slightly negative (+0.01 e/Å)
- Neutral   (≈0.00 e/Å)
- Slightly positive (–0.01 e/Å)
- Highly positive   (–0.02 e/Å)
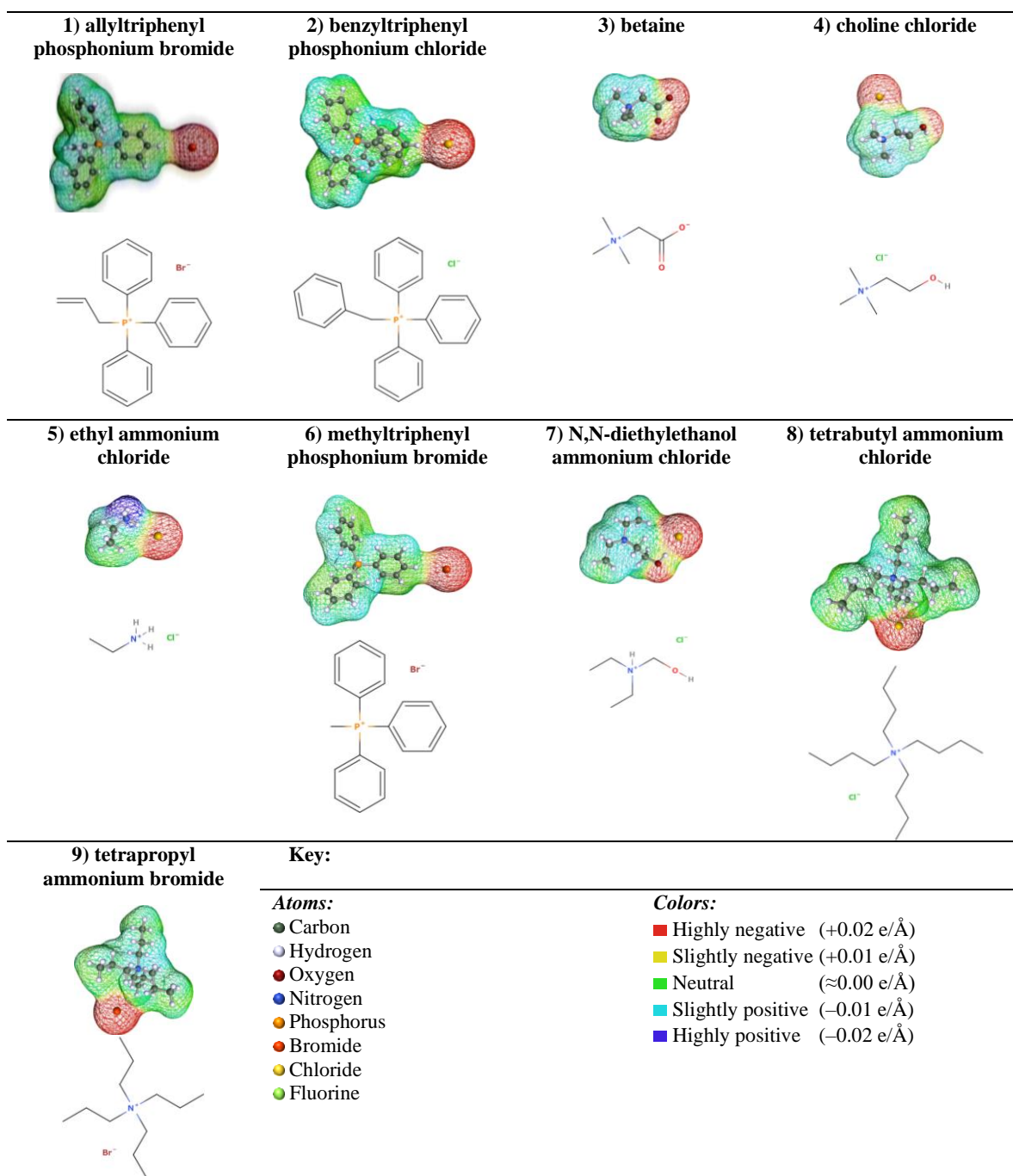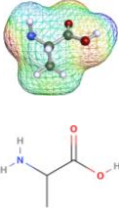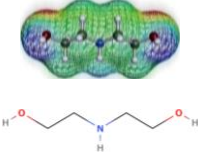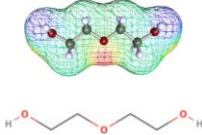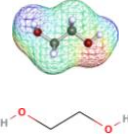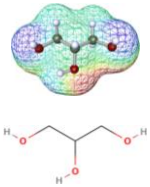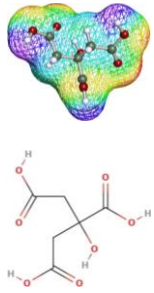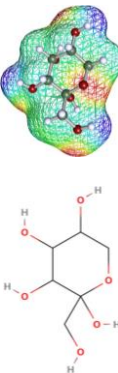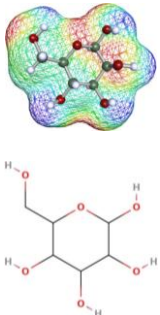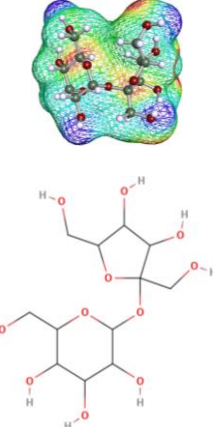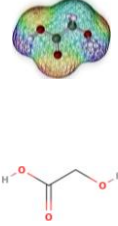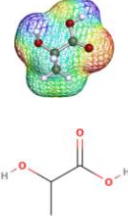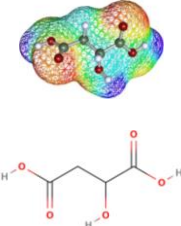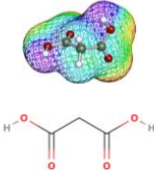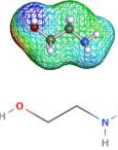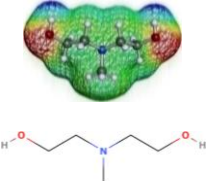
Figure III.26. 3D and 2D molecular structures of the 9 modeled hydrogen bond acceptors (HBAs).

1) alanine

2) diethanolamine

3) diethylene glycol

4) ethylene glycol

5) glycerol

6) citric acid

7) fructose

8) glucose

9) sucrose

10) glycine

11) glycolic acid

12) lactic acid

13) malic acid

14) malonic acid

15) monoethanol amine

16)methyldiethanol amine

17) oxalic acid

18) proline

19) triethanol amine

20) triethylene glycol

21) trifluoro acetamide   **22) water**   **Key:**

Atoms:

- Carbon
- Hydrogen
- Oxygen
- Nitrogen
- Phosphorus
- Bromide
- Chloride
- Fluorine

Colors:

Highly negative	(+0.02 e/Å)
Slightly negative	(+0.01 e/Å)
Neutral	(≈0.00 e/Å)
Slightly positive	(–0.01 e/Å)
Highly positive	(–0.02 e/Å)
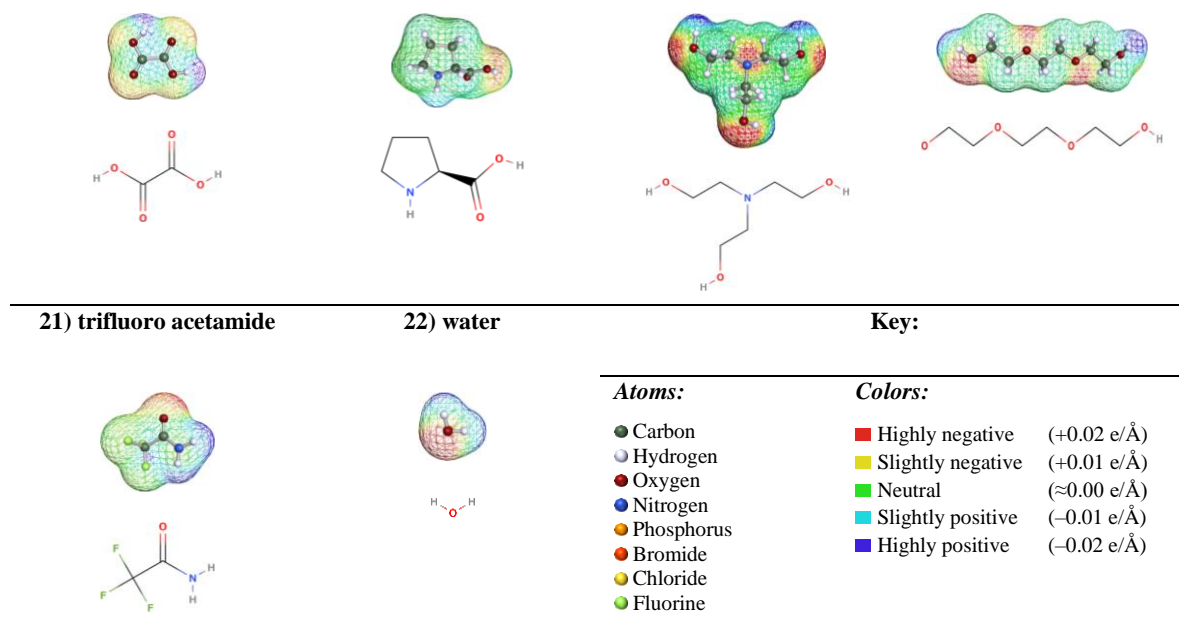
Figure III.27. 3D and 2D molecular structures of the 21 modeled hydrogen bond donors (HBDs) and water.

Utilizing the COSMO-RS structures, the *σ-profile* of each HBA and HBD was determined. Figure III.28 shows the developed *σ-profile* curves of the 9 HBAs and 21 HBDs categorized as follows : (a) salts, (b) amines & water, (c) fatty acids & amino acids, and d) polyols & sugars.
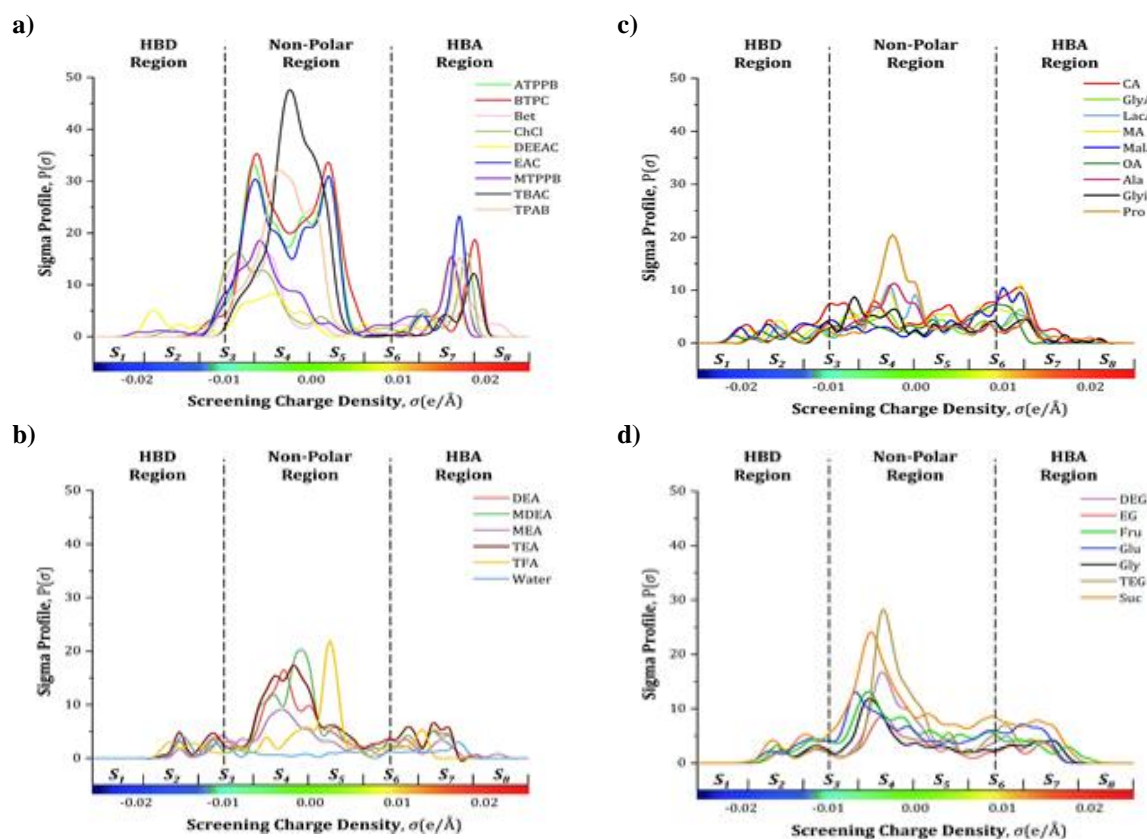
Figure III.28. The calculated *σ-profile* of the 31 constituents modeled as (a) salts, (b) amines & water, (c) fatty acids & amino acids, and d) polyols & sugars.

Chapter III   Physicochemical Properties of Deep Eutectic Solvents

The importance of analyzing the *σ-profile* is that it describes the surface polarity of a molecule and gives the chemical information required in predicting the dispersal, electrostatic, and hydrogen bonding interactions between the constituents of a mixture (Palomar et al., 2009). From Figure III.28, depending on the density charge, the curves can be split into three primary regions; the positive polarity surface "HBD region" covering the σ-range from -0.02500 up until -0.00625, the non-polar region denoted by the σ range of $-0.00625 < \sigma < +0.00625$, and the negative polarity surface "HBA region" with a σ range of $+0.00625 < \sigma < +0.02500$.

The added value of analyzing the *σ-profile* is that the nature of atoms and their concentration in each molecule can be detected. In Figure III.28, the *σ-profile* curves were analyzed and the position of each atom was observed as the following: in the HBD region, the positively charged hydrogen atoms (H^+) were found at $-0.02500 < \sigma < -0.01250$ region, the atoms found in the weak donor region (nearby the vertical dashed lines) were the ammonium (N^+) and phosphonium (P^+) cations located in the $-0.01250 < \sigma < -0.00625$ region, the alkyl groups ($-CH_3$, $-CH_2$, and $-CH$) were found in the non-polar region between $-0.00625 < \sigma < +0.00625$ region, and the double bond atoms ($C=C$) in the aromatics and the carbons in the carbonyl groups ($C=O$) were positioned in weak acceptor region of $+0.00625 < \sigma < +0.01250$ range. The HBA region covered oxygen (O^-) and nitrogen (N^-) atoms that belong to the $O - H$ and $N - H$ groups located in the $+0.01250 < \sigma < +0.01875$ area, and fluoride (F^-), chloride (Cl^-), and bromide (Br^-) anions were found in $+0.01875 < \sigma < +0.02500$.

III.5.4.2. MLR Model

a) Model Development

The dataset was split into two subsets that are "more specific" to certain families of DESs. The two categories were created based on the families of the HBDs as it was found that the nature of the HBD was much more pronounced relative to the effect of HBAs (see section III.5.3). The first category denoted as "Family A" consists of the DESs that are more acidic such as fatty acids and amino acids. Sugars were also added to the Family A group as many DESs in Table III.24 are combinations of acids and sugars (such as MA:Glu and MA:Suc). On the other hand, the other relatively less acidic DESs with higher pH values were grouped in Family B, which consists of amines and polyols. Subsequently, the Family A set contained 45 DESs and the Family B set contained 39 DESs. These divisions were expected to improve the model's predictive power in estimating the pH of the DESs (Fourches et al., 2010). Accordingly, the Family A set consisted of 313 experimental points, while the Family B set consisted of 335 points presenting an extensive range of pH measurements. The divisions of the dataset for both Family A and Family B models

are shown in Table III.25.Consequently, the prediction of new DESs should be made exclusively based on the nature of the HBD, where if the HBD constituent of the DES is a fatty acid, amino acid, hydroxy acid, or sugar then the Family A model must be utilized. On the other hand, if the HBD constituent of the DES is an amine or a polyol then the Family B model must be utilized instead. Otherwise, if the HBD constituent at hand belongs to neither family, then the developed models would not be applicable to predict their pH behavior.

To test the predictivity of the proposed models, the dataset in each model was split into a training set and a testing set. The data in the training set were utilized in the development of the model whereas the data in the testing set were only used to externally evaluate the predictivity of the model. The testing set was fixed to 75% of the DESs, and the remaining 25% were used as the testing set. The selection of the DESs in the testing set was done by first choosing representative external molecules for each family. For instance, in the Family A set, DEEAC was selected as an HBA representative, MalA & OxaA were selected as acid representatives, and Suc was selected as a sugar representative. Conversely, for Family B, BTPC was selected as an HBA representative, DEA was selected as an amine representative, and DEG was selected as a polyol representative. Accordingly, all the DESs comprised of DEEAC, BTPC, MalA, OxaA, Suc, DEA, and DEG were taken for external validation. The selection of these molecules was done based on the number of their data points, where for instance, only 2 DESs were comprised of BTPC. If for instance ChCl would have been chosen as an external representative then 33 DESs would have to be excluded from the training set, which would not be practical for the development of a machine learning-based model. To reach the 25% testing set threshold, the "Ordered Response" technique was utilized (Gramatica et al., 2016). In this technique, first, the pH values of all the DESs at room temperature were organized from lowest to highest. Then, one DES out of each seven DESs of the Family A set and one DES out of each nine DESs of the Family B set were added into the testing set to cover the 25% DES threshold. These 25% DESs in the testing set were not used to develop the models and were only utilized to test the final models. Accordingly, the Family A test set consisted of 12 out of 45 DESs, while the Family B test set consisted of 10 out of 39 DESs. The performance of the models in predicting the testing set was evaluated based on the external regression coefficient ($R^2_{external}$) and various other statistical parameters.

Table III.25. The partitioning of the Family A and Family B datasets.

	Family A	Family B
Total number of DESs	45	39
Training DESs	33	29
External DESs	12	10
Data points	313	335
Training points	222	251
External points	91	84
Training DESs	DESs 9, 13, 15, 16, 17, 19, 20, 22, 23, 24, 25, 26, 37, 38, 39, 63, 64, 65, 67, 68, 70, 71, 72, 73, 74, 75, 76, 77, 78, 79, 80, 81, 83	DESs 4, 6, 12, 21, 28, 29, 31, 33, 34, 35, 41, 42, 43, 44, 45, 46, 47, 48, 49, 50, 51, 52, 54, 55, 57, 58, 59, 60, 62
External DESs	DESs 10, 14, 18, 27, 30, 32, 36, 40, 66, 69, 82, 84	DESs 1, 2, 3, 5, 7, 8, 11, 53, 56, 61
External molecules	DEEAC, MalA, OxaA, Suc	BTPC, DEA, DEG

b) $S_{\sigma\text{-profiles}}$ *Discretization*

The *σ-profile* of most molecules has been reported to contain 51 points within the range of $\pm$ 0.025 e/Å (Lin & Sandler, 2002). In this sense, the discretization of the *σ-profile* curves into 4, 6, 8, 10, and 12 $S_{\sigma\text{-profile}}$ descriptors has been systematically investigated. Figure III.29 represents an example of the discretized $S_{\sigma\text{-profile}}$ descriptors for ethylene glycol.
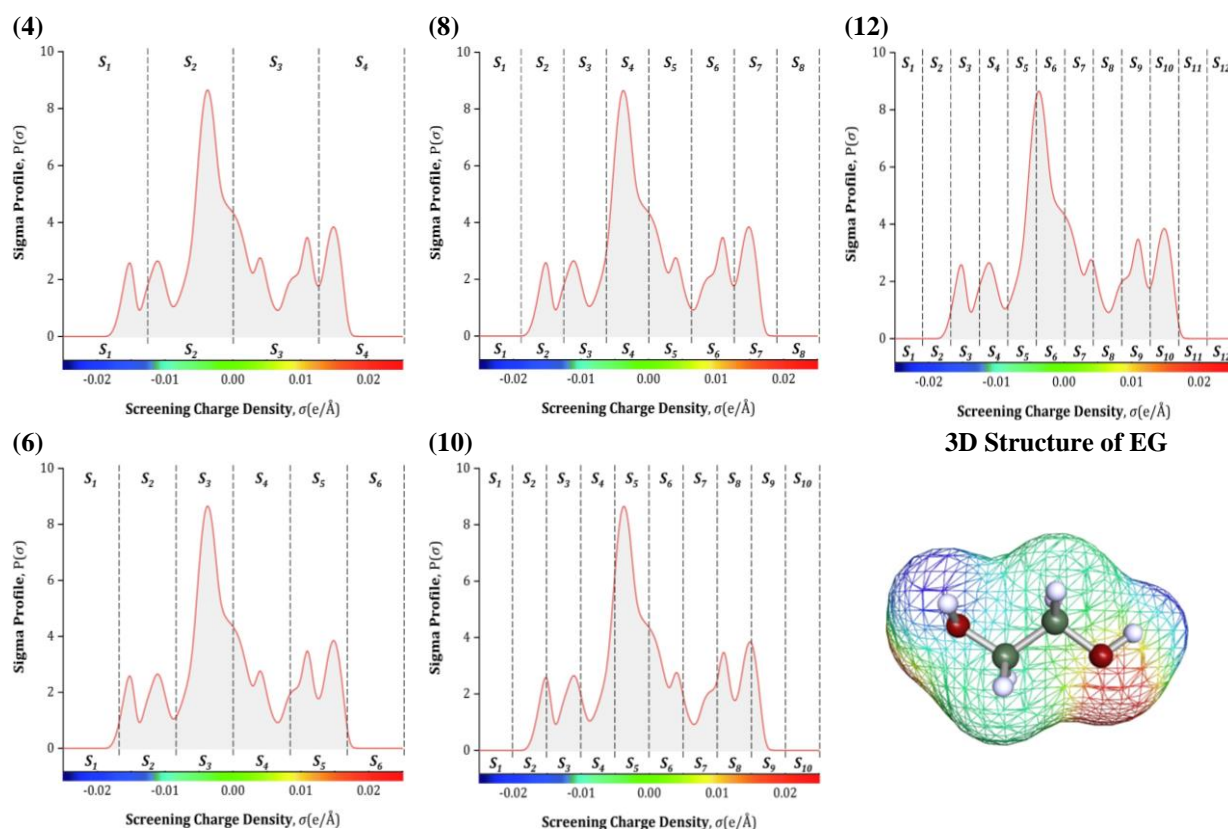
Figure III.29. Representation of the discretized $S_{\sigma\text{-profile}}$ descriptors in 4, 6, 8, 10, and 12 segments for ethylene glycol as an example.

As the discretization of the $S_{\sigma\text{-profile}}$ increases, the accuracy of the developed models is also significantly increased as a result of more fitting parameters. Nevertheless, that would also lead to

Chapter III   Physicochemical Properties of Deep Eutectic Solvents

an increase in the complexity of the resulting model. Thus, a comprise should be made between the number of fitting parameters and the accuracy of the developed model. Figure III.30 presents a heatmap of the regression coefficient (R^2) and the number of fitting parameters based on the partitioning of the $S_{\sigma\text{-}profile}$ for the Family A and Family B models. It can be observed that as the partitioning increases to 12 segments the R^2 values are also improved up to 0.8970 and 0.8580 for Family A and Family B, respectively. However, even though these R^2 values are decent, they may not be considered good enough to facilitate solvent screening studies. These R^2 values also indicate that the machine learning algorithm requires more statistically significant descriptors in order to represent the data more accurately.

(a)

	4 Partitions (S_1–S_4)	6 Partitions (S_1–S_6)	8 Partitions (S_1–S_8)	10 Partitions (S_1–S_{10})	12 Partitions (S_1–S_{12})
Including Interactions	R^2=0.9191 15 coefficients	R^2=0.9644 26 coefficients	**R^2=0.9947** 38 coefficients	R^2=0.9974 53 coefficients	R^2=0.9975 51 coefficients
Excluding Interactions	R^2=0.7664 5 coefficients	R^2=0.8705 7 coefficients	R^2=0.8548 9 coefficients	R^2=0.8851 11 coefficients	R^2=0.8970 13 coefficients

(b)

	4 Partitions (S_1–S_4)	6 Partitions (S_1–S_6)	8 Partitions (S_1–S_8)	10 Partitions (S_1–S_{10})	12 Partitions (S_1–S_{12})
Including Interactions	R^2=0.6767 11 coefficients	R^2=0.9429 24 coefficients	**R^2=0.9969** 40 coefficients	R^2=0.9964 47 coefficients	R^2=0.9981 49 coefficients
Excluding Interactions	R^2=0.4912 5 coefficients	R^2=0.6138 7 coefficients	R^2=0.6390 9 coefficients	R^2=0.8036 10 coefficients	R^2=0.8580 12 coefficients

Figure III.30. Heatmap of the regression coefficient (R^2) in several MLR models based on descriptor interactions and partitioning of $S_{\sigma\text{-}profile}$ for the (a) Family A model, and the (b) Family B model.

Therefore, to improve the performance of the models, the addition of more descriptors (other than $S_{\sigma\text{-}profiles}$) or complexity terms between $S_{\sigma\text{-}profile}$ descriptors could be utilized. However, if more descriptors (such as DES critical properties for instance) were utilized, then the model would lose its ability to provide molecular-level insights as the addition of these macroscopic descriptors would damage the "coherence" of the regression. Other than that, the $S_{\sigma\text{-}profile}$ molecular descriptors were selected as they have a sound physical basis and can easily be obtained through basic COSMO-RS modeling. Other types of descriptors may not have the same physical basis that $S_{\sigma\text{-}profiles}$ have, and may not be as easy to calculate and obtain. Additionally, most DES descriptors assume the DES to be a *pseudo*-pure component, meaning that the descriptors need to be calculated for each DES individually.

The $S_{\sigma\text{-}profile}$ descriptors are a special type of parameters calculated from an atomic basis (Torrecilla et al., 2010). Thus, it takes into account the charged contribution and the relative concentration of each atom that constitutes the "DES mixture", which is very useful in the field of DESs as it removes the need to define the DES as a *pseudo*-pure component, and it easily allows for defining mixtures of DESs with their water content, which are critical in pH studies. Thus, to avoid these issues, the addition of complexity terms between $S_{\sigma\text{-}profile}$ descriptors has been utilized. The complexity terms selected are based on 2nd degree factorials, which can be utilized to investigate the interactions between a pair of descriptors.

The R^2 values after including the binary interaction terms are shown in the heatmap in Figure III.30. It can be observed that the addition of the interaction terms increased the performance of the developed models. Nevertheless, the complexity of the models also increased as a result. Based on the obtained heatmap, the 8-partition model including the binary interactions between the descriptors has been selected as the optimal compromise between accuracy and fitting parameters as it is the simplest model with a regression coefficient above $R^2 > 0.99$. Presumably, the discretization of the σ-*profile* into 8 segments is found to be sufficient enough to reasonably characterize the effect of all the functional groups that exist within the DESs. Using the 8-partition profile, the σ-*profile* curve can be classified into five main regions based on their charges; the HBD region, the weak donor region, the non-polar region, the weak acceptor region, and the HBA region with their representative descriptors being $[S_1, S_2]$, $[S_3]$, $[S_4, S_5]$, $[S_6]$, and $[S_7, S_8]$, respectively. The "chemical information" of strong, regular, and weak donating functional groups is stored in S_1, S_2, and S_3, respectively, while the "chemical information" of strong, regular, and weak accepting functional groups is stored within S_8, S_7, and S_6, respectively.

c) Family A

To develop the Family A MLR model, 33 DESs were utilized in the development of the model (*i.e.,* training), and the remaining 12 DESs were used to test the predictivity of the model (*i.e.,* testing set). The initial step in evaluating the model is to check the impact of each descriptor and their binary interactions on the model. For that reason, an analysis of variance study was conducted and the results are shown in Table III.26.

Chapter III Physicochemical Properties of Deep Eutectic Solvents

Table III.26. The coefficients of the 38 significant descriptors and the intercept of the Family A model.

Category	Term	Estimate	Standard Error	$\|t\text{-}Ratio\|$	$P\text{-}value$
Intercept	a_0	39.31	14.78	2.66	0.0083
HBD	S_1	9401.19	4,821.12	1.95	0.0465
	S_2	-13070.83	3,251.45	4.02	<0.0001
Weak donor	S_3	-3324.20	972.23	3.42	0.0007
Non-polar	S_4	-1346.91	496.74	2.71	0.0071
	S_5	435.42	219.90	1.98	0.0455
Weak acceptor	S_6	4992.10	1509.15	3.31	0.0011
HBA	S_7	8326.25	2334.65	3.57	0.0004
	S_8	37435.97	9315.42	4.02	<0.0001
Temperature	T	-1.29×10^{-2}	8.51×10^{-4}	15.15	<0.0001
{HBD, Temperature}	$(S_1-\bar{S}_1)(T-\bar{T})$	10.29×10^{-1}	6.86×10^{-1}	1.50	0.1125
	$(S_2-\bar{S}_2)(T-\bar{T})$	34.44×10^{-1}	9.69×10^{-1}	3.55	0.0004
{Weak donor, Temperature}	$(S_3-\bar{S}_3)(T-\bar{T})$	-2.95×10^{-2}	1.536×10^{-2}	1.92	0.0482
{Non-polar, Temperature}	$(S_4-\bar{S}_4)(T-\bar{T})$	5.69×10^{-1}	2.50×10^{-1}	2.28	0.0236
	$(S_5-\bar{S}_5)(T-\bar{T})$	-28.99×10^{-1}	6.67×10^{-1}	4.35	<0.0001
{HBA, Temperature}	$(S_8-\bar{S}_8)(T-\bar{T})$	-20.20×10^{-1}	9.77×10^{-1}	2.25	0.0271
{HBD, HBD}	$(S_1-\bar{S}_1)(S_2-\bar{S}_2)$	-35370219.00	12580221.00	2.81	0.0053
{HBD, Weak donor}	$(S_1-\bar{S}_1)(S_3-\bar{S}_3)$	-7380316.00	2627407.00	2.81	0.0053
{HBD, Non-polar}	$(S_1-\bar{S}_1)(S_4-\bar{S}_4)$	-105501.00	32866.36	3.21	0.0015
	$(S_1-\bar{S}_1)(S_5-\bar{S}_5)$	9001733.20	3048929.00	2.95	0.0034
{HBD, Weak acceptor}	$(S_1-\bar{S}_1)(S_6-\bar{S}_6)$	1853102.80	661646.20	2.80	0.0055
	$(S_2-\bar{S}_2)(S_6-\bar{S}_6)$	1272799.70	434961.90	2.93	0.0037
{HBD, HBA}	$(S_1-\bar{S}_1)(S_7-\bar{S}_7)$	12118890.00	4277145.00	2.83	0.0049
	$(S_1-\bar{S}_1)(S_8-\bar{S}_8)$	-56305137.00	17131621.00	3.29	0.0011
	$(S_2-\bar{S}_2)(S_7-\bar{S}_7)$	-1329440.00	500806.20	2.65	0.0084
	$(S_2-\bar{S}_2)(S_8-\bar{S}_8)$	-32845561.00	11364365.00	2.89	0.0042
{Weak donor, Non-polar}	$(S_3-\bar{S}_3)(S_4-\bar{S}_4)$	72611.93	33275.65	2.18	0.0299
	$(S_3-\bar{S}_3)(S_5-\bar{S}_5)$	-2685473.00	989645.80	2.71	0.0071
{Weak donor, Weak acceptor}	$(S_3-\bar{S}_3)(S_6-\bar{S}_6)$	2047090.80	731873.90	2.80	0.0055
{Weak donor, Non-polar}	$(S_3-\bar{S}_3)(S_7-\bar{S}_7)$	-84229.96	32120.71	2.62	0.0092
	$(S_3-\bar{S}_3)(S_8-\bar{S}_8)$	-9971815.00	3085243.00	3.23	0.0014
{Non-polar, Weak acceptor}	$(S_4-\bar{S}_4)(S_6-\bar{S}_6)$	-268050.70	94521.37	2.84	0.0049
{Non-polar, HBA}	$(S_4-\bar{S}_4)(S_7-\bar{S}_7)$	-247666.60	100270.30	2.47	0.0141
	$(S_4-\bar{S}_4)(S_8-\bar{S}_8)$	-5042131.00	1805414.00	2.79	0.0056
	$(S_5-\bar{S}_5)(S_7-\bar{S}_7)$	7438614.10	2752236.00	2.70	0.0073
	$(S_5-\bar{S}_5)(S_8-\bar{S}_8)$	-3346227.00	1820323.00	1.84	0.0671
{Weak acceptor, HBA}	$(S_6-\bar{S}_6)(S_7-\bar{S}_7)$	-4790982.00	1723914.00	2.78	0.0058
	$(S_6-\bar{S}_6)(S_8-\bar{S}_8)$	26080014.00	7454203.00	3.50	0.0005
{HBA, HBA}	$(S_7-\bar{S}_7)(S_8-\bar{S}_8)$	24500561.00	7327952.00	3.34	0.0009

[a] Mean values: $\bar{S}_1=1.10\times10^{-3}$; $\bar{S}_2=8.71\times10^{-3}$; $\bar{S}_3=3.01\times10^{-2}$; $\bar{S}_4=2.34\times10^{-2}$; $\bar{S}_5=1.19\times10^{-2}$; $\bar{S}_6=1.49\times10^{-2}$; $\bar{S}_7=1.47\times10^{-2}$; $\bar{S}_8=3.20\times10^{-4}$; $\bar{T}=316.169$

In Table III.26, it can be seen that the intercept and all the 8 molecular descriptors with the temperature descriptor had a significant influence on the model development as their $P\text{-}values$ were < 5%. The effect of the binary interactions on the model was also analyzed and it was found that the interactions between $\{S_{6,+}, T\}$ and $\{S_{7,+}, T\}$ molecular descriptors and the temperature descriptor were insignificant on the Family A model. The same findings were obtained for the binary interactions between some pairs of molecular descriptors where the $\{S_{2,-}, S_{3,-}\}$, $\{S_{2,-}, S_{4,-}\}$, $\{S_{2,-}, S_{5,+}\}$, $\{S_{4,-}, S_{5,+}\}$, and $\{S_{5,+}, S_{6,+}\}$ pairs did not affect the model. The remaining binary interactions showed a significant effect on the model with $P\text{-}values$ lower than < 5% except for the $\{S_{1,+}, T\}$ and $\{S_{5,+}, S_{8,+}\}$ descriptors where their impact was considered to be less pronounced as their $P\text{-}values$ were above > 5% at 11.25% and 6.71%, respectively. Nonetheless, these descriptors were still considered influential by minimizing the Corrected Akaike Information Criterion (AIC_c), indicating that the descriptors contain valuable information from a statistical viewpoint

and that they improve the model more than they would be expected to by chance. Therefore, based on the stepwise fitting algorithm and the analysis of variance study, the resultant Family A model can be expressed as follows :

$$
\begin{aligned}
pH_{Family\,A} =\ & 39.31 + 9401.19\,(S_1) - 13070.83\,(S_2) - 3324.20\,(S_3) - 1346.91\,(S_4) + 435.42\,(S_5) + 4992.10 \\
& (S_6) + 8326.25\,(S_7) - 37435.97\,S_8) - 1.29\times10^{-2}\,(T) - 35370219.00\,(S_1-\overline{S_1})(S_2-\overline{S_2}) - 7380316.00 \\
& (S_1-\overline{S_1})(S_3-\overline{S_3}) - 105501.00\,(S_1-\overline{S_1})(S_4-\overline{S_4}) + 9001733.20\,(S_1-\overline{S_1})(S_5-\overline{S_5}) + 1853102.80 \\
& (S_1-\overline{S_1})(S_6-\overline{S_6}) + 12118890.00\,(S_1-\overline{S_1})(S_7-\overline{S_7}) - 56305137.00\,(S_1-\overline{S_1})(S_8-\overline{S_8}) + 10.29\times10^{-1} \\
& (S_1-\overline{S_1})(T-\overline{T}) + 1272799.70\,(S_2-\overline{S_2})(S_6-\overline{S_6}) - 1329440.00\,(S_2-\overline{S_2})(S_7-\overline{S_7}) - 32845561.00 \\
& (S_2-\overline{S_2})(S_8-\overline{S_8}) + 34.44\times10^{-1}\,(S_2-\overline{S_2})(T-\overline{T}) + 72611.93\,(S_3-\overline{S_3})(S_4-\overline{S_4}) - 2685473.00 \\
& (S_3-\overline{S_3})(S_5-\overline{S_5}) + 2047090.80\,(S_3-\overline{S_3})(S_6-\overline{S_6}) - 84229.96\,(S_3-\overline{S_3})(S_7-\overline{S_7}) - 9971815.00 \\
& (S_3-\overline{S_3})(S_8-\overline{S_8}) - 2.95\times10^{-2}\,(S_3-\overline{S_3})(T-\overline{T}) - 268050.70\,(S_4-\overline{S_4})(S_6-\overline{S_6}) - 247666.60\,(S_4-\overline{S_4})(S_7-\overline{S_7}) \\
& - 5042131.00\,(S_4-\overline{S_4})(S_8-\overline{S_8}) + 5.69\times10^{-1}\,(S_4-\overline{S_4})(T-\overline{T}) + 7438614.10\,(S_5-\overline{S_5})(S_7-\overline{S_7}) - 3346227.00 \\
& (S_5-\overline{S_5})(S_8-\overline{S_8}) - 28.99\times10^{-1}\,(S_5-\overline{S_5})(T-\overline{T}) - 4790982.00\,(S_6-\overline{S_6})(S_7-\overline{S_7}) + 26080014.00 \\
& (S_6-\overline{S_6})(S_8-\overline{S_8}) + 11958774.00\,(S_7-\overline{S_7})(S_8-\overline{S_8}) - 20.20\times10^{-1}\,(S_8-\overline{S_8})(T-\overline{T})
\end{aligned}
$$

(III.7)

where S_i and $\overline{S_i}$ are the molecular descriptors and their mean values (e/Å^2), respectively, and T is the temperature (K).

After generating the Family A model, its performance was analyzed and the results are summarized in Table III.27. The model showed excellent performance in terms of fitting the experimental data for the pH property with high regression coefficient (R^2= 0.9947). Moreover, the internal robustness of the model was evaluated based on the values of the cross-validation coefficients; The high cross-validation coefficients (Q^2) reflects the stability of the model. Furthermore, several chance correlation tests have been conducted. The low y-scrambling regression coefficient ($R^2_{scramble}$= 0.0072) indicates that the model parameters were not correlated by chance. Similarly, the high Fisher statistics (F_{Ratio} =905.51; $P_{value,\,Fisher}$ <0.0001) suggest that large variations due to systematic variances in the descriptors are exhibited by the model rather than differences caused by chance. This also can be supported by the high adjusted regression coefficient ($R^2_{adjusted}$= 0.9936), indicating that the descriptors enhanced the model more than it would be expected by chance.

Table III.27. Family A's statistical performance.

Parameter	Value
Training set	
DESs	33
Data points	222
R^2	0.9947
$AICc$	-45.1439
$F_{\text{-Ratio}}$	905.51
$P_{\text{-value, Fisher}}$	<0.0001
$R^2_{adjusted}$	0.9936
Q^2_{pH}	0.9939
Q^2_{Mw}	0.9965
Q^2_{Savg}	0.9973
$Q^2_{LMO, 25\%}$	0.9941
Q^2_{LOO}	0.9947
$R^2_{scramble}$	0.0072
$RMSE$	0.1589
SD_{avg}	±0.08
$AARD$	±7.54%
$AD_{coverage}$	100.0%
Testing set	
DESs	12
Data points	91
$R^2_{external}$	0.9942
$RMSE$	0.1722
SD_{avg}	±0.09
$AARD$	±17.38%
$AD_{coverage}$	100.0%

It should be mentioned that although the developed model consists of 38 significant descriptors, the parameters are all essentially constructed based on 8 basic molecular descriptors only ($S_1 - S_8$) and the temperature descriptor (T). The remaining parameters are just basic multiplications of a pair of descriptors expressing the binary interactions between the descriptors. Subsequently, the model at hand can be utilized for studying and predicting the pH of a large amount of acid and sugar-based DESs, which have not been tested experimentally, utilizing 8 basic molecular descriptors only that can be obtained through simple COSMO-RS modeling of the desired HBAs and the HBDs, enabling a straightforward and cheap method for screening new green and sustainable DESs with the required pH for a particular application.

The descriptors and their binary interactions were further analyzed to study their effect on the pH based on their estimated coefficients. As mentioned in section III.5.3.1, the molecular descriptors were calculated based on their *σ-profile*, which is linked to their molecular structure and their molecular-level behaviors. Therefore, analyzing their effect on the model is mandatory to gain insights into each molecular descriptor's physical meaning on the pH. In Table III.26, it can be seen that some descriptors had a positive coefficient indicating a positive effect (proportional relation) on the pH. In contrast, the negative coefficients indicated an inversely proportional relation (negative effect), causing a decrease in the pH values.

The $S_{1,+}$ molecular descriptor was positively affecting the pH, whereas the $S_{2,-}$ molecular descriptor showed a negative effect. Nonetheless, when comparing the absolute coefficient estimates and the t-$_{Ratios}$ of the two descriptors in the HBD region, it can be observed that the $S_{2,-}$ descriptor has a more pronounced effect. Also, it should be noted that by referring to Figure III.29, it can be observed that $S_{1,+}$ descriptor showed minor peaks for a few acids only, which explains the high P-$_{value}$ that the descriptor exhibits (4.65%). On the other hand, the $S_{2,-}$ descriptor showed clear peaks with a P-$_{value}$ lower than 0.1%. As previously mentioned in Table III.17, the $S_{1,+}$ and $S_{2,-}$ descriptors represent hydrogen (H^+), and since the $S_{2,-}$ (the more pronounced descriptor) is negatively correlated it can be concluded that as the concentration of polarizable H atoms increases in the molecular structure of the DES, the lower the acidity due to the increased protonation within the solvent, which was expected as this is a general trend with regards to acids (Skulcova et al., 2018). As for the HBA region, both the molecular descriptors $S_{7,+}$ and $S_{8,+}$ were positively affecting the pH. From Table III.17, it can be observed that $S_{7,+}$ descriptor represents the oxygen ($O^{\delta-}$) and nitrogen ($N^{\delta-}$) atoms of O–H and N–H. Moreover, the negatively charged anions; fluoride (F^-), chloride (Cl^-), and bromide (Br^-) are located in $S_{8,+}$. Presumably, these results suggest that increasing the concentration of these electron-withdrawing groups lowers the protonation ability of the acid and sugar-based DESs as a result of increased hydrogen bonding interactions.

The weak donor region in Table III.17 identifies the cations (N^+, P^+) in $S_{3,-}$, indicating that increasing the concentration of these cations in the structure of the DES negatively affects the pH. Moreover, the alkyl groups represented by both the $S_{4,-}$ and $S_{5,+}$ molecular descriptors showed an opposite effect, but, since the absolute coefficient estimates and the t-$_{Ratios}$ of $S_{4,-}$ are higher than $S_{5,+}$, the negative effect of $S_{4,-}$ is considered to be more pronounced. The weak acceptor region represented by the $S_{6,+}$ identifies the carbon double bonds ($C=C$) and the carbons in the carbonyl groups ($C=O$) in Table III.17. This means that the presence of these structural features in the DES constituents increases the pH of the acid and sugar-based DESs. The temperature descriptor showed a negative correlation with the pH. This result indicates that the molecular vibration exhibited at the molecular-level increases as more energy is being introduced to the system promoting the formation of $[H^+]$ ions and inhibiting the hydrogen bonding between molecules causing the pH to decrease (Saputra et al., 2020), which is in agreement with the experimental findings in section III.5.2. Also, it should be mentioned that the t-$_{Ratio}$ of the temperature descriptor was significantly high, indicating the significant effect of temperature on the pH. Furthermore, when analyzing the binary interactions between the temperature and the descriptors, it can be seen

that a positive effect is exhibited when combined with the $S_{1,+}$, $S_{2,-}$, and $S_{4,-}$ descriptors, and a negative effect is exhibited when combined with the $S_{3,-}$, $S_{5,+}$, and $S_{8,+}$. These results indicate that even though the temperature descriptor was negatively correlated with pH, the binary interactions of H^+ with temperature leads to an increase in the pH, while the binary interactions of N$^+$, P$^+$, Cl^-, Br^-, and F^- with temperature leads to a decrease in the pH. On the other hand, the binary interaction between the pair of molecular surface descriptors showed both correlations; 14 interactions were negatively correlated, while the remaining 9 were positively correlated with pH. Table 4 in (Appendix A) lists a comparison between the original correlated sign of each molecular surface descriptor and the sign of its interaction correlation with other surface descriptors.

From Table A.4 it can be observed that six possible combinations can occur as follows: $[+,+\rightarrow+]$, $[+,+\rightarrow-]$, $[+,-\rightarrow+]$, $[+,-\rightarrow-]$, $[-,-\rightarrow+]$, or $[-,-\rightarrow-]$, where for instance the combination $[+,+\rightarrow+]$ represents an interaction between (i) a "positively" correlated molecular surface descriptor $(S_{i,+})$ and (ii) another "positively" correlated molecular surface descriptor $(S_{j,+})$, resulting in a "positively" correlated interaction between the two surfaces $\{S_{i,+},S_{j,+}\}$. An example of the $[+,+\rightarrow+]$ binary interaction is the interaction between $S_{6,+}$, which is positive, and $S_{8,+}$, which is also positive, resulting in a positively correlated interaction $\{S_{6,+},S_{8,+}\}$. This result was fairly expected as the atoms contain within $S_{6,+}$ (C=C, C=O) and $S_{8,+}$ (Cl^-, Br^-, F^-) were originally observed to be increasing pH, and thus, their interactions denoted as $\{S_{6,+},S_{8,+}\}$, were also expected to increase the value of pH. The $\{S_{1,+},S_{2,-}\}$ interaction (both in the HBD region) presented a $[-,+\rightarrow-]$ behavior, which indicates that the concentration of H atoms that are contained within the $S_{2,-}$ descriptor have a more pronounced effect on decreasing the pH than the effect of the H atoms within the $S_{1,+}$ descriptor, matching the trend observed by their t-$_{Ratios}$. A similar result can be observed when studying the interaction between $\{S_{4,-},S_{6,+}\}$, which exhibited a $[+,-\rightarrow-]$ behavior, indicating that the atoms contained within the $S_{4,-}$ (–CH$_3$, –CH$_2$, and –CH) have a higher effect on decreasing the pH than the effect that C=C, C=O $(S_{6,+})$ have on increasing the pH when the binary interactions between descriptors are considered.

Lastly, the interactions between the HBA region and the weak acceptor region $\{S_{6,+},S_{7,+}\}$ demonstrated a $[+,+\rightarrow-]$ behavior indicating that increasing the concentration of C=C, C=O $(S_{6,+})$ within the vicinity of the O$^{\delta-}$ and N$^{\delta-}$ $(S_{7,+})$, which belong to the O$^{\delta-}$–H and N$^{\delta-}$–H functional groups, increases the protonation ability of the DES as a result of their binary interactions, causing the pH to decrease.

Figure III.31 (a) shows a parity plot of the experimental and the predicted data in the training set. It can be seen that the model can be considered reliable in fitting the experimental data as all the points in training were lying close to the diagonal line showing minor dispersion (R^2=0.9947) and the Root-Mean-Square-Error (*RMSE*) was calculated to be 0.1589. Figure III.31 (b) shows the parity graph plotted for the testing set. It can be seen that the model was able to show high predictive capabilities of the DESs in the testing set ($R^2_{external}$ = 0.9942 and *RMSE* = 0.1722).

(a)

(b)
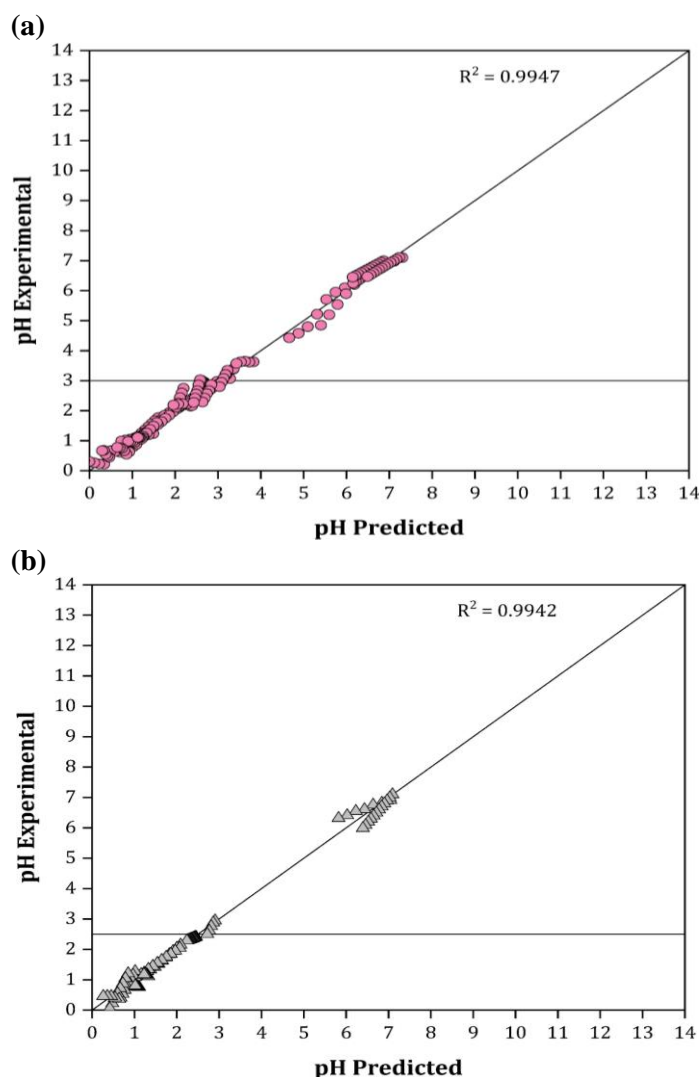
Figure III.31. Parity graph of the experimental and predicted pH values of Family A's MLR model in (a) training, and (b) external testing.

For further model evaluation, the residual plot was utilized to examine the accuracy of the model. Figure III.32 shows the excellence of the proposed model in predicting the pH property of DESs where the residuals were at a range of ±0.5 with an absolute-average-relative-deviation (*AARD*) of ±7.54% in training, and an *AARD* of ±17.38% in testing. It should be mentioned that the reason which the model shows a systematic linear deviation in both Figure III.31 and Figure III.32 is that the pH model was developed for a variety of DES structures and their temperature

dependence, which exhibits a linear behavior (as discussed in section III.5.2. This allows the model's field of investigation to include both the DES structure and the temperature, which is very important for screening new green and sustainable DESs with the required pH for a specific application.
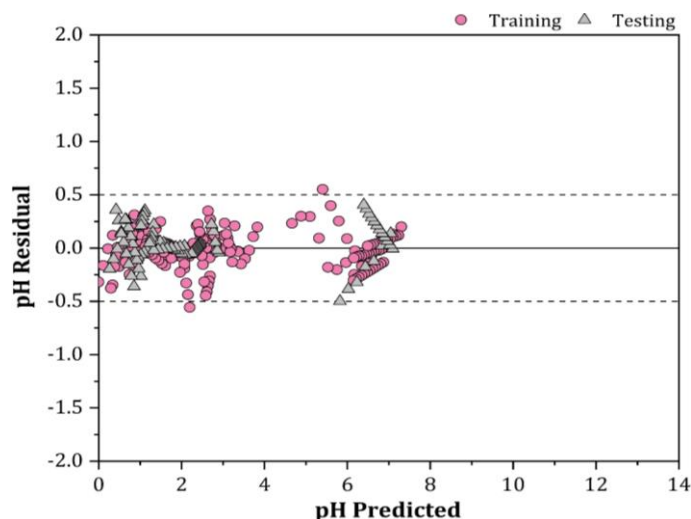
Figure III.32. The residual deviation between the experimentally determined and model predicted pH values in the Family A MLR model.

Moreover, Figure III.33 shows the performance of the Family A MLR model in predicting the pH values of the external molecule DES set as a function of temperature. It can be seen that the model predicts the external molecules of DEEAC:MalA (DES32) and MA:Suc:H_2O (DES40) quite accurately. However, the external performances of ChCl:MalA:H_2O (DES27) and ChCl:OxaA:H_2O (DES30) are a lot lower with standard deviations (SD_{avg}) of ± 0.18 and ± 0.25, respectively. The points represent the experimental data and the solid lines represent the model predictions
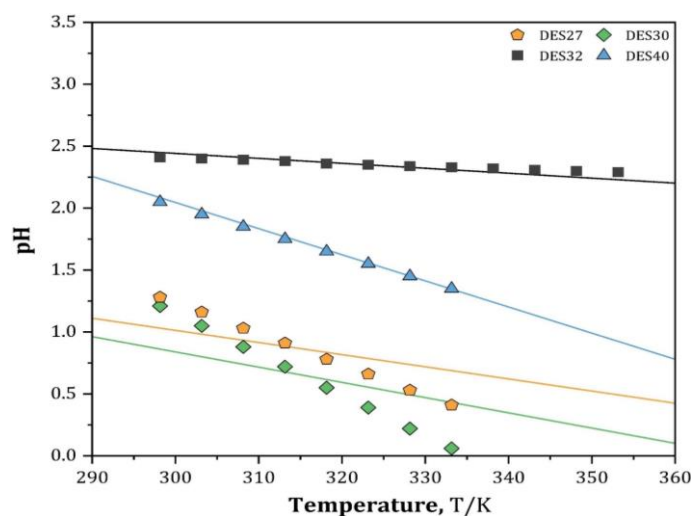
Figure III.33. Experimental and predicted pH values as a function of temperature in external molecule validation for Family A's MLR model.

Chapter III   Physicochemical Properties of Deep Eutectic Solvents

d) Family B

In the second model, 39 amines and polyol-based DESs were selected to develop the model, where 29 DESs were utilized for training, and the remaining 10 DESs were utilized in external validation. The model results are listed in Table III.28.

Table III.28. The coefficients of the 40 significant descriptors and the intercept of the Family B model.

Category	Term	Estimate	Standard Error	$|t\text{-}_{Ratio}|$	$P\text{-}_{value}$
Intercept	a_0	2712.99	998.45	2.72	0.0070
HBD	S_1	12195344.00	919519.90	13.26	<0.0001
	S_2	2007820.40	108337.40	18.53	<0.0001
Weak donor	S_3	1625622.70	64483.41	25.21	<0.0001
Non-polar	S_4	299995.39	11001.01	27.27	<0.0001
	S_5	-1219162.00	53413.79	22.82	<0.0001
Weak acceptor	S_6	-242091.30	17662.87	13.71	<0.0001
HBA	S_7	-2446456.00	94746.93	25.82	<0.0001
	S_8	-3275372.00	125348.20	26.13	<0.0001
Temperature	T	-9.91×10^{-3}	4.38×10^{-4}	22.63	<0.0001
{HBD, Temperature}	$(S_1-\bar{S}_1)(T-\bar{T})$	-40.15×10^{-1}	24.02×10^{-1}	1.67	0.0957
	$(S_2-\bar{S}_2)(T-\bar{T})$	51.57×10^{-1}	6.41×10^{-1}	8.05	<0.0001
{Weak donor, Temperature}	$(S_3-\bar{S}_3)(T-\bar{T})$	-8.32×10^{-1}	1.74×10^{-1}	4.78	<0.0001
{Non-polar, Temperature}	$(S_5-\bar{S}_5)(T-\bar{T})$	5.77×10^{-1}	7.60×10^{-2}	7.59	<0.0001
	$(S_6-\bar{S}_6)(T-\bar{T})$	-7.69×10^{-1}	1.38×10^{-1}	5.56	<0.0001
{HBA, Temperature}	$(S_7-\bar{S}_7)(T-\bar{T})$	25.12×10^{-1}	3.53×10^{-1}	7.11	<0.0001
	$(S_8-\bar{S}_8)(T-\bar{T})$	26.19×10^{-1}	7.76×10^{-1}	3.37	0.0008
{HBD, HBD}	$(S_1-\bar{S}_1)(S_2-\bar{S}_2)$	$2.64\times10^{+10}$	$1.39\times10^{+9}$	18.97	<0.0001
{HBD, Weak donor}	$(S_1-\bar{S}_1)(S_3-\bar{S}_3)$	$7.14\times10^{+9}$	$2.95\times10^{+8}$	24.21	<0.0001
	$(S_2-\bar{S}_2)(S_3-\bar{S}_3)$	$-7.42\times10^{+8}$	34900324.00	21.25	<0.0001
{HBD, Non-polar}	$(S_1-\bar{S}_1)(S_4-\bar{S}_4)$	$2.17\times10^{+9}$	$7.80\times10^{+7}$	27.87	<0.0001
	$(S_1-\bar{S}_1)(S_5-\bar{S}_5)$	$-3.26\times10^{+9}$	$2.28\times10^{+8}$	14.27	<0.0001
	$(S_2-\bar{S}_2)(S_4-\bar{S}_4)$	-46429937.00	2273852.00	20.42	<0.0001
	$(S_2-\bar{S}_2)(S_5-\bar{S}_5)$	93297386.00	4099702.00	22.76	<0.0001
{HBD, Weak acceptor}	$(S_1-\bar{S}_1)(S_6-\bar{S}_6)$	$-5.10\times10^{+9}$	$2.42\times10^{+8}$	21.07	<0.0001
{HBD, HBA}	$(S_1-\bar{S}_1)(S_7-\bar{S}_7)$	$-7.34\times10^{+9}$	$2.81\times10^{+8}$	26.09	<0.0001
	$(S_2-\bar{S}_2)(S_7-\bar{S}_7)$	$1.72\times10^{+9}$	80438510.00	21.33	<0.0001
	$(S_2-\bar{S}_2)(S_8-\bar{S}_8)$	924971536.00	34174322.00	27.07	<0.0001
{Weak donor, Non-polar}	$(S_3-\bar{S}_3)(S_4-\bar{S}_4)$	-33295616.00	1559555.00	21.35	<0.0001
	$(S_3-\bar{S}_3)(S_5-\bar{S}_5)$	38422954.00	2005305.00	19.16	<0.0001
{Weak donor, Weak acceptor}	$(S_3-\bar{S}_3)(S_6-\bar{S}_6)$	151526609.00	6987297.00	21.69	<0.0001
{Weak donor, HBA}	$(S_3-\bar{S}_3)(S_7-\bar{S}_7)$	4999312.60	274929.90	18.18	<0.0001
	$(S_3-\bar{S}_3)(S_8-\bar{S}_8)$	$1.29\times10^{+9}$	50105026.00	25.69	<0.0001
{Non-polar, Non-polar}	$(S_4-\bar{S}_4)(S_5-\bar{S}_5)$	-5079827.00	424574.70	11.96	<0.0001
{Non-polar, HBA}	$(S_4-\bar{S}_4)(S_7-\bar{S}_7)$	77090308.00	3600634.00	21.41	<0.0001
	$(S_4-\bar{S}_4)(S_8-\bar{S}_8)$	187576063.00	7419743.00	25.28	<0.0001
	$(S_5-\bar{S}_5)(S_7-\bar{S}_7)$	-66022050.00	3544836.00	18.62	<0.0001
	$(S_5-\bar{S}_5)(S_8-\bar{S}_8)$	$-1.19\times10^{+9}$	47194228.00	25.24	<0.0001
{Non-polar, Weak acceptor}	$(S_5-\bar{S}_5)(S_6-\bar{S}_6)$	26647478.00	2158303.00	12.35	<0.0001
{ Weak acceptor, HBA}	$(S_6-\bar{S}_6)(S_7-\bar{S}_7)$	$-3.82\times10^{+8}$	17597237.00	21.73	<0.0001
{HBA, HBA}	$(S_7-\bar{S}_7)(S_8-\bar{S}_8)$	$-2.20\times10^{+9}$	83528785.00	26.29	<0.0001

[a]Mean values: $\bar{S}_1 =7.32\times10^{-5}$; $\bar{S}_2 =6.89\times10^{-3}$; $\bar{S}_3 =2.15\times10^{-2}$; $\bar{S}_4 =6.91\times10^{-2}$; $\bar{S}_5 =2.30\times10^{-2}$; $\bar{S}_6 =1.23\times10^{-2}$; $\bar{S}_7 =1.68\times10^{-2}$; $\bar{S}_8 =8.40\times10^{-4}$; $\bar{T} =324.019$

In this model, 40 descriptors were observed to have a strong influence on the pH of DESs. The 8 molecular descriptors had an impact on the model, as their estimated coefficients had $P\text{-}_{values}$ < 5%. As for the binary interaction between each molecular descriptor and the temperature, it was observed that all the interactions pairs $\{S_i, T\}$ were found to be statistically significant and affecting the pH of DESs, except for $\{S_4, T\}$ where its effect was less pronounced and therefore excluded from the model. With regards to the interactions among two surface descriptors, it was observed that the pairs $\{S_1, S_8\}$ $\{S_2, S_6\}$, $\{S_4, S_6\}$, and $\{S_6, S_8\}$ did not affect the pH of DESs. The effect of

all the molecular descriptors and their binary interactions on the developed model was confirmed by the low P_{values}, the high values of t_{Ratio}, and improving the AIC_c information criterion. Consequently, the resulting model can be expressed as follow:

$pH_{Family\ B}$ = 2712.99 + 12195344.00 (S_1) + 2007820.40 (S_2) + 1625622.70 (S_3) + 299995.39 (S_4) − 1219162.00 (S_5) − 242091.30 (S_6) − 2446456.00 (S_7) − 3275372.00 (S_8) − 9.91×10^{-3} (T) + 2.64×10^{+10} $(S_1-\overline{S_1})(S_2-\overline{S_2})$ + 7.14×10^{+9} $(S_1-\overline{S_1})(S_3-\overline{S_3})$ + 2.17×10^{+9} $(S_1-\overline{S_1})(S_4-\overline{S_4})$ − 3.26×10^{+9} $(S_1-\overline{S_1})(S_5-\overline{S_5})$ − 5.10×10^{+9} $(S_1-\overline{S_1})(S_6-\overline{S_6})$ − 7.34×10^{+9} $(S_1-\overline{S_1})(S_7-\overline{S_7})$ − 40.15×10^{-1} $(S_1-\overline{S_1})(T-\overline{T})$ − 7.42×10^{+8} $(S_2-\overline{S_2})(S_3-\overline{S_3})$ − 46429937.00 $(S_2-\overline{S_2})(S_4-\overline{S_4})$ + 93297386.00 $(S_2-\overline{S_2})(S_5-\overline{S_5})$ + 1.72×10^{+9} $(S_2-\overline{S_2})(S_7-\overline{S_7})$ + 924971536.00 $(S_2-\overline{S_2})(S_8-\overline{S_8})$ + 51.57×10^{-1} $(S_2-\overline{S_2})(T-\overline{T})$ − 33295616.00 $(S_3-\overline{S_3})(S_4-\overline{S_4})$ + 38422954.00 $(S_3-\overline{S_3})(S_5-\overline{S_5})$ + 151526609.00 $(S_3-\overline{S_3})(S_6-\overline{S_6})$ + 4999312.60 $(S_3-\overline{S_3})(S_7-\overline{S_7})$ + 1.29×10^{+9} $(S_3-\overline{S_3})(S_8-\overline{S_8})$ − 8.32×10^{-1} $(S_3-\overline{S_3})(T-\overline{T})$ − 5079827.00 $(S_4-\overline{S_4})(S_5-\overline{S_5})$ + 77090308.00 $(S_4-\overline{S_4})(S_7-\overline{S_7})$ + 187576063.00 $(S_4-\overline{S_4})(S_8-\overline{S_8})$ + 26647478.00 $(S_5-\overline{S_5})(S_6-\overline{S_6})$ − 66022050.00 $(S_5-\overline{S_5})(S_7-\overline{S_7})$ − 1.19×10^{+9} $(S_5-\overline{S_5})(S_8-\overline{S_8})$ + 5.77×10^{-1} $(S_5-\overline{S_5})(T-\overline{T})$ − 3.82×10^{+8} $(S_6-\overline{S_6})(S_7-\overline{S_7})$ − 7.69×10^{-1} $(S_6-\overline{S_6})(T-\overline{T})$ − 2.20×10^{+9} $(S_7-\overline{S_7})(S_8-\overline{S_8})$ + 25.12×10^{-1} $(S_7-\overline{S_7})(T-\overline{T})$ + 26.19×10^{-1} $(S_8-\overline{S_8})(T-\overline{T})$

(III.8)

where S_i and $\overline{S_i}$ are the molecular descriptors and their mean values (e/Å^2), respectively, and T is the temperature (K).

Statistical analysis was then performed on the developed model, and the results are summarized in Table III.29. Based on the obtained results, it was concluded that the Family B model also established a strong performance statistically: the regression coefficient (R^2) and the Fisher's statistic (F_{Ratio}) values were high; R^2= 0.9969 and F_{Ratio} =1991.87 with a $P_{value,\ Fisher}$ < 0.0001 confirming the suitability of fitting the experimental pH values, the cross-validation coefficients were high suggesting the robustness of the model, the low value of the y-scrambling regression coefficient ($R^2_{scramble}$ = 0.0056) and high value of adjusted regression coefficient ($R^2_{adjusted}$= 0.9963) indicate the absence of chance regression correlation.

Table III.29. Family B's statistical performance.

Parameter	Value
Training set	
DESs	29
Data points	251
R^2	0.9969
AICc	-329.67
F_{Ratio}	1991.87
$P_{value,\ Fisher}$	<0.0001
$R^2_{adjusted}$	0.9963
Q^2_{pH}	0.9945
Q^2_{Mw}	0.9962
Q^2_{Savg}	0.9979

$Q^2_{LMO, 25\%}$	0.9965
Q^2_{LOO}	0.9969
$R^2_{scramble}$	0.0056
RMSE	0.1205
SD_{avg}	±0.06
AARD	±2.77%
$AD_{coverage}$	100%
Testing set	
DESs	10
Data points	84
$R^2_{external}$	0.9960
RMSE	0.1433
SD_{avg}	± 0.08
AARD	± 3.68%
$AD_{coverage}$	100%

To clarify the effect of each descriptor and their binary interactions on the pH basic model, the estimated coefficients were evaluated. In the HBD region where $S_{1,+}$ and $S_{2,+}$ molecular descriptors are located, both descriptors showed positive effects (positive coefficients) on the pH of Family B's DESs with high absolute coefficients, high t-$_{Ratio}$, and P-$_{values}$< 5% indicating the positive effect of increasing the concentration of polarizable H atoms on increasing the pH of Family B's DESs. Similarly, the two descriptors in the HBA region $S_{7,-}$ and $S_{8,-}$ were also found to be negatively correlated indicating that an increase in the concentration of $O^{\delta-}$, $N^{\delta-}$, Br^-, Cl^-, and F^- anions lead to a decrease in the pH of DESs, which is opposite to the results obtained in the Family A model. In terms of evaluating the t-$_{Ratio}$, it can be observed that the HBA and the HBD descriptors were significant indicating that both are influential to the pH. When analyzing the weak donor region represented by $S_{3,+}$, a significant positive effect was detected where the absolute values of descriptor's coefficient, its t-$_{Ratio}$, and P-$_{values}$ confirm the favorable influence of cations (N^+, P^+) on the pH of Family B's DESs. Moreover, the negative effect of $S_{6,-}$ in the weak acceptor region concludes the decrease in the pH by the presence of carbon double bonds ($C=C$) and carbonyl groups($C=O$) in the DES structure. The non-polar region showed dual behavior; a negative effect found in the $S_{5,-}$ molecular surface descriptors, and a positive effect in $S_{4,+}$ molecular surface descriptor, which is similar to the trends observed in the Family A model. Also, since the t-$_{Ratio}$ of $S_{4,+}$ are higher than $S_{5,-}$, the positive effect of $S_{4,+}$ is considered to be more pronounced concluding that an increase in the concentration of alkyl groups disturbs the protonation of $[H^+]$, and thus, causing the pH to increase. This result agrees with the findings obtained in section III.5.3.1, where it was observed that an increase in the pH values occurs as the alkyl chain length increases, supporting the effect of the $S_{4,+}$ molecular descriptor on the pH model (pH of TBAC:Gly (1:4) > pH of EAC:Gly (1:4)). As for the temperature descriptor, the same observation found in Family A MLR model was obtained in Family B's MLR model where the

effect of temperature on the pH was significant and inversely proportional (high t-$_{Ratio}$, and P-$_{value}$ < 5%).

When analyzing the binary interactions between the temperature and the molecular surface descriptors, it can be observed that the interactions of $\{S_{2,+}, T\}$, $\{S_{5,-}, T\}$, $\{S_{7,-}, T\}$, and $\{S_{8,-}, T\}$ exhibited a positive correlation whereas the interactions of $\{S_{1,+}, T\}$, $\{S_{3,+}, T\}$, and $\{S_{6,-}, T\}$ presented a negative correlation. Based on the analysis of the absolute coefficient estimates, the t-$_{Ratios}$, and Table III.17, it was concluded that although the temperature exhibited a negative correlation with pH, the binary interactions of H^+, $O^{\delta-}$, $N^{\delta-}$, Cl^-, Br^-, F^-, –CH, –CH$_2$, and –CH$_3$ with temperature leads to an increase in the pH, while the binary interactions of $C^{\delta+}$, N^+, P^+, $C=C$, $C=O$ with temperature leads to a decrease in the pH.

Regarding the interaction between two surface descriptors, it was observed that $\{S_{1,+}, S_{2,+}\}$, $\{S_{1,+}, S_{3,+}\}$, and $\{S_{1,+}, S_{4,+}\}$ exhibited a positive $[+, + \rightarrow +]$ correlation, which was expected as the interaction is identically correlated as the original parental descriptors Table 5 in (Appendix A). Conversely, the $\{S_{1,+}, S_{5,-}\}$ and $\{S_{1,+}, S_{7,-}\}$ interaction presented a $[+, - \rightarrow -]$ behavior, which indicates that the concentration –CH, –CH$_2$, and –CH$_3$ and $O^{\delta-}$, $N^{\delta-}$ of O-H and N-H that are contained within the $S_{5,-}$ and $S_{7,-}$ descriptors have a more pronounced effect on decreasing the pH of DESs than the effect of the H atoms within the $S_{1,+}$ descriptor. Moreover, the $\{S_{5,-}, S_{7,-}\}$, $\{S_{5,-}, S_{8,-}\}$, $\{S_{6,-}, S_{7,-}\}$, and $\{S_{7,-}, S_{8,-}\}$ all showed a negative behavior $[-, - \rightarrow -]$, which matches their origin descriptors. Finally, the interactions between $\{S_{2,+}, S_{4,+}\}$ and $\{S_{3,+}, S_{4,+}\}$ showed a $[+, + \rightarrow -]$ behavior suggesting that increasing the concentration of H^+, N^+, and P^+ within the vicinity of the non-polar –CH, –CH$_2$, and –CH$_3$ functional groups, increases the protonation ability of amine and polyol-based DESs as a result of their binary interactions (causing the pH to decrease), even though the original descriptors were positively correlated.

Figure III.34 (a) shows the experimental *versus* the predicted data of the training set. The high regression coefficient indicated the linearity of the model as all the experimental and predicted data were lying on the diagonal line with narrow dispersion (R^2= 0.9969) and the *RMSE* = 0.1205. The external predictivity of the model was then evaluated with 10 DESs used as a testing set. In Figure III.34 (b), it can be seen that the model showed high predictive capabilities as the regression coefficient ($R^2_{external}$) obtained was 0.9960 and the *RMSE* was 0.1433. Figure III.35 further confirms the quality of the model in predicting the pH of Family B's DESs where the residuals were at a range of ±0.50% with an *AARD* of ±3.68% and an SD_{avg} of ±0.08.

(a)

(b)
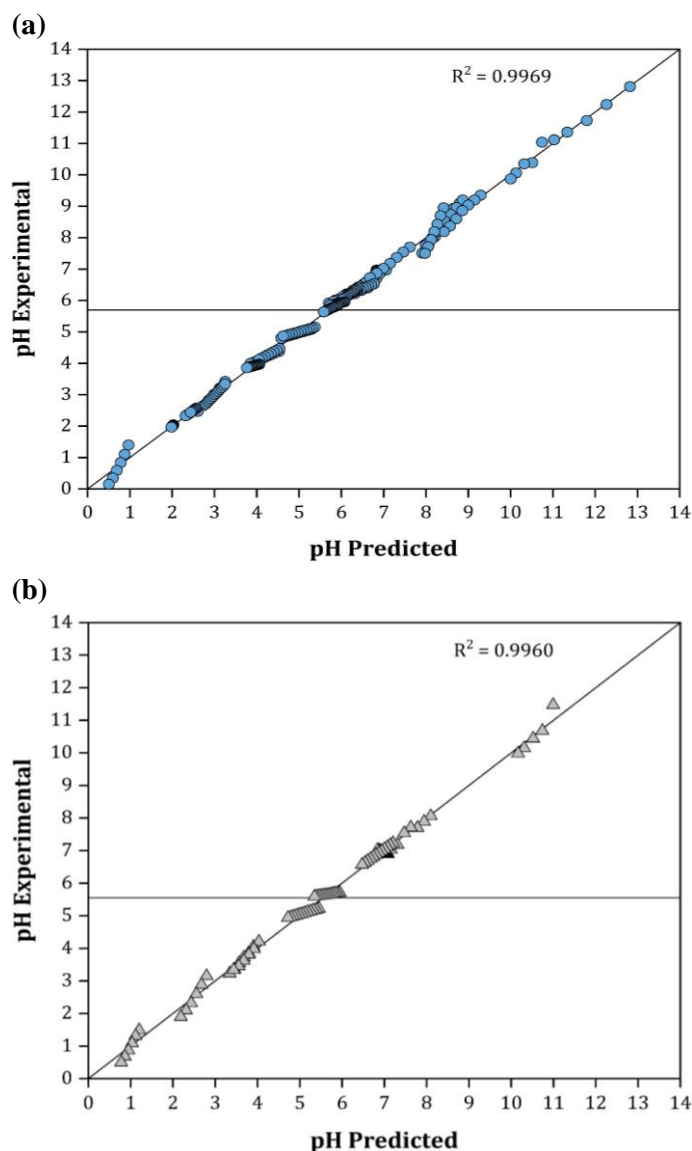
Figure III.34. Parity graph of the experimental and predicted pH values of Family B's MLR model in (a) training, and (b) external testing.
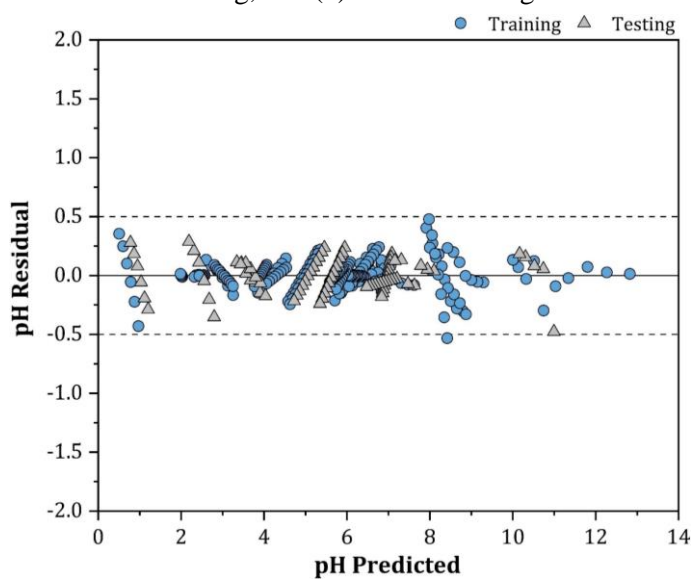
Figure III.35. The residual deviation between the experimentally determined and model predicted pH values in the Family B's MLR model.

Furthermore, Figure III.36 shows the performance of the Family B MLR model in predicting the pH values of the external molecule DES set as a function of temperature. It can be observed that the experimental and the predicted points were fairly overlying indicating high reliability of the proposed model except for ATPPB:DEG:H$_2$O (DES1), BTPC:EG (DES7), and ChCl:DEA (DES11) where their external performance was deviating at lower temperatures. Hence, their average standard deviations were ±0.27, ±0.24, and ±0.30, respectively. Nevertheless, the model still computes the correct qualitative trend with the pH of DES11 > DES7 > DES1, which is consistent with the trend in the experimental data. The points represent the experimental data and the solid lines represent the model predictions.
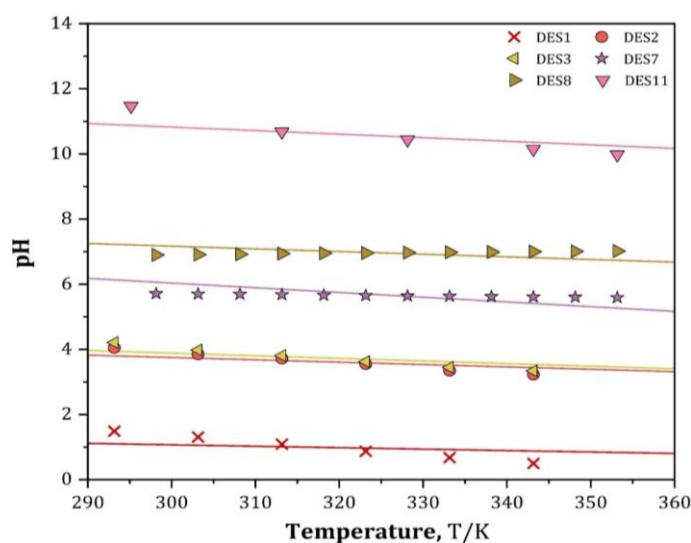
Figure III.36. Experimental and predicted pH values as a function of temperature in external molecule validation for Family B's MLR model.

III.5.4.3. Artificial Neural Network

a) $S_{\sigma\text{-profiles}}$ Discretization and Architecture Optimization

As a comparison to performance of the linear MLR machine learning algorithm, another non-linear model of the experimental pH data of the DESs has also been developed utilizing a feed-forward artificial neural network (ANN). The 4, 6, 8, 10, and 12 discretized $S_{\sigma\text{-profile}}$ descriptors, and the temperature were selected as the network's inputs, while the pH of the DESs was selected as the output. During model development, it was found that an accurate fit for the entire experimental data can be determined using the ANN model (unlike the MLR model) eliminating the need to split the data into two subsets that are "more specific" to certain families of DESs. Out of the 84 DESs, 62 DESs were selected for network learning and the remaining 22 DESs were utilized in external validation.

The number of neurons in the hidden layer is a crucial parameter that has a substantial influence on the accuracy and the complexity of the developed model (Shahbaz et al., 2012; Tu, 1996). Thus, to avoid developing a complicated or overfitted model, several network architectures with 2, 4, 6, 8, 10, and 12 hidden neurons were studied. A heatmap of the regression coefficient (R^2) in several neural network architectures based on the number of hidden neurons and partitioning of $S_{\sigma\text{-profile}}$ is shown in Figure III.37.

Based on the obtained results, the 8-partition network with a neuron architecture of 9-6-1 (*i.e.*, 60 weight coefficients and 7 bias intercepts) has been selected as the optimal compromise between accuracy and fitting parameters as it is the simplest model with a regression coefficient above $R^2 > 0.99$. The selected neural configuration is visually depicted in Figure III.38.

	2 Neurons (3 *intercepts*)	4 Neurons (5 *intercepts*)	6 Neurons (7 *intercepts*)	8 Neurons (9 *intercepts*)	10 Neurons (11 *intercepts*)	12 Neurons (13 *intercepts*)
12 Partitions (S_1–S_{12})	R^2=0.8952 28 coefficients	R^2=0.9814 56 coefficients	R^2=0.9971 84 coefficients	R^2=0.9991 112 coefficients	R^2=0.9997 140 coefficients	R^2=0.9999 168 coefficients
10 Partitions (S_1–S_{10})	R^2=0.8763 24 coefficients	R^2=0.9782 48 coefficients	R^2=0.9964 72 coefficients	R^2=0.9983 96 coefficients	R^2=0.9993 120 coefficients	R^2=0.9996 144 coefficients
8 Partitions (S_1–S_8)	R^2=0.8557 20 coefficients	R^2=0.9679 40 coefficients	**R^2=0.9951** 60 coefficients	R^2=0.9978 80 coefficients	R^2=0.9986 100 coefficients	R^2=0.9992 120 coefficients
6 Partitions (S_1–S_6)	R^2=0.8432 16 coefficients	R^2=0.9408 32 coefficients	R^2=0.9716 48 coefficients	R^2=0.9943 64 coefficients	R^2=0.9968 80 coefficients	R^2=0.9981 96 coefficients
4 Partitions (S_1–S_4)	R^2=0.7645 12 coefficients	R^2=0.8862 24 coefficients	R^2=0.9209 36 coefficients	R^2=0.9635 48 coefficients	R^2=0.9793 60 coefficients	R^2=0.9888 72 coefficients

Figure III.37. Heatmap of the regression coefficient (R^2) in several neural network architectures based on the number of hidden neurons and partitioning of $S_{\sigma\text{-profile}}$.
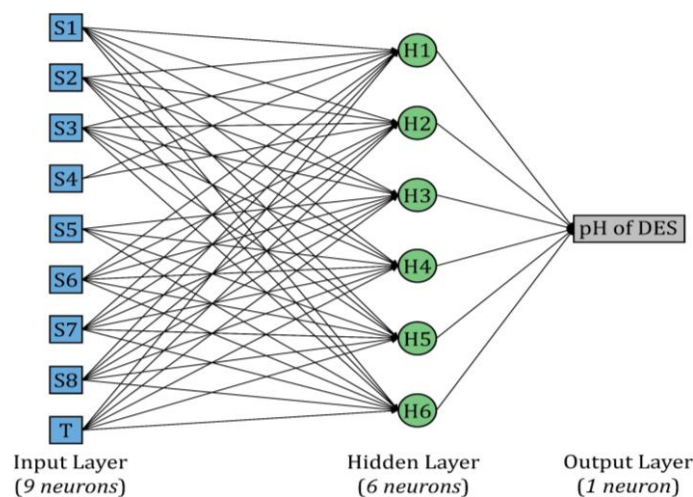
Figure III.38. The 9-6-1 architecture configuration of the artificial neural network for predicting the pH of DESs.

b) Model Evaluation

The weight coefficient and the bias intercept estimates of the 9-6-1 network are listed in Table III.30. Consequently, the resulting ANN model can be expressed as follows:

$$\text{pH} = 2.46(H_1) - 6.87(H_2) + 5.37(H_3) + 4.46(H_4) - 1.14(H_5) - 2.04(H_6) + 2.16 \qquad \text{(III.9)}$$

Where the hidden neurons H_1, H_2, H_3, H_4, H_5, and H_6 are expressed as follows:

$$
\begin{aligned}
H_1 = tanh\Big(\frac{1}{2}(4159.25(S_1) - 6129.54(S_2) + 1125.83(S_3) - 572.51(S_4) - 238.14(S_5) \\
+ 2373.34(S_6) - 2396.48(S_7) + 1882.06(S_8) - 5.67\times10^{-4}(T) + 72.82)\Big)
\end{aligned}
\qquad \text{(III.10)}
$$

$$
\begin{aligned}
H_2 = tanh\Big(\frac{1}{2}(-2166.37(S_1) + 1316.91(S_2) - 929.68(S_3) - 16.38(S_4) + 805.43(S_5) \\
- 80.86(S_6) + 1073.54(S_7) + 205.36(S_8) + 1.21\times10^{-5}(T) - 23.81)\Big)
\end{aligned}
\qquad \text{(III.11)}
$$

$$
\begin{aligned}
H_3 = tanh\Big(\frac{1}{2}(-769.41(S_1) - 492.08(S_2) - 136.95(S_3) - 5.09(S_4) + 305.81(S_5) \\
+ 143.56(S_6) + 600.8(S_7) - 62.57(S_8) - 4.43\times10^{-3}(T) - 7.48)\Big)
\end{aligned}
\qquad \text{(III.12)}
$$

$$
\begin{aligned}
H_4 = tanh\Big(\frac{1}{2}(-28529.31(S_1) - 1669.83(S_2) + 386.62(S_3) + 99.2(S_4) + 34.18(S_5) \\
+ 41.16(S_6) - 1725.9(S_7) - 3654.55(S_8) - 3.76\times10^{-3}(T) + 26.5)\Big)
\end{aligned}
\qquad \text{(III.13)}
$$

$$
\begin{aligned}
H_5 = tanh\Big(\frac{1}{2}(-9600.19(S_1) - 4736.25(S_2) - 812.63(S_3) - 741.55(S_4) + 310.38(S_5) \\
+ 2614.84(S_6) + 1154.73(S_7) + 13877.77(S_8) + 4.49\times10^{-2}(T) + 12.65)\Big)
\end{aligned}
\qquad \text{(III.14)}
$$

$$
\begin{aligned}
H_6 = tanh\Big(\frac{1}{2}(10169.21(S_1) + 4741.2(S_2) - 633.29(S_3) - 340.01(S_4) + 2496.14(S_5) \\
- 746.18(S_6) + 2610.79(S_7) - 11328.32(S_8) - 1.34\times10^{-4}(T) - 70.73)\Big)
\end{aligned}
\qquad \text{(III.15)}
$$

where S_i is the molecular descriptor of region i (e/Å^2) and T is the temperature (K).

Table III.30. The estimates of the 60 weight coefficients and the 7 bias intercepts of the 9-6-1 ANN model.

Neuron	Term	Coefficient Estimate	$P\text{-}value$
H_1	S_1	4159.25	<0.0001
	S_2	-6129.54	<0.0001
	S_3	1125.83	<0.0001
	S_4	-572.51	<0.0001
	S_5	-238.14	<0.0001
	S_6	2373.34	<0.0001
	S_7	-2396.48	<0.0001
	S_8	1882.06	<0.0001
	T	-5.67×10^{-4}	<0.0001
	bias b_1	72.82	<0.0001
H_2	S_1	-2166.37	<0.0001

	S_2	1316.91	<0.0001
	S_3	-929.68	<0.0001
	S_4	-16.38	<0.0001
	S_5	805.43	<0.0001
	S_6	-80.86	<0.0001
	S_7	1073.54	<0.0001
	S_8	205.36	<0.0001
	T	1.21×10^{-5}	<0.0001
	bias b_2	-23.81	<0.0001
H_3	S_1	-769.41	<0.0001
	S_2	-492.08	<0.0001
	S_3	-136.95	<0.0001
	S_4	-5.09	<0.0001
	S_5	305.81	<0.0001
	S_6	143.56	<0.0001
	S_7	600.80	<0.0001
	S_8	-62.57	<0.0001
	T	-4.43×10^{-3}	<0.0001
	bias b_3	-7.48	<0.0001
H_4	S_1	-28529.31	<0.0001
	S_2	-1669.83	<0.0001
	S_3	386.62	<0.0001
	S_4	99.20	<0.0001
	S_5	34.18	<0.0001
	S_6	41.16	<0.0001
	S_7	-1725.90	<0.0001
	S_8	-3654.55	<0.0001
	T	-3.76×10^{-3}	<0.0001
	bias b_4	26.50	<0.0001
H_5	S_1	-9600.19	<0.0001
	S_2	-4736.25	<0.0001
	S_3	-812.63	<0.0001
	S_4	-741.55	<0.0001
	S_5	310.38	<0.0001
	S_6	2614.84	<0.0001
	S_7	1154.73	<0.0001
	S_8	13877.77	<0.0001
	T	4.49×10^{-2}	<0.0001
	bias b_5	12.65	<0.0001
H_6	S_1	10169.21	<0.0001
	S_2	4741.20	<0.0001
	S_3	-633.29	<0.0001
	S_4	-340.01	<0.0001
	S_5	2496.14	<0.0001
	S_6	-746.18	<0.0001
	S_7	2610.79	<0.0001
	S_8	-11328.32	<0.0001
	T	-1.34×10^{-4}	<0.0001
	bias b_6	-70.73	<0.0001
pH	H_1	2.46	<0.0001
	H_2	-6.87	<0.0001
	H_3	5.37	<0.0001
	H_4	4.46	<0.0001
	H_5	-1.14	<0.0001
	H_6	-2.04	<0.0001
	bias b	2.16	<0.0001

A statistical summary of the performance of the ANN model is presented in Table III.31.

When compared to the MLR model, the prediction performance of the ANN model was found to

be better as the model can fit the pH property of acids, sugars, polyols, and amines in a single correlation with an internal R^2 fit of 0.9951. The high regression coefficient can be observed visually in Figure III.39 (a) as the experimental and predicted data were lying on the parity graph's diagonal line with a narrow dispersion ($RMSE = 0.2241$).

Table III.31. The ANN model's statistical performance.

Parameter	Value
Training set	
Number of DESs	62
DESs	DESs 4, 6, 9, 12, 13, 15, 16, 17, 19, 20, 21, 22, 23, 24, 25, 26, 28, 29, 31, 33, 34, 35, 37, 38, 39, 41, 42, 43, 44, 45, 46, 47, 48, 49, 50, 51, 52, 54, 55, 57, 58, 59, 60, 62, 63, 64, 65, 67, 68, 70, 71, 72, 73, 74, 75, 76, 77, 78, 79, 80, 81, 83
Data points	473
R^2	0.9951
AICc	-102.99
P-value, Fisher	<0.0001
$Q^2_{LMO,\ 25\%}$	0.9938
$R^2_{scramble}$	0.1216
$RMSE$	0.2241
SD_{avg}	±0.11
$AARD$	±9.48%
$AD_{coverag}$	98.1%
Number of DESs	62
Testing set	
Number of DESs	22
DESs	DESs 1,2, 3, 5, 7, 8, 10, 11, 14, 18, 27, 30, 32, 36, 40, 53, 56, 61, 66, 69, 82, 84
External molecules	DEEAC, BTPC, MalA, OxaA, Suc, DEA, DEG
Data points	175
$R^2_{externel}$	0.9923
$RMSE$	0.1890
SD_{avg}	±0.11
$AARD$	±11.42%
$AD_{coverag}$	96.0%

(a)

(b)

Figure III.39. Parity graph of the experimental and predicted pH values of the 9-6-1 ANN model in (a) training, and (b) external testing.

The external predictivity of the ANN model was then assessed with a testing set comprised of 22 DESs. It can be seen from that the model showed high predictive capabilities as the $R^2_{external}$ was obtained to be 0.9923. This result was also confirmed by the prediction residuals shown in Figure III.40 where the majority of the residuals were at a range of ±0.5 with an *AARD* of $\pm11.42\%$, and an SD_{avg} of ±0.11.
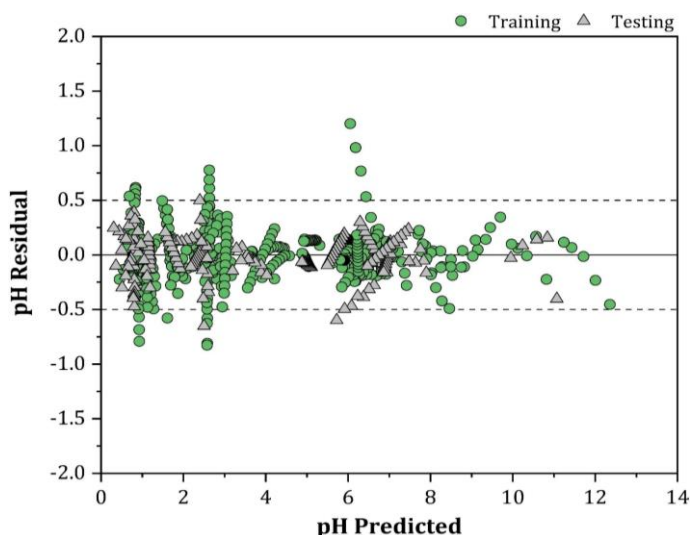
Figure III.40. The residual deviation between the experimentally determined and model predicted pH values in the 9-6-1 ANN model.

Figure III.41 shows the performance of the ANN model in predicting the pH values of the external molecule DES set as a function of temperature. Overall, it can be seen that the model predicts the external molecules quite accurately. However, the performance of ChCl:MalA:H_2O (DES27) is a lot lower than the rest with an SD_{avg} of ±0.30. Moreover, the performance of the general ANN model has been compared to the performance of the Family A and Family B MLR models in Table III.32. Based on the obtained results, it can be concluded that ANN models based on $S_{\sigma\text{-}profile}$ descriptors are also excellent at predicting the pH of DESs, especially when compared to the developed MLR models that required the data to be split into two family-specific subsets. Nonetheless, the ANN model still requires a large amount of estimated fitting parameters, and even though ANNs provide highly accurate and reliable predictive models, one of their well-known shortcomings is the lack of physical interpretation between the inputs and the predicted property(Tu, 1996), unlike the proposed MLR models in the previous sections.
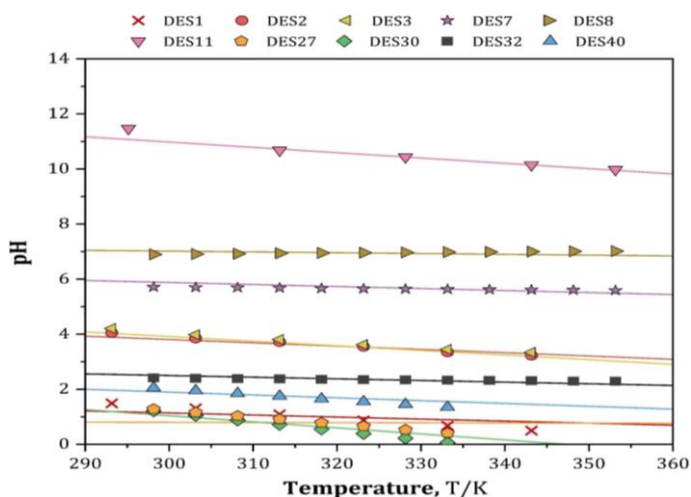
Figure III.41. Experimental and predicted pH values as a function of temperature in external molecule validation for the ANN model.

Table III.32. Comparison of the family-specific MLR models and the general 9-6-1 ANN model in predicting the external molecule DES set.[a]

DES	Temperature	Experimental	MLR prediction	ANN prediction
Family A's external molecule DES set				
DES27, ChCl:MalA:H$_2$O (1:1:0.22)	298.15 – 333.15	1.28 – 0.41	1.02 – 0.67 (SD_{avg} = ±0.18)	0.81 – 0.79 (SD_{avg} = ±0.30)
DES30, ChCl:OxaA: H$_2$O (1:1:2.44)	298.15 – 333.15	1.21 – 0.06	0.85 – 0.42 (SD_{avg} = ±0.25)	1.08 – 0.31 (SD_{avg} = ±0.13)
DES32, DEEAC:MalA (1:1)	298.15 – 353.15	2.41 – 2.29	2.46 – 2.24 (SD_{avg} = ±0.04)	2.51 – 2.18 (SD_{avg} = ±0.07)
DES40, MA:Suc: H$_2$O, (1:1:0.22)	298.15 – 333.15	2.05 – 1.35	2.07 – 1.33 (SD_{avg} = ±0.01)	1.92 – 1.56 (SD_{avg} = ±0.12)
Family B's external molecule DES set				
DES1, ATPPB:DEG: H$_2$O (1:4:0.17)	293.15 – 343.15	1.49 – 0.50	1.10 – 0.88 (SD_{avg} = ±0.27)	1.19 – 0.82 (SD_{avg} = ±0.22)
DES2, ATPPB:DEG: H$_2$O (1:10:0.31)	293.15 – 343.15	4.05 – 3.23	3.80 – 3.44 (SD_{avg} = ±0.16)	3.89 – 3.29 (SD_{avg} = ±0.08)
DES3, ATPPB:DEG: H$_2$O (1:16:0.39)	293.15 – 343.15	4.21 – 3.34	3.94 – 3.54 (SD_{avg} = ±0.17)	4.03 – 3.19 (SD_{avg} = ±0.12)
DES7, BTPC:EG (1:3)	298.15 – 353.15	5.71 – 5.59	6.05 – 5.25 (SD_{avg} = ±0.24)	5.90 – 5.50 (SD_{avg} = ±0.10)
DES8, BTPC:Gly (1:5)	298.15 – 353.15	6.90 – 7.02	7.19 – 6.74 (SD_{avg} = ±0.20)	7.02 – 6.86 (SD_{avg} = ±0.10)
DES11, ChCl:DEA (1:6)	295.15 – 353.15	11.47 – 9.98	10.89 – 10.26 (SD_{avg} = ±0.30)	11.07 – 9.95 (SD_{avg} = ±0.15)

[a]Average standard deviation between the two points (SD_{avg}).

III.5.4.4. Applicability Domain

The AD is defined as follow (i) the x-axis represents the leverage values where $0 < h_i < h^*$, and (ii) the y-axis represents the standardized residuals where $-3 < SDR < +3$ (Gramatica, 2007). Figure III.42 shows the William Plots for the developed models.
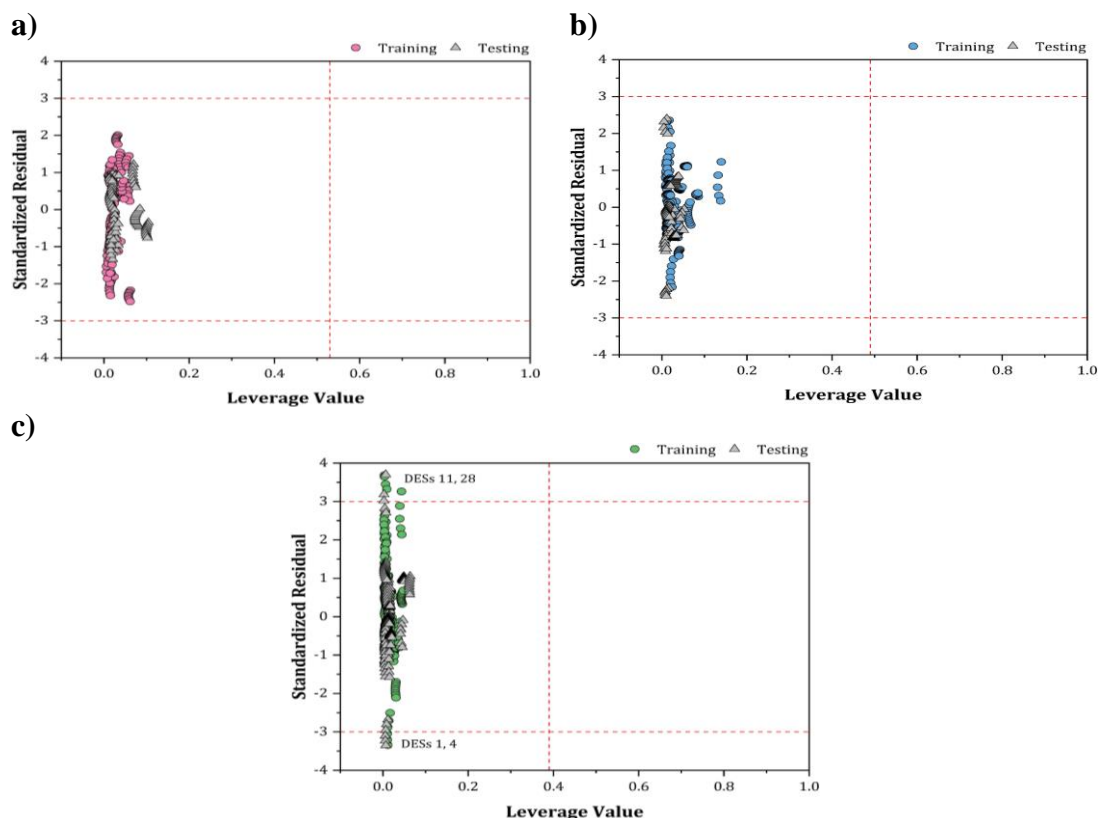
Figure III.42. William plots for the (a) Family A MLR model, the (b) Family B MLR model, and the (c) general ANN model. The dashed lines represent the boundaries of the applicability domain.

In the first step of obtaining the AD, the critical leverage values (h^*) were calculated for the models to be 0.53, 0.49, and 0.38 for the Family A MLR model, the Family B MLR model, and the ANN model, respectively. After calculating h^*, the domains were obtained to test the applicability of each model in covering and predicting a wide range of new DES combinations. From Figure III.42 (a) and (b), it can be seen that all the DESs in the training set and testing set in both Family A and Family B MLR models were within the AD margins and present no outliers with an $AD_{coverage} = 100.0\%$, indicating that the families are homogenous and can be well described by the proposed machine learning algorithm. As for the ANN model in Figure III.42 (c), it can be observed that the model presents no structural outliers as all the points present a leverage value significantly lower than the critical leverage value ($h_i < h^*$). Nonetheless, the estimates of a few DESs were considered as "response outliers" as they exhibit standardized residuals values above the ±3 boundaries, which bring down the $AD_{coverage}$ to 97.5%. The response outliers in the general ANN model include: ATPPB:DEG:H_2O (DES1), ATPPB:TEG:H_2O (DES4), ChCl:DEA (DES11), and ChCl:MDEA (DES28). Based on the obtained AD analysis, it can be concluded that the prediction of a new combination of hydrophilic DESs that (i) are within the model's applicability domain, and (ii) contain similar constituents to the ones utilized in the training set could be considered reliable. However, the prediction of new hydrophilic DESs that are not within the model's applicability domain should be treated with more attention due to their high extrapolation degree.

III.6. Conclusion

Mathematical models for the prediction of physicochemical properties of DESs were developed. The models were derived by a QSPR analysis, after defining the independent (i.e. the Sσ-profile, Temperature, and interaction terms) and the dependent (properties) variables. The DESs were selected so that their constituents have a wide range of chemical structures. The definition of the expression of the models was supported by an in-depth statistical analysis in which the main descriptors exerting a significant influence on the studied properties were considered. The modeling results showed that the proposed models for the investigated DESs properties were able to predict the properties of the DESs and with acceptable accuracy. The developed QSPR models can be considered as a reliable tool for predicting important DESs properties and can be used for their determination in the absence of experimental measurements, allowing a significant economy and time saving, and are useful for a thorough and optimal process design.

References

Abbott, A. P., Alabdullah, S. S. M., Al-Murshedi, A. Y. M., & Ryder, K. S. (2018). Brønsted acidity in deep eutectic solvents and ionic liquids. *Faraday Discussions*, *206*, 365–377. https://doi.org/10.1039/c7fd00153c

Adeyemi, I., Abu-Zahra, M. R. M., & AlNashef, I. M. (2018). Physicochemical properties of alkanolamine-choline chloride deep eutectic solvents: Measurements, group contribution and artificial intelligence prediction techniques. *Journal of Molecular Liquids*, *256*, 581–590. https://doi.org/10.1016/j.molliq.2018.02.085

Aissaoui, T., AlNashef, I. M., & Benguerba, Y. (2016). Dehydration of natural gas using choline chloride based deep eutectic solvents: COSMO-RS prediction. *Journal of Natural Gas Science and Engineering*, *30*, 571–577. https://doi.org/10.1016/j.jngse.2016.02.007

Almustafa, G., Sulaiman, R., Kumar, M., Adeyemi, I., Arafat, H. A., & AlNashef, I. (2020). Boron extraction from aqueous medium using novel hydrophobic deep eutectic solvents. *Chemical Engineering Journal*, *395*(February), 125173. https://doi.org/10.1016/j.cej.2020.125173

Bagh, F. S. G., Shahbaz, K., Mjalli, F. S., AlNashef, I. M., & Hashim, M. A. (2013). Electrical conductivity of ammonium and phosphonium based deep eutectic solvents: Measurements and artificial intelligence-based prediction. *Fluid Phase Equilibria*, *356*, 30–37. https://doi.org/10.1016/j.fluid.2013.07.012

Bahadori, L., Abdul Manan, N. S., Chakrabarti, M. H., Hashim, M. A., Mjalli, F. S., Alnashef, I. M., Hussain, M. A., & Low, C. T. J. (2013). The electrochemical behaviour of ferrocene in deep eutectic solvents based on quaternary ammonium and phosphonium salts. *Physical Chemistry Chemical Physics*, *15*(5), 1707–1714. https://doi.org/10.1039/c2cp43077k

Bahadori, L., Chakrabarti, M. H., Mjalli, F. S., Alnashef, I. M., Manan, N. S. A., & Hashim, M. A. (2013). Physicochemical properties of ammonium-based deep eutectic solvents and their electrochemical evaluation using organometallic reference redox systems. *Electrochimica Acta*, *113*, 205–211. https://doi.org/10.1016/j.electacta.2013.09.102

Carvalheda, C. A., Campos, S. R. R., Machuqueiro, M., & Baptista, A. M. (2013). Structural effects of ph and deacylation on surfactant protein c in an organic solvent mixture: A constant-pH MD study. *Journal of Chemical Information and Modeling*, *53*(11), 2979–2989. https://doi.org/10.1021/ci400479c

Dearden, J. C., Cronin, M. T. D., & Kaiser, K. L. E. (2009). How not to develop a quantitative structure-activity or structure-property relationship (QSAR/QSPR). *SAR and QSAR in Environmental Research*, *20*(3–4), 241–266. https://doi.org/10.1080/10629360902949567

Diedenhofen, M., & Klamt, A. (2010). COSMO-RS as a tool for property prediction of IL mixtures-A review. *Fluid Phase Equilibria*, *294*(1–2), 31–38. https://doi.org/10.1016/j.fluid.2010.02.002

Dietz, C. H. J. T., Creemers, J. T., Meuleman, M. A., Held, C., Sadowski, G., Van Sint Annaland, M., Gallucci, F., & Kroon, M. C. (2019). Determination of the Total Vapor Pressure of Hydrophobic Deep Eutectic Solvents: Experiments and Perturbed-Chain Statistical Associating Fluid Theory Modeling [Research-article]. *ACS Sustainable Chemistry and Engineering*, *7*(4), 4047–4057. https://doi.org/10.1021/acssuschemeng.8b05449

Eckert, F., & Klamt, A. (2002). Fast Solvent Screening via Quantum Chemistry: COSMO-RS Approach. *AIChE Journal*, *48*(2), 369–385. https://doi.org/10.1002/aic.690480220

Farias, F. O., Passos, H., Coutinho, J. A. P., & Mafra, M. R. (2018). PH Effect on the Formation of Deep-Eutectic-Solvent-Based Aqueous Two-Phase Systems. *Industrial and Engineering Chemistry Research*, *57*(49), 16917–16924. https://doi.org/10.1021/acs.iecr.8b04256

Florindo, C., Celia-Silva, L. G., Martins, L. F. G., Branco, L. C., & Marrucho, I. M. (2018). Supramolecular hydrogel based on a sodium deep eutectic solvent. *Chemical Communications*, *54*(54), 7527–7530. https://doi.org/10.1039/c8cc03266a

Florindo, C., Romero, L., Rintoul, I., Branco, L. C., & Marrucho, I. M. (2018). From Phase Change Materials to Green Solvents: Hydrophobic Low Viscous Fatty Acid-Based Deep Eutectic Solvents. *ACS Sustainable Chemistry and Engineering*, *6*(3), 3888–3895. https://doi.org/10.1021/acssuschemeng.7b04235

Fourches, D., Muratov, E., & Tropsha, A. (2010). Trust, but verify: On the importance of chemical structure curation in cheminformatics and QSAR modeling research. *Journal of Chemical Information and Modeling*, *50*(7), 1189–1204. https://doi.org/10.1021/ci100176x

Ghaedi, H., Ayoub, M., Sufian, S., Hailegiorgis, S. M., Murshid, G., & Khan, S. N. (2018). Thermal stability analysis, experimental conductivity and pH of phosphonium-based deep eutectic solvents and their prediction by a new empirical equation. *Journal of Chemical Thermodynamics*, *116*, 50–60. https://doi.org/10.1016/j.jct.2017.08.029

Gilmore, M., McCourt, É. N., Connolly, F., Nockemann, P., Swadźba-Kwaśny, M., & Holbrey, J. D. (2018). Hydrophobic Deep Eutectic Solvents Incorporating Trioctylphosphine Oxide: Advanced Liquid Extractants. *ACS Sustainable Chemistry and Engineering*, *6*(12), 17323–17332. https://doi.org/10.1021/acssuschemeng.8b04843

Gramatica, P. (2007). Principles of QSAR models validation: Internal and external. *QSAR and Combinatorial Science*, *26*(5), 694–701. https://doi.org/10.1002/qsar.200610151

Gramatica, P., Cassani, S., & Sangion, A. (2016). Aquatic ecotoxicity of personal care products: QSAR models and ranking for prioritization and safer alternatives' design. *Green Chemistry*, *18*(16), 4393–4406. https://doi.org/10.1039/c5gc02818c

Hayyan, A., Mjalli, F. S., Alnashef, I. M., Al-Wahaibi, T., Al-Wahaibi, Y. M., & Hashim, M. A. (2012). Fruit sugar-based deep eutectic solvents and their physical properties. *Thermochimica Acta*, *541*, 70–75. https://doi.org/10.1016/j.tca.2012.04.030

Hayyan, A., Mjalli, F. S., Alnashef, I. M., Al-Wahaibi, Y. M., Al-Wahaibi, T., & Hashim, M. A. (2013). Glucose-based deep eutectic solvents: Physical properties. *Journal of Molecular Liquids*, *178*, 137–141. https://doi.org/10.1016/j.molliq.2012.11.025

Jibril, B., Mjalli, F., Naser, J., & Gano, Z. (2014). New tetrapropylammonium bromide-based deep eutectic solvents: Synthesis and characterizations. *Journal of Molecular Liquids*, *199*, 462–469. https://doi.org/10.1016/j.molliq.2014.08.004

Kahlen, J., Masuch, K., & Leonhard, K. (2010). Modelling cellulose solubilities in ionic liquids using COSMO-RS. *Green Chemistry*, *12*(12), 2172–2181. https://doi.org/10.1039/c0gc00200c

Kareem, M. A., Mjalli, F. S., Hashim, M. A., & Alnashef, I. M. (2010). Phosphonium-based ionic liquids analogues and their physical properties. *Journal of Chemical and Engineering Data*, *55*(11), 4632–4637. https://doi.org/10.1021/je100104v

Li, T., Song, Y., Xu, J., & Fan, J. (2019). A hydrophobic deep eutectic solvent mediated sol-gel coating of solid phase microextraction fiber for determination of toluene, ethylbenzene and o-xylene in water

coupled with GC-FID. *Talanta*, *195*(September 2018), 298–305. https://doi.org/10.1016/j.talanta.2018.11.085

Lin, S. T., & Sandler, S. I. (2002). A priori phase equilibrium prediction from a segment contribution solvation model. *Industrial and Engineering Chemistry Research*, *41*(5), 899–913. https://doi.org/10.1021/ie001047w

Martins, M. A. R., Crespo, E. A., Pontes, P. V. A., Silva, L. P., Bülow, M., Maximo, G. J., Batista, E. A. C., Held, C., Pinho, S. P., & Coutinho, J. A. P. (2018). Tunable Hydrophobic Eutectic Solvents Based on Terpenes and Monocarboxylic Acids. *ACS Sustainable Chemistry and Engineering*, *6*(7), 8836–8846. https://doi.org/10.1021/acssuschemeng.8b01203

Martins, M. A. R., Silva, L. P., Schaeffer, N., Abranches, D. O., Maximo, G. J., Pinho, S. P., & Coutinho, J. A. P. (2019). Greener Terpene-Terpene Eutectic Mixtures as Hydrophobic Solvents. *ACS Sustainable Chemistry and Engineering*, *7*(20), 17414–17423. https://doi.org/10.1021/acssuschemeng.9b04614

Mat Hussin, S. A., Varanusupakul, P., Shahabuddin, S., Yih Hui, B., & Mohamad, S. (2020). Synthesis and characterization of green menthol-based low transition temperature mixture with tunable thermophysical properties as hydrophobic low viscosity solvent. *Journal of Molecular Liquids*, *308*, 113015. https://doi.org/10.1016/j.molliq.2020.113015

Mitar, A., Panić, M., Prlić Kardum, J., Halambek, J., Sander, A., Zagajski Kučan, K., Radojčić Redovniković, I., & Radošević, K. (2019). Physicochemical properties, cytotoxicity, and antioxidative activity of natural deep eutectic solvents containing organic acid. *Chemical and Biochemical Engineering Quarterly*, *33*(1), 1–18. https://doi.org/10.15255/CABEQ.2018.1454

Mjalli, F. S., Naser, J., Jibril, B., Alizadeh, V., & Gano, Z. (2014a). Tetrabutylammonium chloride based ionic liquid analogues and their physical properties. *Journal of Chemical and Engineering Data*, *59*(7), 2242–2251. https://doi.org/10.1021/je5002126

Mjalli, F. S., Naser, J., Jibril, B., Alizadeh, V., & Gano, Z. (2014b). Tetrabutylammonium chloride based ionic liquid analogues and their physical properties. *Journal of Chemical and Engineering Data*, *59*(7), 2242–2251.

Moity, L., Durand, M., Benazzouz, A., Pierlot, C., Molinier, V., & Aubry, J. M. (2012). Panorama of sustainable solvents using the COSMO-RS approach. *Green Chemistry*, *14*(4), 1132–1145. https://doi.org/10.1039/c2gc16515e

Palomar, J., Torrecilla, J. S., Lemus, J., Ferroa, V. R., & Rodriguez, F. (2009). A COSMO-RS based guide to analyze/quantify the polarity of ionic liquids and their mixtures with organic cosolvents. *Physical Chemistry Chemical Physics*, *12*, 1991–2000. https://doi.org/10.1039/c001176m

Paris, J., Telzerow, A., Ríos-Lombardía, N., Steiner, K., Schwab, H., Morís, F., Gröger, H., & González-Sabín, J. (2019). Enantioselective One-Pot Synthesis of Biaryl-Substituted Amines by Combining Palladium and Enzyme Catalysis in Deep Eutectic Solvents. *ACS Sustainable Chemistry and Engineering*, *7*(5), 5486–5493. https://doi.org/10.1021/acssuschemeng.8b06715

Ribeiro, B. D., Florindo, C., Iff, L. C., Coelho, M. A. Z., & Marrucho, I. M. (2015). Menthol-based eutectic mixtures: Hydrophobic low viscosity solvents. *ACS Sustainable Chemistry and Engineering*, *3*(10), 2469–2477. https://doi.org/10.1021/acssuschemeng.5b00532

Riveiro, E., González, B., & Domínguez, Á. (2020). Extraction of adipic, levulinic and succinic acids from water using TOPO-based deep eutectic solvents. *Separation and Purification Technology*, *241*(February), 116692. https://doi.org/10.1016/j.seppur.2020.116692

Rocha, M. A. A., Neves, C. M. S. S., Freire, M. G., Russina, O., Triolo, A., Coutinho, J. A. P., & Santos, L. M. N. B. F. (2013). Alkylimidazolium based ionic liquids: Impact of cation symmetry on their nanoscale structural organization. *Journal of Physical Chemistry B*, *117*(37), 10889–10897. https://doi.org/10.1021/jp406374a

Saputra, R., Walvekar, R., Khalid, M., & Mubarak, N. M. (2020). Synthesis and thermophysical properties of ethylammonium chloride-glycerol-ZnCl2 ternary deep eutectic solvent. *Journal of Molecular Liquids*, *310*, 113232. https://doi.org/10.1016/j.molliq.2020.113232

Shahbaz, K., Baroutian, S., Mjalli, F. S., Hashim, M. A., & Alnashef, I. M. (2012). Densities of ammonium and phosphonium based deep eutectic solvents: Prediction using artificial intelligence and group contribution techniques. *Thermochimica Acta*, *527*, 59–66. https://doi.org/10.1016/j.tca.2011.10.010

Shahbaz, K., Mjalli, F. S., Hashim, M. A., & Alnashef, I. M. (2011). Prediction of deep eutectic solvents densities at different temperatures. *Thermochimica Acta*, *515*(1–2), 67–72. https://doi.org/10.1016/j.tca.2010.12.022

Skulcova, A., Russ, A., Jablonsky, M., & Sima, J. (2018). *PEER REVIEWED BRIEF COMMUNICATION The pH Behavior of Seventeen Deep Eutectic Solvents*. 3, 5042–5051.

Tereshatov, E. E., Boltoeva, M. Y., & Folden, C. M. (2016). First evidence of metal transfer into hydrophobic deep eutectic and low-transition-temperature mixtures: Indium extraction from hydrochloric and oxalic acids. *Green Chemistry*, *18*(17), 4616–4622. https://doi.org/10.1039/c5gc03080c

Topliss, J. G., & Costello, R. J. (1972). Chance Correlations in Structure-Activity Studies Using Multiple Regression Analysis. *Journal of Medicinal Chemistry*, *15*(10), 1066–1068. https://doi.org/10.1021/jm00280a017

Torrecilla, J. S., Palomar, J., Lemus, J., & Rodríguez, F. (2010). A quantum-chemical-based guide to analyze/quantify the cytotoxicity of ionic liquids. *Green Chemistry*, *12*(1), 123–13. https://doi.org/10.1039/b919806g

Tropsha, A., Gramatica, P., & Gombar, V. K. (2003). The importance of being earnest: Validation is the absolute essential for successful application and interpretation of QSPR models. *QSAR and Combinatorial Science*, *22*(1), 69–77. https://doi.org/10.1002/qsar.200390007

Tu, J. V. (1996). Advantages and disadvantages of using artificial neural networks versus logistic regression for predicting medical outcomes. *Journal of Clinical Epidemiology*, *49*(11), 1225–1231. https://doi.org/10.1016/S0895-4356(96)00002-9

Uslu, H., & Bamufleh, H. S. (2016). Effect of Solvent and pH on the Extraction of Carbolic Acid from Aqueous Solution by TOMAC. *Journal of Chemical and Engineering Data*, *61*(4), 1676–1680. https://doi.org/10.1021/acs.jced.5b01089

van Osch, D. J. G. P., Dietz, C. H. J. T., Warrag, S. E. E., & Kroon, M. C. (2020). The Curious Case of Hydrophobic Deep Eutectic Solvents: a Story on the Discovery, Design and Applications. *ACS Sustainable Chemistry & Engineering*. https://doi.org/10.1021/acssuschemeng.0c00559

Van Osch, D. J. G. P., Parmentier, D., Dietz, C. H. J. T., Van Den Bruinhorst, A., Tuinier, R., & Kroon, M. C. (2016). Removal of alkali and transition metal ions from water with hydrophobic deep eutectic solvents. *Chemical Communications*, *52*(80), 11987–11990. https://doi.org/10.1039/c6cc06105b

Van Osch, D. J. G. P., Van Spronsen, J., Esteves, A. C. C., Tuinier, R., & Vis, M. (2020). Oil-in-water emulsions based on hydrophobic eutectic systems. *Physical Chemistry Chemical Physics*, *22*(4), 2181–2187. https://doi.org/10.1039/c9cp06762k

Chapter III   Physicochemical Properties of Deep Eutectic Solvents

Van Osch, D. J. G. P., Zubeir, L. F., Van Den Bruinhorst, A., Rocha, M. A. A., & Kroon, M. C. (2015). Hydrophobic deep eutectic solvents as water-immiscible extractants. *Green Chemistry*, *17*(9), 4518–4521. https://doi.org/10.1039/c5gc01451d

Verma, R., & Banerjee, T. (2018). Liquid-Liquid Extraction of Lower Alcohols Using Menthol-Based Hydrophobic Deep Eutectic Solvent: Experiments and COSMO-SAC Predictions. *Industrial and Engineering Chemistry Research*, *57*(9), 3371–3381. https://doi.org/10.1021/acs.iecr.7b05270

Verma, R., & Banerjee, T. (2019). Palmitic-Acid-Based Hydrophobic Deep Eutectic Solvents for the Extraction of Lower Alcohols from Aqueous Media: Liquid–Liquid Equilibria Measurements, Validation and Process Economics. *Global Challenges*, *3*(11), 1900024. https://doi.org/10.1002/gch2.201900024

Zhao, Y., Huang, Y., Zhang, X., & Zhang, S. (2015). A quantitative prediction of the viscosity of ionic liquids using Sσ-profile molecular descriptors. *Physical Chemistry Chemical Physics*, *17*(5), 3761–3767. https://doi.org/10.1039/c4cp04712e

Zubeir, L. F., Van Osch, D. J. G. P., Rocha, M. A. A., Banat, F., & Kroon, M. C. (2018). Carbon Dioxide Solubilities in Decanoic Acid-Based Hydrophobic Deep Eutectic Solvents. *Journal of Chemical and Engineering Data*, *63*(4), 913–919. https://doi.org/10.1021/acs.jced.7b00534

Chapter IV

Deep Eutectic Solvents as Extraction Solvents

IV.1. Introduction

Fuels are considered to be a major environmental pollutant as they are rich in aromatics, sulfur-containing, and nitrogen-containing aromatics (Barker, 1985) that are burnt to produce hazardous air pollutants, such as CO_x, SO_x, and NO_x. Therefore, strict governmental regulations have been introduced to set limits on the content of aromatics, sulfur-containing, and nitrogen-containing aromatics in fuels (EPA, 2014). Industrially, catalytic hydrotreatment is the established process used for the simultaneous dearomatization, desulfurization, and denitrogenation of fuels (Stanislaus & Barry, 1994). DESs have been extensively applied in the separation of aromatics, sulfur-containing, and nitrogen-containing aromatics from *n*-alkanes. However, most studies investigated the separation of only one impurity (either an aromatic, a sulfur-containing aromatic, or a nitrogen-containing aromatic) from *n*-alkanes.

IV.2. Extraction of Impurities from Oil Using Acidic Deep Eutectic Solvents

IV.2.1. Experimental Procedures

IV.2.1.1. Materials
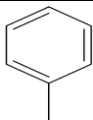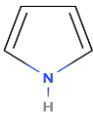
Table IV.1 lists the chemicals used with their respective sources, CAS numbers, and weight fraction purities.

Table IV.1. Chemicals and their corresponding CAS numbers, and purity as identified by the suppliers.

Chemical	CAS number	Purity (*wt%*)	Source
n-decane	124-18-5	≥ 99.0	Sigma-Aldrich
Toluene	108-88-3	≥ 99.5	Sigma-Aldrich
Thiophene	110-02-1	≥ 99.0	Sigma-Aldrich
Pyridine	110-86-1	≥ 99.0	Sigma-Aldrich
Pyrrole	109-97-7	≥ 98.0	Sigma-Aldrich
Tetrapropylammonium bromide	1941-30-6	≥ 98.0	Sigma-Aldrich
Acetic acid	64-19-7	≥ 99.5	Surechem Products
Ethanol	64-17-5	≥ 99.8	Sigma-Aldrich

The chemical structures and formulas of the diesel model components are listed in Table IV.2. All the chemicals used were of 98 wt% or higher purity and were used as obtained from the suppliers.
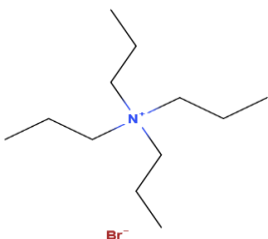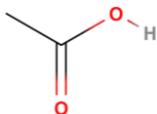
Table IV.2. Chemical structures and formulas of the diesel model components.

Component	Chemical Formula	Structure
n-decane	$C_{10}H_{22}$	
Toluene	C_7H_8	
Thiophene	C_4H_4S	
Pyridine	C_5H_5N	
Pyrrole	C_4H_5N	

IV.2.1.2. DES Preparation and Characterization

The DES as shown in Table IV.3 was prepared by mixing precisely weighed amounts of tetrapropylammonium bromide (TPAB) and acetic acid (AA) with a 1:4 molar ratio in 40 mL screw-capped bottles using a Shimadzu balance AUX220 with a measurement uncertainty of ± 0.0002 g. Then, using a ThermoMixer C (Eppendorf, Germany), the mixture was heated to 338.2 K and stirred at 500 rpm for 2 h to form a clear homogeneous liquid. It is worth noting from Table IV.3 that even though the molar fractions of HBA to HBD is 20 mol% to 80 mol%, in terms of weight fraction, the fractions of HBA to HBD is observed to be more significant, 52.6 wt% compared to 47.4 wt%, respectively.

Table IV.3. The deep eutectic solvent with its chemical structure, formula, molar fraction, and weight fraction.

	Hydrogen bond acceptor	Hydrogen bond donor
Name	Tetrapropylammonium bromide	Acetic acid
Structure		
Chemical formula	$C_{12}H_{28}BrN$	$C_2H_4O_2$
Molar ratio	1	4
Mole percentage (mol%)	20.0%	80.0%
Weight percentage (wt%)	52.6%	47.4%

The physical properties of the solvent; density, dynamic viscosity, water content, and freezing point of TPAB: AA (1:4) were measured. The viscosity was measured at T = 298.2 K

using a Thermo Scientific's HAAKE Rheo Stress 6000 rheometer at a shear rate of 240 s^{-1} for 120 s with an average standard deviation of 8 mPa$\cdot$s. Moreover, Karl-Fischer Titrator (GRS Scientific/Aquamax KF Coulometric) was used to determine the water content of the DES while the density was measured using a DMA 5000 M manufactured by Anton Paar. Finally, the freezing point of the DES was measured using a Perkin Elmer Differential Scanning Calorimeter (DSC 4000). The temperature profile adopted was : (i) cooling from 303.2 K to 193.2 K at a rate of 4 K$\cdot$min^{-1}, (ii) isotherm at 193.2 K for 15 min, and (iii) heating from 193.2 K back to 303.2 K at a rate of 4 K$\cdot$min^{-1}.

IV.2.1.3. Solubility Test

The solubility test was performed for each fuel component in either the DES or the pure acetic acid at T = 298.2 K and P = 1.01 bar using the equilibrium cell method, where 3 g of each fuel component was mixed with either 3 g of DES or 3 g of pure acetic acid in screw-capped 8 mL vials. The vials were then stirred for 4 h at 1000 rpm via a ThermoMixer C at a T = 298.2 K and left to settle for approximately 20 h at a constant temperature of 298.2 K to reach equilibrium. If phase separation is observed, then a 0.5 mL sample from the solvent-rich phase "extract phase" is taken for analysis using a syringe, without disturbing the phases coexistence interface.

IV.2.1.4. Liquid-Liquid Extraction

The *pseudo*-ternary phase diagrams of {*n*-decane (1) + toluene (2) + TPAB : AA (3)}, {*n*-decane (1) + thiophene (2) + TPAB : AA (3)}, {*n*-decane (1) + pyridine (2) + TPAB : AA (3)}, and {*n*-decane (1) + pyrrole (2) + TPAB : AA (3)} were experimentally obtained by preparing 9 arbitrary diesel models with a wide range of compositions, from 95 wt% to 20 wt% *n*-decane. The 9 models were then mixed with TPAB : AA (1 :4) at a fixed solvent-to-feed ratio of 1 :1 in screw-capped vials. The prepared vials were then stirred for 4 h at 1000 rpm via a ThermoMixer C at T = 298.2 K, and left to settle for approximately 20 h at constant temperature of 298.2 K to reach equilibrium. Finally, a 0.5 mL sample from both phases was taken for analysis using a syringe, without disturbing the phases coexistence interface.

The term "*pseudo*" has been introduced to indicate that the DES was treated as a *pseudo*-pure species instead of a mixture of two components. This terminology was later justified experimentally using Fourier Transform Infrared (FT-IR) Spectrometry and Karl Fisher Titration. The FT-IR analysis was conducted using a VERTEX 80v spectrometer manufactured by Bruker. The spectrum was obtained in transmittance mode using 64 scans with a resolution of 4 cm^{-1} between the wavenumber region of 4000 to 400 cm^{-1}.To further understand the behavior of the system, the influence of different parameters such as (1) initial concentration, (2) mixing effect of

fuel impurities, (3) and multi-stage extraction on the performance of DES were studied. In these experiments, an arbitrary diesel model consisting of {5 wt% toluene + 5 wt% thiophene + 5 wt% pyridine + 5 wt% pyrrole + 80 wt% *n*-decane} was selected for the extraction process.

IV.2.1.5. *Analysis of Raffinate and Extract Phases*

The composition of the raffinate ("the *n*-alkane rich-phase") and extract ("the DES rich-phase") after extraction was measured using Gas Chromatography (GC) via an Agilent 6890 N. The specifications and experimental conditions of the analysis used are available in Table 1 in the (Appendix B). The prepared samples were diluted using 1 mL of ethanol as an internal standard. Moreover, since it was not possible to measure the DES concentration via gas chromatography (due to its low volatility), only the concentrations of the fuel components in both phases were measured using the GC, while the concentration of the DES was determined via mass balance calculations. The GC liner, "where nonvolatile materials are collected", was replaced after measuring each system to avoid the contamination of the GC column. The GC's analysis was checked via a method verification test, where samples of known concentrations were run by the GC and the standard deviation between the known concentrations and the GC measured concentrations were within an average of ±0.3 wt%. The statistical uncertainty of the GC measurements was also calculated by running each sample in triplicates and was found to be within an average standard deviation of ±0.3 wt%.

IV.2.2. Results and Discussion

IV.2.2.1. *DES Characterization*

The physiochemical properties of a solvent are of great importance to assess their feasibility as an extracting agent for liquid−liquid extraction. Thus, the properties of TPAB: AA (1:4) including density, dynamic viscosity, water content, and freezing point were measured and are listed in Table IV.4.

Table IV.4. Freezing temperature, density, viscosity, and water content of TPAB: AA (1:4). The density and viscosity were measured at 298.2 K and 1.01 bar.

Freezing Point (T_f) (K)	Density (ρ) (g/cm^3)	Viscosity (η) (mPa·s)	Water Content (wt %)	Water Content (mol%)
249.1 ± 1.1	1.099 ± 0.003	26.4 ± 1.6	0.13 ± 0.01	0.72 ± 0.05

[a]Standard uncertainty in temperature and pressure are $u(T) = ±0.1K$ and $u(P) = ±0.04$ bar, respectively

First, the freezing point of the DES was measured and found to be 249.1 K, which is well below the freezing points of both the individual constituents *i.e.*, 525.4 K and 298.7 K for tetrapropylammonium bromide and acetic acid, respectively. This presumably indicates the

formation of strong intermolecular interactions between both components of the DES. The viscosity of the DES was also measured and was found to be 26.4 mPa·s, which is considered to be low when compared to many other solvents. Also, since DESs are known for their ability to absorb moisture [31,52], the water content of freshly prepared DES was measured and was found to be less than 0.13 wt% ($\approx$ 0.72 mol%). Finally, the density of the DES was measured as a function of temperature from 293.2 K up to 368.2 K as shown in Figure IV.1 (the numerical data are available in Table IV.5). The density data were then correlated using linear regression with an R^2 value of 0.9995 as described by Eq. IV.1.

$$\rho_{(g/cm^3)} = -0.0009T_{(K)} + 1.3534 \tag{IV.1}$$

Table IV.5. Numerical values of density measured between $293.2 \leq T \leq 368.2$ at P (bar) = 1.01.

Temperature, T (K)	Density, ρ (g/cm^3)
293.2	1.103 ±0.002
298.2	1.099 ±0.003
308.2	1.091 ±0.003
318.2	1.083 ±0.003
328.2	1.074 ±0.002
338.2	1.066 ±0.003
348.2	1.057 ±0.002
358.2	1.048 ±0.003
368.2	1.039 ±0.002

[a]Standard uncertainty in temperature and pressure are $u(T) = \pm0.1K$ and $u(P) = \pm0.04$ bar, respectively.
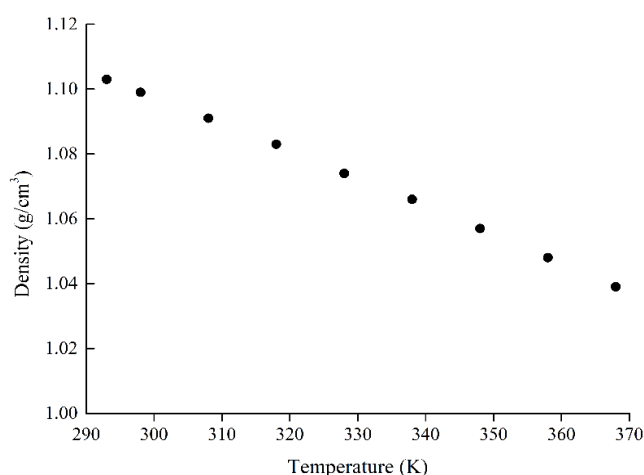
Figure IV.1. The density of TPAB: AA (1:4) versus temperature.

IV.2.2.2. Solubility Test

The aim of conducting an initial solubility test was to check the feasibility of a solvent to extract aromatics from *n*-alkanes. This can be done by checking that (1) the solvent has high solubility of the aromatics to be extracted, and (2) the solvent has no/very low solubility of the *n*-alkane. Therefore, the solubility of each fuel component in both acetic acid and TPAB: AA (1:4) was measured and the results are shown in Figure IV.2. The systems of {thiophene (1) + AA/DES

(2)}, {pyridine (1) + AA/DES (2)}, and {pyrrole (1) + AA/DES (2)} formed clear and homogeneous solutions with no phase separation or turbidity, indicating that thiophene, pyridine, and pyrrole are fully miscible in both the DES and pure acetic acid. This is presumably due to the presence of the electronegative sulfur and nitrogen elements in these molecules, which increased their polar and electrostatic interactions with the DES. Also, since pyrrole contains an N-H bond, it is expected that the pyrrole molecule is not only able to interact with the DES via polar and electrostatic interactions, but also through hydrogen bonding.
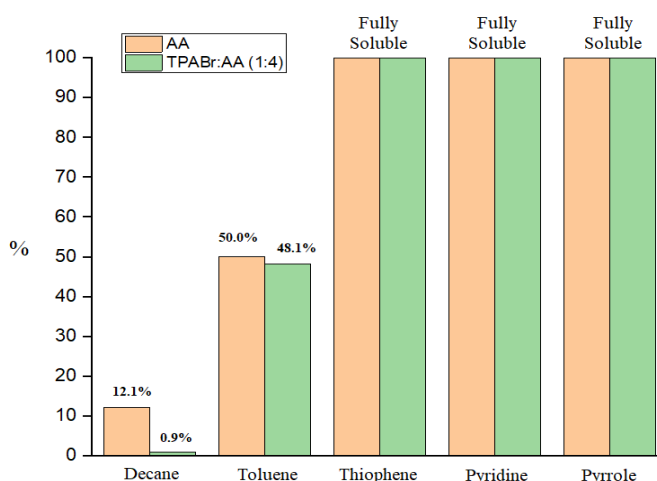
Figure IV.2. Solubilities (wt%) of each fuel component in the solvent-rich phase of either TPAB: AA (1:4) or acetic acid (Conditions: T = 298.2 K, P = 1.01 bar, stirring time = 4 h at 1000 rpm, and settling time = 20 h).

The solubility of *n*-decane in TPAB: AA (1:4) was around 13 times lower than that in pure acetic acid (0.9 wt% compared to 12.1 wt%). This behavior can be attributed to the increased polarity of the solvent upon the addition of the salt "TPAB", which led to a large decrease in the solubility of the nonpolar *n*-decane. The lower solubility of *n*-decane in the DES is expected to improve the recoverability of *n*-decane, consequently, increasing the profitability of the extraction process. As for the system of {toluene (1) + AA/DES (2)}, the toluene was found to be partially soluble in both solvents, with the solubility in pure acetic acid being slightly higher than that of the DES. Nevertheless, the solubility of toluene is still relatively much higher than that of *n*-decane even though they are both considered nonpolar molecules. This is presumably because of the existence of the π-electron cloud surrounding the toluene molecule, which can interact with the DES via electrostatic interactions. Therefore, based on the solubilities obtained, it can be concluded that the TPAB: AA (1:4) could be considered as a potential solvent for simultaneous dearomatization, desulfurization, and denitrogenation and merits further investigation of its single-stage extractive ability.

IV.2.2.3. Single-Stage Liquid-Liquid Extraction from Diesel Model

In this section, the separation of a mixture containing 5 wt% toluene, 5 wt% thiophene, 5 wt% pyridine, and 5 wt% pyrrole from *n*-decane using TPAB: AA (1:4) was conducted at 298.2 K and 1.01 bar. The results were expressed in terms of extraction efficiency (calculated by Eq. II.24) and are listed in Table IV.6. The extraction performance of the DES was then compared to that of pure acetic acid as shown in Figure IV.3. It can be seen that the extraction efficiencies of both thiophene and pyrrole using the DES were around ≈17% higher than that of pure acetic acid even though in section V.4.2 both impurities were fully soluble in either the DES or pure acetic acid. This increase in extraction capacity is presumably due to the aforementioned increase in polarity of the solvent after the addition of the salt. On the other hand, the extraction efficiencies of toluene and pyridine were slightly higher for acetic acid compared to the DES, which is consistent with the results obtained in the solubility measurements in section IV.2.2.2. Additionally, it was found that the addition of the TPAB salt increased the aromatic selectivity of the solvent by decreasing the amount of *n*-decane lost to the extract phase. The weight fraction of *n*-decane in the extract phase of acetic acid was found to be 7.6 wt% compared to 1.4 wt% in the TPAB: AA (1:4) phase. Therefore, based on extraction efficiency and the loss of *n*-decane to the extract phase, it can be concluded that TPAB: AA (1:4) could be considered as a potential solvent in the application of simultaneous dearomatization, desulfurization, and denitrogenation of fuels.

Table IV.6. Weight fractions and single-stage extraction efficiency of each fuel impurity using TPAB: AA (1:4) at a 1:1 solvent-to-feed ratio measured at 298.2 K and 1.01 bar.

Fuel Impurity	$w_{i,Initial}$ (wt%)	$w_{i,Raffinate}$ (wt%)	E (%)
Toluene	5.00	4.14	17.2
Thiophene	5.00	3.18	36.4
Pyridine	5.00	0.27	94.6
Pyrrole	5.00	0.12	97.6

[a]Standard uncertainty in temperature, pressure, and weight fractions are $u(T) = \pm0.1K$, $u(P) = \pm0.04$ bar, and $u(w) = \pm0.30$ wt%, respectively.
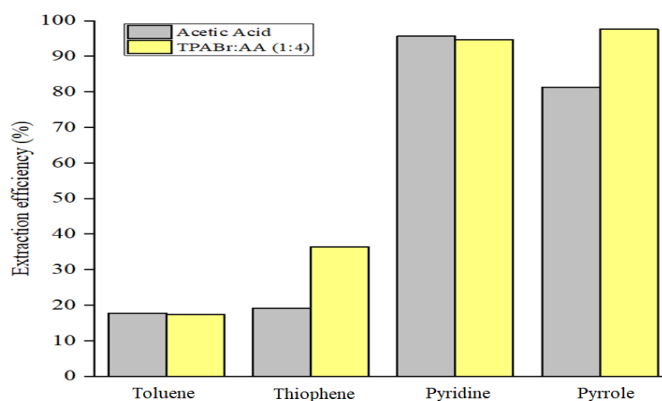
Figure IV.3. Extraction efficiency of each fuel contaminant using acetic acid and TPAB : AA 1 :4. (Conditions : T = 298.2 K, P = 1.01 bar, S : F ratio = 1 :1, stirring time = 4 h at 1000 rpm, and settling time = 20 h).

As for the extraction mechanism, it was found from the results obtained using GC that both the raffinate and extract phases showed a distinctive peak for each impurity and no new peaks were observed after the extraction process. This indicates that the extraction mechanism was based on physical extraction as no reaction occurs between the impurities and the DES. The GC results are available in Figures 1 and 2 in (Appendix B). To verify these results, mass balance calculations were conducted between the initial composition and the compositions of both the *n*-alkane rich phase and the solvent-rich phase, the results showed good mass conservation (within ±0.3 wt% standard deviation). This finding is of great importance as physical extractants are preferred over-reactive extractants because the regeneration of the solvent is usually easier. Another advantage is that the extracted aromatics could be utilized as raw materials for other industries since they do not undergo any chemical changes in structure.

IV.2.2.4. Liquid-Liquid Equilibrium Data

a) Pseudo-ternary LLE

For the purpose of understanding the equilibrium behavior of each impurity with the DES, the *pseudo*-ternary equilibrium data of {*n*-decane (1) + toluene (2) + TPAB : AA (3)}, {*n*-decane (1) + thiophene (2) + TPAB : AA (3)}, {*n*-decane (1) + pyridine (2) + TPAB : AA (3)} and {*n*-decane (1) + pyrrole (2) + TPAB : AA (3)} were determined experimentally at 298.2 K and 1.01 bar. The numerical tie line data in weight fractions are available in Table 2 in the (Appendix B) and are graphically illustrated as triangular phase diagrams in Figure IV.4 The obtained LLE data were also used in order to calculate the distribution ratio (β_2) and the selectivity (*S*) using Eq. II.25 and Eq. II.26, respectively.
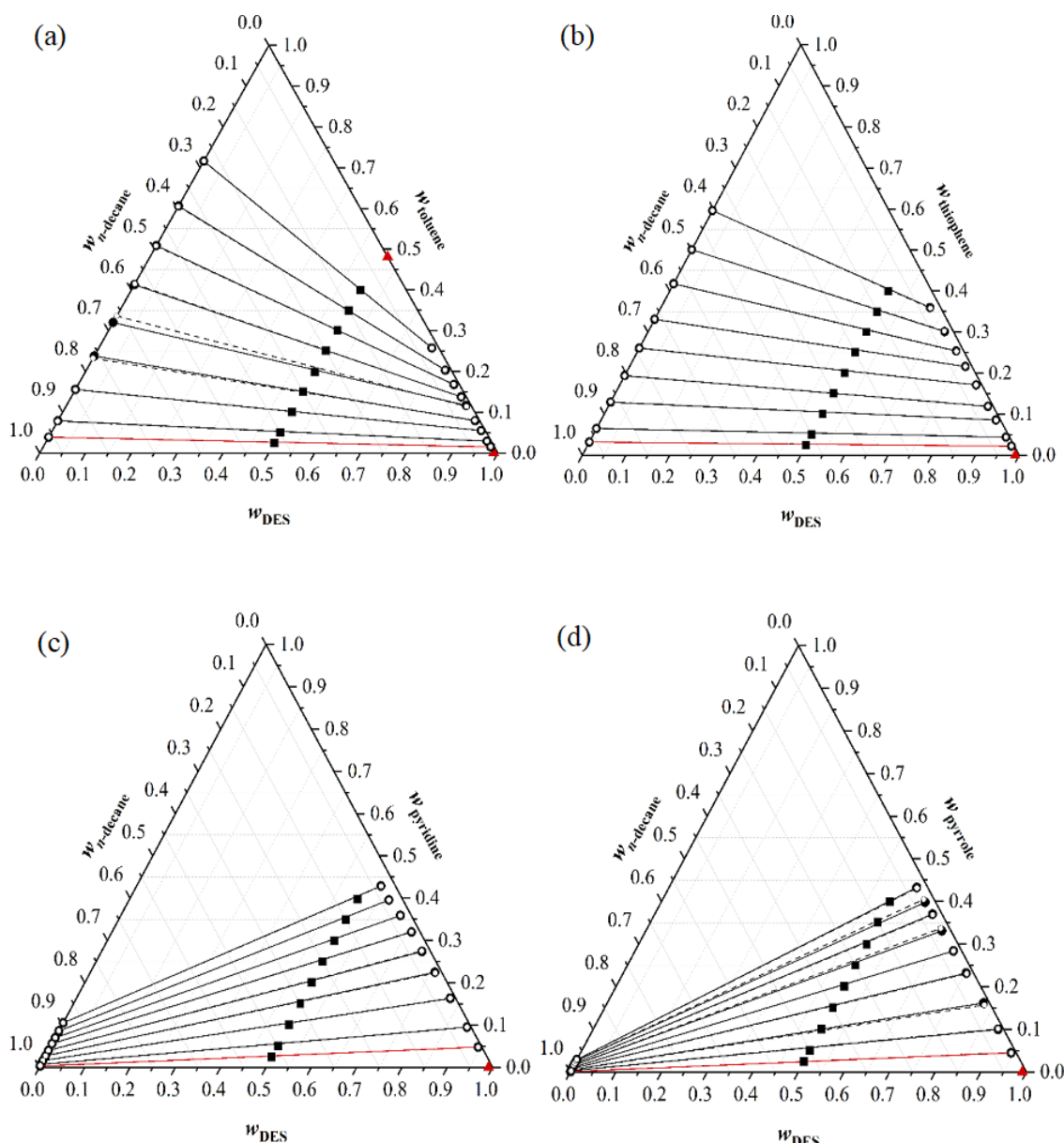
Figure IV.4. Triangular diagrams in weight fractions of the experimental tie lines (●, black solid line) and the calculated tie lines using the NRTL model (○, black dashed line) for systems of {n-decane + (a) toluene / (b) thiophene / (c) pyridine / (d) pyrrole + TPAB: AA} measured at T = 298.2 K and P = 1.01 bar. The initial compositions and solubilities are represented by (■) and (▲), respectively. The red lines correspond to tie lines of 5% toluene, 5% thiophene, 5% pyridine, and 5% pyrrole initial composition.

It can be observed from Figure IV.4 that the immiscibility window was decreasing as follows: toluene > thiophene ≫ pyridine > pyrrole as the range of weight fractions in the raffinate phase for each impurity is decreasing due to the higher extraction. Also, all systems showed small weight fractions of n-decane in the DES-rich phase (< 3.3 wt%), which indicates that low cross-contamination of n-decane into the extract phase occurred. On the other hand, it was found based on mass balance that no cross-contamination of the DES into the n-alkane rich phase occurred ($w_{3,R} = 1 - w_{1,R} - w_{2,R} = 0.000$). This finding was then further verified experimentally by FT-IR analysis. The analysis of a sample raffinate phase after extraction and a sample of the fresh diesel model

showed similar spectrums indicating that no transfer of the DES to the raffinate phase (Figure IV.5). This finding is of great significance as no solvent recovery column would be required after the extraction process to separate the DES from the raffinate phase, which will help to reduce the operational cost of the extraction process.
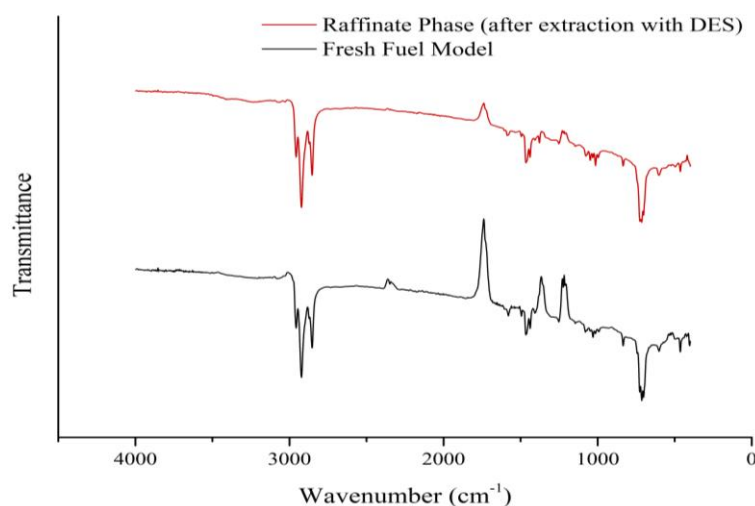
Figure IV.5. FT-IR analysis of the fresh fuel model and the raffinate phase after extraction from an initial mixture of 80 wt% n-decane, 5 wt% toluene, 5 wt% thiophene, 5 wt% pyridine, 5 wt% pyrrole using TPAB (1:4) at a solvent to feed ratio of 1:1.

Moreover, the amount of water was measured for both the extract and raffinate phases after extraction and was found to be $w_{water, E} < 0.0015$ in extract phase "almost similar to the initial water content of the DES" and $w_{water, R} < 0.0001$ in the raffinate phase, which indicates that the water content of the DES remains in the extract phase. These findings also validate the assumption of treating the DES as a pseudo-pure compound. Furthermore, this also validates the uncertainties obtained by the GC analysis, and, the calculations of the DES composition via mass balance.

It can be seen from Figure IV.4 that both systems of pyridine and pyrrole exhibited positive slopes ($\beta_2 > 1$), which indicates that relatively small amounts of TPAB: AA (1:4) are required to achieve separation. On the other hand, negative slopes ($\beta_2 < 1$) were observed for systems of toluene and thiophene, indicating that larger amounts of DES are needed to achieve high efficiencies. The distribution ratios were calculated using Eq.2 and are shown graphically in Figure IV.6 It can be seen that the highest distribution ratios were obtained for pyrrole and pyridine, where β_2 ranged between 45.0 to 14.9 and 16.0 to 4.1, respectively. It was also found that for pyrrole and pyridine the distribution ratio values sharply decrease as the concentration in the raffinate increases. The lowest distribution ratios were observed by the thiophene and toluene systems, with the values of β_2 ranging between 0.7 to 0.6 and 0.4 to 0.3, respectively. Despite these relatively low distribution ratios, it was observed that the distribution ratios were almost independent of the

initial concentration of fuel impurity. This finding is useful from an industrial standpoint as it indicates that regardless of initial concentration "at least up to ≈60 wt%" a fixed amount of solvent would be required to achieve separation.
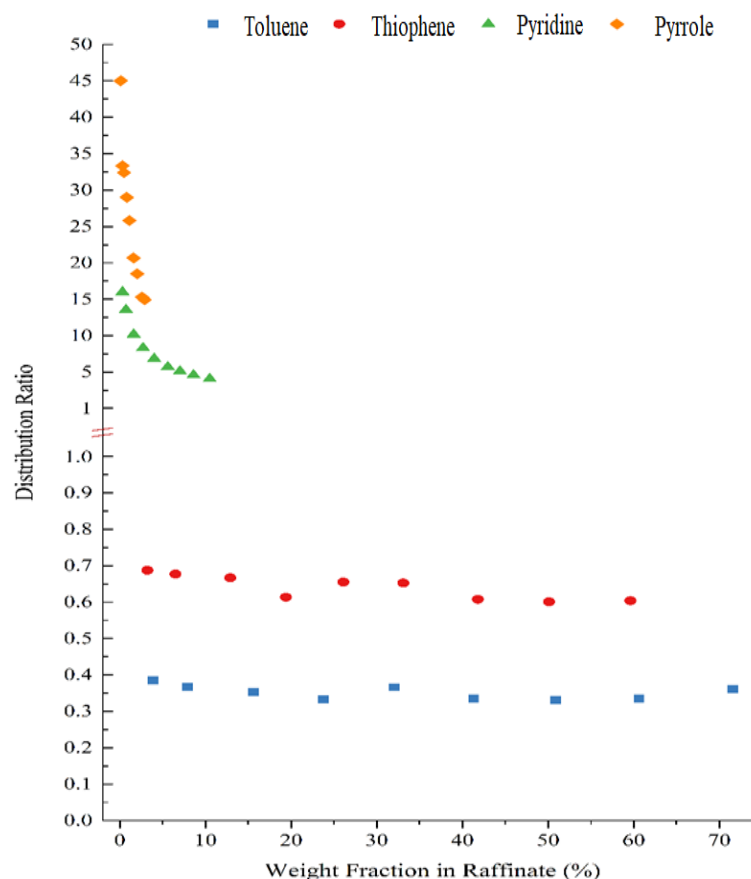
Figure IV.6. Distribution ratio (β_2) of toluene/thiophene/pyridine/pyrrole versus the fraction of fuel contaminant (wt%) in the raffinate phase.

Selectivity measures the affinity of impurities to the DES compared to the affinity of *n*-decane to the DES. Greater selectivity values are desirable as it indicates that fewer equilibrium stages "smaller-size equipment" are required for the targeted separation [19,41], which helps to reduce the capital cost of the extraction unit. Higher selectivities also improve the *n*-decane recovery from the raffinate phase, which also increases the profitability of the extraction process by reducing operational costs. Figure IV.7 shows the selectivity values of toluene, thiophene, pyridine, and pyrrole calculated using Eq. II.26. The calculated selectivities were observed to be greater than unity ($S > 1$) implying that the extraction using TPAB : AA (1 :4) is feasible. It can be observed that the selectivity values were decreasing in the following order : pyrrole > pyridine $\gg$ thiophene > toluene. It was also found that selectivity values for pyrrole and pyridine decrease much more sharply when compared to the decrease in selectivity values of toluene and thiophene. For the systems of pyrrole and pyridine, remarkable selectivity values were found, ranging

between 4087 to 604 and 1994 to 114, respectively. While for the extractions of the thiophene and toluene, the selectivity values ranged between 95 to 10 and 46 to 7, respectively.
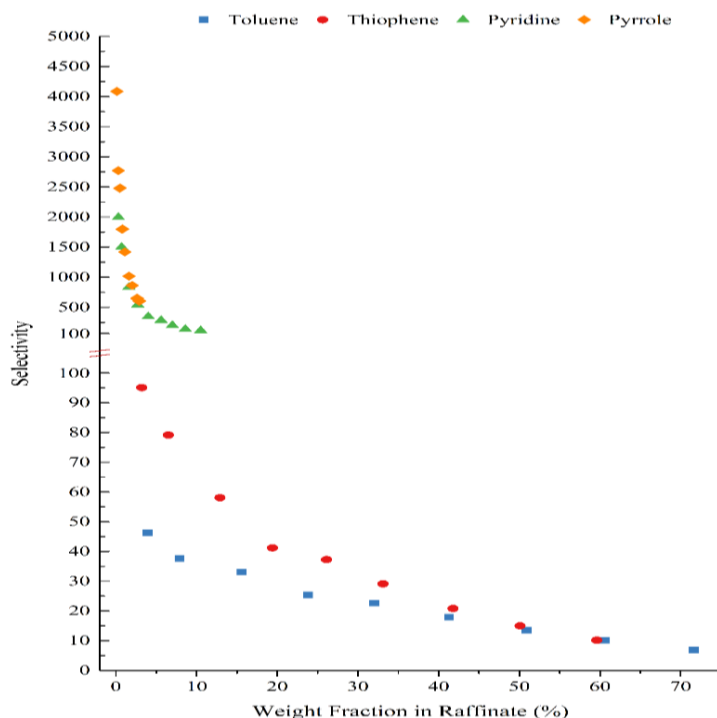
Figure IV.7. Selectivity (*S*) of pyrrole/pyridine/thiophene/toluene versus the fraction of fuel contaminant (wt%) in the raffinate phase.

b) *Consistency Tests*

The experimental equilibrium data, available in mole fractions in Table 3 in (Appendix B), were checked for its consistency via both the Othmer−Tobias empirical correlation (Eq. II.27) and the Hand empirical correlation (Eq. II.28). Table IV.7 lists the empirical parameters calculated via linear regression for both correlations and their least-squares regression values (R^2), while the plots for each *pseudo*-ternary system can be found in Figure IV.8. It was found that all the LLE data measured experimentally show a high degree of consistency as the R^2 values for each system were approaching unity.
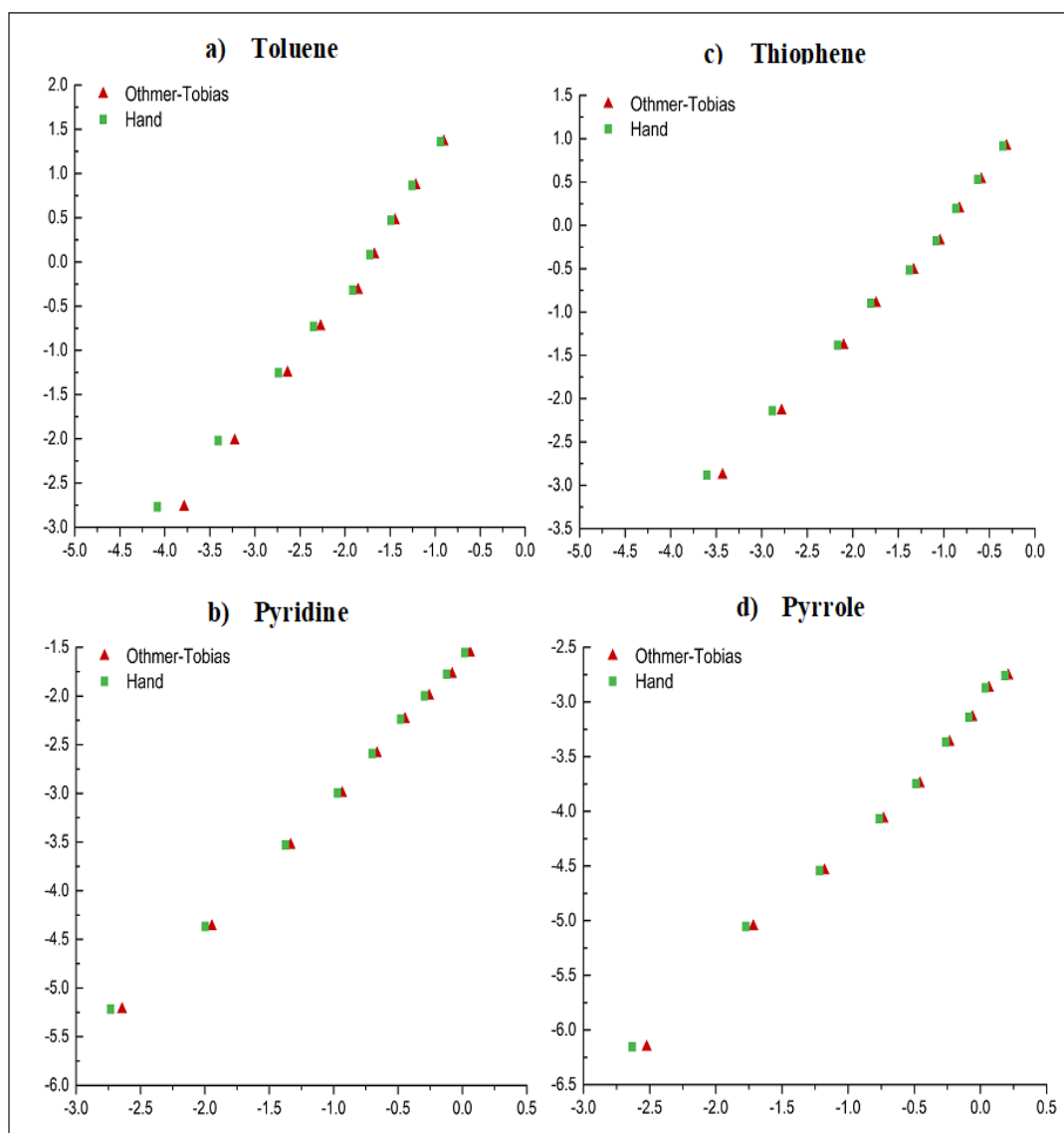
Figure IV.8. Othmer-Tobias and Hand empirical correlations plots for each ternary system.

Table IV.7. Othmer-Tobias and Hand parameters and the values of the least square regression R^2 for each *pseudo*-ternary system.

Ternary system	Othmer-Tobias			Hand		
	a	*b*	R^2	*c*	*d*	R^2
{*n*-decane + Toluene + TPAB:AA}	2.512	1.416	0.995	2.401	1.303	0.991
{*n*-decane + Thiophene + TPAB:AA}	1.187	1.203	0.997	1.190	1.157	0.995
{*n*-decane + Pyridine + TPAB:AA}	-1.666	1.369	0.999	-1.624	1.348	0.998
{*n*-decane + Pyrrole + TPAB:AA}	-3.066	1.224	0.995	-3.041	1.192	0.994

c) NRTL Regression

Obtaining an accurate correlation for the equilibrium data is of great importance as it facilitates the use of simulation programs such as Aspen Plus, which can be used in designing a multi-stage liquid-liquid extraction pilot plant using DESs. Using simulation, it would be possible to investigate the influence of various key parameters on the extraction process. Also, it would

enable further sensitivity and optimization studies. The *pseudo*-ternary equilibrium data were correlated in Aspen Plus via the NRTL thermodynamic model. The estimated binary interaction parameters for each *pseudo*-ternary system and their respective RMSD values are listed in Table IV.8.

It can be seen that the data are well correlated using the NRTL model with an *RMSD* less than <0.35% for all systems. The close agreement of the regression can also be seen visually in the triangular diagrams of Figure IV.4.

Table IV.8. The correlated NRTL binary interaction parameters and their root-mean-square deviations.

Component i	Component j	τ_{ij}	τ_{ji}	α	*RMSD* (%)
{*n*-decane (1) + toluene (2) + TPAB:AA 1:4 (3)}					
n-decane	Toluene	-0.452	1.006	0.25	0.34
n-decane	TPAB:AA	2.713	4.052	0.25	
Toluene	TPAB:AA	2.796	0.314	0.25	
{*n*-decane (1) + thiophene (2) + TPAB:AA 1:4 (3)}					
n-decane	Thiophene	-0.342	2.455	0.25	0.05
n-decane	TPAB:AA	9.197	4.539	0.25	
Thiophene	TPAB:AA	2.325	0.443	0.25	
{*n*-decane (1) + pyridine (2) + TPAB:AA 1:4 (3)}					
n-decane	Pyridine	-1.812	2.735	0.25	0.04
n-decane	TPAB:AA	4.345	3.971	0.25	
Pyridine	TPAB:AA	-0.236	-2.781	0.25	
{n-decane (1) + pyrrole (2) + TPAB:AA 1:4 (3)}					
n-decane	Pyrrole	-0.040	2.643	0.25	0.20
n-decane	TPAB:AA	4.496	3.668	0.25	
Pyrrole	TPAB:AA	1.097	-2.973	0.25	

IV.2.2.5. Literature Comparison

In order to evaluate the performance the TPAB:AA (1:4), the distribution ratios and selectivities obtained were compared with relevant LLE literature for systems of {*n*-decane (1) + toluene / thiophene / pyrrole (2) + solvent (3)} measured at T = 298.2 K / 303.2 K and 1.01 bar. To the best of our knowledge, no LLE data for the system of {*n*-decane (1) + pyridine (2) + solvent (3)} have been previously reported in the literature. However, for comparison, LLE systems of {*n*-octane / *n*-dodecane (1) + pyridine (2) + solvent (3)} have been considered as they are the closest LLE systems available. The comparison is listed in Table IV.9 and is graphically depicted in Figure IV.9.

The distribution ratios and selectivities of all solvents in the literature were converted from a molar basis to a mass basis to account for the differences in molecular masses of the solvents. Also, distribution ratio and selectivity comparisons based on mass are considered to be more realistic and practical for large-scale industrial usage (Rodriguez et al., 2015).

Table IV.9. The distribution ratio (β_2) and selectivity (S) ranges for systems of {n-alkane (1) + toluene / thiophene / pyridine / pyrrole (2) + solvent (3)} found in the literature at 298.2 K or 303.2 K.

Solvent	T (K)	$w_{2,R}$ (%)	$\beta_2{}^{a}$	S^{a}	Ref.
		{n-decane (1) + toluene (2) + solvent (3)}			
TPAB:AA (1:4)	298.2	3.9 – 71.6	0.4 – 0.3	46 – 10	Our work
N-Formylmorpholine	303.2	4.2 – 48.6	0.9 – 0.6	51 – 5	(Brijmohan et al., 2020)
γ-valerolactone	298.2	6.0 – 32.1	0.9 – 0.8	17 – 2	(Klajmon et al., 2016)
[2-HEAF]	303.2	20.9 – 53.5	0.2 – 0.1	8 – 2	(Mesquita et al., 2015a)
Glycerol	303.2	25.5 – 52.0	0.1 – 0.1	123 – 45	
		{n-decane (1) + thiophene (2) + solvent (3)}			
TPAB:AA (1:4)	298.2	3.2 – 59.6	0.7 – 0.6	95 – 10	Our work
[Bmim][SCN]	298.2	1.3 – 18.4	0.9 – 0.8	723 – 279	(Mafi et al., 2018)
[Hmim][SCN]	298.2	0.8 – 31.8	1.2 – 0.9	176 – 50	(Mafi, et al., 2016a)
[Omim][SCN]	298.2	0.7 – 39.3	1.1 – 0.8	36 – 14	
[Bmim][NO$_3$]	298.2	3.5 – 49.0	0.9 – 0.6	546 – 158	(Mafi, et al., 2016b)
[Omim][NO$_3$]	298.2	1.4 – 26.0	1.1 – 0.9	52 – 23	
		{n-alkane (1) + pyridine (2) + solvent (3)}			
TPAB:AA (1:4)	298.2	0.3 – 10.5	16.0 – 4.1	1994 – 114	Our work
MTPPBr:Gly:EG (1:2:2)^{b}	298.2	6.1 – 34.8	3.7 – 1.7	1160 – 18	(Warrag et al., 2020)
MTPPBr:EG (1:4)^{b}	298.2	8.5 – 33.4	3.5 – 1.8	526 – 19	
MTPPBr:Gly (1:4)^{b}	298.2	7.6 – 33.9	2.3 – 1.5	1040 – 109	
[Emim][MeSO$_4$]^{c}	298.2	2.1 – 23.1	2.3 – 1.7	147 – 70	((Chikh Baelhadj et al., 2017)
		{n-decane (1) + pyrrole (2) + solvent (3)}			
TPAB:AA (1:4)	298.2	0.1 – 2.9	45.0 – 14.9	4087 – 604	Our work
N-Methylformamide	298.2	2.6 – 26.3	11.9 – 3.2	3581 – 49	(Cha et al., 2019)

^{a}The distribution ratio and selectivity were calculated on mass basis.^{b}The n-alkane used was n-octane. ^{c}The n-alkane used was n-dodecane.

Remarkably, regarding the denitrogenation of pyrrole and pyridine, it can be seen that the DES studied performed better than the solvents available in the literature for both the distribution ratio and selectivity factors. Instead, although the dearomatization of toluene using TPAB: AA (1 :4) yielded encouraging selectivities, the performance concerning distribution ratios was lower than that of classical solvents such as N-formylmorpholine.

Finally, the desulfurization performance of the selected DES was compared to 5 ionic liquids reported by Mafi *et al*. [53–55]. From Table IV.9, it can be seen that many ILs show better extraction performances than TPAB : AA (1 :4) in both values of distribution ratio and selectivity. However, if the cost and the relatively complicated synthesis routes of ILs are taken into account, DESs could still be considered as potential solvents in this application (Brijmohan & Narasigadu, 2020; Klajmon et al., 2016; Mesquita et al., 2015b; Warrag et al., 2020). Therefore, to make a clear judgment on the performance of DESs further studies should be conducted to check if the higher amount of solvent required for the separation can be compensated through the lower costs associated with DES preparation. Additionally, it is worth noting that even though the performance of the selected DES was lower with regards to desulfurization, the DES's performance in the application of simultaneous dearomization, desulfurization, and denitrogenation of diesel might be better than that of the ILs studied in the literature.
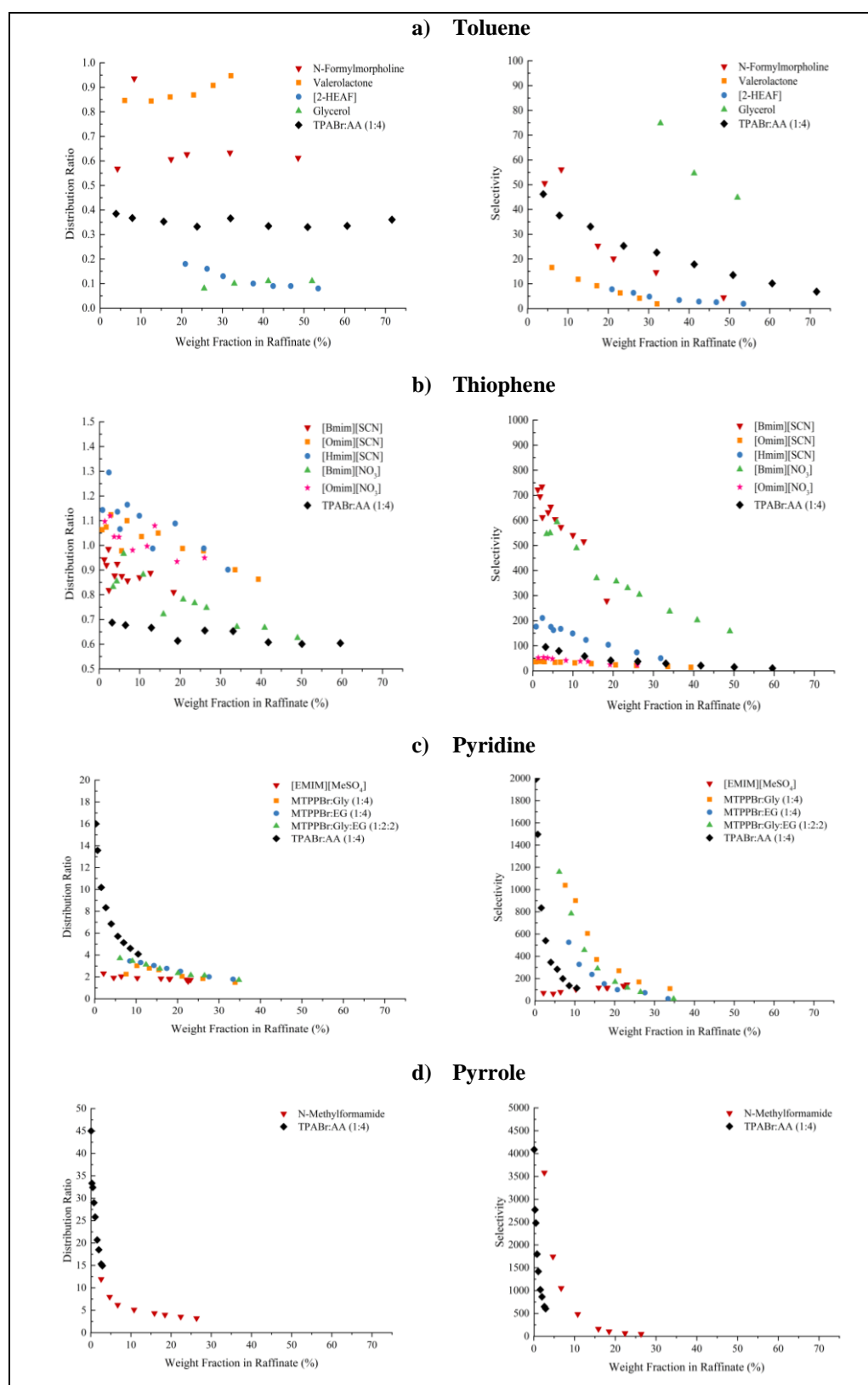
Figure IV.9. Distribution ratio (β_2) and selectivity (S) calculated on mass basis of each fuel impurity verses the fraction of fuel contaminant (wt%) in the raffinate phase for systems of {n-alkane + (a) toluene / (b) thiophene / (c) pyridine / (d) pyrrole + solvent}.

IV.2.2.6. Parametric Study

a) Effect of Initial Concentration

Industrially, the initial concentration of fuel impurities is an important parameter that needs to be considered as fuels have varying levels of impurity concentrations. For that purpose, the effect of initial concentration on the single-stage pure component extraction efficiency has been studied thoroughly using concentrations of 5, 10, 20, 30, 40, 50, 60, 70, and 80 wt%. As shown in Figure IV.10, the extraction efficiencies were always in the order of pyrrole > pyridine > thiophene > toluene regardless of the initial concentration used.

Also, it can be observed that the extraction efficiency of pyrrole was almost independent of initial concentration (between 96 and 97%), even at concentrations as high as 80 wt%. While for pyridine, it can be seen that the extraction efficiency gradually decreases as the initial concentration increases starting at 94.0% and ending with 86.8%. In the case of thiophene, the extraction efficiency was constant at around 35.8% between the initial concentrations of 5 wt% and 30 wt%, then started gradually decreasing between 40 wt% and 80 wt%. This behavior is presumably due to the solvent reaching its maximum capacity as high concentrations of thiophene accumulate in the DES phase inhibiting further extraction. Finally, toluene exhibited similar behavior to thiophene, where the extraction efficiency was almost constant at approximately 21.9% between the initial concentrations of 5 wt% and 20 wt% and then started gradually decreasing between 30 wt% and 80 wt%.
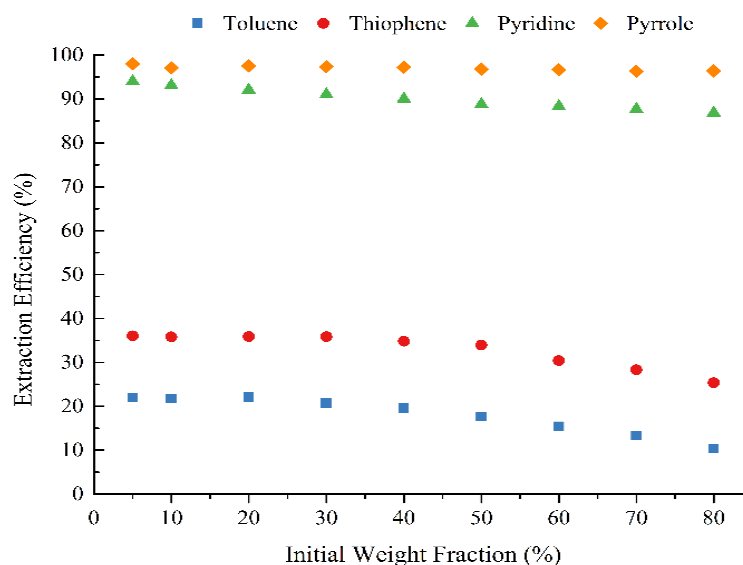
Figure IV.10. Effect of initial concentration on the single-stage extraction efficiency of each fuel contaminant separately in n-decane using TPAB: AA 1:4 (Conditions: T = 298.2 K, P = 1.01 bar, S: F ratio = 1:1, stirring time = 4 h at 1000 rpm, and settling time = 20 h).

b) **Mixture vs. Pure Component Efficiency**

The mixing effects of the impurities on the single-stage extraction efficiency was investigated by comparing (a) the extraction efficiency of a mixture consisting of {5 wt% toluene + 5 wt% thiophene + 5 wt% pyridine + 5 wt% pyrrole + 80 wt% *n*-decane} to the (b) extraction efficiency of 5 wt% of each fuel impurity in 95 wt% *n*-decane. Figure IV.11 shows that the extraction efficiency of thiophene, pyridine, and pyrrole are almost identical in either case. This suggests that the extraction of the sulfur-containing aromatic, the basic nitrogen-containing aromatic, and the non-basic nitrogen-containing aromatic is independent of mixing effects under the studied concentrations. This behavior is presumably due to the molecules occupying different sites in the DES phase (Cassol et al., 2007). However, in the case of toluene, it was found that the presence of competitive molecules (thiophene, pyridine and pyrrole) inhibited the extraction of toluene by approximately ≈5%. This could presumably be due to the DES approaching saturation from the extracted thiophene, pyridine, and pyrrole before being able to extract toluene, which has the lowest selectivity compared to the other impurities.
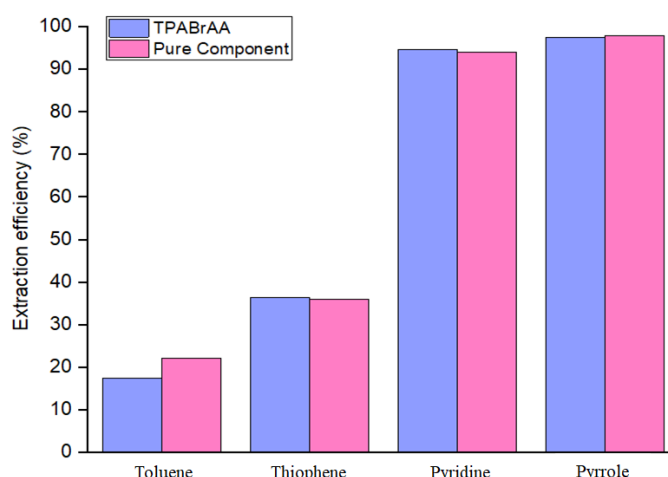
Figure IV.11. Single-stage extraction efficiency of toluene (5 wt%), thiophene (5 wt%), pyridine (5 wt%), and pyrrole (5 wt%) (a) in a mixture containing all four impurities in n-decane (b) in a mixture containing one impurity with n-decane only using TPAB: AA 1:4 (Conditions: T = 298.2 K, P = 1.01 bar, S: F ratio = 1:1, stirring time = 4 h at 1000 rpm, and settling time = 20 h).

c) ***Multi-Stage Liquid-Liquid Extraction from Diesel Model***

Even though DESs are generally cheap, not only for their material costs but also for their cheap preparation techniques, it is still important to investigate the effect of the multi-stage batch experiment to determine the number of stages (cycles) necessary to achieve high extraction efficiencies with minimal solvent. In this experiment, the *n*-decane-rich phase "raffinate" has been separated from the DES-rich phase "extract" after each stage. Then, fresh DES is added to the raffinate phase of the previous stage keeping a 1:1 solvent-to-feed ratio. This procedure was

repeated 5 times from stages 1 through 5 and the concentration of each impurity was determined after each stage. From Figure IV.12 it can be seen that an extraction efficiency of "≈100%" for both pyridine and pyrrole was achieved after 2 stages only.
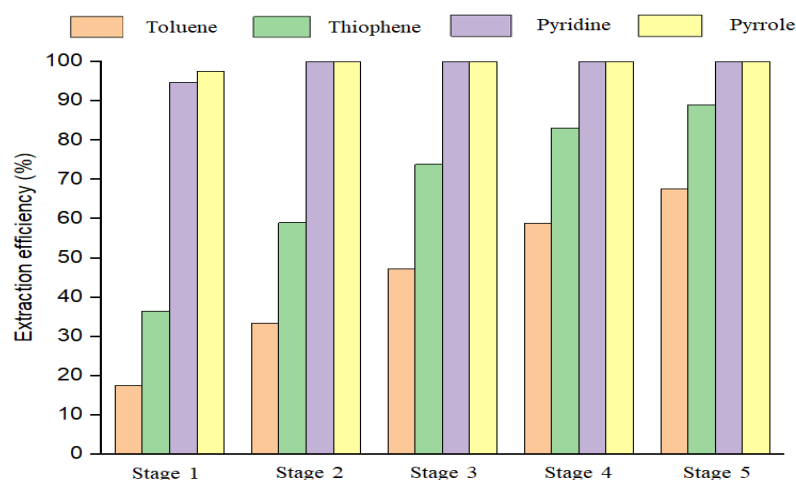
Figure IV.12. Multi-stage extraction efficiency of each fuel contaminant using TPAB: AA (1:4) from a mixture consisting of {5 wt% toluene + 5 wt% thiophene + 5 wt% pyridine + 5 wt% pyrrole + 80 wt% n-decane}. (Conditions: T = 298.2 K, P = 1.01 bar, S: F ratio = 1:1, stirring time = 4 h at 1000 rpm, and settling time = 20 h).

As for toluene and thiophene, extraction efficiency of 67.6% and 89.0%, respectively, were achieved after the 5th stage. The concentration profiles of each fuel impurity throughout the 5 stages is also available in Figure IV.13.
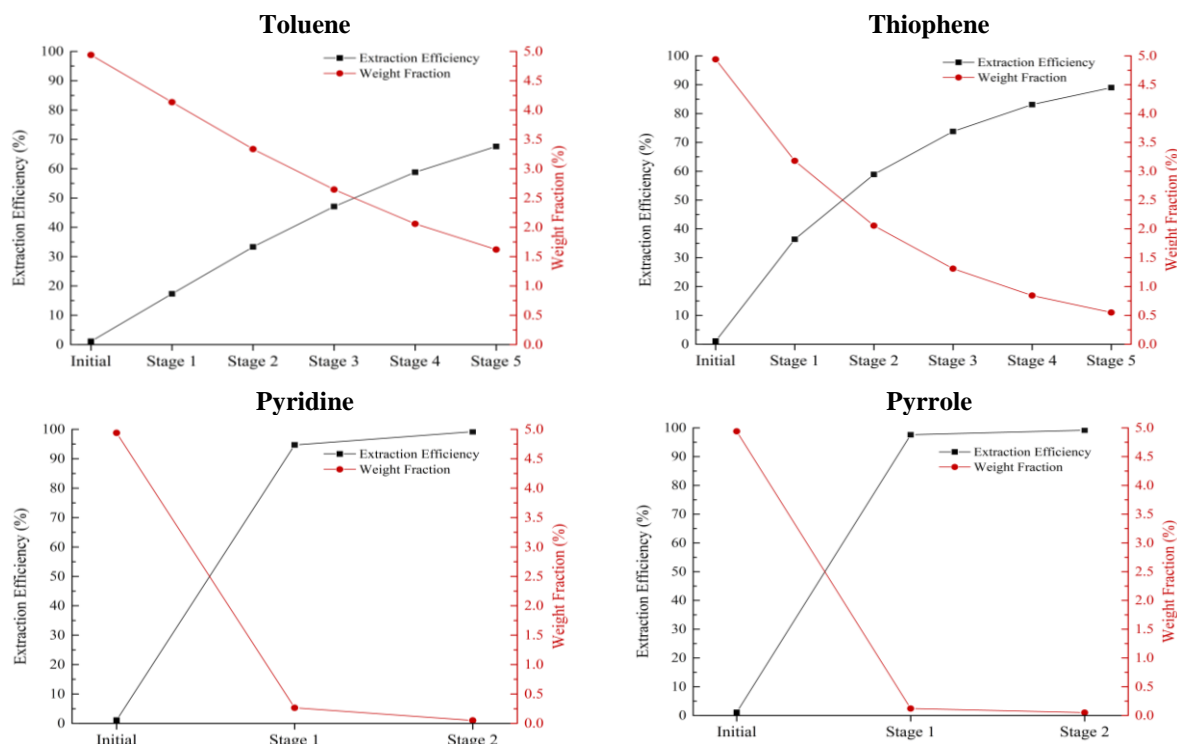
Figure IV.13. Concentration profiles and extraction efficiencies of (a) toluene (b) thiophene (c) pyridine (d) pyrrole at different stages.

In Figure IV.14 the extraction efficiency of toluene and thiophene in each stage was calculated separately by using the initial weight fraction in Eq. II.14 as the weight fraction of the previous stage. It can be seen that the extraction efficiency of thiophene per stage is constant, while in the case of toluene the extraction efficiency gradually increased from stage 1 until stage 3 starting with 17.2% and increasing up until 22.1% and then stayed almost constant between stages 4 and 5. This is presumably due to the reduction in the concentration of the other fuel impurities, which decreases the mixing effects and the competition that inhibits the extraction of toluene.
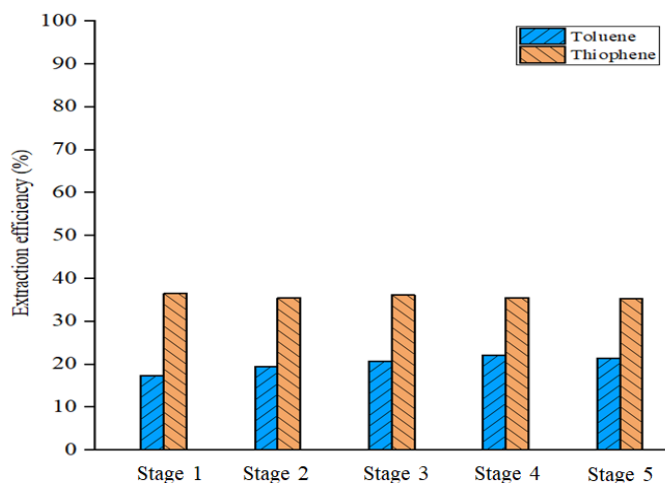
Figure IV.14. Extraction efficiency of toluene and thiophene per stage using TPAB: AA (1:4) (Conditions: T = 298.2 K, P = 1.01 bar, S: F ratio = 1:1, stirring time = 4 h at 1000 rpm, and settling time = 20 h).

Since it was found that the extraction efficiency of thiophene per stage is constant, it is possible to approximately forecast how many stages would be required for a certain extraction efficiency assuming that the behavior stays constant. Thus, if a 99% extraction efficiency is targeted, then the number of stages required can be calculated using Eq.VI.2 as follows:

$$E_{targeted} = 1 - (1 - E_{stage})^n \qquad (IV.2)$$

where $E_{targeted}$ is the targeted extraction efficiency, E_{stage} is the constant single-stage extraction efficiency, and *n* is the theoretical number of stages. Solving Eq.VI.2 for *n* (using $E_{targeted} = 99\%$) and setting the constant single-stage efficiency for thiophene as 35.8%, the theoretical number of stages required would be approximately ≈11 stages.

d) Comparison to Benchmark Solvents

The performance of TPAB:AA (1:4) was also compared to benchmark commercial solvents (*i.e.* sulfolane and dimethyl sulfoxide) based on single-stage liquid-liquid extraction performances. Figure IV.15 shows the results obtained for extracting the mixture of {5 wt% toluene + 5 wt% thiophene + 5 wt% pyridine + 5 wt% pyrrole + 80 wt% *n*-decane} in 1:1 solvent-to-feed ratio. Regarding the denitrogenation extraction efficiency, the DES performed better than both

commercial solvents in extracting both basic and non basic nitrogen-containing compounds. While on the other hand, the commercial solvents had higher extraction efficiencies for toluene and thiophene compared to the DES. Finally, the amount of *n*-decane lost to the extract phase for both commercial solvents was measured and found to be 1.8 wt% and 1.1 wt% for DMSO and sulfolane, respectively, which are comparable to that of the DES at a value of 1.4 wt%. It could be concluded that DESs could be used as potential solvents for the simultaneous dearomatization of fuels with somewhat encouraging results. However, further research is still required to find a more suitable and optimal DES.
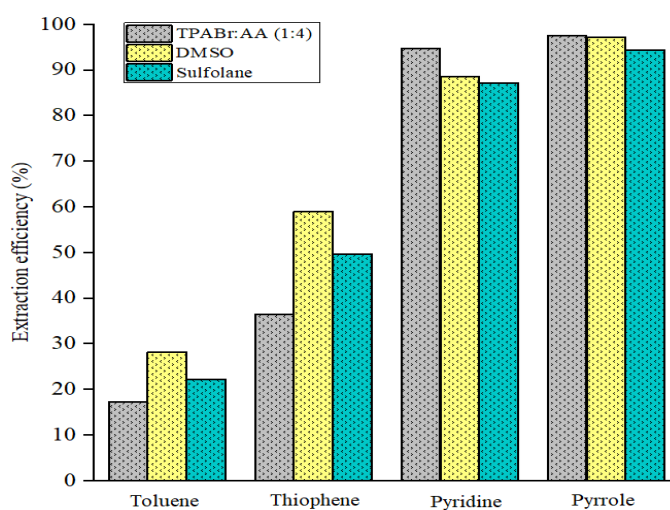
Figure IV.15. Single-stage extraction efficiency of TPAB: AA (1:4) compared to sulfolane and DMSO. (Conditions: T = 298.2 K (303.2 K for sulfolane), P = 1.01 bar, S: F ratio = 1:1, stirring time = 4 h at 1000 rpm, and settling time = 20 h).

IV.3. Extraction of Impurities from Oil Using Naturel Deep Eutectic Solvents

IV.3.1. Experimental Procedure

IV.3.1.1. Chemicals

Table IV.10 lists the chemicals used and their corresponding CAS numbers, purity, and sources as stated by the suppliers. No further purification has been applied for the mentioned chemicals.

Table IV.10. Summary of the Chemicals and their corresponding structure, CAS numbers, and purity.

Chemical	Structure	CAS number	Purity (*wt%*)	Source
Betaine		107-43-7	≥ 98.0	Sigma-Aldrich
Levulinic acid		123-76-2	≥98.0	Acros
n-decane		124-18-5	≥ 99.0	Sigma-Aldrich
Thiophene		110-02-1	≥ 99.0	Sigma-Aldrich
Pyridine		110-86-1	≥ 99.0	Sigma-Aldrich
Toluene		108-88-3	≥ 99.5	Sigma-Aldrich
Ethanol		64-17-5	≥ 99.8	Sigma-Aldrich

IV.3.1.2. Deep Eutectic Solvent Preparation and Ratio Optimization Experiment

The NADES preparation method was adopted by Abbott *et. al* (Abbott et al., 2004). The NADESs were prepared by mixing preciously measured amounts of solid betaine and solid levulinic acid with molar ratios of 2:1, 1:1, 1:2, 1:3, 1:4, 1:5, and 1:7 in screw-capped bottles using Shimadzu balance AUX220 with uncertainty in the measurement of ±0.0002 g. The mixtures were then heated up to 333.15 K for 3 h at 300 rpm using a temperature-controlled incubated shaker (IKA KS 4000) i-control (with temperature stability of ±0.1K). Only mixtures that formed a clear homogeneous liquid were used for the ratio optimization experiment. The liquid-liquid extraction experiment was conducted using the equilibrium cell method at a solvent to feed ratio of 1 :1, by adding 3g of each NADES that were formed to screw-capped 8 mL vials with 3g of an arbitrary fuel model containing {10% thiophene, 10% pyridine, 10% toluene and 70% *n*-decane} on a mass basis. Using an Eppendorf thermomixer, the mixtures were stirred for 4 h at 1000 rpm and T = 298.15 K. They were then kept overnight to reach an equilibrium state. Afterwards, for each vial, the NADES phase and *n*-alkane phase were sampled and analyzed using Gas Chromatography (GC).

All the prepared samples were diluted using ethanol before the GC analysis. The GC method is described in table 1 in (Appendix B). It should be noted that the NADES concentration in each

sample was found by mass balance calculations as it cannot be quantified using GC due to its low volatility. Moreover, all samples were measured in triplicates and the calculated statistical uncertainty was equal to 0.005. Finally, samples of known composition were analyzed using the GC to validate the method. The *RMSD* found was equal to 0.004.

IV.3.1.3. NADES Characterization

After the ratio optimization experiment, the physical properties (density, dynamic viscosity, and water content) of the selected NADES were measured. Anton Paar (DMA 5000 M) with an uncertainty of 0.00001 g.cm^{-3} was used to measure the density. While the viscosity was measured using Thermo Scientific's HAAKE Rheo Stress 6000 rheometer at a shear rate of 240 s^{-1} for 120 s with an average standard deviation of 8 mPa.s. Additionally, the Karl-Fischer titrator (GRS Scientific/Aquamax KF Coulometric) was used to measure the water content of the NADES.

IV.3.1.4. Binary Solubility Test

The binary solubility systems of {thiophene + NADES}, {pyridine + NADES}, {*n*-decane + NADES}, and {toluene + NADES} were tested at 298.15 K and 1.01 bar using the same method described in section IV.3.1.2. Afterward, samples from the NADES phase were taken and analyzed using GC. It should be noted that no phase separation was observed for {thiophene + NADES} and {pyridine + NADES} systems, which implies that both thiophene and pyridine exhibited full miscibility in the NADES.

IV.3.1.5. Pseudo-ternary LLE Data

The *pseudo*-ternary systems of {*n*-decane (1) + thiophene (2) + Bet:LevA (3)}, {*n*-decane (1) + pyridine (2) + Bet:LevA (3)} and {*n*-decane (1) + toluene (2) + Bet:LevA (3)} were obtained at 298.15 K and 1.01 bar using the aforementioned equilibrium cell method in section IV.3.1.2. In this experiment, the fuel model was varied by changing the initial concentration of each fuel impurity from 10% to 80% with a balance of *n*-decane. All experiments were done at a 1:1 solvent to feed ratio. Finally, the assumption of a *pseudo*-ternary system (NADES stays intact in one phase only) was experimentally tested and verified by Karl Fisher Titrator and a Fourier Transform Infrared (FTIR) Spectrometry Analysis. The FTIR analysis was conducted using a Perkin Elmer VERTEX 80v (transmittance mode) in the wavenumber range of 4000-400 cm^{-1}.

IV.3.2. Results and Discussion

IV.3.2.1. Ratio Optimization

The physicochemical properties and extractive ability of NADESs are significantly influenced by the choice of HBA, HBD, and their molar ratio. Thus, in order to select an effective NADES, the effect of the molar ratio should be investigated. Mixtures of Bet and LevA in the molar ratios of 2:1, 1:1, 1:2, 1:3, 1:4, 1:5, and 1:7 were prepared and only the mixtures that formed a clear homogeneous liquid were considered for the single-stage liquid-liquid extraction experiment. The observed states of the mixtures are tabulated in Table IV.11.

Table IV.11. State of betaine and levulinic acid mixture at different molar ratios at 298.15 K and 1.01 bar[a]

HBA: HBD	Mole fraction of HBD	State of the mixture at 298.15 K
Betaine (1:0)	0.0%	Solid
Bet:LevA (2:1)	33.3%	Solid
Bet:LevA (1:1)	50.0%	Solid-liquid mixture
Bet:LevA (1:2)	66.7%	Clear homogeneous liquid
Bet:LevA (1:3)	75.0%	Clear homogeneous liquid
Bet:LevA (1:4)	80.0%	Clear homogeneous liquid
Bet:LevA (1:5)	83.3%	Clear homogeneous liquid
Bet:LevA (1:7)	87.5%	Clear homogeneous liquid
Levulinic acid (0:1)	100.0%	Solid

[a]Standard uncertenity in the DES composition on mass basis $u(w_{HBD}) = u(w_{HBD}) = 0.0002$g

As seen from Figure IV.16, as the molar ratio of the LevA increases, the extraction efficiency of thiophene, pyridine, and toluene increased and the highest overall extraction efficiency was for 1:7 molar ratio. Based on the results obtained, the molar ratio of 1:7 was chosen for the rest of the experiments. Also, it is worth noting that the viscosity of Bet:LevA (1:7) was considerably lower than the reported Bet:LevA (1:2) (Warrag et al., 2018), with viscosities of 117.7 and 1267 mPa.s, respectively. Also, the same molar ratio of Bet:LevA (1:7) has also been found in the literature for the extraction of phenolic compound from spent coffee grounds (Krisanti et al., 2019). Table IV.12 shows the identification summary of the selected NADES Bet:LevA (1:7).
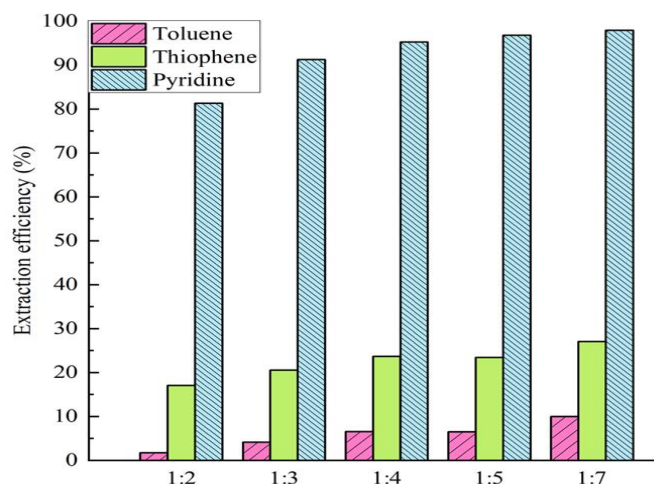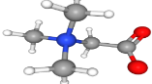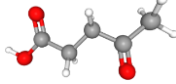
Figure IV.16. Extraction efficiencies of thiophene, pyridine, and toluene using Bet:LevA with different molar ratios.

It should be mentioned that the results obtained from gas chromatography (GC) showed a distinctive peak for each impurity in both NADES phase and *n*-alkane phase. This indicates that no reaction occurs between the NADES and the impurities and that the extraction was based on physical mechanism (The GC results are available in Figures 3 and 4 in the (Appendix B)).

Table IV.12. Summary of selected natural deep eutectic solvent (NADES).

	Hydrogen bond acceptor (HBA)	**Hydrogen bond donor (HBD)**
Common name	Betaine	Levulinic acid
IUPAC name	2-(trimethylazaniumyl) acetate	4-Oxopentanoic acid
Molecular formula	$C_5H_{11}NO_2$	$C_5H_8O_3$
Molecular Structure		
Molar ratio	1	7
NADES molecular weight (*g.mol^{-1}*)	116.25	

IV.3.2.2. NADES Characterization

The density and the dynamic viscosity are considered to be an important physical property for the selection of liquid-liquid extraction solvents (Zhang et al., 2012). Also, since betaine is known for its hygroscopicity and ability to absorb moisture, therefore, measuring the water content of the NADES is very important. Table IV.13 lists the measured density (ρ), dynamic viscosity (η), and water content of Bet:LevA (1:7) at 298.15K and 1.01bar. The viscosity was found to be 117.7 mPa.s, which is considered as moderate, compared to other natural deep eutectic solvents (Kučan et al., 2018). The water content of freshly made NADES was found to be less than 0.80 wt%. However, when converted into molar fraction this amount was found significant (≈ 5 mol%). As reported in literature, the presence of water decreases the NADES viscosity, decreases its

cytotoxic profile, and accordingly improves the performance of NADES (Dai et al., 2015; Mbous et al., 2017).

Table IV.13. Density, dynamic viscosity, and water content of Bet:LevA (1:7) measured at T (K) = 298.15 and P (bar) = 1.01.

Density (ρ) ($g.cm^{-3}$)	Dynamic viscosity (η) ($mPa.s$)	w_{H2O} (wt %)	x_{H2O} (mol%)
1.143 ±0.003	117.7 ±0.6	0.77 ±0.03	4.78 ±0.16

Figure IV.17 shows the measured density of Bet:LevA (1:7) at temperature between 293.15 K and 368.15 K (the numerical data are available in Table IV.14). The density dependence on temperature is well described by the following equation :

$$\rho_{(g/cm^3)} = -0.0009T_{(K)} + 1.3958 \tag{IV.3}$$

Table IV.14. Numerical values for the experimental density measured between $293.15 \leq T\,(K) \leq 368.15$ at P (bar) = 1.01 for Bet:LevA (1:7) DES.

Temperature, T (K)	Density, ρ (g.cm^{-3})
293.15	1.148 ±0.002
298.15	1.143 ±0.003
303.15	1.138 ±0.001
308.15	1.133 ±0.004
313.15	1.128 ±0.002
318.15	1.124 ±0.002
323.15	1.119 ±0.004
328.15	1.115 ±0.003
333.15	1.112 ±0.004
338.15	1.107 ±0.002
343.15	1.102 ±0.001
348.15	1.098 ±0.004
353.15	1.095 ±0.004
358.15	1.092 ±0.004
363.15	1.087 ±0.003
368.15	1.083 ±0.002

[a]The standard uncertainties for pressure and temperate are $u(P) = 0.04$ bar, $u(T) = 0.1$ K, respectively.
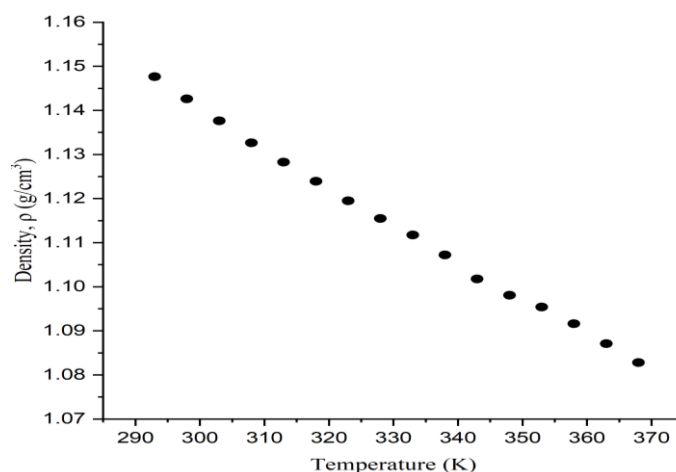
Figure IV.17. Effect of temperature on the density of the Bet:LevA (1:7).

IV.3.2.3. *Binary Solubility Test*

The measured binary solubility for each system {solute + Bet:LevA (1:7)} are shown in Figure IV.18 (standard uncertainty of *u(w)* = 0.002). Both systems of {thiophene + Bet:LevA (1:7)} and {pyridine + Bet:LevA (1:7)} formed clear and homogeneous liquids with no phase separation nor turbidity, which indicates the full solubility of thiophene and pyridine in Bet:LevA (1:7). This can probably be attributed to the existence of the electronegative sulfur and nitrogen elements that increased their reactivity. Therefore, presumably, the full solubility of these molecules is due to a combination of electrostatic and hydrogen-bonding interactions (Rodriguez et al., 2015). On the other hand, the binary system of {*n*-decane + Bet:LevA (1:7)} shows that *n*-decane was barely soluble in the NADES, which can be attributed to its low polarity. Finally, the binary system of {toluene + Bet:LevA (1:7)} exhibited partial solubility. Even though both compounds are non-polar, the solubility of toluene is relatively much higher than *n*-decane. This could be attributed to the presence of π-electrons around toluene component which is absent in the *n*-decane compound. This π-electron generates an electrostatic cloud around the aromatic molecule which facilitate the interaction with the NADES leading to partial solubility (Rodriguez et al., 2015). Therefore, based on the solubilities obtained, it can be inferred that the selected NADES could be considered as a potential extractant for simultaneous desulfurization, denitrogenation, and dearomatization and merits further investigation of its ternary liquid-liquid equilibrium behavior.
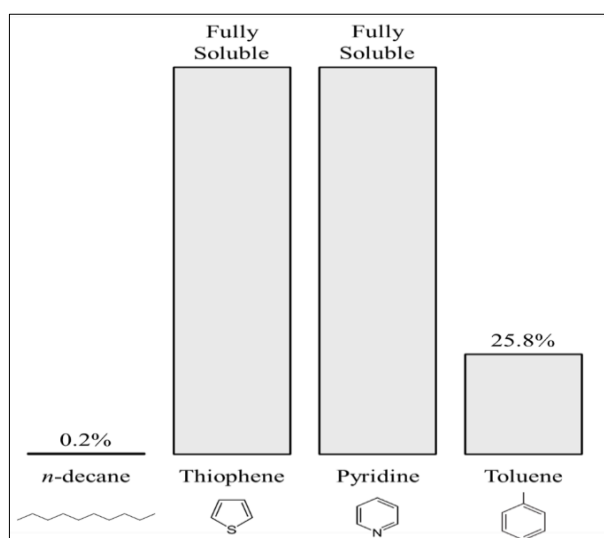
Figure IV.18. Solubility of thiophene, pyridine, toluene, and *n*-decane in the NADES phase measured at 298.15 K and 1.01 bar.

IV.3.2.4. Pseudo-ternary LLE Experiment

The liquid-liquid equilibrium data of binary and *pseudo*-ternary systems were obtained experimentally at 298.15 K and 1.01 bar to observe the performance of Bet:LevA (1:7) with each oil component. The obtained LLE data are presented in Table 4 in (Appendix B) and graphically demonstrated as triangular ternary plots in Figure IV.19. The consistency test was performed using Othmer-Tobias and Hand correlations (Carniti et al., 1978) to test the accuracy of experimental LLE data and the calculated results are found in Table IV.15.

Table IV.15. Parameters of Othmer-Tobias and Hand correlations and the values of least square regression R^2 for each ternary system.

Ternary system	Othmer-Tobias			Hand		
	a	*b*	R^2	*c*	*d*	R^2
{*n*-decane + Thiophene + Bet:LevA (1:7)}	1.539	1.191	0.995	1.555	1.181	0.995
{*n*-decane + Pyridine + Bet:LevA (1:7)}	-2.082	2.182	0.985	-2.035	2.198	0.986
{*n*-decane + Toluene + Bet:LevA (1:7)}	3.233	1.387	0.975	3.152	1.333	0.971

From Figure IV.19, the following observations were found; (1) the immiscibility window was decreasing as follows: toluene > thiophene > pyridine. This behavior can be observed by the decreased range of raffinate weight fractions of each impurity. Pyridine's weight fractions were only ranging between 0.001 and 0.071 while thiophene's and toluene's weight fractions were ranging between 0.073 – 0.650 and 0.086 – 0.749, respectively, (2) the positive slope found for pyridine system infers that a reduced amount of solvent is needed for high extraction. Conversely, negative slopes were observed when extracting thiophene and toluene indicating that the weight fractions in extract phase are lower than that in the *n*-alkane phase, (3) the absence of NADES in the *n*-alkane phase where $w_3 = 0.000$ ($w_3 = 1 - w_1 - w_2$) implying that no further solvent recovery-column is mandatory after the extraction process, which reduces the operational cost of the extraction process.
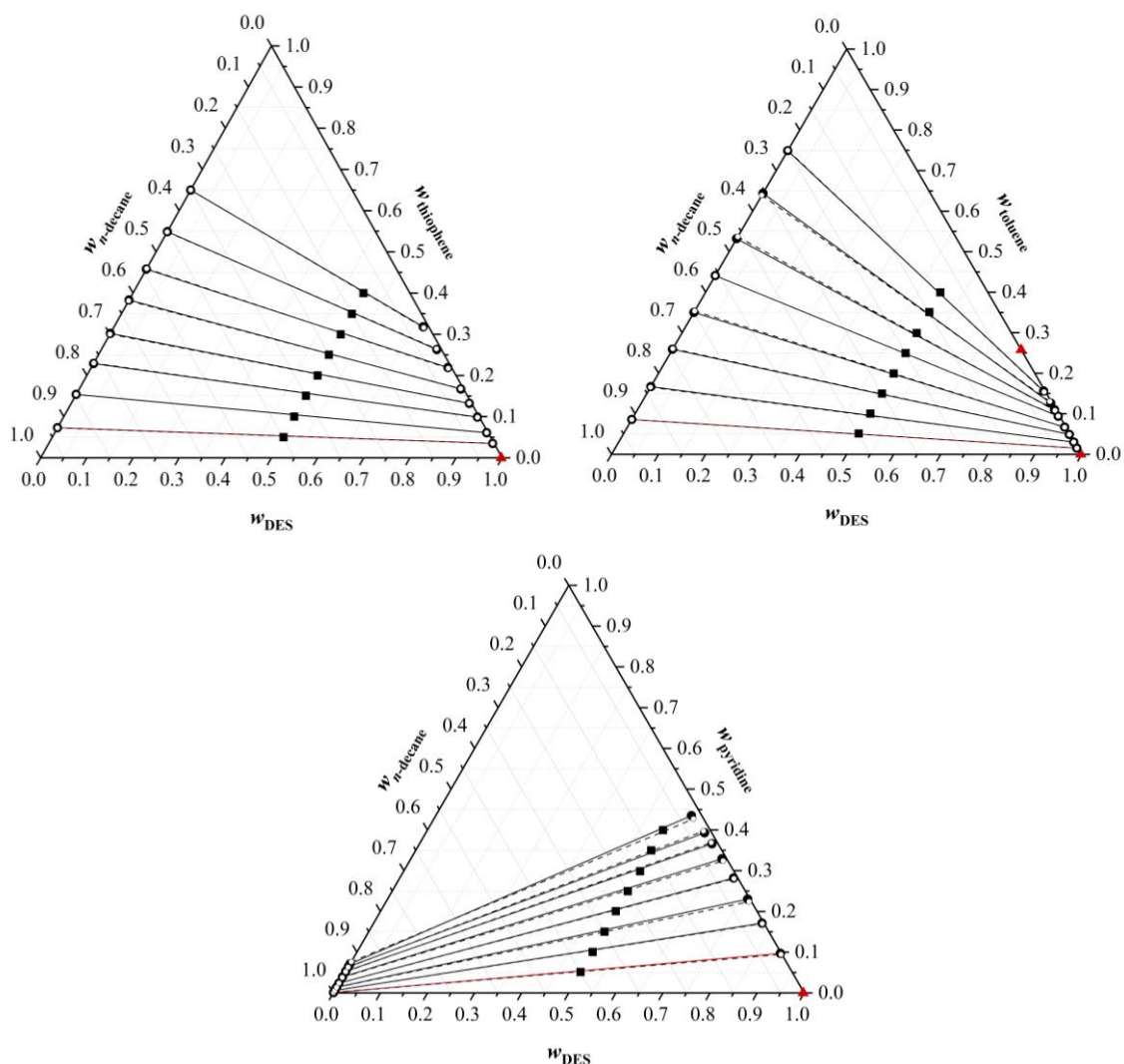
Figure IV.19. Experimental and NRTL model tie lines for the *pseudo*-ternary systems {*n*-alkane + thiophene/toluene/pyridine+ NADES} in weight fractions (●, solid line) with initial composition points as (■), (−, solid line) as the initial concentration of each impurity in the arbitrary fuel model, and binary solubilities as (red▲) measured at 298.15K and 1.01bar. The calculated tie-lines using NRTL model are shown as (○, dashed line).

The water amount (w_{water}) in both extract and *n*-alkane phase after liquid-liquid extraction were measured using Karl Fisher titrator and found to be 0.00078 and 0.0002, respectively. The results indicate the NADES stays intact in the extract phase with no losses to the *n*-alkane phase. This result was confirmed by FTIR analysis shown in Figure IV.20. Therefore, the statement of considering the NADES as *pseudo*-pure species is verified.
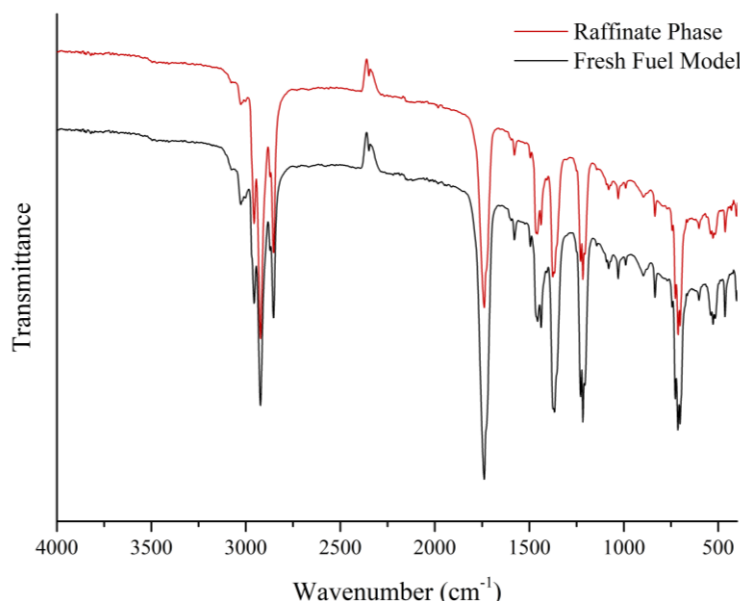
Figure IV.20. FTIR analysis for samples of the fresh fuel model and *n*-alkane phase after extraction from an initial mixture of 70 wt.% *n*-decane, 10 wt.% thiophene, 10 wt.% pyridine, 10 wt.% toluene using Bet:LevA (1:7) at a solvent-to-feed ratio of 1:1.

The characterization parameters (distribution ratio, selectivity, and extraction efficiency) of each system were calculated using the Eqs. II.14-II.16 and the results are found in Table 4 in the (Appendix B), and presented in Figure IV.21-Figure IV.23.

Generally, the values of distribution ratio indicate the amount of solvent needed; the higher the β, the lesser the amount of solvent is required for high extraction. The highest distribution ratios were obtained for {*n*-decane (1) + pyridine + Bet:LevA (1:7) (3)} system where β ranged between 97.00 to 6.12. Also, it can be seen that the values of β decreased sharply as the pyridine's weight fraction in the *n*-alkane phase increases. For the {*n*-decane (1) + thiophene+ Bet:LevA (1:7) (3)} system, the highest β value was 0.49 and the lowest was 0.39. Moreover, the distribution ratio of thiophene was decreasing up to a certain point (at *wt%* = 0.15 and β of 0.39) then started to increase by increasing thiophene's weight fraction in the *n*-alkane phase. The distribution ratio values of toluene were the lowest among the other impurities, which was expected based on its low solubility in the NADES phase, as discussed in Section IV.3.1.4. The $\beta_{toluene}$ values ranged from 0.21 to 0.17 with an almost constant distribution ratio behavior independent of toluene's weight fraction in the raffinate.
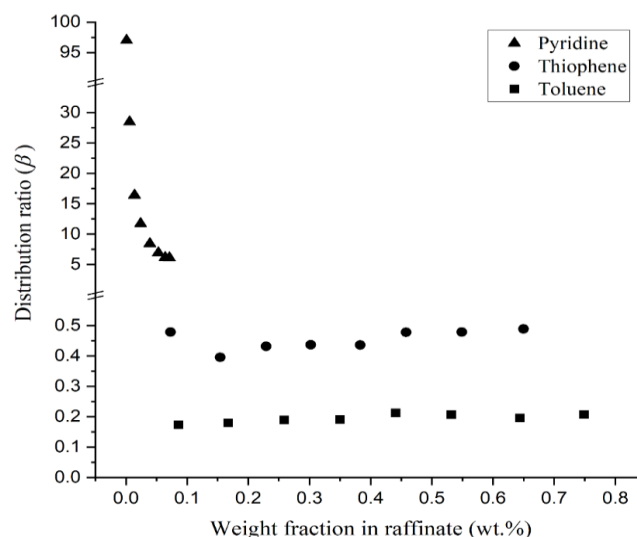
Figure IV.21. The distribution coefficient of solute in the *n*-alkane phase with thiophene as (●), pyridine as (▲), and toluene as (■).

On the other hand, the selectivity separation factor measures the choosiness of each impurity over *n*-alkane. In all three systems, *S* values were found to be greater than unity ($S > 1$), which infers the possibility of separation. The highest values of selectivity were obtained for {*n*-decane (1) + pyridine + Bet:LevA (1:7) (3)} system where a sharp decrease in the selectivity (from 48,500.0 to 255.3) was observed as the pyridine's weight fraction in the raffinate phase increases. The high values of selectivity indicate less number of stages is needed for the targeted separation. Conversely, the selectivity of {*n*-decane (1) + thiophene+ Bet:LevA (1:7) (3)} system showed gradual decrease as the weight fraction of thiophene in the raffinate phase increases, ranging between 159.7 and 14.4. Toluene system {*n*-decane (1) + toluene + Bet:LevA (1:7) (3)} expressed different behavior, where the selectivity values increased from 58.0 to 90.0, then, decreased gradually from 90.0 to 17.3. Also, it can be seen from Figure IV.21 and Figure IV.22 a trend where the range of weight fraction data points were decreasing as follows: toluene > thiophene > pyridine. This behavior corresponds to the aforementioned decrease in the immiscibility window of each impurity in the ternary diagrams as the extraction of pyridine was much higher than that of thiophene and toluene.
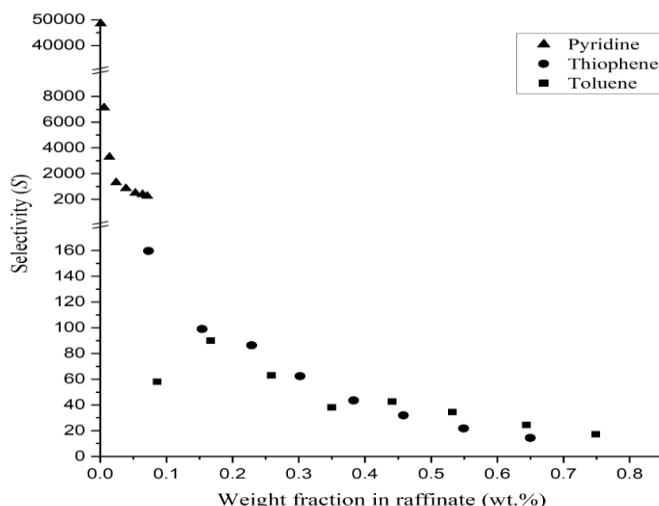
Figure IV.22. The selectivity of solute in the *n*-alkane phase with thiophene as (●), pyridine as (▲), and toluene as (■).

For each impurity, the extraction efficiency was calculated and illustrated in Figure IV.23 It can be observed that increasing the initial weight fraction gradually decreased the extraction efficiency of all impurities. The highest extraction efficiencies were found for pyridine (99.0-90.9%) followed by thiophene and toluene s ranging between (27.0%- 18.6%) and (16.9- 6.1%), respectively. Here, the solvent capacity plays a role where increasing the concentration of each impurity results in accumulating the extracted impurities in the NADES phase which in turn reduces the NADES extraction capability.
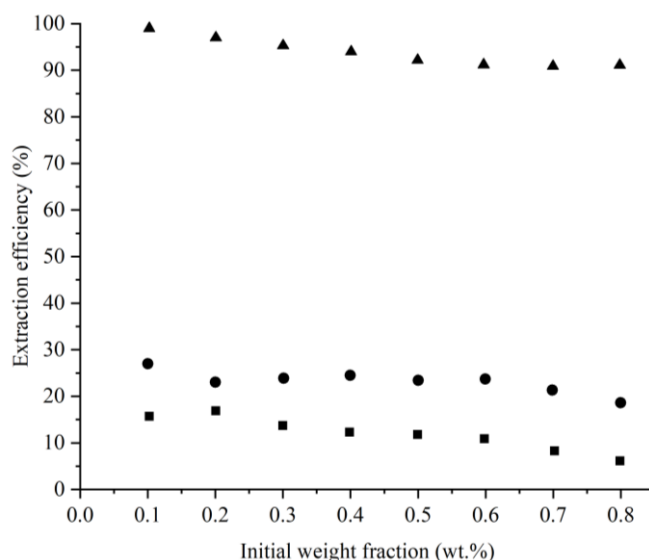
Figure IV.23. The extraction efficiency of solute in the *n*-alkane phase with thiophene as (●), pyridine as (▲), and toluene as (■).

IV.3.2.5. Effect of Mixing

In order to investigate the performance of Bet:LevA (1:7) when extracting either pure or a mixture of different impurities, the extraction of each component (10 wt.% of thiophene, 10 wt.%

of pyridine or 10 wt.% of toluene, also shown in Figure IV.19 as a red tie-line) was investigated separately and again in a mixture containing 10 wt.% of thiophene, 10 wt.% of pyridine and 10 wt.% of toluene in *n*-decane. The results presented in Figure IV.24 show that the extraction efficiency of thiophene and pyridine are almost equal either when mixed or isolated from the other impurities, suggesting that sulfur-containing and nitrogen-containing aromatics occupy different void sites in the NADES phase and do not compete with each other even under those relatively high concentrations. However, in the case of toluene, the presence of thiophene and pyridine inhibits its extraction.
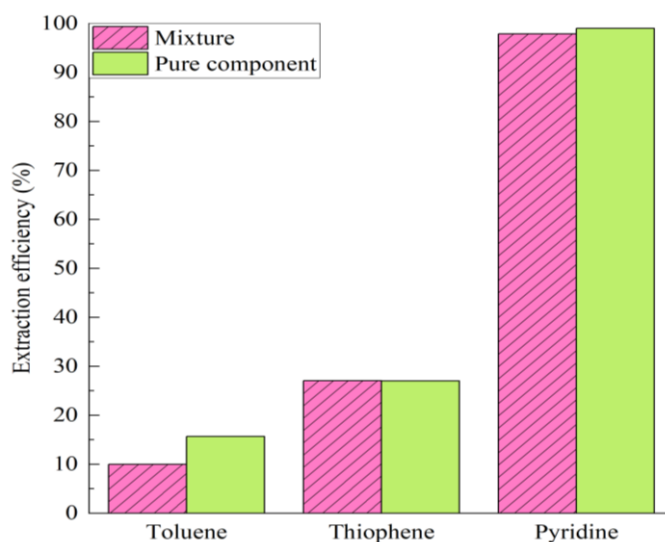
Figure IV.24. Extraction of thiophene (10 wt.%), pyridine (10 wt.%), and toluene (10 wt.%) from *n*-decane (a) in a solution containing all three impurities (b) in separated solutions by Bet:LevA (1:7).

IV.3.2.6. Comparison to Sulfolane

Bet:LevA (1:7) was experimentally compared to sulfolane, a dearomatization benchmark solvent, by single-stage liquid-liquid extraction. The results are shown in Figure IV.25 in terms of extraction efficiency. As observed the highest extraction efficiency of pyridine was found when using Bet:LevA (1:7) as an extracting solvent. On the other hand, the extraction efficiencies of thiophene and toluene were higher when using sulfolane.
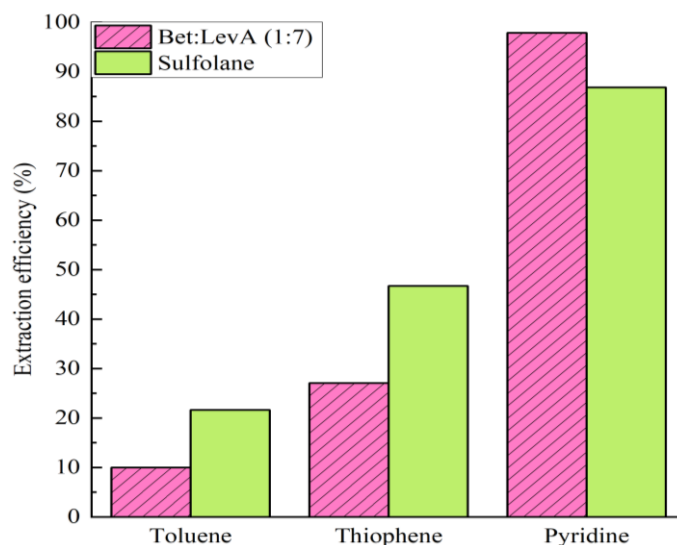
Figure IV.25. Extraction efficiency of Bet:LevA (1:7) compared to sulfolane in the extraction of a mixture of thiophene (10 wt. %), pyridine (10 wt.%), and toluene (10 wt.%) from *n*-decane.

IV.3.2.7. Literature Comparison

The distribution ratio (β) and the selectivity (S) of several solvents previously investigated in literature for each impurity were compared to Bet:LevA (1:7) at 298.15 K and 1.01 bar. Due to the difference in the molar mass of solvents, the tie line data of the solvents were converted from mole fractions to weight fractions wherever needed. The distribution ratios of {*n*-decane + thiophene/pyridine/toluene + solvent} are presented in Figure IV.26-Figure IV.28 where as the selectivity values of {*n*-decane+ thiophene/pyridine and toluene +solvent} are presented in Figure IV.29-Figure IV.31 Based on the author's knowledge, no LLE data for the systems {*n*-decane + pyridine + solvent} were reported in the literature. However, for the sake of comparison, the closest LLE systems found were {*n*-octane + pyridine + MTPPBr:EG / MTPBBr:Gly / MTPPBr:Gly:EG} and {*n*-dodecane + pyridine + [Emim][MeSO$_4$]}.

When comparing Bet:LevA (1:7) to other solvents found in literature, the following has been observed; (1) Bet:LevA (1:7) had the lowest β values when extracting thiophene, (2) for pyridine system, the highest distribution ratios were found when using Bet:LevA (1:7), (3) as for toluene, β values of Bet:LevA (1:7) were lying in-between; higher than Glycerol and [2-HEAF], and lower than N-formylmorpholine, γ-valerolactone, and Sulfolane. In terms of selectivity; (1) when extracting thiophene, Bet:LevA (1:7) had selectivity values higher than [Omim][NO$_3$], [Omim][SCN], similar to [Hmim][SCN] and lower than other ILs. (2) for pyridine system, Bet:LevA (1:7) expressed the highest S values compared to other solvents, (3) as for {*n*-decane + toluene + Bet:LevA (1:7)} system, the selectivity values obtained for each solvent were in the

following order Glycerol>Bet:LevA (1:7)>N-formylmorpholine> Sulfolane> γ-valerolactone> [2-HEAF].

Based on the distribution ratios and selectivities, Bet:LevA (1:7) showed a significant ability as an extraction solvent that could be used for denitrification and desulfurization processes; however, a poorer performance for dearomatization was found. Nevertheless, the absence NADES in the *n*-alkane phase, the low cost, and the difficulty in synthesizing ILs could encourage the use of the NADES in the combined desulfurization, denitrification, and dearomatization processes.
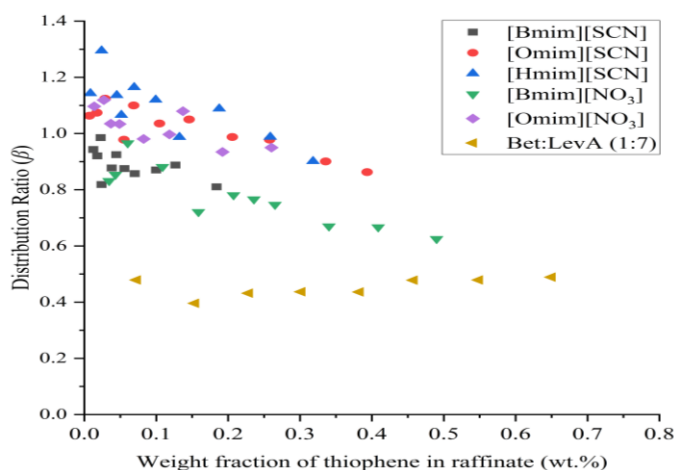
Figure IV.26. Distribution ratios of the systems {*n*-decane + thiophene + solvent} were measured at 298.15 K and 1.01 bar (Mafi et al., 2018; Mafi, Dehghani, et al., 2016; Mafi, et al., 2016).
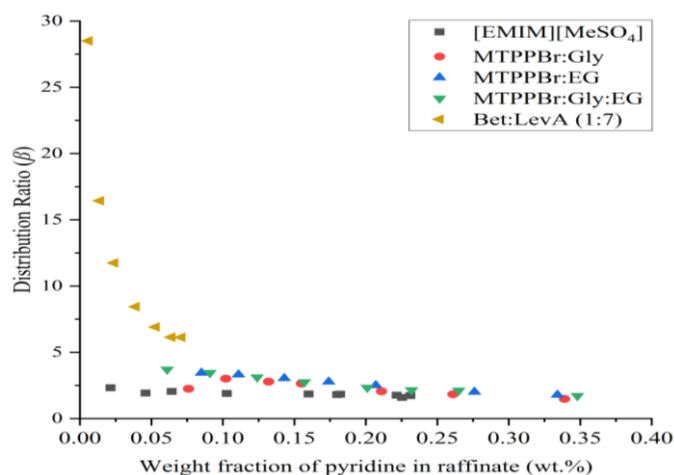
Figure IV.27. Distribution ratios of the systems {*n*-decane + pyridine + Bet:LevA},{*n*-octane + pyridine + MTPPBr:EG/MTPPBr:Gly/MTPPBr:Gly:EG}, {*n*-dodecane + pyridine + [Emim][MeSO₄]} were measured at 298.15 K and 1.01 bar (Chikh Baelhadj & Mutelet, 2017).
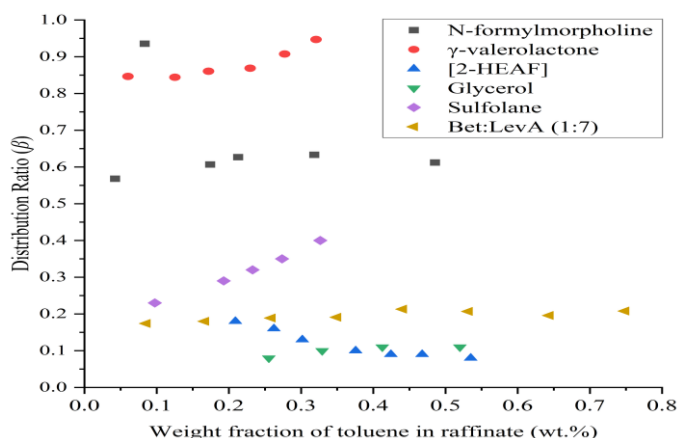
Figure IV.28. Distribution ratios of the systems {*n*-decane + toluene + solvent} were measured at 298.15 K and 1.01 bar except for {*n*-decane + toluene + Sulfolane/[2-HEAF]/Glycerol/ N-formylmorpholine} were measured 303.15 K and 1.01 bar. Data were taken from references (Brijmohan & Narasigadu, 2020; Klajmon et al., 2016; Mesquita et al., 2015a; Pyartman et al., 2006).
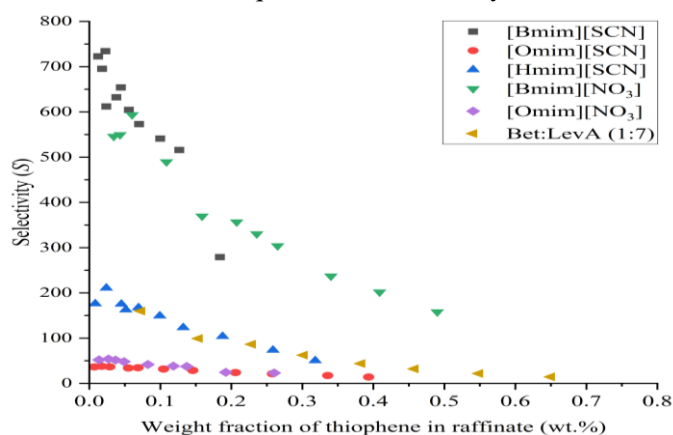
Figure IV.29. Selectivities of the systems {*n*-decane + thiophene + solvent} were measured at 298.15 K and 1.01 bar (Mafi et al., 2018; Mafi, Dehghani, et al., 2016; Mafi, et al., 2016).
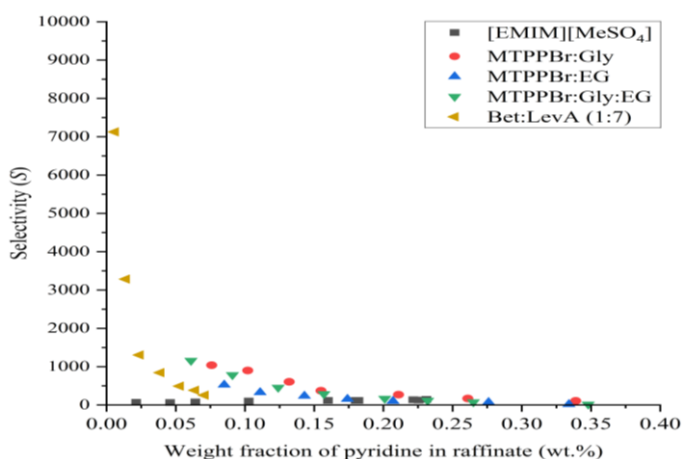
Figure IV.30. Selectivities of the systems {*n*-octane + pyridine + MTPPBr:EG/MTPPBr: Gly/MTPPBr: Gly:EG}, {*n*-decane + pyridine + Bet: LevA}, {*n*-dodecane + pyridine + [Emim][MeSO₄]} were measured at 298.15 K and 1.01 bar (Chikh Baelhadj & Mutelet, 2017).
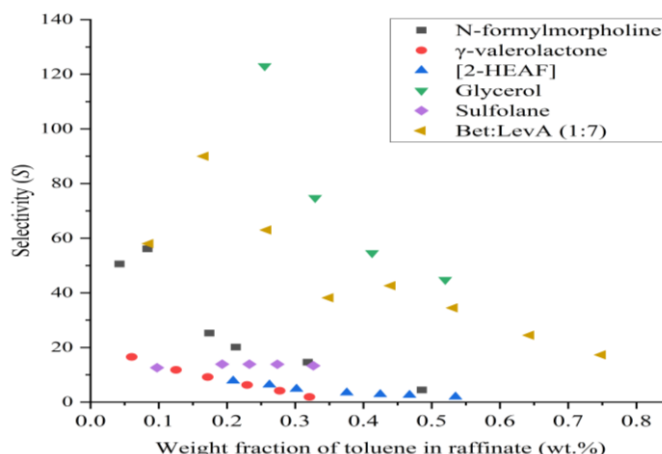
Figure IV.31. Selectivities of the systems {*n*-decane + toluene + solvent} were measured at 298.15 and 1.01 bar except for {*n*-decane + toluene + Sulfolane/[2-HEAF]/Glycerol/ N-formylmorpholine} were measured 303.15 K and 1.01 bar (Brijmohan & Narasigadu, 2020; Klajmon et al., 2016; Mesquita et al., 2015a; Pyartman et al., 2006).

IV.3.2.8. NRTL Regression

The measured LLE data of each ternary system were correlated using NRTL and the obtained tie lines are presented in Figure IV.19 Also, the estimated binary interaction parameters and the *RMSD* are given in Table IV.16. It should be mentioned that all the calculations were based on the weight fraction as the NADES expresses high molecular weight. Also, the non-randomness parameter c_{ij} was set to a value of 0.25 that's within the accepted range of nonpolar components with polar non-associated liquids systems. It can be seen from Figure IV.19 that all the three ternary systems were well correlated using NRTL thermodynamic model as the *RSMD* values were < 1%. This conclude that NRTL thermodynamic model is a good method to represent the experimental LLE data.

Table IV.16. The estimated Binary Interaction Parameters and *RMSD* for NRTL Model.

Component *i*	Component *j*	τ_{ij}	τ_{ji}	α_{ij}	*RMSD* (%)
{*n*-decane + Thiophene + Bet:LevA}					
n-decane	Thiophene	-0.81	2.20	0.25	
n-decane	Bet:LevA (1:7)	5.22	4.98	0.25	0.09
Thiophene	Bet:LevA (1:7)	2.30	0.22	0.25	
{*n*-decane + Pyridine + Bet:LevA}					
n-decane	Pyridine	7.88	3.26	0.25	
n-decane	Bet:LevA (1:7)	17.22	9.84	0.25	0.29
Pyridine	Bet:LevA (1:7)	14.97	6.19	0.25	
{*n*-decane + Toluene + Bet:LevA}					
n-decane	Toluene	16.92	7.17	0.25	
n-decane	Bet:LevA (1:7)	0.11	3.12	0.25	0.19
Toluene	Bet:LevA (1:7)	16.98	3.28	0.25	

IV.4. Conclusion

Deep Eutectic Solvents (DESs) were evaluated for its performance in the application of simultaneous dearomatization, desulfurization, and denitrogenation of diesel fuels *via* liquid-liquid extraction. The performance of the DESs was assessed by the following: (1) solubility of each fuel component in the DES, (2) extraction of the diesel model *via* single-stage liquid-liquid extraction, (3) and comparing the experimentally determined data to benchmark solvents (sulfolane and DMSO) and other solvents reported in the literature.

The results showed an increase in distribution ratio, selectivity, and extraction efficiency as follows; pyridine > thiophene > toluene. The assumption of the *pseudo*-ternary system was justified by FTIR analysis and measuring the water content in the DESs phase and *n*-alkane phase after extraction , and finaly, the NRTL regression model was applied using ASPEN PLUS.

References

Abbott, A. P., Boothby, D., Capper, G., Davies, D. L., & Rasheed, R. K. (2004). Deep Eutectic Solvents formed between choline chloride and carboxylic acids: Versatile alternatives to ionic liquids. *Journal of the American Chemical Society*, *126*(29), 9142–9147. https://doi.org/10.1021/ja048266j

Barker, C. (1985). Origin, Composition and Properties of Petroleum. *Developments in Petroleum Science*, *17*(PA), 11–45. https://doi.org/10.1016/S0376-7361(08)70564-8

Brijmohan, N., & Narasigadu, C. (2020). Ternary Liquid-Liquid Equilibrium Data for the N-Formylmorpholine + Toluene + { n-Nonane or n-Decane} Systems at (303.2, 323.2, and 343.2) K and 101.3 kPa. *Journal of Chemical and Engineering Data*, *65*(2), 788–792. https://doi.org/10.1021/acs.jced.9b01011

Carniti, P., Cori, L., & Ragaini, V. (1978). A critical analysis of the hand and Othmer-Tobias correlations. *Fluid Phase Equilibria*, *2*(1), 39–47. https://doi.org/10.1016/0378-3812(78)80003-X

Cassol, C. C., Umpierre, A. P., Ebeling, G., Ferrera, B., Chiaro, S. S. X., & Dupont, J. (2007). On the extraction of aromatic compounds from hydrocarbons by imidazolium ionic liquids. *International Journal of Molecular Sciences*, *8*(7), 593–605. https://doi.org/10.3390/i8070593

Cha, X., Gao, J., Zhang, Y., Cui, Z., Xu, D., Zhang, L., & Wang, Y. (2019). Liquid-liquid equilibrium for ternary systems of N-Methylformamide + Pyrrole/Indole + Alkanes at 298.15 K: Phase Equilibrium Measurement and Correlation [Research-article]. *Journal of Chemical and Engineering Data*, *64*(7), 3085–3091. https://doi.org/10.1021/acs.jced.9b00202

Chikh Baelhadj, A., & Mutelet, F. (2017). Liquid-Liquid Equilibria for the Ternary Systems Dodecane + Toluene or Thiophene or Pyridine + 1-Ethyl-3-methylimidazolium Methyl Sulfate. *Journal of Chemical and Engineering Data*, *62*(6), 1749–1755. https://doi.org/10.1021/acs.jced.6b00437

Dai, Y., Witkamp, G. J., Verpoorte, R., & Choi, Y. H. (2015). Tailoring properties of natural deep eutectic solvents with water to facilitate their applications. *Food Chemistry*, *187*, 14–19. https://doi.org/10.1016/j.foodchem.2015.03.123

EPA, U. S. (2014). Control of Air Pollution From Motor Vehicles: Tier 3 Motor Vehicle Emission and Fuel Standards. *Federal Register*, *79*(81), 23414–23886. https://doi.org/10.2753/RSH1061-1983310140

García, G., Aparicio, S., Ullah, R., & Atilhan, M. (2015). Deep eutectic solvents: Physicochemical properties and gas separation applications. *Energy and Fuels*, *29*(4), 2616–2644. https://doi.org/10.1021/ef5028873

Klajmon, M., Řehák, K., Matoušová, M., & Morávek, P. (2016). Experimental and Computational Study on Liquid-Liquid Equilibrium in Ternary Systems of γvalerolactone, Toluene, and Hydrocarbons. *Journal of Chemical and Engineering Data*, *61*(1), 391–397. https://doi.org/10.1021/acs.jced.5b00611

Krisanti, E. A., Saputra, K., Arif, M. M., & Mulia, K. (2019). Formulation and characterization of betaine-based deep eutectic solvent for extraction phenolic compound from spent coffee grounds. *AIP Conference Proceedings*, *2175*. https://doi.org/10.1063/1.5134604

Kučan, K. Z., Perković, M., Cmrk, K., Načinović, D., & Rogošić, M. (2018). Betaine + (Glycerol or Ethylene Glycol or Propylene Glycol) Deep Eutectic Solvents for Extractive Purification of Gasoline. *ChemistrySelect*, *3*(44), 12582–12590. https://doi.org/10.1002/slct.201803251

Mafi, M., Dehghani, M. R., & Mokhtarani, B. (2016). Novel liquid-liquid equilibrium data for six ternary systems containing IL, hydrocarbon and thiophene at 25 °C. *Fluid Phase Equilibria*, *412*, 21–28. https://doi.org/10.1016/j.fluid.2015.12.006

Mafi, M., Dehghani, M. R., & Mokhtarani, B. (2018). Liquid-liquid equilibrium data for extractive desulfurization using 1-butyl-3-methyl imidazolium thiocyanate, n-alkane and thiophene. *Fluid Phase Equilibria*, *456*, 109–115. https://doi.org/10.1016/j.fluid.2017.10.017

Mafi, M., Mokhtarani, B., & Dehghani, M. R. (2016). Removal of thiophene from model diesel oil with

nitrate based ionic liquids at several temperatures. *Journal of Molecular Liquids*, *221*, 1104–1110. https://doi.org/10.1016/j.molliq.2016.06.078

Mbous, Y. P., Hayyan, M., Wong, W. F., Looi, C. Y., & Hashim, M. A. (2017). Unraveling the cytotoxicity and metabolic pathways of binary natural deep eutectic solvent systems. *Scientific Reports*, *7*(February), 1–14. https://doi.org/10.1038/srep41257

Mesquita, F. M. R., Pinheiro, R. S., Santiago-Aguiar, R. S., & de Sant'Ana, H. B. (2015a). Measurement of phase equilibria data for the extraction of toluene from alkane using different solvents. *Fluid Phase Equilibria*, *404*, 49–54. https://doi.org/10.1016/j.fluid.2015.06.016

Mesquita, F. M. R., Pinheiro, R. S., Santiago-Aguiar, R. S., & de Sant'Ana, H. B. (2015b). Measurement of phase equilibria data for the extraction of toluene from alkane using different solvents. *Fluid Phase Equilibria*, *404*, 49–54. https://doi.org/10.1016/j.fluid.2015.06.016

Pyartman, A. K., Keskinov, V. A., Lishchuk, V. V., & Spiridonova, I. A. (2006). Influence of temperature on phase separation in the ternary systems [Th(NO3)4(TBP)2]-decane-third organic component. *Radiochemistry*, *48*(3), 272–278. https://doi.org/10.1134/S106636220603012X

Rodriguez, N. R., Requejo, P. F., & Kroon, M. C. (2015). Aliphatic-Aromatic Separation Using Deep Eutectic Solvents as Extracting Agents. *Industrial and Engineering Chemistry Research*, *54*(45), 11404–11412. https://doi.org/10.1021/acs.iecr.5b02611

Stanislaus, A., & Barry, H. C. (1994). Aromatic hydrogenation catalysis: A review. *Catalysis Reviews*, *36*(1), 75–123. https://doi.org/10.1080/01614949408013921

Trivedi, T. J., Lee, J. H., Lee, H. J., Jeong, Y. K., & Choi, J. W. (2016). Deep eutectic solvents as attractive media for CO2 capture. *Green Chemistry*, *18*(9), 2834–2842. https://doi.org/10.1039/c5gc02319j

Warrag, S. E. E., Darwish, A. S., Adeyemi, I. A., Hadj-Kali, M. K., Kroon, M. C., & Alnashef, I. M. (2020). Extraction of pyridine from n-alkane mixtures using methyltriphenylphosphonium bromide-based deep eutectic solvents as extractive denitrogenation agents. *Fluid Phase Equilibria*, *517*, 112622. https://doi.org/10.1016/j.fluid.2020.112622

Warrag, S. E. E., Fetisov, E. O., Van Osch, D. J. G. P., Harwood, D. B., Kroon, M. C., Siepmann, J. I., & Peters, C. J. (2018). Mercury Capture from Petroleum Using Deep Eutectic Solvents. *Industrial and Engineering Chemistry Research*, *57*(28), 9222–9230. https://doi.org/10.1021/acs.iecr.8b00967

Warrag, S. E. E., Rodriguez, N. R., Nashef, I. M., Van Sint Annaland, M., Siepmann, J. I., Kroon, M. C., & Peters, C. J. (2017). Separation of Thiophene from Aliphatic Hydrocarbons Using Tetrahexylammonium-Based Deep Eutectic Solvents as Extracting Agents. *Journal of Chemical and Engineering Data*, *62*(9), 2911–2919. https://doi.org/10.1021/acs.jced.7b00168

Zhang, Q., De Oliveira Vigier, K., Royer, S., & Jérôme, F. (2012). Deep eutectic solvents: Syntheses, properties and applications. *Chemical Society Reviews*, *41*(21), 7108–7146. https://doi.org/10.1039/c2cs35178a

General Conclusion

Deep Eutectic Solvents (DESs) emerged as a new generation of sustainable alternatives to classical organic solvents and Ils. DESs are most commonly described as a mixture of a hydrogen bond acceptor (HBA) and a hydrogen bond donor (HBD) that when mixed interact with each other *via* hydrogen bonding leading to the formation of a eutectic mixture with a freezing point far below that of its constituents. DESs have similar properties to that of ILs in terms of their low vapor pressure and wide liquid range. However, they can be easily prepared by applying heat (no chemical synthesis required), and they are generally cheaper than ILs. DESs have also been described as "designer solvents" as their physical properties and solvation properties can easily be tailored by changing the HBA, the HBD, or their mixing ratio. Therefore, based on the HBA and HBD selection, it is possible to prepare a low-cost, naturally occurring, and biodegradable solvent with high solvation properties. Although the use of naturally occurring DESs offers many advantages. Therefore, more studies investigating the toxicity, biodegradability, and cost of ILs and DESs are of utmost importance in order to facilitate their industrial application. Since their discovery, DESs have been used in many applications such as electrochemistry, catalysis, material preparation, nanotechnology, separation, and analytical chemistry.

The fundamental physical properties of DESs (density, viscosity, electrical conductivity, pH, *etc*.) are critical in investigating the potential and feasibility of utilizing these sustainable solvents in the design, simulation, and optimization of any industrial process. Without knowledge of these properties, any industrial planning is meaningless as these properties are utilized in various thermodynamical models, process simulations, and engineering estimations that are required for studying fluid flow, mass transfer, heat transfer, and reaction kinetics of DESs.

The study presented in this doctoral thesis is built on two projects, each project comprises parts. In the first project, physio-chemical properties of deep eutectic solvents were predicted using COSMO-RS Sigma Profiles as Molecular Descriptors: A Quantitative Structure-Property Relationship (QSPR) Study. This project contains the following four parts :

The first part has been creating new empirical models for the prediction of viscosity and density of DESs were developed. The models were derived by multilinear regression analysis, after defining the independent (i.e. the Sσ- profile, Temperature, and interaction terms) and the dependent (properties) variables. A set of data, including 310 experimental measurements of density and 193 of viscosity for 49 different DESs were used for the development and validation of the model performance. The DESs were selected so that their constituents have a wide range of chemical structures. The definition of the expression of the models was supported by an in-depth statistical analysis in which the main descriptors exerting a significant influence on the studied

properties were considered. The modeling results showed that the proposed models for the investigated DESs properties were able to predict the properties of the DESs with an acceptable accuracy with R^2 value $\in$ [0.9839, 0.9874].

The second part proposes two novel QSPR models developed for predicting the density and viscosity of HDESs. The models are characterized by a wide domain of applicability, verified statistically using several approaches, and were applied in predicting several HDESs using experimental data reported in the literature not included in the training set. The results showed that the proposed models were excellent at externally predicting the properties of the HDESs as indicated by R^2 values of 0.9956 and 0.9871 for density and viscosity, respectively. The main advantage of the approach it is based only on structural information that can be obtained using COSMO-RS, which is a computationally inexpensive and relatively straightforward method for modeling molecules. Consequently, the developed framework can be used for screening *a priori* the density and viscosity of a large number of HDESs (that are yet to be prepared) using only ten simple descriptors, allowing for significant time and cost savings.

In the third part, two new linear QSPR models were developed for the prediction of electrical conductivity of DESs. The proposed models utilized COSMO-RS molecular charge density distributions (S_σ-profiles) as molecular descriptors. The datasets used for the development of the models were obtained from the literature. The data comprised 236 experimental electrical conductivity measurements for 21 ammonium-based and phosphonium-based DESs covering a wide range of temperatures and molar ratios. Multiple Linear Regression was used as a mathematical expression for the proposed QSPR models due to its simplicity. The first model accounted for the structure of the HBA, the HBD, the molar ratio, and temperature, while the second model additionally incorporated the interactions between the molecular descriptors. Results showed that by accounting for the interactions, the regression coefficients (R^2) of the predictive model can be increased from 0.801 to 0.985. In addition, the stability and reliability of the two models were further assessed using applicability domain analysis.

In the fourth part, novel machine learning-based QSPR models were developed to predict the pH of 41 DESs comprised of various combinations of 9 HBAs and 21 HBDs resulting in a total of 648 experimental data points. For the sake of comparing, the performance of the linear machine learning algorithm and another non-linear algorithm were utilized. The results confirmed the validity of the models as they can capture the behavior of the training dataset with high R^2 values and predict the external testing dataset successfully with low standard deviations. Moreover, the models showed a domain of applicability that covered a wide space of molecular structures. The

MLR and ANN approaches could be considered reliable and can be utilized for screening purposes in the absence of experimental data for the determination of the pH property of DESs, particularly for screening new green and sustainable DESs for process design and industrial scale-up. The ANN model presents better predictive capabilities and a more robust method overall, while the MLR model can be considered as more interpretable.

The developed models can be considered as a reliable tool for predicting important DESs properties. The findings showed that QSPR models are excellent at predicting the properties of DESs. These models inspire and stimulate the development of robust models to predict the properties of designer solvents from the drawn molecular structures, which will save time and resources and can be used for their determination in the absence of experimental measurements.

The second project is related to the extraction of fuels impurities using deep eutectic solvents. This project contains the following two parts:

The first part an acidic DES was evaluated for its performance in the application of simultaneous dearomatization, desulfurization, and denitrogenation of diesel fuels *via* liquid-liquid extraction. The selected DES was comprised of tetrapropylammonium bromide (TPABr) as an HBA and acetic acid (AA) as an HBD at a 1:4 molar ratio. The performance of the DES was evaluated by the following: (1) solubility of each fuel component in the DES, (2) extraction of the diesel model *via* single-stage liquid-liquid extraction, (3) and comparing the experimentally determined data to benchmark solvents (sulfolane and DMSO) and other solvents reported in the literature. It was found that the pyrrole, pyridine, and thiophene were fully miscible in the DES, while toluene and *n*-decane exhibited partial solubilities of 48.1 *wt*% and 0.9 *wt*%, which explains the trend of the single-stage liquid-liquid extraction efficiencies obtained as follows: pyrrole 97.6% > pyridine 94.6% > thiophene 36.4% > toluene 17.2%. Thereafter, a parametric study was conducted to examine the influence of (1) initial concentration, (2) mixing effects, (3) multi-stage, and (4) multi-cycle extraction on extraction efficiency. The increase in initial concentration (from 5 to 80 *wt*%) decreased the extraction efficiency of each impurity in different ways based on the nature of the molecule. Moreover, the presence of competitive molecules in a mixture decreased the extraction efficiency of toluene by approximately ≈5%, while on the other hand, the extraction of sulfur- and nitrogen-containing aromatics was independent of mixing effects. The feasibility of deep dearomatization using the DES was evaluated by the multi-stage liquid-liquid extraction experiment. Results showed that complete removal of pyrrole and pyridine can be achieved in 2 stages only. As for toluene and thiophene, extraction efficiencies of 67.6% and 89.0% were

achieved after the 5th stage. Finally, the possibility of re-using the DES in multiple extraction cycles was assessed to evaluate its extraction capacity.

The second part is devoted to a study of a model describing the capability of natural deep eutectic solvents (NADESs) in extracting thiophene, pyridine, and toluene from *n*-decane fuel via ternary liquid-liquid equilibrium. The constituents of the NADES selected were betaine and levulinic acid are naturally occurring. Moreover, the selected NADES, Bet:LevA (1:7) was characterized for its dynamic viscosity, water content, and density at 298.15 K and 1.01 bar. Then, the solubility of thiophene, pyridine, toluene, and *n*-decane in the Bet:LevA (1:7) was measured at 298.15 K and 1.01 bar. The extractive ability of Bet:LevA (1:7) was assessed using the distribution ratio, selectivity, and extraction efficiency values of each of the three solutes calculated from the experimental LLE data at a 1:1 solvent-to-feed mass ratio. The results showed an increase in distribution ratio, selectivity, and extraction efficiency as follows; pyridine > thiophene > toluene. The assumption of the *pseudo*-ternary system was justified by FTIR analysis and measuring the water content in the NADES phase and *n*-alkane phase after extraction. The calculated values were then compared to benchmark solvents such as sulfolane and several other solvents previously investigated in the literature. The NRTL regression model was applied using ASPEN PLUS, the three systems showed values of root-mean-square deviation between 0.29%<RMSD<0.09% which indicates excellent agreement between the experimental and the regressed data.

It was found that the DESs had high extraction capacities towards desulfurization and denitrogenation, however, the dearomatization capacity was lower. Based on the obtained results and the comparison to other solvents, it was concluded that DESs could be used as potential solvents in the application of simultaneous dearomatization, desulfurization, and denitrogenation of fuels with somewhat encouraging results. However, further research is still needed in order to find a more suitable, optimal, and "green" DES for this application.

Appendixes

Appendix A

Table A.1. Experimental density and viscosity data points of all the HDESs. All data points were measured at P = 1.01 bar.

T (K)	ρ (g·cm^{-3})	T (K)	η (mPa·s)	Ref.
HDES1- Decanoic Acid : Tetrabutylammonium Chloride (2:1)				
288.2 ± 0.02	0.9232 ± 0.0005	288.2 ± 0.02	526.39 ± 1.842	
293.2 ± 0.02	0.9199 ± 0.0005	293.2 ± 0.02	368.54 ± 1.289	
298.2 ± 0.02	0.9168 ± 0.0005	298.2 ± 0.02	265.26 ± 0.928	
303.2 ± 0.02	0.9136 ± 0.0005	303.2 ± 0.02	195.05 ± 0.682	(Van Osch et al., 2015)
308.2 ± 0.02	0.9104 ± 0.0005	308.2 ± 0.02	146.16 ± 0.511	
313.2 ± 0.02	0.9073 ± 0.0005	313.2 ± 0.02	111.52 ± 0.390	
318.2 ± 0.02	0.9042 ± 0.0005	318.2 ± 0.02	86.53 ± 0.302	
323.2 ± 0.02	0.9010 ± 0.0005	323.2 ± 0.02	68.27 ± 0.239	
HDES2- Decanoic Acid : Tetraheptylammonium Chloride (2:1)				
288.2 ± 0.02	0.8972 ± 0.0005	288.2 ± 0.02	307.09 ± 1.074	
293.2 ± 0.02	0.8939 ± 0.0005	293.2 ± 0.02	227.96 ± 0.797	
298.2 ± 0.02	0.8907 ± 0.0005	298.2 ± 0.02	172.87 ± 0.605	
303.2 ± 0.02	0.8875 ± 0.0005	303.2 ± 0.02	133.19 ± 0.466	(Van Osch et al., 2015)
308.2 ± 0.02	0.8843 ± 0.0005	308.2 ± 0.02	104.19 ± 0.364	
313.2 ± 0.02	0.8811 ± 0.0005	313.2 ± 0.02	82.73 ± 0.289	
318.2 ± 0.02	0.8779 ± 0.0005	318.2 ± 0.02	66.61 ± 0.233	
323.2 ± 0.02	0.8747 ± 0.0005	323.2 ± 0.02	54.32 ± 0.190	
HDES3- Decanoic Acid : Methyltrioctylammonium Bromide (2:1)				
288.2 ± 0.02	0.9489 ± 0.0005	288.2 ± 0.02	1186.97 ± 4.154	
293.2 ± 0.02	0.9456 ± 0.0005	293.2 ± 0.02	814.53 ± 2.850	
298.2 ± 0.02	0.9422 ± 0.0005	298.2 ± 0.02	576.53 ± 2.017	
303.2 ± 0.02	0.9388 ± 0.0005	303.2 ± 0.02	416.93 ± 1.459	(Van Osch et al., 2015)
308.2 ± 0.02	0.9356 ± 0.0005	308.2 ± 0.02	307.25 ± 1.075	
313.2 ± 0.02	0.9323 ± 0.0005	313.2 ± 0.02	230.39 ± 0.806	
318.2 ± 0.02	0.9290 ± 0.0005	318.2 ± 0.02	175.72 ± 0.615	
323.2 ± 0.02	0.9258 ± 0.0005	323.2 ± 0.02	136.15 ± 0.476	
HDES4- Decanoic Acid : Methyltrioctylammonium Chloride (2:1)				
288.2 ± 0.02	0.9027 ± 0.0005	288.2 ± 0.02	1706.23 ± 5.971	
293.2 ± 0.02	0.8996 ± 0.0005	293.2 ± 0.02	1138.73 ± 3.985	
298.2 ± 0.02	0.8964 ± 0.0005	298.2 ± 0.02	783.41 ± 2.741	
303.2 ± 0.02	0.8932 ± 0.0005	303.2 ± 0.02	552.32 ± 1.933	(Van Osch et al., 2015)
308.2 ± 0.02	0.8900 ± 0.0005	308.2 ± 0.02	398.23 ± 1.393	
313.2 ± 0.02	0.8869 ± 0.0005	313.2 ± 0.02	293.12 ± 1.025	
318.2 ± 0.02	0.8838 ± 0.0005	318.2 ± 0.02	219.87 ± 0.769	
323.2 ± 0.02	0.8807± 0.0005	323.2 ± 0.02	190.56 ± 0.666	
HDES5- Decanoic Acid : Tetraoctylammonium Bromide (2:1)				
88.2 ± 0.02	0.9364 ± 0.0005	288.2 ± 0.02	1273.07 ± 4.455	
293.2 ± 0.02	0.9331 ± 0.0005	293.2 ± 0.02	889.57 ± 3.113	
298.2 ± 0.02	0.9298 ± 0.0005	298.2 ± 0.02	636.36 ± 2.227	
303.2 ± 0.02	0.9265 ± 0.0005	303.2 ± 0.02	464.04 ± 1.624	(Van Osch et al., 2015)
308.2 ± 0.02	0.9232 ± 0.0005	308.2 ± 0.02	344.61 ± 1.206	
313.2 ± 0.02	0.9200 ± 0.0005	313.2 ± 0.02	260.41 ± 0.911	
318.2 ± 0.02	0.9168 ± 0.0005	318.2 ± 0.02	199.89 ± 0.699	
323.2 ± 0.02	0.9136 ± 0.0005	323.2 ± 0.02	155.69 ± 0.544	

HDES6- Decanoic Acid : Tetraoctylammonium Chloride (2:1)				
288.2 ± 0.02	0.8953 ± 0.0005	288.2 ± 0.02	929.18 ± 3.252	
293.2 ± 0.02	0.8921 ± 0.0005	293.2 ± 0.02	654.18 ± 2.291	
298.2 ± 0.02	0.8889 ± 0.0005	298.2 ± 0.02	472.58 ± 1.654	
303.2 ± 0.02	0.8857 ± 0.0005	303.2 ± 0.02	348.61 ± 1.220	
308.2 ± 0.02	0.8825 ± 0.0005	308.2 ± 0.02	261.97 ± 0.916	(Van Osch et al., 2015)
313.2 ± 0.02	0.8794 ± 0.0005	313.2 ± 0.02	200.26 ± 0.700	
318.2 ± 0.02	0.8763 ± 0.0005	318.2 ± 0.02	155.52 ± 0.544	
323.2 ± 0.02	0.8732 ± 0.0005	323.2 ± 0.02	122.61 ± 0.429	
HDES7- Decanoic Acid : Tetraoctylammonium Chloride (1.5:1)				
288.2 ± 0.02	0.8944 ± 0.0005			
293.2 ± 0.02	0.8912 ± 0.0005			
298.2 ± 0.02	0.8881 ± 0.0005			
303.2 ± 0.02	0.8849 ± 0.0005	Not reported		(Zubeir et al., 2018)
308.2 ± 0.02	0.8818 ± 0.0005			
313.2 ± 0.02	0.8787 ± 0.0005			
318.2 ± 0.02	0.8756 ± 0.0005			
323.2 ± 0.02	0.8725 ± 0.0005			
HDES8- Decanoic Acid : Lidocaine (2:1)				
293.2 ± 0.02	0.9624 ± 0.0005	293.2 ± 0.03	352.50 ± 5.000	
298.2 ± 0.02	0.9583 ± 0.0005	298.2 ± 0.03	237.50 ± 5.000	
303.2 ± 0.02	0.9540 ± 0.0005	303.2 ± 0.03	160.00 ± 5.000	
308.2 ± 0.02	0.9497 ± 0.0005	308.2 ± 0.03	111.00 ± 5.000	(Dietz et al., 2019; Van Osch et al., 2016)
313.2 ± 0.02	0.9455 ± 0.0005	313.2 ± 0.03	78.60 ± 5.000	
318.2 ± 0.02	0.9412 ± 0.0005	318.2 ± 0.03	57.15 ± 5.000	
323.2 ± 0.02	0.9370 ± 0.0005	323.2 ± 0.03	42.45 ± 5.000	
HDES9- Decanoic Acid : Lidocaine (3:1)				
293.2 ± 0.02	0.9540 ± 0.0005	293.2 ± 0.03	302.00 ± 5.000	
298.2 ± 0.02	0.9497 ± 0.0005	298.2 ± 0.03	208.50 ± 5.000	
303.2 ± 0.02	0.9454 ± 0.0005	303.2 ± 0.03	141.50 ± 5.000	
308.2 ± 0.02	0.9411 ± 0.0005	308.2 ± 0.03	98.45 ± 5.000	(Dietz et al., 2019; Van Osch et al., 2016)
313.2 ± 0.02	0.9368 ± 0.0005	313.2 ± 0.03	70.20 ± 5.000	
318.2 ± 0.02	0.9325 ± 0.0005	318.2 ± 0.03	51.10 ± 5.000	
323.2 ± 0.02	0.9282 ± 0.0005	323.2 ± 0.03	38.05 ± 5.000	
HDES10- Decanoic Acid : Lidocaine (4:1)				
293.2 ± 0.02	0.9461 ± 0.0005	293.2 ± 0.03	197.50 ± 5.000	
298.2 ± 0.02	0.9419 ± 0.0005	298.2 ± 0.03	142.00 ± 5.000	
303.2 ± 0.02	0.9377 ± 0.0005	303.2 ± 0.03	100.30 ± 5.000	
308.2 ± 0.02	0.9335 ± 0.0005	308.2 ± 0.03	71.95 ± 5.000	(Dietz et al., 2019; Van Osch et al., 2016)
313.2 ± 0.02	0.9293 ± 0.0005	313.2 ± 0.03	52.70 ± 5.000	
318.2 ± 0.02	0.9251 ± 0.0005	318.2 ± 0.03	39.35 ± 5.000	
323.2 ± 0.02	0.9208 ± 0.0005	323.2 ± 0.03	29.95 ± 5.000	
HDES11- Decanoic Acid : Sodium Dodecanoate (4:1)				
293.2 ± 0.01	0.9280 ± 0.0005	293.2 ± 0.01	76.59 ± 0.191	
298.2 ± 0.01	0.9240 ± 0.0005	298.2 ± 0.01	60.48 ± 0.151	
303.2 ± 0.01	0.9210 ± 0.0005	303.2 ± 0.01	48.43 ± 0.211	
308.2 ± 0.01	0.9170 ± 0.0005	308.2 ± 0.01	39.29 ± 0.098	(Florindo, Celia-Silva, et al., 2018)
313.2 ± 0.01	0.9130 ± 0.0005	313.2 ± 0.01	32.27 ± 0.080	
318.2 ± 0.01	0.9100 ± 0.0005	318.2 ± 0.01	26.79 ± 0.066	
323.2 ± 0.01	0.9060 ± 0.0005	323.2 ± 0.01	22.48 ± 0.056	

328.2 ± 0.01	0.9020 ± 0.0005	328.2 ± 0.01	19.04 ± 0.047	
333.2 ± 0.01	0.8990 ± 0.0005	333.2 ± 0.01	16.27 ± 0.040	
338.2 ± 0.01	0.8950 ± 0.0005	338.2 ± 0.01	14.02 ± 0.035	
343.2 ± 0.01	0.8920 ± 0.0005	343.2 ± 0.01	12.16 ± 0.030	
348.2 ± 0.01	0.8880 ± 0.0005	348.2 ± 0.01	10.63 ± 0.026	
353.2 ± 0.01	0.8840 ± 0.0005	353.2 ± 0.01	9.35 ± 0.023	
HDES12- Dodecanoic Acid : Octanoic Acid (1:3)				
293.2 ± 0.01	0.9040 ± 0.0005	293.2 ± 0.01	8.22 ± 0.020	
298.2 ± 0.01	0.9010 ± 0.0005	298.2 ± 0.01	7.09 ± 0.017	
303.2 ± 0.01	0.8970 ± 0.0005	303.2 ± 0.01	6.16 ± 0.015	
308.2 ± 0.01	0.8930 ± 0.0005	308.2 ± 0.01	5.39 ± 0.013	
313.2 ± 0.01	0.8890 ± 0.0005	313.2 ± 0.01	4.76 ± 0.011	
318.2 ± 0.01	0.8850 ± 0.0005	318.2 ± 0.01	4.23 ± 0.010	
323.2 ± 0.01	0.8810 ± 0.0005	323.2 ± 0.01	3.78 ± 0.009	(Florindo, Romero, et al., 2018)
328.2 ± 0.01	0.8770 ± 0.0005	328.2 ± 0.01	3.39 ± 0.008	
333.2 ± 0.01	0.8730 ± 0.0005	333.2 ± 0.01	3.06 ± 0.007	
338.2 ± 0.01	0.8690 ± 0.0005	338.2 ± 0.01	2.78 ± 0.006	
343.2 ± 0.01	0.8650 ± 0.0005	343.2 ± 0.01	2.53 ± 0.006	
348.2 ± 0.01	0.8610 ± 0.0005	348.2 ± 0.01	2.31 ± 0.005	
353.2 ± 0.01	0.8580 ± 0.0005	353.2 ± 0.01	2.12 ± 0.005	
HDES13- Dodecanoic Acid : Nonanoic Acid (1:3)				
293.2 ± 0.01	0.9010 ± 0.0005	293.2 ± 0.01	10.12 ± 0.025	
298.2 ± 0.01	0.8970 ± 0.0005	298.2 ± 0.01	8.64 ± 0.021	
303.2 ± 0.01	0.8930 ± 0.0005	303.2 ± 0.01	7.44 ± 0.018	
308.2 ± 0.01	0.8900 ± 0.0005	308.2 ± 0.01	6.47 ± 0.016	
313.2 ± 0.01	0.8860 ± 0.0005	313.2 ± 0.01	5.67 ± 0.014	
318.2 ± 0.01	0.8820 ± 0.0005	318.2 ± 0.01	5.00 ± 0.012	
323.2 ± 0.01	0.8780 ± 0.0005	323.2 ± 0.01	4.44 ± 0.011	(Florindo, Romero, et al., 2018)
328.2 ± 0.01	0.8740 ± 0.0005	328.2 ± 0.01	3.97 ± 0.009	
333.2 ± 0.01	0.8700 ± 0.0005	333.2 ± 0.01	3.57 ± 0.008	
338.2 ± 0.01	0.8660 ± 0.0005	338.2 ± 0.01	3.22 ± 0.008	
343.2 ± 0.01	0.8630 ± 0.0005	343.2 ± 0.01	2.92 ± 0.007	
348.2 ± 0.01	0.8590 ± 0.0005	348.2 ± 0.01	2.66 ± 0.006	
353.2 ± 0.01	0.8550 ± 0.0005	353.2 ± 0.01	2.43 ± 0.006	
HDES14- Dodecanoic Acid : Decanoic Acid (1:2)				
293.2 ± 0.01	0.8980 ± 0.0005	293.2 ± 0.01	12.89 ± 0.032	
298.2 ± 0.01	0.8940 ± 0.0005	298.2 ± 0.01	10.76 ± 0.026	
303.2 ± 0.01	0.8890 ± 0.0005	303.2 ± 0.01	9.20 ± 0.023	
308.2 ± 0.01	0.8860 ± 0.0005	308.2 ± 0.01	7.94 ± 0.019	
313.2 ± 0.01	0.8820 ± 0.0005	313.2 ± 0.01	6.91 ± 0.017	
318.2 ± 0.01	0.8790 ± 0.0005	318.2 ± 0.01	6.06 ± 0.015	
323.2 ± 0.01	0.8750 ± 0.0005	323.2 ± 0.01	5.35 ± 0.013	(Florindo, Romero, et al., 2018)
328.2 ± 0.01	0.8710 ± 0.0005	328.2 ± 0.01	4.75 ± 0.011	
333.2 ± 0.01	0.8670 ± 0.0005	333.2 ± 0.01	4.25 ± 0.010	
338.2 ± 0.01	0.8640 ± 0.0005	338.2 ± 0.01	3.82 ± 0.009	
343.2 ± 0.01	0.8600 ± 0.0005	343.2 ± 0.01	3.44 ± 0.008	
348.2 ± 0.01	0.8560 ± 0.0005	348.2 ± 0.01	3.12 ± 0.007	
353.2 ± 0.01	0.8520 ± 0.0005	353.2 ± 0.01	2.84 ± 0.007	
HDES15- Ethylparaben : Methyltrioctylammonium Chloride (2:1)				
298.2 ± 0.01	0.9950 ± 0.0005	298.2 ± 0.01	957.50 ± 0.0005	(Li et al., 2019)

303.2 ± 0.01	0.9916 ± 0.0005	303.2 ± 0.01	599.80 ± 0.0005	
308.2 ± 0.01	0.9882 ± 0.0005	313.2 ± 0.01	300.50 ± 0.0005	
313.2 ± 0.01	0.9848 ± 0.0005	323.2 ± 0.01	180.30 ± 0.0005	
318.2 ± 0.01	0.9814 ± 0.0005			
323.2 ± 0.01	0.9780± 0.0005			
HDES16- Ibuprofen :Tetraheptylammonium Chloride (3:7)				
298.2 ± 0.01	0.8920 ± 0.009	298.2 ± 0.01	1029.00 ± 0.100	
313.2 ± 0.01	0.8820 ± 0.009	313.2 ± 0.01	400.10 ± 0.400	(Tereshatov et al., 2016)
328.2 ± 0.01	0.8730 ± 0.009	328.2 ± 0.01	181.70 ± 0.300	
343.2 ± 0.01	0.8630 ± 0.009	343.2 ± 0.01	96.67 ± 0.110	
HDES17- DL-Menthol : Acetic Acid (1:1)				
293.2 ± 0.02	0.9350 ± 0.0005	293.2 ± 0.02	11.30 ± 0.039	
298.2 ± 0.02	0.9310 ± 0.0005	298.2 ± 0.02	8.69 ± 0.030	
303.2 ± 0.02	0.9270 ± 0.0005	303.2 ± 0.02	6.90 ± 0.024	
308.2 ± 0.02	0.9230 ± 0.0005	308.2 ± 0.02	5.59 ± 0.019	
313.2 ± 0.02	0.9190 ± 0.0005	313.2 ± 0.02	4.56 ± 0.015	
318.2 ± 0.02	0.9150 ± 0.0005	318.2 ± 0.02	3.84 ± 0.013	
323.2 ± 0.02	0.9110 ± 0.0005	323.2 ± 0.02	3.25 ± 0.011	(Ribeiro et al., 2015)
328.2 ± 0.02	0.9060 ± 0.0005	328.2 ± 0.02	2.78 ± 0.009	
333.2 ± 0.02	0.9020 ± 0.0005	333.2 ± 0.02	2.39 ± 0.008	
338.2 ± 0.02	0.8980 ± 0.0005	338.2 ± 0.02	2.09 ± 0.007	
343.2 ± 0.02	0.8940 ± 0.0005	343.2 ± 0.02	1.84 ± 0.006	
348.2 ± 0.02	0.8890 ± 0.0005	348.2 ± 0.02	1.63 ± 0.005	
353.2 ± 0.02	0.8840 ± 0.0005	353.2 ± 0.02	1.46 ± 0.005	
HDES18- DL-Menthol : Lactic Acid (1:2)				
93.2 ± 0.02	1.0380 ± 0.0005	293.2 ± 0.02	370.86 ± 1.298	
298.2 ± 0.02	1.0330 ± 0.0005	298.2 ± 0.02	218.93 ± 0.766	
303.2 ± 0.02	1.0290 ± 0.0005	303.2 ± 0.02	134.25 ± 0.469	
308.2 ± 0.02	1.0250 ± 0.0005	308.2 ± 0.02	86.53 ± 0.302	
313.2 ± 0.02	1.0210 ± 0.0005	313.2 ± 0.02	58.84 ± 0.205	
318.2 ± 0.02	1.0170 ± 0.0005	318.2 ± 0.02	40.71 ± 0.142	
323.2 ± 0.02	1.0130 ± 0.0005	323.2 ± 0.02	29.47 ± 0.103	(Ribeiro et al., 2015)
328.2 ± 0.02	1.0090 ± 0.0005	328.2 ± 0.02	21.95 ± 0.076	
333.2 ± 0.02	1.0050 ± 0.0005	333.2 ± 0.02	16.95 ± 0.059	
338.2 ± 0.02	1.0010 ± 0.0005	338.2 ± 0.02	13.12 ± 0.045	
343.2 ± 0.02	0.9970 ± 0.0005	343.2 ± 0.02	10.46 ± 0.036	
348.2 ± 0.02	0.9920 ± 0.0005	348.2 ± 0.02	8.49 ± 0.029	
353.2 ± 0.02	0.9880 ± 0.0005	353.2 ± 0.02	7.01 ± 0.024	
HDES19- DL-Menthol : Pyruvic Acid (1:2)				
293.2 ± 0.02	0.9990 ± 0.0005	293.2 ± 0.02	44.64 ± 0.156	
298.2 ± 0.02	0.9950 ± 0.0005	298.2 ± 0.02	29.95 ± 0.104	
303.2 ± 0.02	0.9910 ± 0.0005	303.2 ± 0.02	21.24 ± 0.074	
308.2 ± 0.02	0.9870 ± 0.0005	308.2 ± 0.02	15.67 ± 0.054	
313.2 ± 0.02	0.9830 ± 0.0005	313.2 ± 0.02	11.88 ± 0.041	
318.2 ± 0.02	0.9780 ± 0.0005	318.2 ± 0.02	9.36 ± 0.032	(Ribeiro et al., 2015)
323.2 ± 0.02	0.9740 ± 0.0005	323.2 ± 0.02	7.51 ± 0.026	
328.2 ± 0.02	0.9700 ± 0.0005	328.2 ± 0.02	6.14 ± 0.021	
333.2 ± 0.02	0.9660 ± 0.0005	333.2 ± 0.02	5.03 ± 0.017	
338.2 ± 0.02	0.9620 ± 0.0005	338.2 ± 0.02	4.32 ± 0.015	
343.2 ± 0.02	0.9580 ± 0.0005	343.2 ± 0.02	3.70 ± 0.012	

348.2 ± 0.02	0.9530 ± 0.0005	348.2 ± 0.02	3.20 ± 0.011	
353.2 ± 0.02	0.9480 ± 0.0005	353.2 ± 0.02	2.74 ± 0.009	

HDES20- DL-Menthol : Dodecanoic Acid (2:1)

293.2 ± 0.02	0.8970 ± 0.0005	293.2 ± 0.02	33.06 ± 0.115	
298.2 ± 0.02	0.8940 ± 0.0005	298.2 ± 0.02	24.42 ± 0.085	
303.2 ± 0.02	0.8900 ± 0.0005	303.2 ± 0.02	18.63 ± 0.065	
308.2 ± 0.02	0.8860 ± 0.0005	308.2 ± 0.02	14.51 ± 0.050	
313.2 ± 0.02	0.8830 ± 0.0005	313.2 ± 0.02	11.45 ± 0.040	
318.2 ± 0.02	0.8790 ± 0.0005	318.2 ± 0.02	9.29 ± 0.032	
323.2 ± 0.02	0.8760 ± 0.0005	323.2 ± 0.02	7.61 ± 0.026	(Ribeiro et al., 2015; Verma & Banerjee, 2018)
328.2 ± 0.02	0.8720 ± 0.0005	328.2 ± 0.02	6.32 ± 0.022	
333.2 ± 0.02	0.8680 ± 0.0005	333.2 ± 0.02	5.23 ± 0.018	
338.2 ± 0.02	0.8650 ± 0.0005	338.2 ± 0.02	4.51 ± 0.015	
343.2 ± 0.02	0.8610 ± 0.0005	343.2 ± 0.02	3.86 ± 0.013	
348.2 ± 0.02	0.8570 ± 0.0005	348.2 ± 0.02	3.34 ± 0.011	
353.2 ± 0.02	0.8530 ± 0.0005	353.2 ± 0.02	2.86 ± 0.010	

HDES21- DL-Menthol : Hexadecanoic Acid (12:1)

293.2 ± 0.02	0.8938 ± 0.0005		
298.2 ± 0.02	0.8900 ± 0.0005		
303.2 ± 0.02	0.8863 ± 0.0005		
308.2 ± 0.02	0.8826 ± 0.0005		
313.2 ± 0.02	0.8788 ± 0.0005		
318.2 ± 0.02	0.8751 ± 0.0005		
323.2 ± 0.02	0.8714 ± 0.0005		
328.2 ± 0.02	0.8677 ± 0.0005	Not reported	(Verma & Banerjee, 2019)
333.2 ± 0.02	0.8639 ± 0.0005		
338.2 ± 0.02	0.8602 ± 0.0005		
343.2 ± 0.02	0.8565 ± 0.0005		
348.2 ± 0.02	0.8528 ± 0.0005		
353.2 ± 0.02	0.8490 ± 0.0005		
358.2 ± 0.02	0.8453± 0.0005		

HDES22- DL-Menthol : 3-Hydroxy Benzoic Acid (7:1)

298.2 ± 0.02	0.9197 ± 0.0001		
303.2 ± 0.02	0.9157 ± 0.0001		
313.2 ± 0.02	0.9077 ± 0.0001		
323.2 ± 0.02	0.8997 ± 0.0001	Not reported	(Mat Hussin et al., 2020)
333.2 ± 0.02	0.8917 ± 0.0001		
343.2 ± 0.02	0.8837 ± 0.0001		
353.2 ± 0.02	0.8757 ± 0.0001		

HDES23- DL-Menthol : 2-Methyl-2,4-pentanediol (2:1)

293.2 ± 0.02	0.9040 ± 0.00015		
298.2 ± 0.02	0.9010 ± 0.00015		
303.2 ± 0.02	0.8970 ± 0.00015		
308.2 ± 0.02	0.8930 ± 0.00015		
313.2 ± 0.02	0.8900 ± 0.00015	Not reported	(Almustafa et al., 2020)
323.2 ± 0.02	0.8820 ± 0.00015		
333.2 ± 0.02	0.8750 ± 0.00015		
343.2 ± 0.02	0.8670 ± 0.00015		
353.2 ± 0.02	0.8590 ± 0.00015		

HDES24- DL-Menthol : 1-Decanol (2:1)

293.2 ± 0.02	0.8740 ± 0.00002			
298.2 ± 0.02	0.8700 ± 0.00002			
303.2 ± 0.02	0.8670 ± 0.00002			
308.2± 0.02	0.8630 ± 0.00002			
313.2 ± 0.02	0.8590 ± 0.00002	Not reported		(Almustafa et al., 2020)
323.2 ± 0.02	0.8520 ± 0.00002			
333.2 ± 0.02	0.8440 ± 0.00002			
343.2 ± 0.02	0.8370 ± 0.00002			
353.2 ± 0.02	0.8290 ± 0.00002			
HDES25- DL-Menthol : Sesamol (1:1)				
298.2 ± 0.02	1.0716 ± 0.0001			
303.2 ± 0.02	1.0676 ± 0.0001			
313.2 ± 0.02	1.0596 ± 0.0001			
323.2 ± 0.02	1.0516 ± 0.0001	Not reported		(Mat Hussin et al., 2020)
333.2 ± 0.02	1.0436 ± 0.0001			
343.2 ± 0.02	1.0356 ± 0.0001			
353.2 ± 0.02	1.0276 ± 0.0001			
HDES26- DL-Menthol : Thymol (1:1)				
298.2 ± 0.02	0.9287 ± 0.0001			
303.2 ± 0.02	0.9247 ± 0.0001			
313.2 ± 0.02	0.9167 ± 0.0001			
323.2 ± 0.02	0.9087 ± 0.0001	Not reported		(Mat Hussin et al., 2020)
333.2 ± 0.02	0.9007 ± 0.0001			
343.2 ± 0.02	0.8927 ± 0.0001			
353.2 ± 0.02	0.8847 ± 0.0001			
HDES27- L-Menthol : Octanoic Acid (1.5:1)				
278.2 ± 0.02	0.9148 ± 0.0005	278.2 ± 0.02	50.64 ± 0.177	
283.2 ± 0.02	0.9110 ± 0.0005	283.2 ± 0.02	35.97 ± 0.125	
288.2 ± 0.02	0.9073 ± 0.0005	288.2 ± 0.02	26.38 ± 0.092	
293.2 ± 0.02	0.9036 ± 0.0005	293.2 ± 0.02	19.83 ± 0.069	
298.2 ± 0.02	0.8998 ± 0.0005	298.2 ± 0.02	15.29 ± 0.053	
303.2 ± 0.02	0.8961 ± 0.0005	303.2 ± 0.02	12.01 ± 0.042	
308.2 ± 0.02	0.8924 ± 0.0005	308.2 ± 0.02	9.58 ± 0.033	
313.2 ± 0.02	0.8887 ± 0.0005	313.2 ± 0.02	7.80 ± 0.027	
318.2 ± 0.02	0.8849 ± 0.0005	318.2 ± 0.02	6.43 ± 0.022	
323.2 ± 0.02	0.8811 ± 0.0005	323.2 ± 0.02	5.37 ± 0.018	
328.2 ± 0.02	0.8773 ± 0.0005	328.2 ± 0.02	4.54 ± 0.015	(Martins et al., 2018)
333.2 ± 0.02	0.8735 ± 0.0005	333.2 ± 0.02	3.88 ± 0.013	
338.2 ± 0.02	0.8697 ± 0.0005	338.2 ± 0.02	3.34 ± 0.011	
343.2 ± 0.02	0.8658 ± 0.0005	343.2 ± 0.02	2.91 ± 0.010	
348.2 ± 0.02	0.8619 ± 0.0005	348.2 ± 0.02	2.55 ± 0.008	
353.2 ± 0.02	0.8580 ± 0.0005	353.2 ± 0.02	2.25 ± 0.007	
358.2 ± 0.02	0.8541± 0.0005	358.2 ± 0.02	2.00 ± 0.007	
363.2 ± 0.02	0.8502 ± 0.0005	363.2 ± 0.02	1.79 ± 0.006	
368.2 ± 0.02	0.8462 ± 0.0005	368.2 ± 0.02	1.61 ± 0.005	
373.2 ± 0.02	0.8422 ± 0.0005	373.2 ± 0.02	1.45 ± 0.005	
HDES28- L-Menthol : Decanoic Acid (1.5:1)				
283.2 ± 0.02	0.9075 ± 0.0005	283.2 ± 0.02	45.50 ± 0.159	
288.2 ± 0.02	0.9039 ± 0.0005	288.2 ± 0.02	33.05 ± 0.115	(Martins et al., 2018)
293.2 ± 0.02	0.9002 ± 0.0005	293.2 ± 0.02	24.68 ± 0.086	

298.2 ± 0.02	0.8965 ± 0.0005	298.2 ± 0.02	18.85 ± 0.065
303.2 ± 0.02	0.8929 ± 0.0005	303.2 ± 0.02	14.70 ± 0.051
308.2 ± 0.02	0.8892 ± 0.0005	308.2 ± 0.02	11.68 ± 0.040
313.2 ± 0.02	0.8855 ± 0.0005	313.2 ± 0.02	9.43 ± 0.033
318.2 ± 0.02	0.8818 ± 0.0005	318.2 ± 0.02	7.73 ± 0.027
323.2 ± 0.02	0.8780 ± 0.0005	323.2 ± 0.02	6.42 ± 0.022
328.2 ± 0.02	0.8743 ± 0.0005	328.2 ± 0.02	5.39 ± 0.018
333.2 ± 0.02	0.8705 ± 0.0005	333.2 ± 0.02	4.58 ± 0.016
338.2 ± 0.02	0.8667 ± 0.0005	338.2 ± 0.02	3.92 ± 0.013
343.2 ± 0.02	0.8629 ± 0.0005	343.2 ± 0.02	3.40 ± 0.011
348.2 ± 0.02	0.8591 ± 0.0005	348.2 ± 0.02	2.97 ± 0.010
353.2 ± 0.02	0.8553 ± 0.0005	353.2 ± 0.02	2.61 ± 0.009
358.2 ± 0.02	0.8514 ± 0.0005	358.2 ± 0.02	2.31 ± 0.008
363.2 ± 0.02	0.8476 ± 0.0005	363.2 ± 0.02	2.06 ± 0.007
368.2 ± 0.02	0.8437 ± 0.0005	368.2 ± 0.02	1.84 ± 0.006
373.2 ± 0.02	0.8397 ± 0.0005	373.2 ± 0.02	1.66 ± 0.005
HDES29- L-Menthol : Decanoic Acid (1:1)			
		293.2 ± 0.03	28.00 ± 5.000
		298.2 ± 0.03	22.00 ± 5.000
		303.2 ± 0.03	17.00 ± 5.000
Not reported		308.2 ± 0.03	14.00 ± 5.000
		313.2 ± 0.03	11.00 ± 5.000
		318.2 ± 0.03	9.00 ± 5.000
		323.2 ± 0.03	7.00 ± 5.000
		328.2 ± 0.03	6.00 ± 5.000
HDES30- L-Menthol : Dodecanoic Acid (3:1)			
298.2 ± 0.02	0.8930 ± 0.0005	298.2 ± 0.02	28.10 ± 0.098
303.2 ± 0.02	0.8894 ± 0.0005	303.2 ± 0.02	20.91 ± 0.073
308.2 ± 0.02	0.8859 ± 0.0005	308.2 ± 0.02	15.93 ± 0.055
313.2 ± 0.02	0.8823 ± 0.0005	313.2 ± 0.02	12.40 ± 0.043
318.2 ± 0.02	0.8787 ± 0.0005	318.2 ± 0.02	9.84 ± 0.034
323.2 ± 0.02	0.8751 ± 0.0005	323.2 ± 0.02	7.94 ± 0.027
328.2 ± 0.02	0.8714 ± 0.0005	328.2 ± 0.02	6.50 ± 0.022
333.2 ± 0.02	0.8677 ± 0.0005	333.2 ± 0.02	5.40 ± 0.018
338.2 ± 0.02	0.8639 ± 0.0005	338.2 ± 0.02	4.54 ± 0.015
343.2 ± 0.02	0.8601 ± 0.0005	343.2 ± 0.02	3.86 ± 0.013
348.2 ± 0.02	0.8562 ± 0.0005	348.2 ± 0.02	3.32 ± 0.011
353.2 ± 0.02	0.8523 ± 0.0005	353.2 ± 0.02	2.87 ± 0.010
358.2 ± 0.02	0.8485 ± 0.0005	358.2 ± 0.02	2.51 ± 0.008
363.2 ± 0.02	0.8447 ± 0.0005	363.2 ± 0.02	2.21 ± 0.007
368.2 ± 0.02	0.8410 ± 0.0005	368.2 ± 0.02	1.96 ± 0.006
373.2 ± 0.02	0.8372 ± 0.0005	373.2 ± 0.02	1.75 ± 0.006
HDES31- L-Menthol : Tetradecanoic Acid (4:1)			
298.2 ± 0.02	0.8921 ± 0.0005	298.2 ± 0.02	33.99 ± 0.118
303.2 ± 0.02	0.8884 ± 0.0005	303.2 ± 0.02	24.78 ± 0.086
308.2 ± 0.02	0.8848 ± 0.0005	308.2 ± 0.02	18.54 ± 0.064
313.2 ± 0.02	0.8812 ± 0.0005	313.2 ± 0.02	14.21 ± 0.049
318.2 ± 0.02	0.8776 ± 0.0005	318.2 ± 0.02	11.11 ± 0.038
323.2 ± 0.02	0.8739 ± 0.0005	323.2 ± 0.02	8.85 ± 0.030
328.2 ± 0.02	0.8702 ± 0.0005	328.2 ± 0.02	7.17 ± 0.025
333.2 ± 0.02	0.8665 ± 0.0005	333.2 ± 0.02	5.89 ± 0.020

The references (Dietz et al., 2019) apply to HDES29 and (Martins et al., 2018) apply to HDES30 and HDES31.

338.2 ± 0.02	0.8628 ± 0.0005	338.2 ± 0.02	4.91 ± 0.017	
343.2 ± 0.02	0.8590 ± 0.0005	343.2 ± 0.02	4.14 ± 0.014	
348.2 ± 0.02	0.8553 ± 0.0005	348.2 ± 0.02	3.53 ± 0.012	
353.2 ± 0.02	0.8515 ± 0.0005	353.2 ± 0.02	3.04 ± 0.010	
358.2 ± 0.02	0.8476 ± 0.0005	358.2 ± 0.02	2.65 ± 0.009	
363.2 ± 0.02	0.8438 ± 0.0005	363.2 ± 0.02	2.32 ± 0.008	
368.2 ± 0.02	0.8398 ± 0.0005	368.2 ± 0.02	2.05 ± 0.007	
373.2 ± 0.02	0.8359 ± 0.0005	373.2 ± 0.02	1.82 ± 0.006	
HDES32- L-Menthol : Hexadecanoic Acid (5.67:1)				
313.2 ± 0.02	0.8814 ± 0.0005	313.2 ± 0.02	15.25 ± 0.053	
318.2 ± 0.02	0.8777 ± 0.0005	318.2 ± 0.02	11.78 ± 0.041	
323.2 ± 0.02	0.8741 ± 0.0005	323.2 ± 0.02	9.29 ± 0.032	
328.2 ± 0.02	0.8703 ± 0.0005	328.2 ± 0.02	7.46 ± 0.026	
333.2 ± 0.02	0.8666 ± 0.0005	333.2 ± 0.02	6.09 ± 0.021	
338.2 ± 0.02	0.8629 ± 0.0005	338.2 ± 0.02	5.04 ± 0.017	
343.2 ± 0.02	0.8591 ± 0.0005	343.2 ± 0.02	4.21 ± 0.014	(Martins et al., 2018)
348.2 ± 0.02	0.8553 ± 0.0005	348.2 ± 0.02	3.57 ± 0.012	
353.2 ± 0.02	0.8513 ± 0.0005	353.2 ± 0.02	3.06 ± 0.010	
358.2 ± 0.02	0.8475 ± 0.0005	358.2 ± 0.02	2.65 ± 0.009	
363.2 ± 0.02	0.8436 ± 0.0005	363.2 ± 0.02	2.32 ± 0.008	
368.2 ± 0.02	0.8396 ± 0.0005	368.2 ± 0.02	2.04 ± 0.007	
373.2 ± 0.02	0.8355 ± 0.0005	373.2 ± 0.02	1.81 ± 0.006	
HDES33- L-Menthol : Octadecanoic Acid (9:1)				
313.2 ± 0.02	0.8810 ± 0.0005	313.2 ± 0.02	16.61 ± 0.058	
318.2 ± 0.02	0.8774 ± 0.0005	318.2 ± 0.02	12.62 ± 0.044	
323.2 ± 0.02	0.8737 ± 0.0005	323.2 ± 0.02	9.81 ± 0.034	
328.2 ± 0.02	0.8700 ± 0.0005	328.2 ± 0.02	7.77 ± 0.027	
333.2 ± 0.02	0.8662 ± 0.0005	333.2 ± 0.02	6.27 ± 0.021	
338.2 ± 0.02	0.8624 ± 0.0005	338.2 ± 0.02	5.14 ± 0.017	
343.2 ± 0.02	0.8587 ± 0.0005	343.2 ± 0.02	4.27 ± 0.014	(Martins et al., 2018)
348.2 ± 0.02	0.8549 ± 0.0005	348.2 ± 0.02	3.59 ± 0.012	
353.2 ± 0.02	0.8511 ± 0.0005	353.2 ± 0.02	3.06 ± 0.010	
358.2 ± 0.02	0.8472 ± 0.0005	358.2 ± 0.02	2.63 ± 0.009	
363.2 ± 0.02	0.8433 ± 0.0005	363.2 ± 0.02	2.29 ± 0.008	
368.2 ± 0.02	0.8393 ± 0.0005	368.2 ± 0.02	2.00 ± 0.007	
373.2 ± 0.02	0.8353 ± 0.0005	373.2 ± 0.02	1.77 ± 0.006	
HDES34- L-Menthol : 1-Tetradecanol (2:1)				
293.2 ± 0.05	0.8733 ± 0.00005	293.2 ± 0.05	44.17 ± 0.089	
298.2 ± 0.05	0.8697 ± 0.00005	298.2 ± 0.05	31.71± 0.063	
303.2 ± 0.05	0.8662 ± 0.00005	303.2 ± 0.05	23.34 ± 0.046	
308.2 ± 0.05	0.8626 ± 0.00005	308.2 ± 0.05	17.57 ± 0.035	
313.2 ± 0.05	0.8591 ± 0.00005	313.2 ± 0.05	13.49 ± 0.026	
318.2 ± 0.05	0.8555 ± 0.00005	318.2 ± 0.05	10.55 ± 0.021	
323.2 ± 0.05	0.8520 ± 0.00005	323.2 ± 0.05	8.38 ± 0.016	
328.2 ± 0.05	0.8484 ± 0.00005	328.2 ± 0.05	6.76 ± 0.013	(Van Osch et al., 2020)
333.2 ± 0.05	0.8449 ± 0.00005	333.2 ± 0.05	5.52 ± 0.011	
338.2 ± 0.05	0.8413 ± 0.00005			
343.2 ± 0.05	0.8378 ± 0.00005			
348.2 ± 0.05	0.8342 ± 0.00005			
353.2 ± 0.05	0.8307 ± 0.00005			
358.2 ± 0.05	0.8271 ± 0.00005			

363.2 ± 0.05	0.8236 ± 0.00005			
368.2 ± 0.05	0.8200 ± 0.00005			

		HDES35- L-Menthol : Borneol (7:3)		
278.2 ± 0.02	0.9295 ± 0.0005	278.2 ± 0.02	1431.00 ± 5.008	
283.2 ± 0.02	0.9257 ± 0.0005	283.2 ± 0.02	680.52 ± 2.381	
288.2 ± 0.02	0.9222 ± 0.0005	288.2 ± 0.02	345.99 ± 1.210	
293.2 ± 0.02	0.9186 ± 0.0005	293.2 ± 0.02	189.27 ± 0.662	
298.2 ± 0.02	0.9149 ± 0.0005	298.2 ± 0.02	110.40 ± 0.386	
303.2 ± 0.02	0.9113 ± 0.0005	303.2 ± 0.02	68.06 ± 0.238	
308.2 ± 0.02	0.9076 ± 0.0005	308.2 ± 0.02	44.00 ± 0.154	
313.2 ± 0.02	0.9039 ± 0.0005	313.2 ± 0.02	29.65 ± 0.103	
318.2 ± 0.02	0.9001 ± 0.0005	318.2 ± 0.02	20.73 ± 0.072	
323.2 ± 0.02	0.8963 ± 0.0005	323.2 ± 0.02	14.97 ± 0.052	(Martins et al., 2019)
328.2 ± 0.02	0.8925 ± 0.0005	328.2 ± 0.02	11.12 ± 0.038	
333.2 ± 0.02	0.8887 ± 0.0005	333.2 ± 0.02	8.47 ± 0.029	
338.2 ± 0.02	0.8848 ± 0.0005	338.2 ± 0.02	6.60 ± 0.023	
343.2 ± 0.02	0.8809 ± 0.0005	343.2 ± 0.02	5.26 ± 0.018	
348.2 ± 0.02	0.8770 ± 0.0005	348.2 ± 0.02	4.26 ± 0.014	
353.2 ± 0.02	0.8730 ± 0.0005	353.2 ± 0.02	3.51 ± 0.012	
358.2 ± 0.02	0.8689 ± 0.0005	358.2 ± 0.02	2.94 ± 0.010	
363.2 ± 0.02	0.8649 ± 0.0005	363.2 ± 0.02	2.50 ± 0.008	
368.2 ± 0.02	0.8608 ± 0.0005	368.2 ± 0.02	2.14 ± 0.007	
373.2 ± 0.02	0.8566 ± 0.0005	373.2 ± 0.02	1.86 ± 0.006	

		HDES36- L-Menthol : Camphor (1:1)		
298.2 ± 0.02	0.9237 ± 0.0005	298.2 ± 0.02	16.42 ± 0.057	
303.2 ± 0.02	0.9199 ± 0.0005	303.2 ± 0.02	12.59 ± 0.044	
308.2 ± 0.02	0.9161 ± 0.0005	308.2 ± 0.02	9.87 ± 0.034	
313.2 ± 0.02	0.9122 ± 0.0005	313.2 ± 0.02	7.89 ± 0.027	
318.2 ± 0.02	0.9084 ± 0.0005	318.2 ± 0.02	6.41 ± 0.022	
323.2 ± 0.02	0.9045 ± 0.0005	323.2 ± 0.02	5.30 ± 0.018	
328.2 ± 0.02	0.9006 ± 0.0005	328.2 ± 0.02	4.44 ± 0.015	
333.2 ± 0.02	0.8967 ± 0.0005	333.2 ± 0.02	3.77 ± 0.013	
338.2 ± 0.02	0.8928 ± 0.0005	338.2 ± 0.02	3.23 ± 0.011	(Martins et al., 2019)
343.2 ± 0.02	0.8888 ± 0.0005	343.2 ± 0.02	2.80 ± 0.009	
348.2 ± 0.02	0.8849 ± 0.0005	348.2 ± 0.02	2.45 ± 0.008	
353.2 ± 0.02	0.8809 ± 0.0005	353.2 ± 0.02	2.17 ± 0.007	
358.2 ± 0.02	0.8769 ± 0.0005	358.2 ± 0.02	1.93 ± 0.006	
363.2 ± 0.02	0.8729 ± 0.0005	363.2 ± 0.02	1.73 ± 0.006	
368.2 ± 0.02	0.8689 ± 0.0005	368.2 ± 0.02	1.56 ± 0.005	
373.2 ± 0.02	0.8645 ± 0.0005	373.2 ± 0.02	1.42 ± 0.004	

		HDES37- L-Menthol : Sobrerol (19:1)		
333.2 ± 0.02	0.8755 ± 0.0005	333.2 ± 0.02	6.72 ± 0.023	
338.2 ± 0.02	0.8717 ± 0.0005	338.2 ± 0.02	5.25 ± 0.018	
343.2 ± 0.02	0.8679 ± 0.0005	343.2 ± 0.02	4.21 ± 0.014	
348.2 ± 0.02	0.8640 ± 0.0005	348.2 ± 0.02	3.42 ± 0.011	
353.2 ± 0.02	0.8600 ± 0.0005	353.2 ± 0.02	2.84 ± 0.009	(Martins et al., 2019)
358.2 ± 0.02	0.8560 ± 0.0005	358.2 ± 0.02	2.39 ± 0.008	
363.2 ± 0.02	0.8519 ± 0.0005	363.2 ± 0.02	2.03 ± 0.007	
368.2 ± 0.02	0.8478 ± 0.0005	368.2 ± 0.02	1.75 ± 0.006	
373.2 ± 0.02	0.8437 ± 0.0005	373.2 ± 0.02	1.53 ± 0.005	

		HDES38- L-Menthol : Thymol (1:1)		

176

278.2 ± 0.02	0.9478 ± 0.0005	278.2 ± 0.02	293.22 ± 1.026	
283.2 ± 0.02	0.9439 ± 0.0005	283.2 ± 0.02	159.37 ± 0.557	
288.2 ± 0.02	0.9402 ± 0.0005	288.2 ± 0.02	92.96 ± 0.325	
293.2 ± 0.02	0.9365 ± 0.0005	293.2 ± 0.02	57.88 ± 0.202	
298.2 ± 0.02	0.9327 ± 0.0005	298.2 ± 0.02	38.08 ± 0.133	
303.2 ± 0.02	0.9290 ± 0.0005	303.2 ± 0.02	26.19 ± 0.091	
308.2 ± 0.02	0.9253 ± 0.0005	308.2 ± 0.02	18.68 ± 0.065	
313.2 ± 0.02	0.9215 ± 0.0005	313.2 ± 0.02	13.75 ± 0.048	
318.2 ± 0.02	0.9177 ± 0.0005	318.2 ± 0.02	10.42 ± 0.036	
323.2 ± 0.02	0.9139 ± 0.0005	323.2 ± 0.02	8.10 ± 0.028	(Martins et al., 2019)
328.2 ± 0.02	0.9101 ± 0.0005	328.2 ± 0.02	6.43 ± 0.022	
333.2 ± 0.02	0.9062 ± 0.0005	333.2 ± 0.02	5.20 ± 0.018	
338.2 ± 0.02	0.9024 ± 0.0005	338.2 ± 0.02	4.29 ± 0.015	
343.2 ± 0.02	0.8985 ± 0.0005	343.2 ± 0.02	3.58 ± 0.012	
348.2 ± 0.02	0.8946 ± 0.0005	348.2 ± 0.02	3.03 ± 0.010	
353.2 ± 0.02	0.8907 ± 0.0005	353.2 ± 0.02	2.60 ± 0.009	
358.2 ± 0.02	0.8867 ± 0.0005	358.2 ± 0.02	2.25 ± 0.007	
363.2 ± 0.02	0.8827 ± 0.0005	363.2 ± 0.02	1.97 ± 0.006	
368.2 ± 0.02	0.8787 ± 0.0005	368.2 ± 0.02	1.73 ± 0.006	
373.2 ± 0.02	0.8747 ± 0.0005	373.2 ± 0.02	1.54 ± 0.005	
HDES39- Oleic Acid :Tetraheptylammonium Chloride (2:1)				
298.2 ± 0.01	0.8670 ± 0.009	298.2 ± 0.01	244.70 ± 0.400	
313.2 ± 0.01	0.8520 ± 0.009	313.2 ± 0.01	121.01± 0.060	(Tereshatov et al., 2016)
328.2 ± 0.01	0.8430 ± 0.009	328.2 ± 0.01	67.69 ± 0.020	
343.2 ± 0.01	0.8340 ± 0.009	343.2 ± 0.01	41.64 ± 0.040	
HDES40- Thymol : 2-Methyl-2,4-pentanediol (2:1)				
293.2 ± 0.02	0.9630 ± 0.0002			
298.2 ± 0.02	0.9590 ± 0.0002			
303.2 ± 0.02	0.9550 ± 0.0002			
308.2 ± 0.02	0.9510 ± 0.0002			
313.2 ± 0.02	0.9480 ± 0.0002		Not reported	(Almustafa et al., 2020)
323.2 ± 0.02	0.9400 ± 0.0002			
333.2 ± 0.02	0.9320 ± 0.0002			
343.2 ± 0.02	0.9240 ± 0.0002			
353.2 ± 0.02	0.9160 ± 0.0002			
HDES41- Thymol : 1-Decanol (2:1)				
293.2 ± 0.02	0.9190 ± 0.0002			
298.2 ± 0.02	0.9150 ± 0.0002			
303.2 ± 0.02	0.9110 ± 0.0002			
308.2 ± 0.02	0.9080 ± 0.0002			
313.2 ± 0.02	0.9040 ± 0.0002		Not reported	(Almustafa et al., 2020)
323.2 ± 0.02	0.8960 ± 0.0002			
333.2 ± 0.02	0.8890 ± 0.0002			
343.2 ± 0.02	0.8810 ± 0.0002			
353.2 ± 0.02	0.8730 ± 0.0002			
HDES42-Thymol : Octanoic Acid (0.73:1)				

278.2 ± 0.02	0.9461 ± 0.0005	278.2 ± 0.02	19.22 ± 0.067	
283.2 ± 0.02	0.9421 ± 0.0005	283.2 ± 0.02	15.02 ± 0.052	
288.2 ± 0.02	0.9381 ± 0.0005	288.2 ± 0.02	11.97 ± 0.041	
293.2 ± 0.02	0.9341 ± 0.0005	293.2 ± 0.02	9.71 ± 0.033	
298.2 ± 0.02	0.9301 ± 0.0005	298.2 ± 0.02	8.00 ± 0.028	
303.2 ± 0.02	0.9261 ± 0.0005	303.2 ± 0.02	6.68 ± 0.023	
308.2 ± 0.02	0.9221 ± 0.0005	308.2 ± 0.02	5.65 ± 0.019	
313.2 ± 0.02	0.9181 ± 0.0005	313.2 ± 0.02	4.83 ± 0.016	
318.2 ± 0.02	0.9140 ± 0.0005	318.2 ± 0.02	4.17 ± 0.014	
323.2 ± 0.02	0.9100 ± 0.0005	323.2 ± 0.02	3.64 ± 0.012	(Martins et al., 2018)
328.2 ± 0.02	0.9060 ± 0.0005	328.2 ± 0.02	3.20 ± 0.011	
333.2 ± 0.02	0.9020 ± 0.0005	333.2 ± 0.02	2.83 ± 0.009	
338.2 ± 0.02	0.8979 ± 0.0005	338.2 ± 0.02	2.53 ± 0.008	
343.2 ± 0.02	0.8939 ± 0.0005	343.2 ± 0.02	2.27 ± 0.007	
348.2 ± 0.02	0.8898 ± 0.0005	348.2 ± 0.02	2.05 ± 0.007	
353.2 ± 0.02	0.8858 ± 0.0005	353.2 ± 0.02	1.86 ± 0.006	
358.2 ± 0.02	0.8817 ± 0.0005	358.2 ± 0.02	1.69 ± 0.005	
363.2 ± 0.02	0.8776 ± 0.0005	363.2 ± 0.02	1.54 ± 0.005	
368.2 ± 0.02	0.8735 ± 0.0005	368.2 ± 0.02	1.41 ± 0.004	
373.2 ± 0.02	0.8694 ± 0.0005	373.2 ± 0.02	1.30 ± 0.004	
HDES43-Thymol : Decanoic Acid (1:1)				
293.2 ± 0.02	0.9340 ± 0.0005	293.2 ± 0.02	15.28 ± 0.053	
298.2 ± 0.02	0.9301 ± 0.0005	298.2 ± 0.02	12.16 ± 0.042	
303.2 ± 0.02	0.9263 ± 0.0005	303.2 ± 0.02	9.86 ± 0.034	
308.2 ± 0.02	0.9224 ± 0.0005	308.2 ± 0.02	8.12 ± 0.028	
313.2 ± 0.02	0.9186 ± 0.0005	313.2 ± 0.02	6.78 ± 0.023	
318.2 ± 0.02	0.9147 ± 0.0005	318.2 ± 0.02	5.74 ± 0.020	
323.2 ± 0.02	0.9108 ± 0.0005	323.2 ± 0.02	4.91 ± 0.017	
328.2 ± 0.02	0.9070 ± 0.0005	328.2 ± 0.02	4.24 ± 0.014	
333.2 ± 0.02	0.9031 ± 0.0005	333.2 ± 0.02	3.70 ± 0.012	(Dietz et al., 2019; Martins et al., 2018)
338.2 ± 0.02	0.8992 ± 0.0005	338.2 ± 0.02	3.26 ± 0.011	
343.2 ± 0.02	0.8953 ± 0.0005	343.2 ± 0.02	2.88 ± 0.010	
348.2 ± 0.02	0.8914 ± 0.0005	348.2 ± 0.02	2.57 ± 0.008	
353.2 ± 0.02	0.8874 ± 0.0005	353.2 ± 0.02	2.31 ± 0.008	
358.2 ± 0.02	0.8835 ± 0.0005	358.2 ± 0.02	2.08 ± 0.007	
363.2 ± 0.02	0.8795 ± 0.0005	363.2 ± 0.02	1.89 ± 0.006	
368.2 ± 0.02	0.8755 ± 0.0005	368.2 ± 0.02	1.72 ± 0.006	
373.2 ± 0.02	0.8715 ± 0.0005	373.2 ± 0.02	1.57 ± 0.005	
HDES44-Thymol : Dodecanoic Acid (1.22:1)				
303.2 ± 0.02	0.9221 ± 0.0005	303.2 ± 0.02	12.43 ± 0.043	
308.2 ± 0.02	0.9183 ± 0.0005	308.2 ± 0.02	10.12 ± 0.035	
313.2 ± 0.02	0.9145 ± 0.0005	313.2 ± 0.02	8.37 ± 0.029	
318.2 ± 0.02	0.9107 ± 0.0005	318.2 ± 0.02	7.01 ± 0.024	
323.2 ± 0.02	0.9069 ± 0.0005	323.2 ± 0.02	5.95 ± 0.020	
328.2 ± 0.02	0.9031± 0.0005	328.2 ± 0.02	5.10 ± 0.017	
333.2 ± 0.02	0.8992 ± 0.0005	333.2 ± 0.02	4.42 ± 0.015	(Martins et al., 2018)
338.2 ± 0.02	0.8954 ± 0.0005	338.2 ± 0.02	3.86 ± 0.013	
343.2 ± 0.02	0.8916 ± 0.0005	343.2 ± 0.02	3.40 ± 0.011	
348.2 ± 0.02	0.8878 ± 0.0005	348.2 ± 0.02	3.02 ± 0.010	
353.2 ± 0.02	0.8842 ± 0.0005	353.2 ± 0.02	2.70 ± 0.009	
358.2 ± 0.02	0.8803 ± 0.0005	358.2 ± 0.02	2.42 ± 0.008	

363.2 ± 0.02	0.8764 ± 0.0005	363.2 ± 0.02	2.19 ± 0.007	
368.2 ± 0.02	0.8724 ± 0.0005	368.2 ± 0.02	1.98 ± 0.006	
373.2 ± 0.02	0.8685 ± 0.0005	373.2 ± 0.02	1.80 ± 0.006	
HDES45-Thymol : Tetradecanoic Acid (3:1)				
313.2 ± 0.02	0.9279 ± 0.0005	313.2 ± 0.02	8.69 ± 0.030	
318.2 ± 0.02	0.9240 ± 0.0005	318.2 ± 0.02	7.16 ± 0.025	
323.2 ± 0.02	0.9202 ± 0.0005	323.2 ± 0.02	5.98 ± 0.020	
328.2 ± 0.02	0.9164 ± 0.0005	328.2 ± 0.02	5.07 ± 0.017	
333.2 ± 0.02	0.9126 ± 0.0005	333.2 ± 0.02	4.34 ± 0.015	
338.2 ± 0.02	0.9087 ± 0.0005	338.2 ± 0.02	3.76 ± 0.013	
343.2 ± 0.02	0.9049 ± 0.0005	343.2 ± 0.02	3.28 ± 0.011	(Martins et al., 2018)
348.2 ± 0.02	0.9010 ± 0.0005	348.2 ± 0.02	2.89 ± 0.010	
353.2 ± 0.02	0.8971 ± 0.0005	353.2 ± 0.02	2.57 ± 0.008	
358.2 ± 0.02	0.8933 ± 0.0005	358.2 ± 0.02	2.30 ± 0.008	
363.2 ± 0.02	0.8893 ± 0.0005	363.2 ± 0.02	2.06 ± 0.007	
368.2 ± 0.02	0.8853 ± 0.0005	368.2 ± 0.02	1.86 ± 0.006	
373.2 ± 0.02	0.8814 ± 0.0005	373.2 ± 0.02	1.69 ± 0.005	
HDES46-Thymol : Hexadecanoic Acid (4:1)				
313.2 ± 0.02	0.9294 ± 0.0005	313.2 ± 0.02	9.21 ± 0.032	
318.2 ± 0.02	0.9255 ± 0.0005	318.2 ± 0.02	7.54 ± 0.026	
323.2 ± 0.02	0.9217 ± 0.0005	323.2 ± 0.02	6.29 ± 0.022	
328.2 ± 0.02	0.9179 ± 0.0005	328.2 ± 0.02	5.31 ± 0.018	
333.2 ± 0.02	0.9140 ± 0.0005	333.2 ± 0.02	4.53 ± 0.015	
338.2 ± 0.02	0.9102 ± 0.0005	338.2 ± 0.02	3.91 ± 0.013	
343.2 ± 0.02	0.9063 ± 0.0005	343.2 ± 0.02	3.41 ± 0.011	(Martins et al., 2018)
348.2 ± 0.02	0.9024 ± 0.0005	348.2 ± 0.02	3.00 ± 0.010	
353.2 ± 0.02	0.8986 ± 0.0005	353.2 ± 0.02	2.65 ± 0.008	
358.2 ± 0.02	0.8946 ± 0.0005	358.2 ± 0.02	2.37 ± 0.008	
363.2 ± 0.02	0.8906 ± 0.0005	363.2 ± 0.02	2.12 ± 0.007	
368.2 ± 0.02	0.8867 ± 0.0005	368.2 ± 0.02	1.92 ± 0.006	
373.2 ± 0.02	0.8828 ± 0.0005	373.2 ± 0.02	1.74 ± 0.006	
HDES47-Thymol : Octadecanoic Acid (9:1)				
318.2 ± 0.02	0.9357 ± 0.0005	318.2 ± 0.02	6.88 ± 0.024	
323.2 ± 0.02	0.9318 ± 0.0005	323.2 ± 0.02	5.68 ± 0.019	
328.2 ± 0.02	0.9279 ± 0.0005	328.2 ± 0.02	4.77 ± 0.016	
333.2 ± 0.02	0.9240 ± 0.0005	333.2 ± 0.02	4.06 ± 0.014	
338.2 ± 0.02	0.9201 ± 0.0005	338.2 ± 0.02	3.49 ± 0.012	
343.2 ± 0.02	0.9162 ± 0.0005	343.2 ± 0.02	3.03 ± 0.010	
348.2 ± 0.02	0.9123 ± 0.0005	348.2 ± 0.02	2.66 ± 0.009	(Martins et al., 2018)
353.2 ± 0.02	0.9083 ± 0.0005	353.2 ± 0.02	2.35 ± 0.008	
358.2 ± 0.02	0.9044 ± 0.0005	358.2 ± 0.02	2.10 ± 0.007	
363.2 ± 0.02	0.9003 ± 0.0005	363.2 ± 0.02	1.88 ± 0.006	
368.2 ± 0.02	0.8963 ± 0.0005	368.2 ± 0.02	1.70 ± 0.005	
373.2 ± 0.02	0.8923 ± 0.0005	373.2 ± 0.02	1.54 ± 0.005	
HDES48-Thymol : Borneol (1:1)				
308.2 ± 0.02	0.9631 ± 0.0005	308.2 ± 0.02	43.10 ± 0.150	
313.2 ± 0.02	0.9593 ± 0.0005	313.2 ± 0.02	30.29 ± 0.106	
318.2 ± 0.02	0.9556 ± 0.0005	318.2 ± 0.02	21.98 ± 0.076	(Martins et al., 2019)
323.2 ± 0.02	0.9518 ± 0.0005	323.2 ± 0.02	16.41 ± 0.057	
328.2 ± 0.02	0.9479 ± 0.0005	328.2 ± 0.02	12.56 ± 0.043	

333.2 ± 0.02	0.9440 ± 0.0005	333.2 ± 0.02	9.83 ± 0.034	
338.2 ± 0.02	0.9401 ± 0.0005	338.2 ± 0.02	7.85 ± 0.027	
343.2 ± 0.02	0.9362 ± 0.0005	343.2 ± 0.02	6.37 ± 0.022	
348.2 ± 0.02	0.9323 ± 0.0005	348.2 ± 0.02	5.26 ± 0.018	
353.2 ± 0.02	0.9283 ± 0.0005	353.2 ± 0.02	4.41 ± 0.015	
358.2 ± 0.02	0.9243 ± 0.0005	358.2 ± 0.02	3.74 ± 0.013	
363.2 ± 0.02	0.9202 ± 0.0005	363.2 ± 0.02	3.21 ± 0.011	
368.2 ± 0.02	0.9161 ± 0.0005	368.2 ± 0.02	2.79 ± 0.009	
373.2 ± 0.02	0.9119 ± 0.0005	373.2 ± 0.02	2.45 ± 0.008	
HDES49-Thymol : Camphor (1:1)				
278.2 ± 0.02	0.9821 ± 0.0005	278.2 ± 0.02	74.83 ± 0.261	
283.2 ± 0.02	0.9782 ± 0.0005	283.2 ± 0.02	52.13 ± 0.182	
288.2 ± 0.02	0.9744 ± 0.0005	288.2 ± 0.02	37.34 ± 0.130	
293.2 ± 0.02	0.9706 ± 0.0005	293.2 ± 0.02	27.51 ± 0.096	
298.2 ± 0.02	0.9668 ± 0.0005	298.2 ± 0.02	20.80 ± 0.072	
303.2 ± 0.02	0.9631 ± 0.0005	303.2 ± 0.02	16.10 ± 0.056	
308.2 ± 0.02	0.9593 ± 0.0005	308.2 ± 0.02	12.72 ± 0.044	
313.2 ± 0.02	0.9555 ± 0.0005	313.2 ± 0.02	10.23 ± 0.035	
318.2 ± 0.02	0.9517 ± 0.0005	318.2 ± 0.02	8.36 ± 0.029	
323.2 ± 0.02	0.9479 ± 0.0005	323.2 ± 0.02	6.93 ± 0.024	
328.2 ± 0.02	0.9441 ± 0.0005	328.2 ± 0.02	5.83 ± 0.020	(Martins et al., 2019)
333.2 ± 0.02	0.9403 ± 0.0005	333.2 ± 0.02	4.95 ± 0.017	
338.2 ± 0.02	0.9364 ± 0.0005	338.2 ± 0.02	4.25 ± 0.014	
343.2 ± 0.02	0.9326 ± 0.0005	343.2 ± 0.02	3.69 ± 0.012	
348.2 ± 0.02	0.9288 ± 0.0005	348.2 ± 0.02	3.23 ± 0.011	
353.2 ± 0.02	0.9249 ± 0.0005	353.2 ± 0.02	2.85 ± 0.009	
358.2 ± 0.02	0.9210 ± 0.0005	358.2 ± 0.02	2.53 ± 0.008	
363.2 ± 0.02	0.9171 ± 0.0005	363.2 ± 0.02	2.26 ± 0.007	
368.2 ± 0.02	0.9132 ± 0.0005	368.2 ± 0.02	2.03 ± 0.007	
373.2 ± 0.02	0.9093 ± 0.0005	373.2 ± 0.02	1.84 ± 0.006	
HDES50-Thymol : Lidocaine (2:1)				
		293.2 ± 0.03	124.00 ± 5.000	
		298.2 ± 0.03	99.00 ± 5.000	
		303.2 ± 0.03	68.00 ± 5.000	
		308.2 ± 0.03	48.00 ± 5.000	
Not reported		313.2 ± 0.03	35.00 ± 5.000	(Dietz et al., 2019)
		318.2 ± 0.03	26.00 ± 5.000	
		323.2 ± 0.03	20.00 ± 5.000	
		328.2 ± 0.03	16.00 ± 5.000	
HDES51-Trioctylphosphine Oxide : Decanoic Acid (1:1)				
293.2 ± 0.02	0.8847 ± 0.0003	293.2 ± 0.02	48.55 ± 0.030	
298.2 ± 0.02	0.8813 ± 0.0003	298.2 ± 0.02	39.03 ± 0.030	
303.2 ± 0.02	0.8779 ± 0.0003	303.2 ± 0.02	31.58 ± 0.030	
308.2 ± 0.02	0.8746 ± 0.0003	308.2 ± 0.02	25.61 ± 0.030	
313.2 ± 0.02	0.8712 ± 0.0003	313.2 ± 0.02	21.00 ± 0.030	
318.2 ± 0.02	0.8679 ± 0.0003	318.2 ± 0.02	17.08 ± 0.030	(Riveiro et al., 2020)
323.2 ± 0.02	0.8645 ± 0.0003	323.2 ± 0.02	14.82 ± 0.030	
328.2 ± 0.02	0.8612 ± 0.0003	328.2 ± 0.02	12.40 ± 0.030	
333.2 ± 0.02	0.8579 ± 0.0003	333.2 ± 0.02	10.59 ± 0.030	
338.2 ± 0.02	0.8545 ± 0.0003	338.2 ± 0.02	9.10 ± 0.030	
343.2 ± 0.02	0.8512 ± 0.0003	343.2 ± 0.02	7.85 ± 0.030	

HDES52- Trioctylphosphine Oxide: Dodecanoic Acid (1:1)				
293.2 ± 0.02	0.8828 ± 0.0003	293.2 ± 0.02	58.75 ± 0.030	
298.2 ± 0.02	0.8795 ± 0.0003	298.2 ± 0.02	46.51 ± 0.030	
303.2 ± 0.02	0.8762 ± 0.0003	303.2 ± 0.02	37.23 ± 0.030	
308.2 ± 0.02	0.8728 ± 0.0003	308.2 ± 0.02	30.14 ± 0.030	
313.2 ± 0.02	0.8695 ± 0.0003	313.2 ± 0.02	24.76 ± 0.030	
318.2 ± 0.02	0.8662 ± 0.0003	318.2 ± 0.02	20.61 ± 0.030	(Riveiro et al., 2020)
323.2 ± 0.02	0.8629 ± 0.0003	323.2 ± 0.02	17.12 ± 0.030	
328.2 ± 0.02	0.8595 ± 0.0003	328.2 ± 0.02	14.61 ± 0.030	
333.2 ± 0.02	0.8562 ± 0.0003	333.2 ± 0.02	12.49 ± 0.030	
338.2 ± 0.02	0.8529 ± 0.0003	338.2 ± 0.02	10.71 ± 0.030	
343.2 ± 0.02	0.8496 ± 0.0003	343.2 ± 0.02	9.23 ± 0.030	
HDES53- Trioctylphosphine Oxide: Phenol (1:2)				
293.2 ± 0.02	0.9350 ± 0.0005	293.2 ± 0.02	16.47 ± 0.500	
298.2 ± 0.02	0.9330 ± 0.0005	298.2 ± 0.02	12.38 ± 0.500	
303.2 ± 0.02	0.9270 ± 0.0005	303.2 ± 0.02	9.52 ± 0.500	
313.2 ± 0.02	0.9230 ± 0.0005	313.2 ± 0.02	6.18 ± 0.500	
323.2 ± 0.02	0.9120 ± 0.0005	323.2 ± 0.02	4.35 ± 0.500	(Gilmore et al., 2018)
333.2 ± 0.02	0.9050 ± 0.0005	333.2 ± 0.02	3.24 ± 0.500	
343.2 ± 0.02	0.9020 ± 0.0005	343.2 ± 0.02	2.53 ± 0.500	
353.2 ± 0.02	0.8950 ± 0.0005	353.2 ± 0.02	2.04 ± 0.500	
363.2 ± 0.02	0.8880 ± 0.0005	363.2 ± 0.02	1.73 ± 0.500	
HDES54- Trioctylphosphine Oxide: Phenol (1:1)				
293.2 ± 0.02	0.9100 ± 0.0005	293.2 ± 0.02	54.00 ± 0.500	
298.2 ± 0.02	0.9070 ± 0.0005	298.2 ± 0.02	43.00 ± 0.500	
303.2 ± 0.02	0.9040 ± 0.0005	313.2 ± 0.02	22.00 ± 0.500	
323.2 ± 0.02	0.8900 ± 0.0005	323.2 ± 0.02	15.02 ± 0.500	
333.2 ± 0.02	0.8830 ± 0.0005	333.2 ± 0.02	10.76 ± 0.500	(Gilmore et al., 2018)
343.2 ± 0.02	0.8770 ± 0.0005			
353.2 ± 0.02	0.8700 ± 0.0005			
363.2 ± 0.02	0.8630 ± 0.0005			

Table A.2. Experimental electrical conductivity data [mS·cm^{-1}] of the DESs measured at P = 1.01 bar.

T (K)	k (mS.cm^{-1})	Ref.	T (K)	k (mS.cm^{-1})	Ref.
DES1- BTPPCl:EG (1:3)			**DES2-** BTPPCl:Gly (1:5)		
328.15	0.485		328.15	0.163	
338.15	0.199		338.15	0.019	
348.15	0.016	(Kareem et al., 2010)	348.15	0.017	(Kareem et al., 2010)
358.15	0.015		358.15	0.015	
368.15	0.014		368.15	0.014	
DES3- MTPPBr:EG (1:5.25)			**DES4-** MTPPBr:EG (1:4)		
298.15	1.942		298.15	1.557	
303.15	2.570	(Bagh et al., 2013)	303.15	2.193	(Kareem et al., 2010)
308.15	3.103		308.15	2.649	
313.15	3.845		313.15	3.246	

T	Value		T	Value
318.15	4.437		318.15	3.858
323.15	5.072		323.15	4.405
328.15	6.279		328.15	5.395
333.15	7.110		333.15	6.221
338.15	8.169		338.15	7.423
343.15	9.496		343.15	8.192
348.15	10.310		348.15	9.074
353.15	11.196		353.15	10.027

DES5- MTPPBr:EG (1:3)			**DES6-** MTPPBr:Gly (1:4)		
298.15	1.092		298.15	0.116	
303.15	1.598		303.15	0.198	
308.15	1.9136		308.15	0.37	
313.15	2.502		313.15	0.41	
318.15	2.964		318.15	0.607	
323.15	3.265	(Bagh et al., 2013)	323.15	0.816	(Bagh et al., 2013)
328.15	4.307		328.15	0.965	
333.15	5.129		333.15	1.233	
338.15	5.797		338.15	1.608	
343.15	6.723		343.15	1.971	
348.15	7.372		348.15	2.874	
353.15	8.114		353.15	3.594	

DES7- MTPPBr:Gly (1:3)			**DES8-** MTPPBr:Gly (1:1.75)		
298.15	0.103		298.15	0.062	
303.15	0.172		303.15	0.124	
308.15	0.319		308.15	0.186	
313.15	0.394		313.15	0.277	
318.15	0.549		318.15	0.405	
323.15	0.719	(Bagh et al., 2013)	323.15	0.496	(Bagh et al., 2013)
328.15	0.927		328.15	0.701	
333.15	1.124		333.15	0.858	
338.15	1.487		338.15	1.16	
343.15	1.778		343.15	1.493	
348.15	2.196		348.15	1.811	
353.15	2.599		353.15	2.154	

DES9- MTPPBr:TFA (1:8)			**DES10-** ChCl:EG (1:2.5)		
278.15	0.134		298.15	8.317	
288.15	0.351		303.15	10.665	
298.15	0.848		308.15	12.07	
308.15	1.821		313.15	14.133	
318.15	2.820		318.15	16.558	
328.15	3.490	(Bagh et al., 2013)	323.15	17.977	(Bagh et al., 2013)
338.15	4.180		328.15	21.257	
348.15	4.820		333.15	24.247	
358.15	5.500		338.15	25.152	
368.15	6.090		343.15	26.275	
			348.15	27.799	
			353.15	28.690	

DES11- ChCl:EG (1:2)			**DES12-** ChCl:EG (1:1.75)		
298.15	7.332	(Bagh et al., 2013)	298.15	6.801	(Bagh et al., 2013)
303.15	10.191		303.15	9.138	

308.15	11.407		308.15	10.857	
313.15	13.553		313.15	12.935	
318.15	15.895		318.15	14.794	
323.15	17.185		323.15	16.335	
328.15	20.227		328.15	18.393	
333.15	22.991		333.15	20.102	
338.15	24.200		338.15	21.773	
343.15	25.599		343.15	23.474	
348.15	27.065		348.15	24.750	
353.15	28.072		353.15	26.043	
DES13- ChCl:Gly (1:3)			**DES14-** ChCl:Gly (1:2)		
298.15	1.463		298.15	1.749	
303.15	1.553		303.15	1.951	
308.15	2.035		308.15	2.549	
313.15	2.570		313.15	3.004	
318.15	3.112		318.15	3.991	
323.15	3.816	(Bagh et al., 2013)	323.15	5.120	(Bagh et al., 2013)
328.15	4.811		328.15	6.046	
333.15	5.757		333.15	7.187	
338.15	6.717		338.15	8.160	
343.15	7.805		343.15	8.955	
348.15	9.286		348.15	10.629	
353.15	10.800		353.15	12.191	
DES15- ChCl:Gly (1:1)			**DES16-** DEACl:EG (1:4)		
298.15	1.929		298.15	5.661	
303.15	2.191		303.15	6.994	
308.15	3.161		308.15	8.245	
313.15	4.603		313.15	9.699	
318.15	5.864		318.15	11.579	
323.15	6.668	(Bagh et al., 2013)	323.15	13.408	(Bagh et al., 2013)
328.15	7.805		328.15	15.086	
333.15	8.980		333.15	17.137	
338.15	9.863		338.15	18.755	
343.15	11.548		343.15	20.286	
348.15	11.548		348.15	22.262	
353.15	12.954		353.15	24.053	
DES17- DEACl:EG (1:3)			**DES18-** DEACl:EG (1:2.5)		
298.15	5.429		298.15	5.120	
303.15	6.878		303.15	6.627	
308.15	8.305		308.15	7.940	
313.15	9.486		313.15	9.283	
318.15	11.339		318.15	10.955	
323.15	13.147	(Bagh et al., 2013)	323.15	12.539	(Bagh et al., 2013)
328.15	14.769		328.15	14.330	
333.15	16.664		333.15	16.161	
338.15	18.395		338.15	17.779	
343.15	19.900		343.15	19.417	
348.15	21.924		348.15	21.347	
353.15	23.667		353.15	23.097	
DES19- DEACl:Gly (1:4)			**DES20-** DEACl:Gly (1:3)		

T (K)			T (K)		
298.15	0.487		298.15	0.602	
303.15	0.78		303.15	0.958	
308.15	1.099		308.15	1.041	
313.15	1.387		313.15	1.562	
318.15	1.878		318.15	2.112	
323.15	2.357	(Bagh et al., 2013)	323.15	2.637	(Bagh et al., 2013)
328.15	2.716		328.15	3.426	
333.15	3.246		333.15	4.086	
338.15	3.962		338.15	4.916	
343.15	4.646		343.15	5.748	
348.15	5.335		348.15	6.474	
353.15	6.095		353.15	7.1	

DES21- DEACl:Gly (1:2)

T (K)	pH	Ref.
298.15	0.75	
303.15	1.177	
308.15	1.635	
313.15	2.067	
318.15	2.716	
323.15	3.381	(Bagh et al., 2013)
328.15	3.903	
333.15	4.878	
338.15	5.754	
343.15	6.521	
348.15	7.754	
353.15	9.109	

Table A.3. Experimental pH data of the DESs measured at P = 1.01 bar.

T (K)	pH	Ref.	T (K)	pH	Ref.
DES1 - ATPPB:DEG:H_2O (1:4:0.17)			**DES1.1 - ATPPB:DEG:H_2O (1:10:0.31)**		
293.15	1.49		293.15	4.05	
303.15	1.31		303.15	3.85	
313.15	1.09	(Ghaedi et al., 2018)	313.15	3.72	(Ghaedi et al., 2018)
323.15	0.87		323.15	3.55	
333.15	0.68		333.15	3.35	
343.15	0.50		343.15	3.23	
DES1.2 - ATPPB:DEG:H_2O (1:16:0.39)			**DES2 - ATPPB:TEG:H_2O (1:4:0.18)**		
293.15	4.21		293.15	1.40	
303.15	3.98		303.15	1.10	
313.15	3.81	(Ghaedi et al., 2018)	313.15	0.84	(Ghaedi et al., 2018)
323.15	3.62		323.15	0.59	
333.15	3.45		333.15	0.35	
343.15	3.34		343.15	0.15	
DES2.1 - ATPPB:TEG:H_2O (1:10:0.35)			**DES2.2 - ATPPB:TEG: :H_2O (1:16:0.56)**		
293.15	3.15		293.15	3.42	
303.15	2.88		303.15	3.21	
313.15	2.60	(Ghaedi et al., 2018)	313.15	3.01	(Ghaedi et al., 2018)
323.15	2.32		323.15	2.82	
333.15	2.10		333.15	2.65	

343.15	1.90		343.15	2.47	
DES3 - BTPC:EG (1:3)			**DES4 -** BTPC:Gly (1:5)		
298.15	5.71		298.15	6.90	
303.15	5.70		303.15	6.91	
308.15	5.69		308.15	6.92	
313.15	5.68		313.15	6.94	
318.15	5.66		318.15	6.95	
323.15	5.65	(Kareem et al., 2010)	323.15	6.96	(Kareem et al., 2010)
328.15	5.64		328.15	6.97	
333.15	5.63		333.15	6.98	
338.15	5.62		338.15	6.99	
343.15	5.61		343.15	7.00	
348.15	5.60		348.15	7.01	
353.15	5.59		353.15	7.02	
DES5 - ChCl:CA:H_2O (1:1:1.33)			**DES5.1** - ChCl:CA:H_2O (2:1:1.44)		
298.15	1.72		298.15	1.33	
303.15	1.61		303.15	1.28	
308.15	1.49		308.15	1.23	
313.15	1.38		313.15	1.18	
318.15	1.26	(Skulcova et al., 2018)	318.15	1.13	(Skulcova et al., 2018)
323.15	1.15		323.15	1.08	
328.15	1.03		328.15	1.03	
333.15	0.92		333.15	0.98	
DES6 - ChCl:DEA (1:6)			**DES7 -** ChCl:EG:H_2O (1:2:0.33)		
295.15	11.47		298.15	4.38	
313.15	10.68		303.15	4.33	
328.15	10.44	(Adeyemi et al., 2018)	308.15	4.27	
343.15	10.15		313.15	4.22	
353.15	9.98		318.15	4.16	(Skulcova et al., 2018)
			323.15	4.11	
			328.15	4.05	
			333.15	4.00	
DES8 - ChCl:Fru (1:1)			**DES8.1** - ChCl:Fru (1.5:1)		
298.15	6.10		298.15	6.91	
308.15	5.95		308.15	6.82	
318.15	5.71		318.15	6.76	
328.15	5.22	(Hayyan et al., 2012)	328.15	6.61	(Hayyan et al., 2012)
338.15	4.80		338.15	6.55	
348.15	4.58		348.15	6.41	
358.15	4.43		358.15	6.32	
DES8.2 - ChCl:Fru (2:1)			**DES8.3** - ChCl:Fru (2.5:1)		
298.15	6.65		298.15	7.10	
308.15	6.45		308.15	6.98	
318.15	6.21		318.15	6.88	
328.15	5.90	(Hayyan et al., 2012)	328.15	6.75	(Hayyan et al., 2012)
338.15	5.54		338.15	6.63	
348.15	5.20		348.15	6.52	
358.15	4.85		358.15	6.41	
DES9 - ChCl:Glu (1:1)			**DES9.1** - ChCl:Glu (1.5:1)		
298.15	6.83	(Hayyan et al., 2013)	298.15	7.10	(Hayyan et al., 2013)

303.15	6.78		303.15	7.00	
308.15	6.72		308.15	6.90	
313.15	6.67		313.15	6.80	
318.15	6.62		318.15	6.70	
323.15	6.57		323.15	6.60	
328.15	6.51		328.15	6.50	
333.15	6.46		333.15	6.40	
338.15	6.41		338.15	6.30	
343.15	6.35		343.15	6.20	
348.15	6.30		348.15	6.09	
353.15	6.25		353.15	5.99	
DES9.2 - ChCl:Glu (2:1)			**DES9.3** - ChCl:Glu (2.5:1)		
298.15	7.00		298.15	7.11	
303.15	6.95		303.15	7.05	
308.15	6.90		308.15	6.99	
313.15	6.85		313.15	6.94	
318.15	6.80		318.15	6.88	
323.15	6.75	(Hayyan et al., 2013)	323.15	6.82	(Hayyan et al., 2013)
328.15	6.70		328.15	6.76	
333.15	6.65		333.15	6.71	
338.15	6.60		338.15	6.65	
343.15	6.55		343.15	6.59	
348.15	6.50		348.15	6.53	
353.15	6.45		353.15	6.47	
DES10 - ChCl:Gly:H_2O (1:2:0.33)			**DES11** - ChCl:GlyA:H_2O (1:3:0.44)		
298.15	4.47		298.15	1.24	
303.15	4.42		303.15	1.20	
308.15	4.37		308.15	1.17	
313.15	4.32	(Skulcova et al., 2018)	313.15	1.13	(Skulcova et al., 2018)
318.15	4.27		318.15	1.10	
323.15	4.22		323.15	1.06	
328.15	4.17		328.15	1.03	
333.15	4.12		333.15	0.99	
DES12 - ChCl:LacA:H_2O (1:5:0.67)			**DES12.1** - ChCl:LacA:H_2O (1:10:1.22)		
298.15	1.73		298.15	1.77	
303.15	1.62		303.15	1.67	
308.15	1.52		308.15	1.56	
313.15	1.41	(Skulcova et al., 2018)	313.15	1.46	(Skulcova et al., 2018)
318.15	1.31		318.15	1.35	
323.15	1.20		323.15	1.25	
328.15	1.10		328.15	1.14	
333.15	0.99		333.15	1.04	
DES13 - ChCl:MA:H_2O (1:1:0.22)			**DES13.1** - ChCl:MA:H_2O (2:1:0.33)		
298.15	1.61		298.15	1.93	
303.15	1.51		303.15	1.82	
308.15	1.42		308.15	1.72	
313.15	1.32	(Skulcova et al., 2018)	313.15	1.61	(Skulcova et al., 2018)
318.15	1.23		318.15	1.51	
323.15	1.13		323.15	1.40	
328.15	1.04		328.15	1.30	

333.15	0.94		333.15	1.19	
ES14 - ChCl:MalA:H_2O (1:1:0.22)			**ES15 -** ChCl:MDEA (1:6)		
298.15	1.28		295.15	11.04	
303.15	1.16		313.15	10.39	
308.15	1.03		328.15	10.35	(Adeyemi et al., 2018)
313.15	0.91		343.15	10.06	
318.15	0.78	(Skulcova et al., 2018)	353.15	9.87	
323.15	0.66				
328.15	0.53				
333.15	0.41				
DES16 - ChCl:MEA (1:6)			**DES17** - ChCl:OxaA:H_2O (1:1:2.44)		
295.15	12.81		298.15	1.21	
313.15	12.24		303.15	1.05	
328.15	11.73	(Adeyemi et al., 2018)	308.15	0.88	
343.15	11.36		313.15	0.72	
353.15	11.12		318.15	0.55	(Skulcova et al., 2018)
			323.15	0.39	
			328.15	0.22	
			333.15	0.06	
DES18 - ChCl:TFA (1:2)			**DES19** - DEEAC:MalA (1:1)		
298.15	3.97		298.15	2.41	
303.15	3.96		303.15	2.40	
308.15	3.95		308.15	2.39	
313.15	3.94		313.15	2.38	
318.15	3.93		318.15	2.36	
323.15	3.92		323.15	2.35	
328.15	3.91	(Bahadori et al., 2013)	328.15	2.34	(Bahadori et al., 2013)
333.15	3.90		333.15	2.33	
338.15	3.89		338.15	2.32	
343.15	3.88		343.15	2.31	
348.15	3.87		348.15	2.30	
353.15	3.86		353.15	2.29	
DES20 - EAC:Gly: :H_2O (1:3:0.64)			**DES20.1** - EAC:Gly:H_2O (1:4:0.95)		
303.15	2.04		303.15	2.42	
313.15	2.03		313.15	2.40	
323.15	2.01		323.15	2.38	
333.15	2.00	(Saputra et al., 2020)	333.15	2.36	(Saputra et al., 2020)
343.15	1.99		343.15	2.35	
353.15	1.97		353.15	2.33	
DES20.2 - EAC:Gly:H_2O (1:5:1.02)			**DES21** - LacA:Ala:H_2O (9:1:1.11)		
303.15	2.57		298.15	2.15	
313.15	2.54		303.15	2.05	
323.15	2.52	(Saputra et al., 2020)	308.15	1.94	
333.15	2.49		313.15	1.84	
343.15	2.47		318.15	1.73	(Skulcova et al., 2018)
353.15	2.44		323.15	1.63	
			328.15	1.52	
			333.15	1.42	
DES22 - LacA:Bet:H_2O (2:1:0.33)			**DES23** - LacA:Glyi:H_2O (2:1:0.33)		
298.15	2.45	(Skulcova et al., 2018)	298.15	2.74	(Skulcova et al., 2018)

303.15	2.36		303.15	2.66	
308.15	2.28		308.15	2.58	
313.15	2.19		313.15	2.50	
318.15	2.11		318.15	2.42	
323.15	2.02		323.15	2.34	
328.15	1.94		328.15	2.26	
333.15	1.85		333.15	2.18	
DES23.1 - LacA:Glyi:H$_2$O (9:1:1.11)			**DES24** - MA:Suc:H$_2$O (1:1:0.22)		
298.15	2.27		298.15	2.05	
303.15	2.17		303.15	1.95	
308.15	2.06		308.15	1.85	
313.15	1.96	(Skulcova et al., 2018)	313.15	1.75	(Skulcova et al., 2018)
318.15	1.85		318.15	1.65	
323.15	1.75		323.15	1.55	
328.15	1.64		328.15	1.45	
333.15	1.54		333.15	1.35	
DES25 - MTPB:EG (1:4)			**DES26** - MTPB:Gly (1:1.75)		
298.15	6.35		298.15	6.97	
303.15	6.30		303.15	6.94	
308.15	6.26		308.15	6.92	
313.15	6.22		313.15	6.89	
318.15	6.17		318.15	6.87	
323.15	6.13		323.15	6.84	
328.15	6.08	(Kareem et al., 2010)	328.15	6.82	(Kareem et al., 2010)
333.15	6.04		333.15	6.79	
338.15	5.99		338.15	6.77	
343.15	5.95		343.15	6.75	
348.15	5.90		348.15	6.72	
353.15	5.86		353.15	6.70	
DES27 - MTPB: TFA (1:8)			**DES28 -** TBAC:EG (1:2)		
298.15	2.71		293.15	9.10	
303.15	2.77		303.15	8.93	
308.15	2.83		313.15	8.72	
313.15	2.88		323.15	8.39	(Mjalli et al., 2014)
318.15	2.94		333.15	8.03	
323.15	3.00		343.15	7.79	
328.15	3.05	(Kareem et al., 2010)	353.15	7.51	
333.15	3.11				
338.15	3.17				
343.15	3.22				
348.15	3.28				
353.15	3.34				
DES28.1 - TBAC:EG (1:3)			**DES28.2 -** TBAC:EG (1:4)		
293.15	9.20		293.15	9.35	
303.15	8.96		303.15	9.20	
313.15	8.74		313.15	9.04	
323.15	8.54	(Mjalli et al., 2014)	323.15	8.86	(Mjalli et al., 2014)
333.15	8.21		333.15	8.60	
343.15	7.99		343.15	8.37	
353.15	7.76		353.15	8.19	

DES29 - TBAC:Gly (1:3)			DES29.1 - TBAC:Gly (1:4)		
293.15	6.51		293.15	8.95	
303.15	6.45		303.15	8.70	
313.15	6.38		313.15	8.43	
323.15	6.31	(Mjalli et al., 2014)	323.15	8.19	(Mjalli et al., 2014)
333.15	6.25		333.15	7.94	
343.15	6.19		343.15	7.71	
353.15	6.11		353.15	7.50	
DES29.2 - TBAC:Gly (1:5)			DES30 - TBAC:TEG (1:1)		
293.15	6.81		293.15	6.40	
303.15	6.74		303.15	6.32	
313.15	6.67		313.15	6.22	
323.15	6.60	(Mjalli et al., 2014)	323.15	6.16	(Mjalli et al., 2014)
333.15	6.53		333.15	6.07	
343.15	6.46		343.15	6.01	
353.15	6.42		353.15	5.92	
DES30.1 - TBAC:TEG (2:1)			DES30.2 - TBAC:TEG (3:1)		
293.15	6.97		293.15	7.70	
303.15	6.84		303.15	7.54	
313.15	6.72		313.15	7.37	
323.15	6.58	(Mjalli et al., 2014)	323.15	7.18	(Mjalli et al., 2014)
333.15	6.45		333.15	7.02	
343.15	6.33		343.15	6.87	
353.15	6.21		353.15	6.73	
DES30.3 - TBAC:TEG (4:1)			DES31 - TPAB:EG (1:3)		
293.15	8.06		298.15	6.41	
303.15	7.89		303.15	6.37	
313.15	7.70		308.15	6.33	
323.15	7.71	(Mjalli et al., 2014)	313.15	6.29	
333.15	7.54		318.15	6.25	
343.15	7.18		323.15	6.21	
353.15	7.03		328.15	6.17	(Jibril et al., 2014)
			333.15	6.13	
			338.15	6.09	
			343.15	6.05	
			348.15	6.01	
			353.15	5.97	
DES31.1 - TPAB:EG (1:4)			DES31.2 - TPAB:EG (1:5)		
298.15	6.53		298.15	7.23	
303.15	6.49		303.15	7.17	
308.15	6.46		308.15	7.11	
313.15	6.42		313.15	7.05	
318.15	6.39		318.15	6.99	
323.15	6.35		323.15	6.93	
328.15	6.32	(Jibril et al., 2014)	328.15	6.87	(Jibril et al., 2014)
333.15	6.28		333.15	6.81	
338.15	6.25		338.15	6.75	
343.15	6.21		343.15	6.69	
348.15	6.18		348.15	6.63	
353.15	6.14		353.15	6.57	

DES32 - TPAB:Gly (1:2)			DES32.1 - TPAB:Gly (1:3)		
298.15	6.40		298.15	5.96	
303.15	6.36		303.15	5.95	
308.15	6.33		308.15	5.94	
313.15	6.30		313.15	5.93	
318.15	6.26		318.15	5.92	
323.15	6.23	(Jibril et al., 2014)	323.15	5.91	(Jibril et al., 2014)
328.15	6.20		328.15	5.90	
333.15	6.17		333.15	5.89	
338.15	6.13		338.15	5.88	
343.15	6.10		343.15	5.87	
348.15	6.07		348.15	5.86	
353.15	6.03		353.15	5.85	
DES32.2 - TPAB:Gly (1:4)			**DES33 - TPAB:TEG (1:2.5)**		
298.15	5.85		298.15	5.09	
303.15	5.83		303.15	5.06	
308.15	5.81		308.15	5.04	
313.15	5.79		313.15	5.01	
318.15	5.78		318.15	4.99	
323.15	5.76	(Jibril et al., 2014)	323.15	4.96	(Jibril et al., 2014)
328.15	5.74		328.15	4.93	
333.15	5.72		333.15	4.91	
338.15	5.70		338.15	4.88	
343.15	5.68		343.15	4.86	
348.15	5.66		348.15	4.83	
353.15	5.64		353.15	4.80	
DES33.1 - TPAB:TEG (1:3)			**DES33.2 - TPAB:TEG (1:4)**		
298.15	5.22		298.15	5.15	
303.15	5.19		303.15	5.12	
308.15	5.17		308.15	5.10	
313.15	5.14		313.15	5.07	
318.15	5.12		318.15	5.05	
323.15	5.09	(Jibril et al., 2014)	323.15	5.02	(Jibril et al., 2014)
328.15	5.06		328.15	4.99	
333.15	5.04		333.15	4.97	
338.15	5.01		338.15	4.94	
343.15	4.99		343.15	4.92	
348.15	4.96		348.15	4.89	
353.15	4.94		353.15	4.87	
DES34 - ChCl:LacA:H_2O (1:9:1.11)			**DES35 - Bet:MA:H_2O (1:1:1.5)**		
298.15	1.61		288.15	3.39	
303.15	1.49		298.15	3.16	
308.15	1.38		308.15	2.98	(Mitar et al., 2019)
313.15	1.26		318.15	2.83	
318.15	1.15	(Skulcova et al., 2018)	328.15	2.62	
323.15	1.03				
328.15	0.92				
333.15	0.80				
DES35.1 - Bet:MA:H_2O (1:1:6)			**DES35.2 - Bet:MA:H_2O (1:1:13.9)**		
288.15	3.40	(Mitar et al., 2019)	288.15	2.95	(Mitar et al., 2019)

T (K)	value	ref	T (K)	value	ref
298.15	3.07		298.15	2.88	
308.15	3.20		308.15	2.76	
318.15	3.01		318.15	2.61	
328.15	2.90		328.15	2.50	
DES36 - ChCl:CA:H$_2$O (2:1:3)			**DES36.1 -** ChCl:CA:H$_2$O (2:1:11.5)		
288.15	0.63		288.15	0.88	
298.15	0.62		298.15	0.93	
308.15	0.62	(Mitar et al., 2019)	308.15	0.96	(Mitar et al., 2019)
318.15	0.65		318.15	0.97	
328.15	0.67		328.15	0.98	
DES36.2 - ChCl:CA:H$_2$O (2:1:26.7)			**DES37 -** ChCl:MA:H$_2$O (1:1:1.7)		
288.15	1.11		288.15	0.22	
298.15	1.16		298.15	0.23	
308.15	1.18	(Mitar et al., 2019)	308.15	0.27	(Mitar et al., 2019)
318.15	1.19		318.15	0.31	
328.15	1.18		328.15	0.34	
ES37.1 - ChCl:MA:H$_2$O (1:1:6.5)			**ES37.2 -** ChCl:MA:H$_2$O (1:1:15.2)		
288.15	0.55		288.15	1.10	
298.15	0.67		298.15	1.06	
308.15	0.75	(Mitar et al., 2019)	308.15	1.10	(Mitar et al., 2019)
318.15	0.77		318.15	1.11	
328.15	0.78		328.15	1.11	
DES38 - Bet:CA:H$_2$O (1:1:1.9)			**DES38.1 -** Bet:CA:H$_2$O (1:1:7.4)		
288.15	2.81		288.15	2.77	
298.15	2.63		298.15	2.60	
308.15	2.46	(Mitar et al., 2019)	308.15	2.44	(Mitar et al., 2019)
318.15	2.29		318.15	2.30	
328.15	2.15		328.15	2.15	
DES38.2 - Bet:CA:H$_2$O (1:1:17.2)			**DES39 -** ChCl:Pro:MA:H$_2$O (1:1:1:2.4)		
288.15	2.75		288.15	3.63	
298.15	2.59		298.15	3.62	
308.15	2.44	(Mitar et al., 2019)	308.15	3.65	(Mitar et al., 2019)
318.15	2.26		318.15	3.63	
328.15	2.12		328.15	3.58	
DES39.1 - ChCl:Pro:MA:H$_2$O (1:1:1:9.3)			**DES39.2 -** ChCl:Pro:MA:H$_2$O (1:1:1:21.6)		
288.15	3.35		288.15	2.95	
298.15	3.21		298.15	2.97	
308.15	3.08	(Mitar et al., 2019)	308.15	2.99	(Mitar et al., 2019)
318.15	2.95		318.15	3.02	
328.15	2.80		328.15	3.03	
DES40 - Pro:MA:H$_2$O (1:1:1.5)			**DES40.1 -** Pro:MA:H$_2$O (1:1:5.9)		
288.15	2.17		288.15	2.87	
298.15	2.24		298.15	2.67	
308.15	2.23	(Mitar et al., 2019)	308.15	2.57	(Mitar et al., 2019)
318.15	2.22		318.15	2.42	
328.15	2.19		328.15	2.29	
DES40.2 - Pro:MA:H$_2$O (1:1:13.8)			**DES41 -** MA:Glu:H$_2$O (1:1:1.9)		
288.15	2.86		288.15	0.37	
298.15	2.67	(Mitar et al., 2019)	298.15	0.41	(Mitar et al., 2019)
308.15	2.56		308.15	0.46	

318.15	2.42		318.15	0.46	
328.15	2.28		328.15	0.46	
DES41.1 - MA:Glu:H$_2$O (1:1:7.5)			**DES41.2 -** MA:Glu:H$_2$O (1:1:17.4)		
288.15	0.45		288.15	0.76	
298.15	0.49		298.15	0.76	
308.15	0.55	(Mitar et al., 2019)	308.15	0.77	(Mitar et al., 2019)
318.15	0.68		318.15	0.79	
328.15	0.67		328.15	0.81	

Table A.4. Family A's model comparison between the original correlated sign of each descriptor and the sign of its interaction correlation with other descriptors.

	S$_1$ (+)	S$_2$ (−)	S$_3$ (−)	S$_4$ (−)	S$_5$ (+)	S$_6$ (+)	S$_7$ (+)	S$_8$ (+)	T (−)
S$_1$ (+)		−	−	−	+	+	+	−	+
S$_2$ (−)	−		x	x	x	+	−	−	+
S$_3$ (+)	−	x		+	−	+	−	−	−
S$_4$ (−)	−	x	+		x	−	−	−	+
S$_5$ (+)	+	x	−	x		x	+	−	−
S$_6$ (+)	+	+	+	−	x		−	+	x
S$_7$ (+)	+	−	−	−	+	−		+	x
S$_8$ (+)	−	−	−	−	−	+	+		−
T (−)	+	+	−	+	−	x	x	−	

Table A.5. Family B's model comparison between the original correlated sign of each descriptor and the sign of its interaction correlation with other descriptors.

	S$_1$ (+)	S$_2$ (+)	S$_3$ (+)	S$_4$ (+)	S$_5$ (−)	S$_6$ (−)	S$_7$ (−)	S$_8$ (−)	T (−)
S$_1$ (+)		+	−	+	−	−	−	x	−
S$_2$ (+)	+		+	+	+	x	+	+	+
S$_3$ (+)	+	+		−	+	+	+	+	−
S$_4$ (+)	+	+	−		−	x	+	+	x
S$_5$ (−)	−	+	+	−		−	−	−	+
S$_6$ (−)	−	x	+	x	−		−	x	−
S$_7$ (−)	−	+	+	+	−	−		−	+
S$_8$ (−)	x	+	+	+	−	x	−		+
T (−)	−	+	−	x	+	−	+	+	

Appendix B

Table B.1. Specifications and experimental conditions of Agilent 6890 N.

Column	Agilent J&W HP-5 (30 m $\times$ 0.32 mm $\times$ 0.25 μm)
Detector	Flame ionization detector (FID)
Injector temperature	548.2 K
Oven temperature profile	(1) 323.15 K isotherm for 1 min,
	(2) 323.15 – 373.15 K at 20 K.min^{-1},
	(3) 373.15 – 408.15 K at 4 K.min^{-1},
	(4) 408.15 – 588.15 K at 35 K.min^{-1},
	(5) 588.15 K isotherm for 2 min.
Detector temperature	473.2 K
Carrier gas	Helium
Gas flow rate	2 mL.min^{-1}
Injection volume	1 μL
Retention time repeatability	±0.004
Method verification (average standard deviation)	±0.003
Statistical uncertainty (average standard deviation)	±0.003

```
Injection Date   :  11/20/2019 11:55:38 AM
```

```
=====================================================
             Customized Report:   PI Chem 02
=====================================================
 Sorted By       RT
```

Peak #	RT [min]	Type	Width [min]	Area	Area %	Name
1	1.692	VB	0.018	17121.500	47.700	
2	2.250	VV	0.014	443.372	1.235	
3	0.000		0.000	0.000	0.000	
4	2.676	PV	0.019	207.100	0.577	
5	2.733	VV	0.035	50.886	0.142	
6	2.827	VB	0.015	1474.444	4.108	
7	4.949	VV	0.042	16568.809	46.160	
8	0.000		0.000	0.000	0.000	
9	14.491	PV	0.043	28.090	0.078	

```
=====================================================
                *** End of Report ***
```
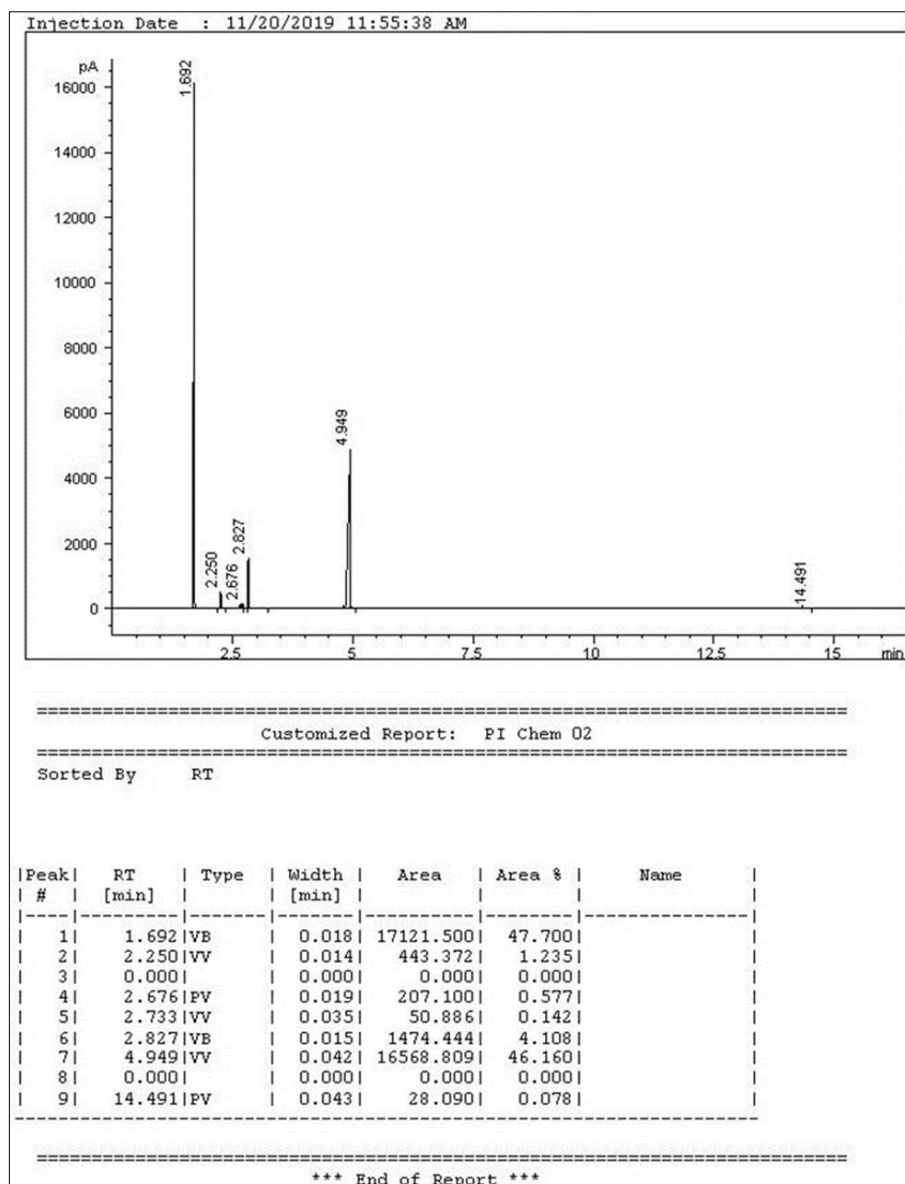
Figure B.1. The GC report of the raffinate phase after extraction from an initial mixture of 80 wt% n-decane, 5 wt% toluene, 5 wt% thiophene, 5 wt% pyridine, 5 wt% pyrrole using TPABr (1:4) at a solvent to feed ratio of 1:1

```
Injection Date   : 11/20/2019 2:19:06 PM
```

```
==============================================================
                 Customized Report:  PI Chem 02
==============================================================
Sorted By      RT


|Peak|   RT    | Type  | Width |   Area   | Area % |    Name      |
| #  | [min]  |       | [min] |          |        |              |
|----|--------|-------|-------|----------|--------|--------------|
|  1 |  1.691 |PV     | 0.018 |17125.977 | 51.937 |              |
|  2 |  1.899 |VV     | 0.045 |   23.009 |  0.070 |              |
|  3 |  2.249 |VV     | 0.014 | 1076.427 |  3.264 |              |
|  4 |  0.000 |       | 0.000 |    0.000 |  0.000 |              |
|  5 |  2.668 |VV     | 0.015 | 1535.131 |  4.656 |              |
|  6 |  2.729 |VV     | 0.038 | 1033.044 |  3.133 |              |
|  7 |  2.826 |VV     | 0.023 | 2373.837 |  7.199 |              |
|  8 |  3.513 |VV     | 0.085 | 8807.969 | 26.712 |              |
|  9 |  3.739 |VV     | 0.160 |  279.046 |  0.846 |              |
| 10 |  4.124 |VV     | 0.070 |  130.914 |  0.397 |              |
| 11 |  4.450 |VV     | 0.168 |   52.245 |  0.158 |              |
| 12 |  4.860 |VV     | 0.020 |  452.843 |  1.373 |              |
| 13 |  0.000 |       | 0.000 |    0.000 |  0.000 |              |
| 14 |  8.025 |PV     | 0.181 |   35.734 |  0.108 |              |
| 15 |  8.372 |VB     | 0.143 |   22.647 |  0.069 |              |
| 16 | 14.492 |PV     | 0.047 |   25.610 |  0.078 |              |
-----------------------------------------------------------------


==============================================================
                  *** End of Report ***
```

Figure B.2. The GC report of the extract phase after extraction from an initial mixture of 80 wt% *n*-decane, 5 wt% toluene, 5 wt% thiophene, 5 wt% pyridine, 5 wt% pyrrole using TPABr (1:4) at a solvent to feed ratio of 1:1

Table B.2. The experimental solubility and *pseudo*-ternary LLE data in weight fractions for systems of {n-decane (1) + toluene/thiophene/pyridine/pyrrole (2) + TPABr:AA 1:4 (3)} measured at 298.2 K and 1.01 bar at a 1:1 solvent to feed ratio. β, S and E are the calculated distribution ratio, selectivity and extraction efficiency values, respectively. The DES weight fraction (w_3) in both phases can be calculated by $w_3 = 1 - w_1 - w_2$.[a]

$w_{2,i}$	alkane-rich phase				DES-rich phase				β_2	β_1	S	E
	$w_{1,R}$		$w_{2,R}$		$w_{1,E}$		$w_{2,E}$					
{*n*-decane (1) + toluene (2) + TPABr:AA 1:4 (3)}												
0%	1.000	±0.000	—	—	0.009	±0.001	—	—	—	0.009	—	—
5%	0.961	±0.001	0.039	±0.001	0.008	±0.001	0.015	±0.001	0.385	0.008	48.1	21.9
10%	0.921	±0.001	0.079	±0.001	0.009	±0.001	0.029	±0.001	0.367	0.010	36.7	21.8
20%	0.844	±0.001	0.156	±0.001	0.009	±0.001	0.055	±0.001	0.353	0.011	32.1	22.1
30%	0.762	±0.003	0.238	±0.003	0.010	±0.001	0.079	±0.001	0.332	0.013	25.5	20.8
40%	0.680	±0.002	0.320	±0.002	0.011	±0.001	0.117	±0.001	0.366	0.016	22.9	19.6
50%	0.587	±0.002	0.413	±0.002	0.011	±0.001	0.138	±0.002	0.334	0.019	17.6	17.6
60%	0.491	±0.003	0.509	±0.003	0.012	±0.001	0.168	±0.001	0.330	0.024	13.8	15.4
70%	0.394	±0.002	0.606	±0.002	0.013	±0.001	0.203	±0.001	0.335	0.033	10.2	13.3
80%	0.284	±0.001	0.716	±0.001	0.015	±0.001	0.258	±0.008	0.360	0.053	6.8	10.4
100%	—	—	1.000	±0.000	—	—	0.481	±0.002	0.481	—	—	—
{*n*-decane (1) + thiophene (2) + TPABr:AA 1:4 (3)}												
0%	1.000	±0.000	—	—	0.009	±0.001	—	—	—	0.009	—	—
5%	0.968	±0.002	0.032	±0.001	0.007	±0.001	0.022	±0.001	0.688	0.007	98.3	35.8
10%	0.935	±0.002	0.065	±0.002	0.008	±0.001	0.044	±0.001	0.677	0.009	75.2	35.8
20%	0.871	±0.001	0.129	±0.001	0.010	±0.001	0.086	±0.001	0.667	0.011	60.6	35.9
30%	0.806	±0.002	0.194	±0.002	0.012	±0.001	0.119	±0.001	0.613	0.015	40.9	35.8
40%	0.739	±0.003	0.261	±0.003	0.013	±0.001	0.171	±0.001	0.655	0.018	36.4	34.8
50%	0.669	±0.008	0.331	±0.008	0.015	±0.001	0.216	±0.001	0.653	0.022	29.7	33.9
60%	0.582	±0.002	0.418	±0.002	0.017	±0.001	0.254	±0.002	0.608	0.029	21.0	30.4
70%	0.499	±0.002	0.501	±0.002	0.020	±0.001	0.301	±0.002	0.601	0.040	15.0	28.3
80%	0.404	±0.002	0.596	±0.002	0.024	±0.001	0.360	±0.001	0.604	0.059	10.2	25.4
100%		Fully miscible, no phase separation.							—	—	—	—
{*n*-decane (1) + pyridine (2) + TPABr:AA 1:4 (3)}												
0%	1.000	±0.000	—	—	0.009	±0.001	—	—	—	0.009	—	—
5%	0.997	±0.001	0.003	±0.001	0.008	±0.001	0.048	±0.001	16.000	0.008	2000.0	94.0
10%	0.993	±0.001	0.007	±0.001	0.009	±0.001	0.095	±0.002	13.571	0.009	1507.9	93.1
20%	0.984	±0.001	0.016	±0.001	0.012	±0.001	0.163	±0.003	10.188	0.012	849.0	92.1
30%	0.973	±0.001	0.027	±0.001	0.015	±0.001	0.225	±0.001	8.333	0.015	555.5	91.0
40%	0.960	±0.002	0.040	±0.002	0.019	±0.001	0.274	±0.002	6.850	0.020	342.5	90.0
50%	0.944	±0.001	0.056	±0.001	0.019	±0.001	0.320	±0.003	5.714	0.020	285.7	88.8
60%	0.930	±0.002	0.070	±0.002	0.024	±0.001	0.359	±0.009	5.129	0.026	197.3	88.3
70%	0.914	±0.001	0.086	±0.001	0.031	±0.001	0.396	±0.006	4.605	0.034	135.4	87.7
80%	0.895	±0.002	0.105	±0.002	0.032	±0.001	0.429	±0.014	4.086	0.036	113.5	86.8
100%		Fully miscible, no phase separation.							—	—	—	—
{*n*-decane (1) + pyrrole (2) + TPABr:AA 1:4 (3)}												
0%	1.000	±0.000	—	—	0.009	±0.001	—	—	—	0.009	—	—
5%	0.999	±0.001	0.001	±0.001	0.011	±0.001	0.045	±0.001	45.000	0.011	4090.9	98.1

10%	0.997	±0.001	0.003	±0.001	0.012	±0.001	0.100	±0.002	33.333	0.012	2777.8	97.0
20%	0.995	±0.001	0.005	±0.001	0.013	±0.001	0.162	±0.002	32.400	0.013	2492.3	97.5
30%	0.992	±0.001	0.008	±0.001	0.016	±0.001	0.232	±0.005	29.000	0.016	1812.5	97.3
40%	0.989	±0.001	0.011	±0.001	0.018	±0.001	0.284	±0.008	25.818	0.018	1434.3	97.3
50%	0.984	±0.001	0.016	±0.001	0.020	±0.001	0.331	±0.010	20.688	0.020	1034.4	96.8
60%	0.980	±0.001	0.020	±0.001	0.021	±0.001	0.370	±0.011	18.500	0.021	881.0	96.7
70%	0.974	±0.001	0.026	±0.001	0.023	±0.001	0.398	±0.006	15.308	0.024	637.8	96.3
80%	0.971	±0.003	0.029	±0.003	0.024	±0.001	0.433	±0.001	14.931	0.025	597.2	96.4
100%	Fully miscible, no phase separation.								—	—	—	—

^aStandard uncertainty in temperature and pressure are $u(T) = ±0.1K$ and $u(P) = ±0.04$ bar, respectively

Table B.3. The experimental solubility and *pseudo*-ternary LLE data in mole fractions for systems of {*n*-decane (1) + toluene/thiophene/pyridine/pyrrole (2) + TPABr:AA 1:4 (3)} measured at 298.2 K and 1.01 bar at a 1:1 solvent to feed ratio.

alkane-rich phase		DES-rich phase	
$x_{1, R}$	$x_{2, R}$	$x_{1, E}$	$x_{2, E}$
{*n*-decane (1) + toluene (2) + TPABr:AA 1:4 (3)}			
1.000	—	0.006	—
0.941	0.059	0.006	0.017
0.883	0.117	0.006	0.032
0.778	0.222	0.006	0.060
0.675	0.325	0.007	0.086
0.579	0.421	0.008	0.128
0.479	0.521	0.008	0.150
0.384	0.616	0.008	0.182
0.296	0.704	0.009	0.220
0.204	0.796	0.010	0.278
—	1.000	—	0.505
{*n*-decane (1) + thiophene (2) + TPABr:AA 1:4 (3)}			
1.000	—	0.006	—
0.947	0.053	0.005	0.026
0.895	0.105	0.006	0.053
0.800	0.200	0.007	0.102
0.711	0.289	0.008	0.140
0.626	0.374	0.009	0.200
0.544	0.456	0.010	0.250
0.452	0.548	0.012	0.292
0.371	0.629	0.013	0.343
0.286	0.714	0.016	0.406
{*n*-decane (1) + pyridine (2) + TPABr:AA 1:4 (3)}			
1.000	—	0.006	—
0.995	0.005	0.006	0.061
0.987	0.013	0.006	0.119
0.972	0.028	0.008	0.200
0.952	0.048	0.010	0.272
0.930	0.070	0.013	0.327

0.904	0.096	0.012	0.378
0.881	0.119	0.016	0.420
0.855	0.145	0.020	0.460
0.826	0.174	0.021	0.494
{*n*-decane (1) + pyrrole (2) + TPABr:AA 1:4 (3)}			
1.000	—	0.006	—
0.998	0.002	0.008	0.067
0.994	0.006	0.008	0.144
0.989	0.011	0.009	0.227
0.983	0.017	0.010	0.315
0.977	0.023	0.011	0.376
0.967	0.033	0.012	0.430
0.959	0.041	0.013	0.472
0.946	0.054	0.014	0.502
0.940	0.060	0.014	0.539

[a]The standard uncertainties of temperature, pressure, and mole fractions are $u(T) = \pm 0.1$ K, $u(P) = \pm 0.04$ bar, and $u(x) = \pm 0.002$, respectively. The DES mole fraction (x_3) in both phases can be calculated by $x_3 = 1 - x_1 - x_2$.[a]
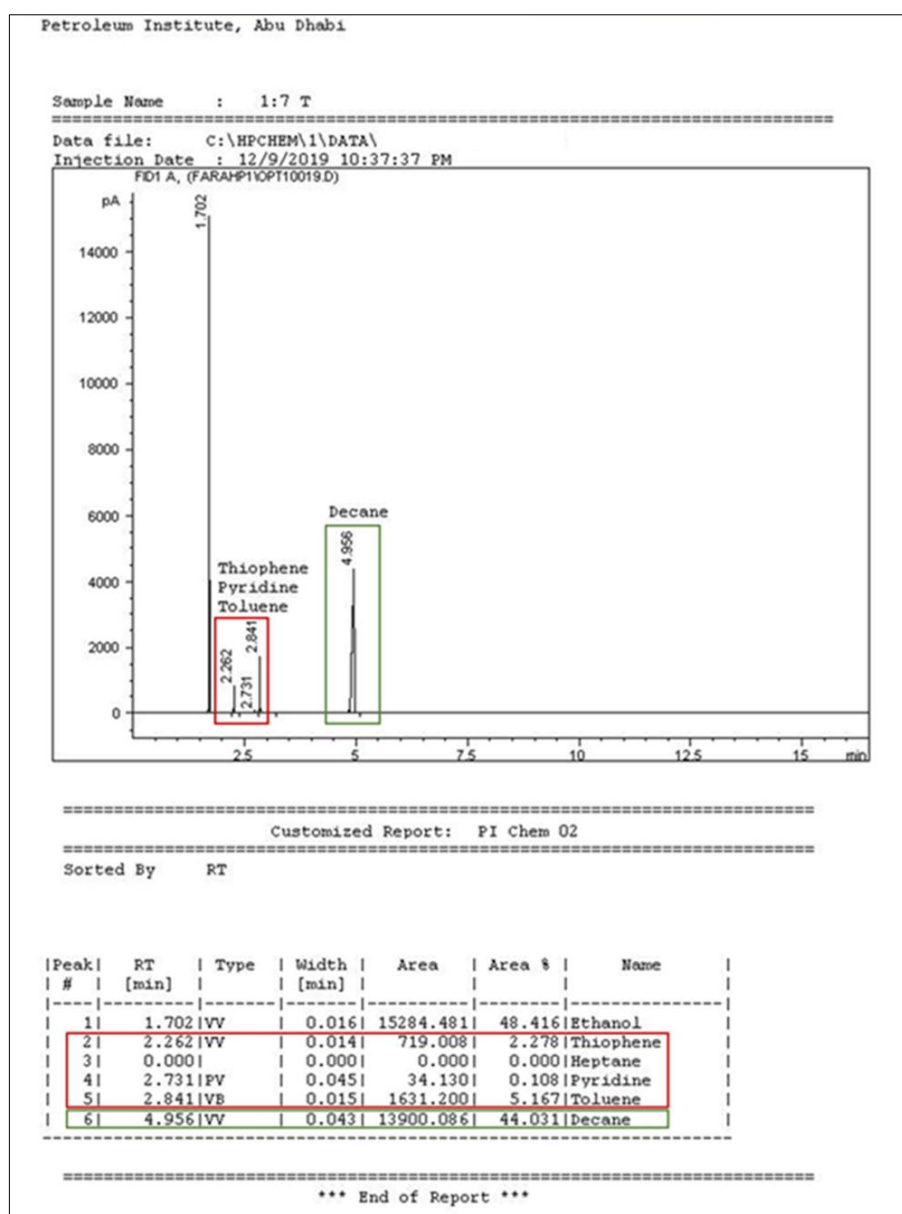
Figure B.3. The GC report for a sample of the *n*-alkane phase after extraction from an initial mixture of 70 wt.% *n*-decane, 10 wt.% thiophene, 10 wt.% pyridine, 10 wt.% toluene using Bet:LevA (1:7) at a solvent-to-feed ratio of 1:1.

```
Petroleum Institute, Abu Dhabi


Sample Name    :   1:7 B
===================================================================================
Data file:     C:\HPCHEM\1\DATA\
Injection Date  :  12/10/2019 1:48:50 AM
         FID1 A, (FARAHP1\OPT10027.D)
```

```
===================================================================================
                      Customized Report:   PI Chem 02
===================================================================================
Sorted By      RT
```

Peak #	RT [min]	Type	Width [min]	Area	Area %	Name
1	1.702	VB	0.019	19785.980	64.014	Ethanol
2	2.262	VB	0.014	725.247	2.346	Thiophene
3	0.000		0.000	0.000	0.000	Heptane
4	2.731	PV	0.017	2035.557	6.586	Pyridine
5	2.841	VV	0.016	529.256	1.712	Toluene
6	3.658	BP	0.249	29.225	0.095	
7	4.956	BV	0.020	40.680	0.132	Decane
8	5.655	PV	0.025	105.992	0.343	
9	6.039	VV	0.079	1431.646	4.632	
10	6.160	VV	0.064	584.961	1.893	
11	6.377	VV	0.129	1798.488	5.819	
12	6.505	VV	0.084	1412.021	4.568	
13	6.531	VV	0.020	317.133	1.026	
14	6.664	VV	0.100	2038.714	6.596	
15	7.043	VV	0.111	49.108	0.159	
16	7.645	VV	0.109	24.808	0.080	

```
-----------------------------------------------------------------------------------

===================================================================================
                      *** End of Report ***
```

Figure B.4. The GC report for a sample of the NADES phase after extraction from an initial mixture of 70 wt.% *n*-decane, 10 wt.% thiophene, 10 wt.% pyridine, 10 wt.% toluene using Bet:LevA (1:7) at a solvent-to-feed ratio of 1:1.

Table B.4. Experimental binary and pseudo-ternary LLE data for systems {*n*-decane (1) + thiophene/pyridine/toluene (2) + Bet:LevA 1:7 (3)} are measured at 298.15 K and 1.01 bar in terms of weight fractions. The calculated distribution coefficient *(β)*, selectivity *(S)* values and extraction efficiency (*E*) are at a 1:1 solvent to feed ratio. The NADES concentration (w_3) in extract phase and raffinate phase can be calculated from the mass balance [a].

	Fuel model-rich phase				NADES-rich phase				β_2	β_1	S	E
$w_{2,i}$	$w_{1,R}$		$w_{2,R}$		$w_{1,E}$		$w_{2,E}$					
{*n*-decane (1) + thiophene (2) + Bet:LevA 1:7 (3)}												
0%	1.000	±0.000	-	-	0.002	±0.001	-	-	-	0.002	-	-
10%	0.927	±0.001	0.073	±0.001	0.003	±0.001	0.035	±0.002	0.479	0.003	159.7	27.0%
20%	0.846	±0.005	0.154	±0.005	0.003	±0.001	0.061	±0.002	0.396	0.004	99.0	23.0%
30%	0.771	±0.002	0.229	±0.002	0.004	±0.001	0.099	±0.003	0.432	0.005	86.4	23.9%
40%	0.698	±0.011	0.302	±0.011	0.005	±0.001	0.132	±0.003	0.437	0.007	62.4	24.5%
50%	0.617	±0.005	0.383	±0.005	0.006	±0.001	0.167	±0.007	0.436	0.010	43.6	23.4%
60%	0.542	±0.009	0.458	±0.009	0.008	±0.001	0.219	±0.008	0.478	0.015	31.9	23.7%
70%	0.451	±0.018	0.549	±0.018	0.010	±0.001	0.263	±0.009	0.479	0.022	21.8	21.3%
80%	0.350	±0.008	0.650	±0.008	0.012	±0.001	0.318	±0.017	0.489	0.034	14.4	18.6%
100%		Fully soluble, no phase separation.							-	-	-	-
{*n*-decane (1) + pyridine (2) + Bet:LevA 1:7 (3)}												
0%	1.000	±0.000	-	-	0.002	±0.001	-	-	-	0.002	-	-
10%	0.999	±0.001	0.001	±0.001	0.002	±0.001	0.097	±0.001	97.00	0.002	48500	99.0%
20%	0.994	±0.001	0.006	±0.001	0.004	±0.001	0.171	±0.004	28.50	0.004	7125	97.0%
30%	0.986	±0.001	0.014	±0.001	0.005	±0.001	0.230	±0.004	16.429	0.005	3285.8	95.3%
40%	0.976	±0.001	0.024	±0.001	0.009	±0.001	0.282	±0.010	11.750	0.009	1305.6	94.0%
50%	0.961	±0.001	0.039	±0.001	0.010	±0.001	0.329	±0.007	8.436	0.010	843.6	92.2%
60%	0.947	±0.003	0.053	±0.003	0.013	±0.001	0.366	±0.019	6.906	0.014	493.3	91.2%
70%	0.936	±0.001	0.064	±0.001	0.015	±0.001	0.393	±0.013	6.141	0.016	383.8	90.9%
80%	0.929	±0.003	0.071	±0.003	0.022	±0.001	0.435	±0.003	6.127	0.024	255.3	91.1%
100%		Fully soluble, no phase separation.							-	-	-	-
{*n*-decane (1) + toluene (2) + Bet:LevA 1:7 (3)}												
0%	1.000	±0.000	-	-	0.002	±0.001	-	-	-	0.002	-	-
10%	0.914	±0.001	0.086	±0.001	0.003	±0.001	0.015	±0.001	0.174	0.003	58.0	15.7%
20%	0.833	±0.006	0.167	±0.006	0.002	±0.001	0.030	±0.001	0.180	0.002	90.0	16.9%
30%	0.741	±0.009	0.259	±0.009	0.002	±0.001	0.049	±0.001	0.189	0.003	63.0	13.7%
40%	0.650	±0.003	0.350	±0.003	0.003	±0.001	0.067	±0.001	0.191	0.005	38.2	12.3%
50%	0.559	±0.008	0.441	±0.008	0.003	±0.001	0.094	±0.004	0.213	0.005	42.6	11.8%
60%	0.468	±0.006	0.532	±0.006	0.003	±0.001	0.110	±0.014	0.207	0.006	34.5	10.9%
70%	0.356	±0.001	0.644	±0.001	0.003	±0.001	0.126	±0.005	0.196	0.008	24.5	8.3%
80%	0.251	±0.004	0.749	±0.004	0.003	±0.001	0.156	±0.002	0.208	0.012	17.3	6.1%
100%	-	-	1.000	±0.000	-	-	0.258	±0.004	0.258	-	-	-

[a]The standard uncertainties are $u(T)$=0.1K, $u(P)$=0.04 bar, and for the NADES; $u(w_{HBA})$=$u(w_{HBD})$=$u(w_{H2O})$ =0.0003

References

Adeyemi, I., Abu-Zahra, M. R. M., & AlNashef, I. M. (2018). Physicochemical properties of alkanolamine-choline chloride deep eutectic solvents: Measurements, group contribution and artificial intelligence prediction techniques. *Journal of Molecular Liquids*, *256*, 581–590. https://doi.org/10.1016/j.molliq.2018.02.085

Almustafa, G., Sulaiman, R., Kumar, M., Adeyemi, I., Arafat, H. A., & AlNashef, I. (2020). Boron extraction from aqueous medium using novel hydrophobic deep eutectic solvents. *Chemical Engineering Journal*, *395*(February), 125173. https://doi.org/10.1016/j.cej.2020.125173

Bagh, F. S. G., Shahbaz, K., Mjalli, F. S., AlNashef, I. M., & Hashim, M. A. (2013). Electrical conductivity of ammonium and phosphonium based deep eutectic solvents: Measurements and artificial intelligence-based prediction. *Fluid Phase Equilibria*, *356*, 30–37. https://doi.org/10.1016/j.fluid.2013.07.012

Bahadori, L., Chakrabarti, M. H., Mjalli, F. S., Alnashef, I. M., Manan, N. S. A., & Hashim, M. A. (2013). Physicochemical properties of ammonium-based deep eutectic solvents and their electrochemical evaluation using organometallic reference redox systems. *Electrochimica Acta*, *113*, 205–211. https://doi.org/10.1016/j.electacta.2013.09.102

Dietz, C. H. J. T., Creemers, J. T., Meuleman, M. A., Held, C., Sadowski, G., Van Sint Annaland, M., Gallucci, F., & Kroon, M. C. (2019). Determination of the Total Vapor Pressure of Hydrophobic Deep Eutectic Solvents: Experiments and Perturbed-Chain Statistical Associating Fluid Theory Modeling [Research-article]. *ACS Sustainable Chemistry and Engineering*, *7*(4), 4047–4057. https://doi.org/10.1021/acssuschemeng.8b05449

Florindo, C., Celia-Silva, L. G., Martins, L. F. G., Branco, L. C., & Marrucho, I. M. (2018). Supramolecular hydrogel based on a sodium deep eutectic solvent. *Chemical Communications*, *54*(54), 7527–7530. https://doi.org/10.1039/c8cc03266a

Florindo, C., Romero, L., Rintoul, I., Branco, L. C., & Marrucho, I. M. (2018). From Phase Change Materials to Green Solvents: Hydrophobic Low Viscous Fatty Acid-Based Deep Eutectic Solvents. *ACS Sustainable Chemistry and Engineering*, *6*(3), 3888–3895. https://doi.org/10.1021/acssuschemeng.7b04235

Ghaedi, H., Ayoub, M., Sufian, S., Hailegiorgis, S. M., Murshid, G., & Khan, S. N. (2018). Thermal stability analysis, experimental conductivity and pH of phosphonium-based deep eutectic solvents and their prediction by a new empirical equation. *Journal of Chemical Thermodynamics*, *116*, 50–60. https://doi.org/10.1016/j.jct.2017.08.029

Gilmore, M., McCourt, É. N., Connolly, F., Nockemann, P., Swadźba-Kwaśny, M., & Holbrey, J. D. (2018). Hydrophobic Deep Eutectic Solvents Incorporating Trioctylphosphine Oxide: Advanced Liquid Extractants. *ACS Sustainable Chemistry and Engineering*, *6*(12), 17323–17332. https://doi.org/10.1021/acssuschemeng.8b04843

Hayyan, A., Mjalli, F. S., Alnashef, I. M., Al-Wahaibi, T., Al-Wahaibi, Y. M., & Hashim, M. A. (2012). Fruit sugar-based deep eutectic solvents and their physical properties. *Thermochimica Acta*, *541*, 70–75. https://doi.org/10.1016/j.tca.2012.04.030

Hayyan, A., Mjalli, F. S., Alnashef, I. M., Al-Wahaibi, Y. M., Al-Wahaibi, T., & Hashim, M. A. (2013). Glucose-based deep eutectic solvents: Physical properties. *Journal of Molecular Liquids*, *178*, 137–141. https://doi.org/10.1016/j.molliq.2012.11.025

Jibril, B., Mjalli, F., Naser, J., & Gano, Z. (2014). New tetrapropylammonium bromide-based deep eutectic

solvents: Synthesis and characterizations. *Journal of Molecular Liquids*, *199*, 462–469. https://doi.org/10.1016/j.molliq.2014.08.004

Kareem, M. A., Mjalli, F. S., Hashim, M. A., & Alnashef, I. M. (2010). Phosphonium-based ionic liquids analogues and their physical properties. *Journal of Chemical and Engineering Data*, *55*(11), 4632–4637. https://doi.org/10.1021/je100104v

Li, T., Song, Y., Xu, J., & Fan, J. (2019). A hydrophobic deep eutectic solvent mediated sol-gel coating of solid phase microextraction fiber for determination of toluene, ethylbenzene and o-xylene in water coupled with GC-FID. *Talanta*, *195*(September 2018), 298–305. https://doi.org/10.1016/j.talanta.2018.11.085

Martins, M. A. R., Crespo, E. A., Pontes, P. V. A., Silva, L. P., Bülow, M., Maximo, G. J., Batista, E. A. C., Held, C., Pinho, S. P., & Coutinho, J. A. P. (2018). Tunable Hydrophobic Eutectic Solvents Based on Terpenes and Monocarboxylic Acids. *ACS Sustainable Chemistry and Engineering*, *6*(7), 8836–8846. https://doi.org/10.1021/acssuschemeng.8b01203

Martins, M. A. R., Silva, L. P., Schaeffer, N., Abranches, D. O., Maximo, G. J., Pinho, S. P., & Coutinho, J. A. P. (2019). Greener Terpene-Terpene Eutectic Mixtures as Hydrophobic Solvents. *ACS Sustainable Chemistry and Engineering*, *7*(20), 17414–17423. https://doi.org/10.1021/acssuschemeng.9b04614

Mat Hussin, S. A., Varanusupakul, P., Shahabuddin, S., Yih Hui, B., & Mohamad, S. (2020). Synthesis and characterization of green menthol-based low transition temperature mixture with tunable thermophysical properties as hydrophobic low viscosity solvent. *Journal of Molecular Liquids*, *308*, 113015. https://doi.org/10.1016/j.molliq.2020.113015

Mitar, A., Panić, M., Prlić Kardum, J., Halambek, J., Sander, A., Zagajski Kučan, K., Radojčić Redovniković, I., & Radošević, K. (2019). Physicochemical properties, cytotoxicity, and antioxidative activity of natural deep eutectic solvents containing organic acid. *Chemical and Biochemical Engineering Quarterly*, *33*(1), 1–18. https://doi.org/10.15255/CABEQ.2018.1454

Mjalli, F. S., Naser, J., Jibril, B., Alizadeh, V., & Gano, Z. (2014). Tetrabutylammonium chloride based ionic liquid analogues and their physical properties. *Journal of Chemical and Engineering Data*, *59*(7), 2242–2251. https://doi.org/10.1021/je5002126

Ribeiro, B. D., Florindo, C., Iff, L. C., Coelho, M. A. Z., & Marrucho, I. M. (2015). Menthol-based eutectic mixtures: Hydrophobic low viscosity solvents. *ACS Sustainable Chemistry and Engineering*, *3*(10), 2469–2477. https://doi.org/10.1021/acssuschemeng.5b00532

Riveiro, E., González, B., & Domínguez, Á. (2020). Extraction of adipic, levulinic and succinic acids from water using TOPO-based deep eutectic solvents. *Separation and Purification Technology*, *241*(February), 116692. https://doi.org/10.1016/j.seppur.2020.116692

Saputra, R., Walvekar, R., Khalid, M., & Mubarak, N. M. (2020). Synthesis and thermophysical properties of ethylammonium chloride-glycerol-ZnCl2 ternary deep eutectic solvent. *Journal of Molecular Liquids*, *310*, 113232. https://doi.org/10.1016/j.molliq.2020.113232

Skulcova, A., Russ, A., Jablonsky, M., & Sima, J. (2018). *PEER REVIEWED BRIEF COMMUNICATION The pH Behavior of Seventeen Deep Eutectic Solvents*. *3*, 5042–5051.

Tereshatov, E. E., Boltoeva, M. Y., & Folden, C. M. (2016). First evidence of metal transfer into hydrophobic deep eutectic and low-transition-temperature mixtures: Indium extraction from hydrochloric and oxalic acids. *Green Chemistry*, *18*(17), 4616–4622. https://doi.org/10.1039/c5gc03080c

Van Osch, D. J. G. P., Parmentier, D., Dietz, C. H. J. T., Van Den Bruinhorst, A., Tuinier, R., & Kroon, M. C. (2016). Removal of alkali and transition metal ions from water with hydrophobic deep eutectic solvents. *Chemical Communications*, *52*(80), 11987–11990. https://doi.org/10.1039/c6cc06105b

Van Osch, D. J. G. P., Van Spronsen, J., Esteves, A. C. C., Tuinier, R., & Vis, M. (2020). Oil-in-water emulsions based on hydrophobic eutectic systems. *Physical Chemistry Chemical Physics*, *22*(4), 2181–2187. https://doi.org/10.1039/c9cp06762k

Van Osch, D. J. G. P., Zubeir, L. F., Van Den Bruinhorst, A., Rocha, M. A. A., & Kroon, M. C. (2015). Hydrophobic deep eutectic solvents as water-immiscible extractants. *Green Chemistry*, *17*(9), 4518–4521. https://doi.org/10.1039/c5gc01451d

Verma, R., & Banerjee, T. (2018). Liquid-Liquid Extraction of Lower Alcohols Using Menthol-Based Hydrophobic Deep Eutectic Solvent: Experiments and COSMO-SAC Predictions. *Industrial and Engineering Chemistry Research*, *57*(9), 3371–3381. https://doi.org/10.1021/acs.iecr.7b05270

Verma, R., & Banerjee, T. (2019). Palmitic-Acid-Based Hydrophobic Deep Eutectic Solvents for the Extraction of Lower Alcohols from Aqueous Media: Liquid–Liquid Equilibria Measurements, Validation and Process Economics. *Global Challenges*, *3*(11), 1900024. https://doi.org/10.1002/gch2.201900024

Zubeir, L. F., Van Osch, D. J. G. P., Rocha, M. A. A., Banat, F., & Kroon, M. C. (2018). Carbon Dioxide Solubilities in Decanoic Acid-Based Hydrophobic Deep Eutectic Solvents. *Journal of Chemical and Engineering Data*, *63*(4), 913–919. https://doi.org/10.1021/acs.jced.7b00534

Publications

Quantitative structure properties relationship for deep eutectic solvents using $S_{\sigma\text{-profile}}$ as molecular descriptors

Tarek Lemaoui [a], Nour El Houda Hammoudi [a], Inas M. Alnashef [b], Marco Balsamo [c], Alessandro Erto [d], Barbara Ernst [e], Yacine Benguerba [a,*]

[a] Laboratoire des Matériaux Polymères Multiphasiques, LMPMP, Université Ferhat ABBAS Sétif-1, 19000 Sétif, Algeria
[b] Department of Chemical Engineering, Khalifa University, Sas Al Nakhl campus, Abu Dhabi 127788, United Arab Emirates
[c] Dipartimento di Scienze Chimiche, Università degli Studi di Napoli Federico II, Complesso Universitario di Monte Sant'Angelo, 80126 Napoli, Italy
[d] Dipartimento di Ingegneria Chimica, dei Materiali e della Produzione Industriale, Università di Napoli Federico II, P. le Tecchio, 80, 80125 Napoli, Italy
[e] Université de Strasbourg, CNRS, IPHC UMR 7178, Laboratoire de Reconnaissance et Procédés de Séparation Moléculaire (RePSeM), ECPM 25 rue Becquerel, F-67000 Strasbourg, France

ABSTRACT

Computer assisted Quantitative Structure Property Relationship (QSPRs) has proven to be an accurate, reliable and cost-effective method for predicting the physicochemical properties of DESs, via a set of molecular descriptors. In this work, experimental data on the properties of DESs at different temperatures were taken from different bibliographic sources. The Conductor like Screen Model for Real Solutions (COSMO-RS) was used to predict the thermodynamic properties of DESs. A modeling analysis was conducted in order to provide a model for the prediction of specific DESs properties, such as viscosity density, etc. The used methodology allowed achieving reliable results as all the models showed high regression performances. The corresponding model parameters were determined and an analysis of variance allowed identification of the most significant factors of the retrieved models. Finally, an independent set of experimental data relevant to the modelled physical properties of DESs was used to test the obtained models. In most cases, there was a good agreement between the experimental and predicted values of the investigated properties.

© 2020 Elsevier B.V. All rights reserved.

1. Introduction

The use of solvents in many industrial applications is of paramount importance. Large-scale applications include industrial separations in different fields such as pharmaceutical, food, metal refining, biochemical, and in wastewater treatment. While the extraction methods have now become a routine procedure in separation technologies, the correct identification of the optimal solvent with adequate properties for a specific application still represents one of the challenges in this research field.

In fact, the choice of an appropriate solvent is essential for both technical and economic reasons, since it represents about 80% of the total volume of chemicals used in a generic process [1]. Solvents present many environmental, health and safety concerns, including human and ecotoxicological problems, process safety hazards and waste management issues [2]. Most organic solvents do not fulfil the requirements

for their use in green technologies because they have an intrinsic toxicity and a high volatility [1].

In recent decades, efforts have been made to replace organic solvents with alternative classes of chemical compounds. These approaches include the use of easily recyclable systems, such as fluorinated solvents, the elimination of solvents from productive cycle (whenever possible) and the use of non-volatile compounds, such as ionic liquids (ILs) and deep eutectic solvents (DESs).

Ionic Liquids are salts that are usually liquid below 100 °C. Over the last two decades, the number of published articles about ILs has increased exponentially [3]. The great advantage of ILs is that they can be tuned by combining different cations and anions. However, their main disadvantages include the difficulty of their processing, mainly due to their general high viscosity. In addition, the cost of ILs is high compared to commercially available solvents. This is due to their relatively complicated synthesis and purification [4]. To overcome these disadvantages, DESs have been proposed as a new class of analogues of the ILs. Although they share many characteristics and properties with ILs, they represent a different type of solvents and have different chemical nature [5].

PAPER

Check for updates

Predicting the density and viscosity of hydrophobic eutectic solvents: towards the development of sustainable solvents†

Tarek Lemaoui, [ID] ‡[a] Ahmad S. Darwish, [ID] ‡[b,c,d] Ayoub Attoui,[a]
Farah Abu Hatab, [ID] [b,c] Nour El Houda Hammoudi,[a] Yacine Benguerba, [ID] [a]
Lourdes F. Vega [ID] [b,d,e] and Inas M. Alnashef [ID] ⋆[b,c,d]

The interest in green and sustainable solvents has been dramatically increasing in recent years because of the growing awareness of the impact of classical organic solvents on environmental pollution and human health. As a solution to these issues, several greener and more sustainable solvents have been proposed in recent years such as the novel Hydrophobic Eutectic Solvents (HESs). HESs have many advantageous characteristics and could be considered as a potential replacement for both ionic liquids and classical solvents. However, choosing the right HES with the required physiochemical properties for a certain application is an extremely difficult task, especially since large-scale experimental measurements are expensive and time-consuming. Thus, the development of predictive models capable of estimating the properties of these solvents could be considered as a powerful tool in screening new green and sustainable HESs. This work presents two novel Quantitative Structure–Property Relationship (QSPR) models for predicting the density and viscosity of HESs using Conductor-like Screening Model for Real Solvents (COSMO-RS) based descriptors. The data set used includes all the experimental measurements reported in the literature up to the date of writing this work to ensure that the developed models are highly reliable and robust. The results show that the proposed models were excellent at predicting the properties of HES not included in the training set as R^2 values of 0.9956 and 0.9871 were obtained for density and viscosity, respectively. This work presents an initiative towards the development of reliable models for predicting the properties of HESs as a means to promote an efficient solvent design approach that can aid in designing and simulating new processes utilizing these novel HESs.

1. Introduction

Since the introduction of the "twelve principles" to Green Chemistry by Anastas and Warner *et al.*[1] an emphasis on designing chemical processes that eliminate the utilization or generation of harmful chemicals has been born. As such, the development of green solvents capable of replacing these classical organic solvents has become a top priority of the scientific community.[2–5] Several breakthrough advances in obtaining green and sustainable solvents have been achieved in the literature,[6] such as the application of supercritical fluids,[7–9] switchable solvents,[10] liquid polymers,[11] and "designer solvents" like Ionic Liquids[12,13] (ILs) and, more recently, Deep Eutectic Solvents[14,15] (DESs).

DESs were introduced as a novel class of solvents that could potentially be used as an alternative to ILs, as they share some physicochemical properties.[14] ILs are most commonly defined as liquid organic salts that have a freezing point lower than 373 K.[12] Conversely, the definition of DESs has not been refined and finalized as of yet. Attempts with the goal of finding a clear and uniform definition for DESs have been made by several papers,[3,15–17] however, more improvements to the definition are still required.[18–22] According to Martins *et al.*[22] "*a 'deep eutectic solvent' is a mixture of two or more pure compounds for which the eutectic point temperature is below that of an ideal liquid mixture,*

[a]*Laboratoire des Matériaux Polymères Multiphasiques (LMPMP), Université Ferhat ABBAS Sétif-1, 19000 Sétif, Algeria*
[b]*Chemical Engineering Department, Khalifa University, Abu Dhabi, P.O. Box 127788, United Arab Emirates (UAE). E-mail: enas.nashef@ku.ac.ae*
[c]*Center for Membrane and Advanced Water Technology (CMAT), Khalifa University, Abu Dhabi, P.O. Box 127788, United Arab Emirates (UAE)*
[d]*Research and Innovation Center on CO2 and H2 (RICH), Khalifa University, Abu Dhabi, P.O. Box 127788, United Arab Emirates (UAE)*
[e]*Center for Catalysis and Separation (CeCaS), Khalifa University, Abu Dhabi, P.O. Box 127788, United Arab Emirates (UAE)*

†Electronic supplementary information (ESI) available: Table S.1: list of all the density and viscosity experimental data used in this work, Table S.2: list of all the 66 descriptors, Table S.3: summary of the analysis of variance results of both density and viscosity models, and Figure S.1: predicted densities and viscosities compared to their experimental uncertainties. See DOI: 10.1039/d0gc03077e
‡Shared first authorship between Tarek Lemaoui and Ahmad S. Darwish.

Article

Prediction of Electrical Conductivity of Deep Eutectic Solvents Using COSMO-RS Sigma Profiles as Molecular Descriptors: A Quantitative Structure−Property Relationship Study

Tarek Lemaoui,[§] Ahmad S. Darwish,[§] Nour El Houda Hammoudi, Farah Abu Hatab, Ayoub Attoui, Inas M. Alnashef, and Yacine Benguerba*

Cite This: https://dx.doi.org/10.1021/acs.iecr.0c02542

Read Online

ACCESS | 📊 Metrics & More | 📰 Article Recommendations | 🆂🅸 Supporting Information

ABSTRACT: This work presents the development of molecular-based mathematical models for the prediction of electrical conductivity of deep eutectic solvents (DESs). Two new quantitative structure−property relationship (QSPR) models based on conductor-like screening model for real solvent (COSMO-RS) molecular charge density distributions (S_σ-profiles) were developed using the data obtained from the literature. The data comprise 236 experimental electrical conductivity measurements for 21 ammonium- and phosphonium-based DESs, covering a wide range of temperatures and molar ratios. First, the hydrogen-bond acceptors (HBAs) and hydrogen-bond donors (HBDs) of each DES were successfully modeled using COSMO-RS. Then, the calculated S_σ-profiles were used as molecular descriptors. The relation between the conductivity and the descriptors in both models has been expressed *via* multiple linear regression. The first model accounted for the structure of the HBA, the HBD, the molar ratio, and temperature, whereas the second model additionally incorporated the interactions between the molecular descriptors. The results showed that by accounting for the interactions, the regression coefficient (R^2) of the predictive model can be increased from 0.801 to 0.985. Additionally, the scope and reliability of the models were further assessed using the applicability domain analysis. The findings showed that QSPR models based on S_σ-profiles as molecular descriptors are excellent at describing the properties of DESs. Accordingly, the obtained model in this work can be used as a useful guideline in selecting DESs with the desired electrical conductivity for industrial applications.
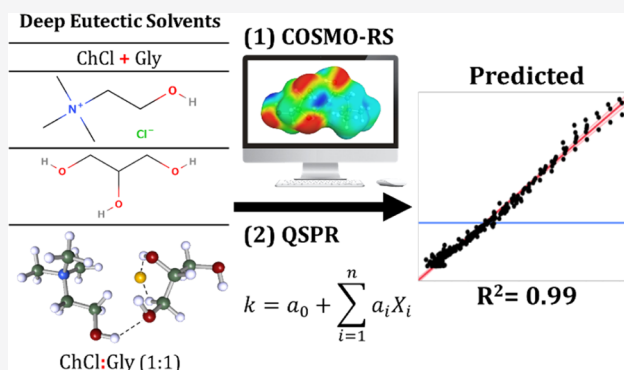
1. INTRODUCTION

Solvents are of vital importance in many industrial applications, which include cosmetics, metal refining, biochemistry, food, pharmaceuticals, and wastewater treatment fields.[1,2] Also, as solvents account for around four-fifths of the total volume of chemical products utilized in a process,[3] the selection of an optimal solvent with desirable properties for a given application is of paramount importance. However, classical organic solvents have raised many concerns related to their inherent toxicity, volatility, and impact on health, safety, and environment.[4] Some of the disadvantages of classical organic solvents include solvent losses because of volatility, environmental emissions, and poor biodegradability, which cause ecotoxicological and waste management issues.[5] Therefore, research efforts aimed at the development of novel "green" solvents are of immense significance.[4]

In an effort to avoid the disadvantages associated with these classical organic solvents, ionic liquids (ILs) have been considered as "green" alternatives.[1,6] ILs are liquid organic salts that are usually liquid below 100 °C. The deployment of ILs offers several advantages over classical organic solvents as they are commonly characterized by their high tunability, low freezing point, low volatility, high chemical/thermal stability, high conductivity, and low flammability.[1,6] Nonetheless, ILs still have several disadvantages that hinder their industrial application, which include their expensive/complex synthesis, and several studies have reported the poor toxicity and biodegradability of some ILs.[7,8]

Deep eutectic solvents (DESs) have also been proposed as novel "green" alternatives to classical organic solvents.[9,10] DESs were first reported in the literature in 2003 by Abbott *et al.*,[11] in which a mixture of choline chloride and urea was presented.

Molecular-Based Guide to Predict the pH of Eutectic Solvents: Promoting an Efficient Design Approach for New Green Solvents

Tarek Lemaoui,[⊥] Farah Abu Hatab,[⊥] Ahmad S. Darwish, Ayoub Attoui, Nour El Houda Hammoudi, Ghaiath Almustafa, Mohamed Benaicha, Yacine Benguerba, and Inas M. Alnashef*

| ACCESS | | Metrics & More | | Article Recommendations | | Supporting Information |

ABSTRACT: The case of sustainable solvents is of great interest both academically and industrially. With research communities becoming more aware of the negative impacts of conventional organic solvents, a range of greener and more sustainable solvents have been developed to counter the harmful drawbacks associated with conventional solvents. Among these, eutectic solvents (ESs) attracted considerable attention for their "green" properties and have proven their usefulness as environmentally benign alternatives to classical solvents. Among the various desirable characteristics of ESs, pH is a key property with significant implications for the design and control of industrial-scale applications. However, selecting an ES with the required pH for a particular application is a challenging task, especially with extensive experimentally determined data being time consuming and expensive. Therefore, in this work, the pH of various ESs have been predicted via novel quantitative structure−property relationships (QSPR) models using two machine learning algorithms, a multiple linear regression (MLR) and an artificial neural network (ANN), with a set of molecular descriptors generated by COSMO-RS. A total of 648 experimental points for 41 chemically unique ESs prepared from 9 HBAs and 21 HBDs at different temperatures were utilized for sufficient data set representation. On the basis of the statistical analysis of the models, it can be concluded that both approaches can be utilized as powerful predictive tools in estimating the pH of new ESs with the ANN model having better predictive capabilities and the MLR model being more interpretable. These models inspire and stimulate the development of robust models to predict the properties of designer solvents from the drawn molecular structures, which will save time and resources.

KEYWORDS: Green solvents, pH, Eutectic solvents (ESs), Quantitative structure−property relationships (QSPR), Multiple linear regression (MLR), Artificial neural networks (ANN)
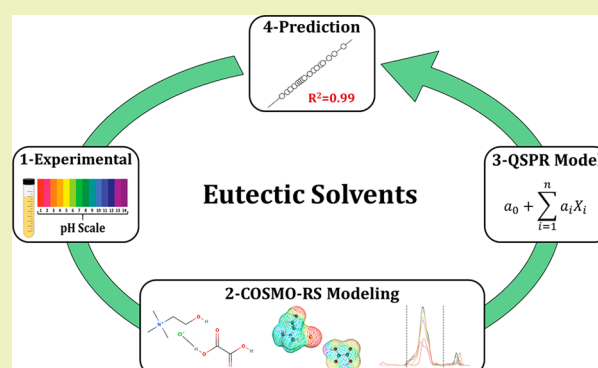
1. INTRODUCTION

With the appearance of the green chemistry concept, and since new solvents for sustainable chemical processes are in constant demand nowadays, the selection and optimization of solvent systems are vital to many industrial applications including fuel purification, biochemical, metal refining, and water/wastewater treatment.[1−4] The organic solvents traditionally used in such industries are often associated with a high toxicity profile.[5−7] The volatility of these conventional solvents not only increases their exposure rate to the environment but also incurs significant economic losses due to solvent evaporation.[8] Modern chemistry and chemical engineering practices reached considerable milestones in replacing conventional organic solvents with less hazardous ones.[7,9] One of the major steps taken in this direction was the development made in the field of ionic liquids (ILs).[10,11] Although ILs are chemically and thermally stable, highly nonvolatile, and tunable, they suffer from high production costs and potential toxic manifestations.[12−14] Consequently, these challenges stunt their application as feasible alternatives.

For this reason, green technology has actively sought to obtain new solvents to replace ILs.

A more recent milestone was achieved in 2003, when deep eutectic solvents (DES) emerged as potential analogs for ILs.[15] In general, DESs are mixtures of two or more hydrogen-bond acceptors (HBA) and hydrogen-bond donors (HBD) that are associated with each other through hydrogen-bond interactions.[16] The resulting eutectic mixture has a decreased melting point relative to the individual components. As the DESs are still considered in their infant stages, different arguments have been raised when defining DES, and several papers were arguing the objective of finding a distinct and

Simultaneous dearomatization, desulfurization, and denitrogenation of diesel fuels using acidic deep eutectic solvents as extractive agents: A parametric study

Tarek Lemaoui [a], Yacine Benguerba [a, *], Ahmad S. Darwish [b], Farah Abu Hatab [b], Samah E. E. Warrag [b], Maaike C. Kroon [b], Inas M. Alnashef [b]

[a] Laboratoire des Matériaux Polymères Multiphasiques (LMPMP), Université Ferhat ABBAS, Département de Génie des Procédés, Sétif-1, 19000 Sétif, Algeria
[b] Khalifa University of Science and Technology, Center for Membrane and Advanced Water Technology (CMAT), Chemical Engineering Department, P.O. Box 54224, Abu Dhabi, United Arab Emirates

A B S T R A C T

Based on the literature, deep eutectic solvents (DESs) have been proven to be promising candidates for the separation of aromatics or heteroaromatics ("sulfur-/nitrogen- containing aromatics") from fuels. However, most studies investigated the separation of a single fuel impurity (aromatics or heteroaromatics) from n-alkanes. Thus, to realistically represent a process that simulates the treatment of both types of aromatics, this work investigated the application of DESs in simultaneous dearomatization, desulfurization, and denitrogenation of fuels, particularly "diesel" using an arbitrary fuel model consisting of {5 wt% toluene + 5 wt% thiophene + 5 wt% pyridine + 5 wt% pyrrole + 80 wt% n-decane}. The selected DES was comprised of tetrapropylammonium bromide and acetic acid at a 1:4 M ratio. The DES performance was evaluated based on single-stage liquid–liquid extraction, the Liquid-Liquid Equilibrium (LLE) data of each impurity, multi-stage, and multi-cycle extraction of the diesel model. Furthermore, the influence of initial concentration and mixing effects of impurities were also studied. The results showed that complete removal of pyrrole and pyridine ("≈100%") can be achieved in 2 stages only, while extraction efficiencies of 68% and 89% for toluene and thiophene, respectively, were achieved after the 5th stage. Based on the obtained results, it was concluded that acidic DESs could be considered as potential solvents for the simultaneous dearomatization, desulfurization, and denitrogenation of diesel fuels.

1. Introduction

Fuels are considered to be a major environmental pollutant as they are rich in aromatics, sulfur-containing, and nitrogen-containing aromatics [1] that are burnt to produce hazardous air pollutants, such as CO_x, SO_x, and NO_x. Therefore, strict governmental regulations have been introduced to set limits on the content of aromatics, sulfur-containing, and nitrogen-containing aromatics in fuels [2].

Industrially, catalytic hydrotreatment is the established process used for the simultaneous dearomatization, desulfurization, and denitrogenation of fuels [3]. In this process, the fuel impurities "aromatics and the heteroaromatics" are catalytically hydrogenated to paraffins at high temperatures and pressures (600–700 K; 20–50 bar) [4]. Despite the workability of this process, it has many drawbacks [4], including (1) severe temperature and pressure operating conditions, (2) excessive hydrogen consumption, (3) use of expensive catalysts, and (4) reduction of the products' cetane number due to hydrocracking side reactions.

Extraction of Thiophene, Pyridine, and Toluene from *n*-Decane as a Diesel Model Using Betaine-Based Natural Deep Eutectic Solvents

Farah Abu Hatab,[§] Ahmad S. Darwish,[§] Tarek Lemaoui, Samah E. E. Warrag, Yacine Benguerba, Maaike C. Kroon, and Inas M. AlNashef*

ACCESS | 📊 Metrics & More | 📖 Article Recommendations | 🆂🅸 Supporting Information

ABSTRACT: In an attempt to develop an alternative process that meets the criteria of "green" and economically sound technology in fuel purification, simultaneous extractive desulfurization, denitrification, and dearomatization using natural deep eutectic solvents (NADESs) were investigated. A NADES composed of betaine (Bet) as a hydrogen bond acceptor (HBA) and levulinic acid (LevA) as a hydrogen bond donor (HBD) was investigated for its extraction capacity of thiophene, pyridine, and toluene from *n*-decane via liquid−liquid extraction. First, the HBA/HBD molar ratio was optimized based on the highest overall extraction efficiency, which was achieved for Bet/LevA (1:7). Furthermore, the selected NADES was characterized by measuring its density, dynamic viscosity, and water content. Then, the solubility of each fuel impurity in the NADES was measured. Moreover, the liquid−liquid equilibrium (LLE) data of the *pseudo*-ternary systems {*n*-decane (1) + thiophene/pyridine/ toluene (2) + Bet/LevA (1:7) (3)} were determined at 298.15 K and 1.01 bar. The assumption of a *pseudo*-ternary system, which means that the NADES stays intact in one phase, was validated experimentally. The solute distribution ratios, selectivities, and the extraction efficiencies of each impurity at a 1:1 solvent-to-feed mass ratio were calculated from the experimental LLE data and compared to a benchmark solvent (i.e. sulfolane) and other ionic liquids and DESs reported in the literature. The LLE data were also correlated using the nonrandom two-liquid thermodynamic model. The regressed LLE data showed good agreement with the experimental data as the root-mean-square deviation was found to be ≤0.29%. Finally, it is clear that Bet/LevA (1:7) can be considered as a potential natural solvent for combined desulfurization, denitrification, and dearomatization processes.
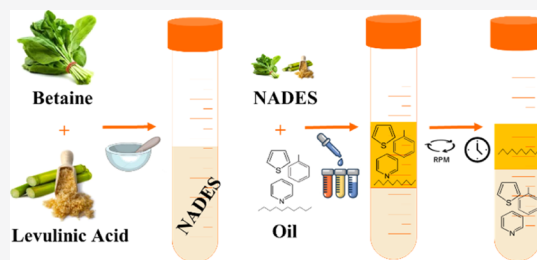
1. INTRODUCTION

The production of fuels with a low content of aromatics is one of the main challenges in the petroleum industry.[1] Various processes have been applied to purify fuels from their impurities.[2] The established industrial process for this application is catalytic hydrotreatment, in which the aromatic species are saturated with large amounts of hydrogen under severe operating conditions (temperatures between 573.15 and 673.15 K and pressures between 3.5 and 7.0 MPa).[3] Although this process is capable of deep dearomatization of the fuel impurities, it has several drawbacks including harsh operating conditions, production of undesirable compounds, namely, hydrogen sulfide (H_2S) and ammonia (NH_3), and consumption of excessive amounts of hydrogen.[4]

Extractive desulfurization, denitrification, or dearomatization via liquid−liquid extraction are one of the effective alternatives for hydrotreatment processes, in which organic solvents such as dimethyl sulfoxide[5] (DMSO), *N*-formylmorpholine[6] (NFM), and sulfolane[7] can be used to extract the aromatic impurities from fuels. However, these organic solvents are generally toxic and difficult to regenerate and exhibit low selectivity to some aromatics which in turn increases the cost of the process.[8,9] These drawbacks encouraged the develop-

ment of alternative solvents to overcome the disadvantages of these organic solvents.

Ionic liquids[10,11] (ILs) were investigated as a replacement for the organic solvents in extractive desulfurization,[12,13] denitrification,[14,15] or dearomatization.[16,17] This novel solvent captured the attention of many researchers due to the ease of tuning its properties, low volatility, and high extraction efficiency.[18−20] However, the toxicity, poor biodegradability, high cost, and difficulty in synthesizing ILs restricted their commercial use as extractive solvents.[21]

A new generation of low-volatile solvents so-called "deep eutectic solvents" (DESs) were first reported by Abbott[22] (where the mixture of solid choline chloride and solid urea formed a eutectic mixture, i.e., liquid at ambient conditions). DESs are simply a mixture of two or more constituents, hydrogen bond acceptors (HBA) and hydrogen bond donors

Multicomponent extraction of aromatics and heteroaromatics from diesel using acidic eutectic solvents: Experimental and COSMO-RS predictions

Ahmad S. Darwish [a,1], Farah Abu Hatab [a,1], Tarek Lemaoui [b], Omar A. Z. Ibrahim [a], Ghaiath Almustafa [a], Botagoz Zhuman [a], Samah E. E. Warrag [a], Mohamed K. Hadj-Kali [c], Yacine Benguerba [b,*], Inas M. Alnashef [a,*]

[a] Center for Membrane and Advanced Water Technology (CMAT), Chemical Engineering Department, Khalifa University, Abu Dhabi, P.O. Box 127788, United Arab Emirates
[b] Laboratoire des Matériaux Polymères Multiphasiques (LMPMP) and Energetics and Solid-State Electrochemistry Laboratory (LEES), Université Ferhat ABBAS Sétif-1, 19000 Sétif, Algeria
[c] Chemical Engineering Department, King Saud University, Riyadh 11421, P.O. Box 800, Saudi Arabia

ARTICLE INFO

ABSTRACT

Eutectic solvents (ESs) have been extensively studied in the literature for the purification of fuels. Nevertheless, most studies investigated the extraction of a single type of aromatic from n-alkanes. In this work, aiming to provide insights about the performance of ESs in a process that mimics the multicomponent dearomatization used industrially, a salt-acid-based ES, comprised of methyltriphenyl-phosphonium bromide and acetic acid, was applied in simultaneously extracting toluene, thiophene, quinoline, and pyrrole from n-decane. First, the DES was characterized for its eutectic composition, physicochemical, and critical properties. Then, an initial screening to determine the molecular-level interactions and extraction mechanism were studied experimentally and using COSMO-RS screening charge density profiles and potentials. A physical mechanism was confirmed for the extraction of pyrrole, thiophene, and toluene while for quinoline, an acid-base reaction was the predominant extraction mechanism. The phase diagrams of each impurity were also experimentally determined, predicted using the COSMO-RS model, and correlated using the NRTL model in Aspen Plus. Lastly, a parametric investigation studying the impact of key parameters including stirring time, initial concentration, mixing effects, solvent-to-feed ratio, multi-stage extraction, and repetitive usage of solvent was conducted. On multi-stage extraction, full recovery of pyrrole and quinoline ($\approx$99.9%) was achieved in only 2-stages, whereas for thiophene and toluene efficiencies of 82.2% and 58.4% were reached after the 5th stage, respectively.

© 2021 Elsevier B.V. All rights reserved.

1. Introduction

The combustion of diesel fuel leads to the production of particulate matters and various harmful gaseous pollutants that include

* Corresponding authors.

E-mail address: enas.nashef@ku.ac.ae (I.M. Alnashef).

[1] Shared first authorship between Ahmad S. Darwish and Farah Abu Hatab.

carbon oxides (CO_x), sulfur oxides (SO_x), and nitrogen oxides (NO_x) as they are rich in aromatics and heteroaromatics (*i.e.*, sulfur-/nitrogen- containing aromatics) [1]. Thus, stringent legislations were introduced worldwide to control the aromatic and heteroaromatic content in diesel [2]. Catalytic hydrotreatment is the conventional process utilized in the industry for the simultaneous dearomatization of diesel [3]. However, this process suffers from numerous drawbacks, most notably, its harsh operating conditions (600–700 K; 20–50 bar) and its production of poisonous by-products such H_2S and NH_3 [3]. Therefore, the development of novel "greener" purification methods for diesel fuels has been a hot research topic, especially since the demand for diesel fuels as an energy source is increasing with the rapid industrial development and economic growth [4].

Based on the literature [4–7], liquid-liquid extraction (LLX) has been proposed as a promising alternative for the hydrotreatment
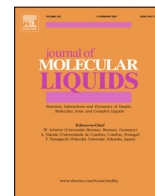
Computational modeling of polydecanediol-*co*-citrate using benzalkonium chloride-based hydrophobic eutectic solvents: COSMO-RS, reactivity, and compatibility insights

Samira Benabid [a], Nacerddine Haddaoui [a], Tarek Lemaoui [b], Ahmad S. Darwish [c], Yacine Benguerba [b], Inas M. Alnashef [c,*]

[a] *Laboratoire de Physico-Chimie des Hauts Polymères (LPCHP), Département de Génie des Procédés, Faculté de Technologie, Université Ferhat ABBAS Sétif-1, Sétif, Algeria*
[b] *Laboratoire des Matériaux Polymères Multiphasiques (LMPMP), Université Ferhat ABBAS, Département de Génie des Procédés, Sétif-1, 19000 Sétif, Algeria*
[c] *Center for Membrane and Advanced Water Technology (CMAT), Chemical Engineering Department, Khalifa University, Abu Dhabi, P.O. Box 127788, United Arab Emirates*

A R T I C L E I N F O

A B S T R A C T

Eutectic solvents (ESs) have been extensively explored in polymer chemistry. Nevertheless, studies utilizing ESs as a constituent of biodegradable poly(diol-*co*-citrate) (PDCA) polyesters are lacking in the literature. In this work, we propose utilizing benzalkonium chloride (BAC) based hydrophobic eutectic solvents (HESs) as a constituent of PDCAs. Spotting the light on the molecular-level interactions and mechanisms, a theoretical computational study was conducted to evaluate the feasibility of the process by exploiting a combination of geometrical optimizations, COSMO-RS quantum chemical calculations, density functional theory (DFT) calculations, reactivity calculations, and a blends compatibility study. The studied HES is comprised of dodecyldimethylbenzyl ammonium chloride (DDBAC) as an HBA and 1,10-decanediol ($D_{10}DO$) as the diol HBD at a 1:3 M ratio. Based on the obtained results, it was found that DDBAC-based HESs can be considered as potential solvents for antimicrobial PDCAs. Additionally, the modeling framework reported in this work can be utilized for screening new types of ESs promoting an efficient design approach of new PDCAs with tailored properties based on the choice of the ES's HBA.

© 2021 Elsevier B.V. All rights reserved.

1. Introduction

The rapid growth of human civilization and industry over the past century has resulted in prevalent negative impacts on the environment due to excessive pollution and energy usage [1]. Solutions to these undeniable negative impacts are of paramount importance as a means to suppress and mitigate their effects on our planet. One of the leading culprits of pollution is the excessive

consumption of solvents in the chemical industry that are harmful to the environment or hazardous, hence been non-sustainable [1,2]. Conventionally, chemical processes rely on a disproportionate amount of organic solvents for several applications, which include: separation and purification, extraction, and dissolving reagents, *etc* [1]. Previous studies have estimated that these classical organic solvents account for approximately eighty percent of the total amount of chemicals utilized in a generic process [3]. Even though these classical organic solvents have numerous advantages, they still have several unsustainable drawbacks that include high volatility, toxicity, flammability, and their inherently non-biodegradable nature, which pose risks to both the environment and human health [1,4]. In this sense, investigations and developments focusing on the design of new types of green and sustainable solvents became a hot research topic [1,2], which include the application of "designer solvents" like ionic liquids [5] (ILs) and, more recently, deep eutectic solvents [6,7] (DESs).

ILs are generally defined as salts consisting of organic cations and anions having a freezing point below 100°C. In contrast, as with any relatively young field, a clear definition of DESs has not

Conferences

جامعة بجاية
Tasdawit n Bgayet
Université de Béjaïa

N° : 149 /CIPCQ 2019/UAMB

Attestation de participation

Le comité d'organisation du **3ème Congrès International de Physique et Chimie Quantique (CIPCQ'19)**, qui a eu lieu à l'Université de Béjaïa du 04 au 06 novembre 2019, atteste que
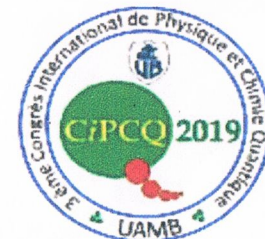
Mme /Melle /M.

Nom : **LEMAOUI**

Prénom : **Tarek**

Etablissement: **Université de Sétif**

a présenté une communication **Poster**

Intitulée : **Quantitative structure properties relationship for DESs using Sσ-profile as molecular descriptors and their molecular interaction by COSMO-RS**

Thème : **(D) Chimie Quantique**

Auteurs : **Tarek LEMAOUI, Yacine BENGUERBA**

Fait à Béjaïa le 06 novembre 2019
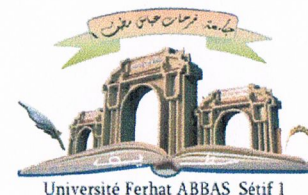P/Le Comité d'Organisation

164

Ferhat ABBAS University Sétif 1, ALGERIA

Faculty of Technology

Department of Engineering Processes

First International Workshop on Environmental Engineering

IWEE 2019

Certificate of Participation

This is to certify that:

LEMAOUI Tarek

has successfully participated with a Poster Presentation titled: **Synthèse de nouveaux solvants eutectiques profonds et l'applicationdans le domaine de la chimie verte**

Co-Authors: BENAICHA Mohamed, BENGUERBA Yacine

in the First International Workshop on Environmental Engineering held from November 16 to 17 2019, in Sétif 1 University, Algeria.
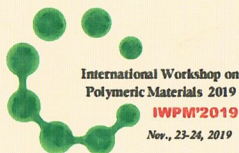
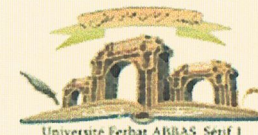**Organizing committee Chairman**

Dr. CHEBLI Derradji

Dr.CHEBLI Derradji

IWEE'19 Chairman

IWEE'19

Université Ferhat ABBAS Sétif 1

International Workshop on Polymeric Materials 2019
IWPM'2019
Nov., 23-24, 2019

Ferhat ABBAS SETIF – 1 UNIVERSITY

Faculty of Technology - Department of Engineering Processes

Université Ferhat ABBAS Setif 1

Ref.: CP-10

International Workshop on Polymeric Materials 2019

Certificate of Attendance

Mr. / Ms. : **Tarek LEMAOUI**

Attended the **International Workshop on Polymeric Materials 2019 (IWPM 2019)**

which was held on 23rd and 24rd November 2019 at Ferhat ABBAS SETIF-1 University (ALGERIA),

with a **POSTER** Presentation

Title : **Application des solvants eutectiques profonds à la science des polymères pour la synthèse de nouveaux matériaux**

Co-authors: Mohamed BENAICHA, Yacine BENGUERBA

Chair of Workshop Organizing Committee

Prof. N. HADDAOUI

IWPM'2019 Chairman

University of Ferhat ABBAS Setif 1 — IWPM'2019

PRIMA

الملخص:

تكتسي المذيبات المستدامة أهمية كبيرة من الناحيتين الأكاديمية والصناعية. مع زيادة وعي المجتمعات البحثية بالآثار السلبية للمذيبات العضوية التقليدية، طوّرَتْ مجموعة من المذيبات الأكثر خضرة واستدامة لمواجهة العيوب الضارة المرتبطة المذيبات التقليدية. من بين هذه المذيبات، المذيبات المنصهرة بعمق الذي جذبت إهتماماً كبيراً بخصائصها "الخضراء" وأثبتت فائدتها كبدائل حميدة بيئياً للمذيبات التقليدية.

تهدف هذه الأطروحة إلى تطوير نماذج جديدة للتنبؤ بالخصائص الفيزيائية الكيميائية للمذيبات المنصهرة بعمق وذلك بإستعمال العلاقة الكمية بين الهيكل والخاصية. تم تطوير النماذج بإستخدام طريقتي، الإنحدار الخطي المتعدد والشبكة العصبية الاصطناعية. من خلال الأدبيات، تم جمع مجموعة بيانات تتكون من أكثر من 100 مذيب منصهر بعمق وأكثر من 2500 تجربة تشمل قياس الخصائص الفيزيائية الكيميائية لهذه المذيبات، من بين هذه الخصائص الكثافة، اللزوجة، الموصلية الكهربائية والأس الهيدروجيني. أظهرت النتائج أن النماذج المقترحة قادرة على التنبؤ بخواص هذه المذيبات بدقة عالية جدا ويمكن إستخدامها في غياب القياسات التجريبية، كذلك تسمح بإقتصاد كبير وتوفير للوقت، وهي مفيدة في عملية شاملة ومثلى. بالإضافة إلى ذلك، تم استعمال المذيبات المنصهرة بعمق في إستخراج الثيوفين، البيريدين، والبيرول، والتولوين من الألكان بطريقة إستخراج السائل - السائل. أولاً، تم قياس الكثافة، اللزوجة الديناميكية ومحتوى الماء لهذه المذيبات. ثم تم قياس مدى ذوبان كل شوائب الوقود في هذه المذيبات. فضلاً عن ذلك فقد تم تحديد بيانات التوازن السائل/السائل للأنظمة الثلاثة (ألكان / ثيوفين + بيريدين + بيرول + تولوين / المذيبات المنصهرة بعمق) تحت درجة 298.15 كلفن و 1.01 بار. تم حساب نسب التوزيع للمذيبات، الإختيارات وكفاءات الاستخراج لكل شوائب بنسبة 1:1 من كتلة المذيب وكذلك مقارنتها بالمذيبات المرجعية وغيره من السوائل الأيونية الواردة في الأدبيات. وإستنادا إلى النتائج المتحصل عليها، خلص إلى أنه يمكن إعتبار المذيبات المنصهرة بعمق فعالة لاستخراج شوائب الوقود وبالتالي يمكن إستخدامها على النطاق الصناعي.

الكلمات المفتاحية :

المذيبات المنصهرة بعمق، العلاقة الكمية بين الهيكل والخاصية، الإنحدار الخطي المتعدد، الشبكة العصبية الاصطناعية، إستخراج السائل-السائل.

Résumé:

Les solvants durables sont d'une grande importance académique et industrielle. Les communautés de recherche deviennent plus conscientes des impacts négatifs des solvants organiques classiques. elles ont développé une gamme de solvants plus écologiques et plus durables pour remédier aux défauts nocifs associés aux solvants classiques. Parmi ces solvants, les solvants eutectiques profonds (SEPs) qui ont attiré une grande attention sur leurs propriétés « vertes » et se sont révélés utiles comme alternatives respectueuses de l'environnement aux solvants conventionnels.

L'objectif de cette thèse est de développer de nouveaux modèles pour prédire les propriétés physico-chimiques des SEPs en utilisant la relation quantitative entre la structure et la propriété. Les modèles ont été développés à l'aide de deux méthodes, la régression linéaire multiple (RLM) et le réseau neuronal artificiel (RNA). Un jeu de données composé de plus de 100 SEPs et de 2500 expériences de mesure impliquant les propriétés physicochimiques (densité, viscosité, conductivité électrique et pH) de ces solvants a été utilisé. Les résultats ont montré que les modèles proposés sont capables de prédire les propriétés des SEPs avec une très grande précision et peuvent être utilisés pour leur détermination en l'absence de mesures expérimentales, réduisant ainsi les couts et le temps pour une conception optimale. De plus, ces SEPs ont été utilisés pour leur capacité d'extraction du thiophène, de la pyridine, du pyrrole et du toluène à partir du n-décane via une extraction liquide-liquide (ELL). Premièrement, les SEPs sélectionnés ont été caractérisés en mesurant leur densité, leur viscosité dynamique et leur teneur en eau. Ensuite, la solubilité de chaque impureté de carburant dans les SEPs a été mesurée. Aussi, les données d'équilibre liquide-liquide des systèmes pseudo-ternaires {n-décane (1) + thiophène /pyridine /pyrrole /toluène (2) + SEPs (3)} ont été déterminées à 298,15 K et 1,01 bar. Les rapports de distribution des solutés, les sélectivités et les efficacités d'extraction de chaque impureté à un rapport de la masse du solvant 1:1 ont été calculés à partir des données expérimentales du ELL et comparés à un solvant de référence, autres liquides ioniques (LIs) et SEPs rapportés dans la littérature. Sur la base des résultats obtenus, il a été conclu que les SEPs pouvaient être considérés comme des solvants efficaces pour l'extraction des impuretés des carburants et peuvent donc être utilisés à l'échelle industrielle.

Mots clés :

Solvants eutectiques profonds, Relations quantitatives structure-propriété, Régression linéaire multiple, Réseaux neuronaux artificiels, Extraction liquide-liquide.

Abstract:

The case of sustainable solvents is of great interest both academically and industrially. With research communities becoming more aware of the negative impacts of conventional organic solvents, a range of greener and more sustainable solvents have been developed to counter the harmful drawbacks associated with conventional solvents. Among these, deep eutectic solvents (DESs) attracted considerable attention for their "green" properties and have proven their usefulness as environmentally benign alternatives to classical solvents.

The main objective of this thesis is to develop novel models to predict the physio-chemical properties of DESs using the quantitative composition-property relationship (QSPR). The models were developed using the two methods, multiple linear regression (MLR) and artificial neural network (ANN). From the literature, a data set of more than 100 DES and more than 2500 experiment points measuring the physicochemical properties of these DESs, including density, viscosity, electrical conductivity, and pH were collected. The results showed that the proposed models are able to predict the properties of DESs with very high accuracy and can be used for their determination in the absence of experimental measurements, hence reducing the cost, and time for an optimal process design. In addition to this, DESs were investigated for their extraction capacity of thiophene, pyridine, pyrrole, and toluene from n-decane via liquid−liquid extraction (LLE). First, the selected DESs were characterized by measuring their density, dynamic viscosity, and water content. Then, the solubility of each fuel impurity in the DESs was measured. Moreover, the liquid−liquid equilibrium (LLE) data of the pseudo-ternary systems {n-decane (1) + thiophene/pyridine/pyrrole/toluene (2) + DESs (3)} were determined at 298.15 K and 1.01 bar. The solute distribution ratios, selectivities, and the extraction efficiencies of each impurity at a 1:1 solvent-to-feed mass ratio were calculated from the experimental LLE data and compared to a benchmark solvent, other ionic liquids (Ils), and DESs reported in the literature. Based on the obtained results, it was concluded that DESs could be considered as effective solvents for the extraction of fuels impurities and can therefore be used in an industrial zone.

Keywords:

الملخص:

الهدف من هذه الأطروحة هو تطوير نماذج جديدة للتنبؤ بالخصائص الفيزيائية الكيميائية للمذيبات المنصهرة بعمق وذلك باستعمال العلاقة الكمية بين الهيكل والخاصية. تم تطوير النماذج باستخدام طريقتي ، الانحدار الخطي المتعدد والشبكة العصبية الاصطناعية. من خلال الأدبيات ، تم جمع مجموعة بيانات تتكون من أكثر من 100 مذيب منصهر بعمق وأكثر من 2500 تجربة تشمل قياس الخصائص الفيزيائية الكيميائية لهذه المذيبات ، من بين هذه الخصائص الكثافة ، اللزوجة ، الموصلية الكهربائية والأس الهيدروجيني. أظهرت النتائج أن النماذج المقترحة قادرة على التنبؤ بخواص هذه المذيبات بدقة عالية جدا ويمكن استخدامها في غياب القياسات التجريبية ، كذلك تسمح باقتصاد كبير وتوفير للوقت ، وهي مفيدة في عملية شاملة ومثلى. بالإضافة إلى ذلك ، تم استعمال المذيبات المنصهرة بعمق في استخراج الثيوفين ، البيريدين ، والبيرول ، والتولوين من الألكان بطريقة استخراج السائل ـ السائل. أولاً ، تم قياس الكثافة ، اللزوجة الديناميكية و محتوى الماء لهذه المذيبات. ثم تم قياس مدى ذوبان كل شوائب الوقود في هذه المذيبات. فضلاً عن ذلك فقد تم تحديد بيانات التوازن السائل/السائل للأنظمة الثلاثة (ألكان / ثيوفين + بيريدين + بيرول + تولوين / المذيبات المنصهرة بعمق) تحت درجة 298.15 كلفن و 1.01 بار. تم حساب نسب التوزيع للمذيبات ، الاختيارات وكفاءات الاستخراج لكل شوائب بنسبة 1:1 من كتلة المذيب وكذلك مقارنتها بالمذيبات المرجعية وغيره من السوائل الأيونية الواردة في الأدبيات. واستنادا إلى النتائج المتحصل عليها ، خلص الى أنه يمكن اعتبار المذيبات المنصهرة بعمق فعالة لاستخراج شوائب الوقود وبالتالي يمكن استخدامها على النطاق الصناعي.

الكلمات المفتاحية :

المذيبات المنصهرة بعمق ، العلاقة الكمية بين الهيكل والخاصية ، الانحدار الخطي المتعدد ، الشبكة العصبية الاصطناعية ، استخراج السائل-السائل.

Résumé:

L'objectif de cette thèse est de développer de nouveaux modèles pour prédire les propriétés physico-chimiques des SEPs en utilisant la relation quantitative entre la structure et la propriété. Les modèles ont été développés à l'aide de deux méthodes, la régression linéaire multiple (RLM) et le réseau neuronal artificiel (RNA). Un jeu de données composé de plus de 100 SEPs et de 2500 expériences de mesure impliquant les propriétés physicochimiques (densité, viscosité, conductivité électrique et pH) de ces solvants a été utilisé. Les résultats ont montré que les modèles proposés sont capables de prédire les propriétés des SEPs avec une très grande précision et peuvent être utilisés pour leur détermination en l'absence de mesures expérimentales, réduisant ainsi les couts et le temps pour une conception optimale. De plus, ces SEPs ont été utilisés pour leur capacité d'extraction du thiophène, de la pyridine, du pyrrole et du toluène à partir du n-décane via une extraction liquide-liquide (ELL). Premièrement, les SEPs sélectionnés ont été caractérisés en mesurant leur densité, leur viscosité dynamique et leur teneur en eau. Ensuite, la solubilité de chaque impureté de carburant dans les SEPs a été mesurée. Aussi, les données d'équilibre liquide-liquide des systèmes pseudo-ternaires {n-décane (1) + thiophène /pyridine /pyrrole /toluène (2) + SEPs (3)} ont été déterminées à 298,15 K et 1,01 bar. Les rapports de distribution des solutés, les sélectivités et les efficacités d'extraction de chaque impureté à un rapport de la masse du solvant 1:1 ont été calculés à partir des données expérimentales du ELL et comparés à un solvant de référence, autres liquides ioniques (LIs) et SEPs rapportés dans la littérature. Sur la base des résultats obtenus, il a été conclu que les SEPs pouvaient être considérés comme des solvants efficaces pour l'extraction des impuretés des carburants et peuvent donc être utilisés à l'échelle industrielle.

Mots clés :

Solvants eutectiques profonds, Relations quantitatives structure-propriété, Régression linéaire multiple, Réseaux neuronaux artificiels, Extraction liquide-liquide.

Abstract:

The main objective of this thesis is to develop novel models to predict the physio-chemical properties of DESs using the quantitative composition-property relationship (QSPR). The models were developed using the two methods, multiple linear regression (MLR) and artificial neural network (ANN). From the literature, a data set of more than 100 DES and more than 2500 experiment points measuring the physicochemical properties of these DESs, including density, viscosity, electrical conductivity, and pH were collected. The results showed that the proposed models are able to predict the properties of DESs with very high accuracy and can be used for their determination in the absence of experimental measurements, hence reducing the cost, and time for an optimal process design. In addition to this, DESs were investigated for their extraction capacity of thiophene, pyridine, pyrrole, and toluene from n-decane via liquid−liquid extraction (LLE). First, the selected DESs were characterized by measuring their density, dynamic viscosity, and water content. Then, the solubility of each fuel impurity in the DESs was measured. Moreover, the liquid−liquid equilibrium (LLE) data of the pseudo-ternary systems {n-decane (1) + thiophene/pyridine/pyrrole/toluene (2) + DESs (3)} were determined at 298.15 K and 1.01 bar. The solute distribution ratios, selectivities, and the extraction efficiencies of each impurity at a 1:1 solvent-to-feed mass ratio were calculated from the experimental LLE data and compared to a benchmark solvent, other ionic liquids (Ils), and DESs reported in the literature. Based on the obtained results, it was concluded that DESs could be considered as effective solvents for the extraction of fuels impurities and can therefore be used in an industrial zone.

Keywords:

Deep eutectic solvents, Quantitative structure-property relationships, Multiple linear regression, Artificial neural networks, Liquid-liquid extraction.